Using independent components analysis to identify visually driven regions and networks in the human brain, using data collected during movie watching.

Phoebe M. Asquith

A thesis submitted to Cardiff University

for the degree of Doctor of Philosophy.

EPSRC
Engineering and Physical Sciences Research Council

Summary of Thesis

Traditionally, regions involved in visual processing are mapped in the brain using simple localisers and/or anatomical techniques. As a more efficient (and interesting) alternative, Bartels & Zeki (2004) suggested that independent components analysis (ICA) could be used to segment the brain into functional regions, using data collected during movie watching.

The first aim of this thesis was to explore the potential of this technique for reliable identification of visually driven regions and networks. In Chapter 2 I thoroughly and systematically explore the sensitivity of tensor ICA (TICA) to common pre-processing parameters and identify an optimal analysis pipeline. Despite some sensitivity of TICA to the parameters tested, robust components in visually responsive regions could be identified across outputs. Using an optimized pipeline, in Chapter 3 I demonstrate that visually driven components (in particular, peak voxels) are consistent across different samples and movie clips, supporting the use of this technique. In Chapter 4 I show that established resting state networks can be identified in an ICA analysis using movies, and that by increasing dimensionality sub-regions of these networks can be identified. Chapter 5 shows how these reliable components represented visual regions in the motion processing pathway. Based on the success of the technique at the group level, in Chapter 6 I apply the technique to individual observer data. Results show that functional networks and visual regions of interest can be reliably identified, supporting its use in future neuroscientific research.

To address the short-comings of BOLD, the second aim of this thesis was to investigate whether MEG frequency data and fMRI bold data could be combined for analysis in a novel technique using TICA. First in Chapter 7 I address some prerequisites for a combined MEG frequency analysis using the technique. On the back of these results, I use the technique to generate interesting cross-frequency components (Chapter 8) and cross modality components using combined MEG and fMRI data (Chapter 9). These results show exciting promise for potential use in future neuroscientific work.

In the final chapter, I investigate the potential use of ICA and changing dimensionality for mapping the functional hierarchy of the visual system. With development this could be a useful tool for understanding connectivity between sub-regions of functional networks. These results have important implications for the identification of visually responsive regions and for understanding neural activity during natural viewing.

Declaration

This work has not been submitted in substance for any other degree or award at this or any other university or place of learning, nor is being submitted concurrently in candidature for any degree or other award.

Signed …… (candidate) Date:

STATEMENT 1

This thesis is being submitted in partial fulfillment of the requirements for the degree of PhD.

Signed …… (candidate) Date:

STATEMENT 2

This thesis is the result of my own independent work/investigation, except where otherwise stated.

Other sources are acknowledged by explicit references. The views expressed are my own.

Signed …… (candidate) Date:

STATEMENT 3

I hereby give consent for my thesis, if accepted, to be available online in the University's Open Access repository and for inter-library loan, and for the title and summary to be made available to outside organizations.

Signed …… (candidate) Date:

STATEMENT 4: PREVIOUSLY APPROVED BAR ON ACCESS

I hereby give consent for my thesis, if accepted, to be available online in the University's Open Access repository and for inter-library loans **after expiry of a bar on access previously approved by the Academic Standards & Quality Committee.**

Signed …… (candidate) Date:

NOTICE OF SUBMISSION OF THESIS: POSTGRADUATE RESEARCH DEGREES

Please TYPE or write in BLACK ink and use BLOCK capitals

SECTION A: TO BE COMPLETED BY THE CANDIDATE AND SUBMITTED WITH THE THESIS

CANDIDATE'S LAST name	ASQUITH		
CANDIDATE'S First name(s)	PHOEBE MAY		
CANDIDATE'S ID NUMBER	C1455729		
School	PSYCHOLOGY		
TITLE OF DEGREE	PHD		
FULL TITLE OF THESIS			
IS THIS A RESUBMISSION?	NO		
IS A BAR ON ACCESS OR LIBRARY DEPOSIT REQUIRED?	Bar on access: Library Deposit:		
THESIS SUBMITTED FOR EXAMINATION IN	Permanent binding: Temporary binding:		
CANDIDATE SIGNATURE		DATE	

Acknowledgments

I appreciate all the help and support of so many people. A huge and special thank you to:

My family, who are always there for me. I will treasure you always!

My kind and beautiful friends.

Tom, for your unwavering care, humor and interest.

My supervisor Simon, for your patience, pragmatism and encouragement.

I feel very lucky to be able to submit my PhD thesis, when millions of women and girls are denied their chance to an education, due to their sex. I hope we can make change, so others around the world can have the same opportunities I have enjoyed, in the future.

Impact of this thesis

Parts of Chapters 1, 2, 8 and 9 have been presented as posters at national and international conferences:

2018 "Using ICA to investigate cross-frequency band networks during movie watching" Poster presented at MEGUK 2018, Ulster University, Londonderry – Derry, NI.

2017"Anticipation of motion: identifying the motion processing pathway" Poster presented at AVA 2017, Queen Mary University of London, London, UK.

2017"The Components of James Bond" Poster Cardiff University, School of Psychology Postgraduate Conference, Cardiff, UK.

2017"Matching corresponding visual areas across fMRI and MEG" Poster presented at VSS 2016, St Pete's Beach, Florida, USA.

2016"Identifying the motion processing pathway" Talk presented at Cardiff University, School of Psychology Postgraduate Conference, Cardiff, UK.

2015"The neural of optic flow parsing" Poster presented at BVI Young Researchers Colloquium 2015, Bristol University, Bristol, UK.

Abbreviations

ATC	Activity timecourse (used in the context of functional neural regions)
BOLD	Blood oxygen level dependent
CICA	Concatenated independent components analysis (temporal concatenation)
EEG	Electroencephalography
ERP	Event-related potential
fMRI	Functional magnetic resonance imaging
ICA	Independent components analysis
IPS	Intraparietal sulcus
LO	Lateral occipital region
MEG	Magnetoencephalography
MRI	Magnetic resonance imaging
MT	Medial temporal region of the brain (motion area)
MT+	Medial temporal region of the brain in humans (motion area), includes MST subdivisions
MST	Medial superior temporal region of the brain, which shows ipsilateral activation
MSTl	Lateral portion of the medial superior temporal region of the brain
MSTd	Dorsal portion of the medial superior temporal region of the brain
RS	Resting state (data), data collected while a participant is at rest
RSN	Resting state network, functional networks identified using ICA with data collected during rest
TICA	Tensor independent components analysis
V1	Visual area 1, also referred to as the primary visual cortex
V2	Visual area 2
V3	Visual area 3
V3A	Visual area 3, subdivision A
V4	Visual area 4
V5	Motion area, also referred to as MT+

Contents

Summary of Thesis 2

Declaration 3

Acknowledgments 5

Impact of this thesis 6

Abbreviations 7

Contents 8

Chapter 1: General introduction 15

1.1 General introduction 15

1.1.1 Background: ICA analysis 20

1.1.2 Background: The BOLD signal 26

1.1.3 Background: Roles of MEG frequency bands in the brain 27

1.1.4 Cross frequency coupling 28

1.1.5 Background: MEG – MRI coupling 29

1.2 Overview of Thesis 31

1.3 Methods report 33

1.2.1 Movie stimuli 33

1.2.1 MRI data collection 34

1.2.2 MEG data collection 36

Chapter 2: A sensitivity analysis of independent component analysis (ICA) 38

2.1 Introduction 38

2.1 Cross subject correlation 40

2.1.1 Methods 40

2.1.2 Results 40
2.2 ICA: the brain order effect 41
2.2.1 Methods 42
2.2.2 Effect of brain order: Random permutations 44
2.2.3 What is driving the brain order effect? 46
2.2.4 Representativeness and the number of components 49
2.2.5 Number of brains in the ICA 50
2.3 Exploiting the ICA variation caused by switching the first brain 53
2.3.1 Removal of motion 55
2.3.2 Grey matter masking 60
2.3.3 Comparing ICA outputs across analysis pipelines 65
2.3.4 Changing ICA parameters 66
2.3.5 Comparing the magnitude of effect across data manipulations 71
2.4 Summary of parameter effects 72
2.4.1 Combining optimal parameters 73
2.5 Restricting the number of components 73
2.5.1 How do you choose the number of components to use? 76
2.6 Chapter summary 76
Chapter 3: The reliability of ICA results across different samples and movie clips. 78
3.1 Introduction 78
3.2 General Methods 79
3.3 Across different movie clips 79
3.3.1 Methods 79

3.3.2 Within-clip reliability (half the movie length) 80
3.3.3 Different movie clips 81
3.4 Across samples 89
3.4.1 Methods 89
3.4.2 Within-sample reliability (smaller sample of 11 participants) 89
3.4.4 Different samples 90
3.4.5 Summary 95
3.5 Length of movie clip 95
3.5.1 Methods 95
3.5.2 ICA outputs: spatial correspondence 95
3.5.3 Networks identified across movie lengths 98
3.6 Summary: Chapter 3 107
Chapter 4: Comparing group ICA components to established resting state networks 108
4.1 Introduction 108
4.2 Methods 109
4.3 Results 110
4.3.1 Visual network 1 112
4.3.2 Visual Network 2 116
4.3.3 Visual Network 3 120
4.3.4 Default mode network 125
4.3.5 Sensorimotor 126
4.3.6 Auditory 127
4.3.7 Executive control 129

4.3.8 Frontoparietal (lateralised) 130
4.4 Summary: Chapter 4 131
Chapter 5: The reliable components identified using a movie stimulus and group TICA 133
5.1 Introduction 133
5.2 Methods 134
5.3 Regions of interest: motion processing pathway 139
5.3.1 pVIP 139
5.3.2 V3A 140
5.3.3 MT+ 142
5.3.4 V6 144
5.3.5 CSv 146
5.3.6 V1/V2/V3 147
5.4 Summary: Chapter 5 150
Chapter 6: Single subject ICA and movie stimuli 152
6.1. Introduction 152
6.2 General Methods 153
6.3 Across subject ICA comparisons 153
6.3.1. Methods 153
6.3.2. Results 154
6.4 Single subject networks vs. Known visual networks 156
6.4.1 Methods 156
6.4.2 Results 156
6.5 Components identified at high dimensionality 167

6.5.1 Methods 167
6.5.2 Results 168
6.7 Summary: Chapter 6 179
Chapter 7: Using movies and ICA to segment oscillatory activity in the brain 180
7.1. Introduction 180
7.2 Can we identify visually driven components in a single MEG band? 183
7.2.1 Methods 184
7.2.2. Results 186
7.3 Are there differences in the relationships between frequency bands in visually driven regions? 192
7.3.1 Methods 192
7.3.2 Results 192
7.4 Are multiband TICA outputs reliable across permutations? 195
7.4.1 Methods 196
7.4.2 Results 197
7.5 Summary: Chapter 7 198
Chapter 8: A novel combined-frequency technique to investigate MEG cross-frequency networks during natural viewing 199
8.1 Introduction 199
8.2 Methods 199
8.3 Results 200
8.3.1 Low dimensionality 200
8.3.2 Higher dimensionality 207
8.4 Summary: Chapter 8 211

Chapter 9: Combining MRI and MEG data collected during natural viewing 213
9.1 Introduction 213
9.2 Methods 214
9.3 Voxel-wise correlation between MEG and MR data 214
9.3.1 Methods 214
9.3.2 Results 214
9.4 Correlation between fMRI component timeseries and MEG voxel timeseries 223
9.4.1 Methods 223
9.4.2 Results 226
9.5 Combined BOLD and single band TICA 227
9.5.1 Methods 228
9.5.2 Results 228
9.6 Combined BOLD and multi-band TICA 229
9.6.1 Methods 229
9.6.2 Results 229
9.7 Summary: Chapter 9 236
Chapter 10: Investigating neural hierarchies by changing ICA dimensionality 237
10.1 Introduction 237
10.2 Tracking components across dimensionalities: a case study 239
10.2.1 Methods 239
10.2.2 Results 240
10.2.3 Discussion: Case study 247
10.3 How do the components merge and split across dimensionalities? 247

10.3.1 Methods 247
10.3.2 Results 248
10.4 Summary: Chapter 10 251
Chapter 11: General discussion 253
11.1 Overview 253
11.2 Implications and future directions 254
Appendices 259
Chapter 2 259
Chapter 3 265
Chapter 4 267
Chapter 5 269
Chapter 6 270
Chapter 7 273
Chapter 8 275
Chapter 9 277
References 283

Chapter 1: General introduction

1.1 General introduction

Containing over 100 billion connected cells, the human brain is probably the most complex organ on the planet. Over hundreds of years philosophers and scientists have tried to understand and characterize this biological black-box, however many functional processes within the brain remain unknown. Today, key questions persist around the mechanisms underpinning our complex cognitive and perceptual processes and abilities. To understand a complex system such as the brain, we must find and describe the component parts and how they interact. One method of addressing this in neuroscientific research has been to divide the human brain into regions of functional specificity (e.g. Kanwisher, 2010). Being able to map neural regions that process different information is important across a range of basic science applications, as well as in clinical settings.

In particular, processing visual information is very important for effective interaction with our environment. For example, our brains can use information from the retina to understand the trajectory of moving objects or navigate through an environment, with little conscious effort. It is reported that ~50% of our neural tissue is directly or indirectly related to vision (Fixot, 1957), therefore being able to map the visual regions is of key interest for understanding the human brain and its functions.

Research has shown that there are multiple regions processing visual information, and different regions play different roles. When visual information first enters the cortex, it reaches the primary visual cortex (V1), which has a topographic organization (Holmes, 1945; Benson et.al., 2012). This means it represents the visual field, preserving information about relative location. Other early visual regions lie next to V1 and represent the whole visual field in separate topographical maps (Wandell, Dumoulin & Brewer, 2007). Visual input is then processed in neural pathways running dorsally and ventrally from the early occipital regions, involving multiple neural regions that are sensitive to different elements of the visual scene such as motion or colour (e.g. Goodale & Milner, 1992). A challenge of neuroscientific research has been to accurately map these visual regions and understand the functional role that each plays.

Recently, an interesting approach pioneered by Bartels and Zeki (2004;2005) suggested that visually responsive regions can be identified using a movie stimulus and independent components analysis (ICA), a data driven clustering technique. By showing a movie to a subject, multiple visual regions are engaged to process the rich broadband input and these regions can in theory be identified in parallel. If proven to be reliable, this would offer an efficient and exciting method for identifying visual regions. Traditionally, visual regions been located using brain anatomy (e.g. Hinds et.al., 2008; Dumoulin et.al., 2000; Bridge et.al., 2005; Glasser & Van Essen, 2011) or by presenting stimuli that isolate elements of the natural visual scene. If shown to a participant while they are in a neuroimaging scanner, regions that respond preferentially to this isolated visual feature can be identified. For example, when identifying the motion responsive region V5/MT+, participants are often shown experimental blocks alternating between an array of stationary, flickering dots and an array of moving dots (e.g. Huk & Heeger, 2002). The activity across the brain can be subtracted between one condition and another to identify where a change in response has occurred, i.e. where the brain is preferentially responding to motion. Once an area has been identified functionally and/or anatomically, the activation of this region during certain tasks can be established. An example here may be identifying whether the MT+ region is activated during action observation.

Using simple stimuli as localisers has allowed for many functional regions to be identified (e.g. Downing, Jiang, Shuman & Kanwisher, 2001; Zeki et.al., 1991; Ishai, Ungerleider, Martin, Schouten & Haxby, 1999) and has helped to identify functional subdivisions in neural organization that were not discernable using only architectural information (e.g. Zeki, 1974). However, there are problems with this process that can lead to the reduced validity of results. If using anatomical landmarks for the identification of regions, this could fall foul to the anatomical differences between individuals. Functional localisers can address this problem as there is no reliance on anatomical features, however if trying to identify a functional *network* many localisers may be needed to identify all the possible regions of interest. For example, if the visual pathway processing optic flow were to be examined, retinotopy would be used for identification of early visual maps (e.g. Dumoulin & Wandell, 2008); a motion versus flickering contrast would be needed to identify motion sensitive regions (Huk & Heeger, 2002); and stimuli simulating different types global optic flow patterns would also be appropriate (Amano, Wandell & Dumoulin, 2009). Presenting multiple localisers

can be unrealistic if there are time restraints on a scan. Additionally, and importantly, participants are likely to lose focus or fixation, thus reducing the effectiveness of the stimuli.

As well as often being impractical for identifying multiple regions, simple functional localisers are an unnatural stimulus that do not represent the richness of the natural visual experience. The technique can tell you that an area is involved in processing a certain aspect of the visual scene but does not directly address how these elements are combined to provide us with our rich and complete visual experience. Use of independent unnatural localisers segments visual networks into regions, but there is more than a single area involved in any task. To attempt to understand the relationship between visual regions during a task, timeseries of activity are usually correlated across the different regions. The correlation value is used to infer the dependence between the processes across the different areas. This seems inefficient and relies on the validity and effectiveness of the localisers being used, as well as having localisers for all the areas in the network being examined.

Bartels and Zeki's alternative approach uses a more natural, broadband stimuli which is much more representative of the natural visual environment and would be easier for an observer to attend to in a scanner. The ICA clustering technique groups voxels that show a correlation in underlying BOLD functional activity (section 1.1.1 provides a breakdown of how this technique works). It is based in the idea that functional specificity has developed in the brain in a complex and rich visual environment and therefore it makes sense that even when observing broadband natural stimuli, functional specificity remains when processing the input. This being the case, it means functionally distinct regions will each have their own characteristic activity timecourse (ATC), responding to features in the stimulus. Bartels and Zeki (2004; 2005) found that by using ICA, regions including the frontal eye fields, LO1, V1, V2/3 and the auditory cortex could be identified in individuals, based on their specific ATC at high dimensionalities.

Bartels and Zeki's technique does not try to segment the visual experience into different elements as a battery of localisers does, but instead finds functional separations in an organic and data-driven way. The potential of this method for identifying a multitude of visual and attentional regions and networks is clear. If reliable, it would provide a way to locate functional regions and networks in the context of natural viewing. It would remove the need for multiple functional localisers and provide a more efficient method and interesting stimulus for observers to attend to. Importantly, as well as being more efficient, this method would allow for

the investigation of temporal locking across networks during natural viewing, and across participants when watching the same movie stimulus.

However, there are many potential issues with the reliability of this technique that need to be examined. First, the sensitivity of ICA to pre-processing pipelines and parameters including motion correction, grey matter masking, smoothing and resampling. The ICA components identified by Bartels and Zeki showed correspondence across eight subjects in their timecourse and spatial map, suggesting that the technique is useful for identifying visual ROI and that the ROI were timelocked to the movie. However, the reliability of results across different groups and movie clips is still undetermined.

To address these concerns, the first section of this thesis will investigate the sensitivity of ICA to different processing parameters. An optimal pipeline will be identified so the robust components can be assessed for their usefulness for identifying multiple visual regions at the group and individual level.

Following the work by Bartels and Zeki (2004), the first section of this thesis will use blood oxygen-level dependent (BOLD) signals collected using fMRI during natural viewing. fMRI measures the oxygenation of blood in the brain, and it is inferred that an increase in oxygenated blood flow corresponds to an increase in neural activity. However, there are other more direct methods of recording neural activity. Since the discovery of the electroencephalogram (EEG) in 1929 (Berger), the oscillatory patterns of the brain's electrical activity have been measurable from the scalp. By 1972 developments had led to the reliable recording of the magnetic fields associated with these electrical signals, using a MEG scanner (Cohen, 1972).

Recording the BOLD signal and MEG signals have different benefits; fMRI data can provide good spatial resolution, while MEG data is a more direct measure of neuronal activity and provides a better temporal resolution. If both techniques can be combined, it provides an opportunity to exploit both strengths to understand neural processing. Secondly, it can help us to understand the relationship between neural signals and the BOLD response. In previous research, combining fMRI and MEG has been accomplished by running the same task in both MEG and MRI scanners and relating the results. For example, Cichy, Pantazis and Oliva achieved a successful combination of both modalities to show content-specific correspondence between early MEG responses and primary visual cortex (V1), and later MEG responses and inferior temporal (IT)

cortex (2014). This meant the processing stages located using BOLD could be pulled apart using the temporal resolution of MEG.

Using a movie clip a temporal structure is applied to visually responsive regions in the brain (Hasson et.al., 2010). If an observer watches the clip in both MRI and MEG scanners, the responses can be compared and combined. ICA identifies groups of voxels that may be spatially distal but that show correlation across time, if MEG and BOLD data were spatially concatenated it is possible that components can be identified across the modalities.

In the second section of this thesis I look to see whether reliable and sensible looking visually driven components can be identified using MEG data. I then investigate a novel technique for exploring the relationship between the different MEG frequency bands and the BOLD signal, using ICA.

Having explored a novel technique for understanding cross-frequency and cross-modality correlations, the question of network hierarchy has been left unaddressed. Bartels and Zeki (2005) used the timeseries of their functional components to examine the hierarchy of the regions identified in individual subjects. They correlated the timeseries of components and mapped the hierarchy based on these values. Another way to potentially examine this hierarchy is to exploit the ICA parcellation process by varying the number of components that the output is restricted to. When using a low number of components, multiple regions that show some functional synchronization will be included in one component (Smith, 2012). If more components are output, the sub-regions within this network should 'split' off and form separate functional components. The pattern of this splitting should, in theory, indicate the structure of the functional hierarchy. Regions that show the least similar activity to the network should split and form a separate component first. The pattern of component splitting across dimensionalities is explored in the final chapter as a novel technique for mapping the hierarchy of visually driven regions. A benefit of this technique over correlating component timeseries from a single ICA output is that the relationship between functional networks and their sub-regions can be explored. This is in contrast with choosing an arbitrary dimensionality and comparing the components within this dimensionality. Using our alternative technique, a more comprehensive account of the functional networks and regions active during natural viewing may be mapped.

The final experimental chapter of this thesis will explore the potential usefulness of exploiting the parcellation of ICA for mapping visual functional hierarchies.

In the next section of this general introduction I will provide some background on the key concepts addressed in this thesis. First, I breakdown the process of ICA and how it can be applied to BOLD data collected using fMRI (section 1.1.1). Next, I summarize the roles different oscillatory frequency bands are thought to play in neural processes (section 1.1.2). In section 1.1.3 I outline current understandings of synchronization across oscillatory activity in the brain. Finally, I provide some background to exploring the relationship between oscillatory activity (measured using MEG) and the BOLD signal (section 1.1.4).

1.1.1 Background: ICA analysis

What is ICA?

Independent components analysis (ICA) is widely used for the analysis of both resting state and task-based fMRI data (e.g. McKeown, Varadarajan, Huettel & McCarthy, 2002; Calhoun, Liu, & Adalı, 2009; Beckmann, Mackay, Filippini & Smith, 2009) and electro-magnetic MEG/EEG data (e.g. Vigário et.al., 2000; Brookes et.al., 2011). It is a data-driven technique and therefore can identify unexpected patterns in a dataset. It has provided an alternative to the explicitly defined classic general linear models as a way of identifying functionally distinct regions in the brain (Jung et.al., 2000; McKeown, 2002).

ICA is used to separate a linear combination signals ("mixed" signals). For example, if two signals (A and B, below) are combined using different linear combinations (e.g. A – 2*B and A*1.2+B*3), the output signals are different mixes of the original signals (C and D, below):

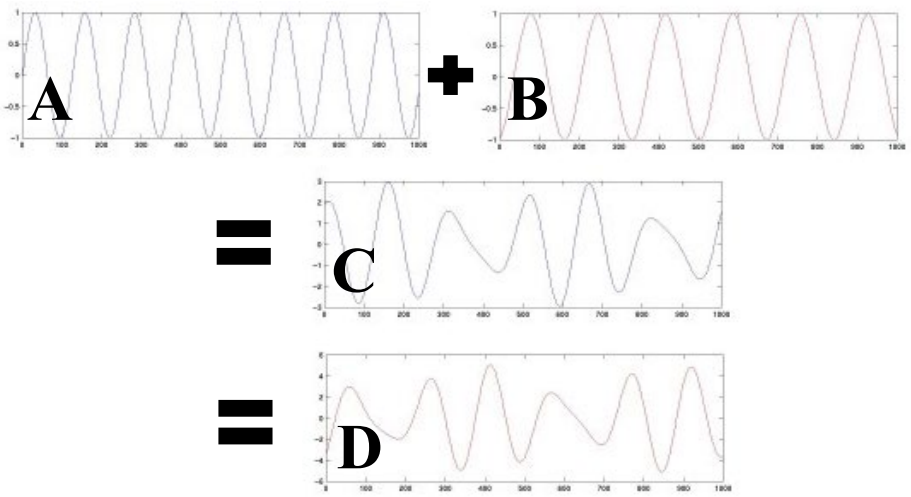

ICA can take the mixed signals C and D and recover the original signals, A and B. This is useful in the context of the BOLD timeseries, as voxel timeseries represent a mix of noise, physiological processes and functional responses to features in a stimulus. The ICA algorithm un-mixes this signal to recover the independent processes underlying BOLD activity.

How is ICA applied to work with the voxel timeseries?

In this thesis the voxels are driven by features in a movie clip presented to participants ("Skyfall" movie, 2012). Because visually driven voxels are responding to the same stimulus, they will share some underlying functional signal when responding to the same features of the movie. This means voxel timeseries are dependent rather than independent to each other, across visually responsive regions. ICA removes the dependence between voxel signals, by identifying the independent source signals underlying the activity. For example, if a neurons within a voxel are responding both to faces and to motion, the timecourse of activity relating to faces will be separated and identified as an independent signal to the activity that is driven by motion:

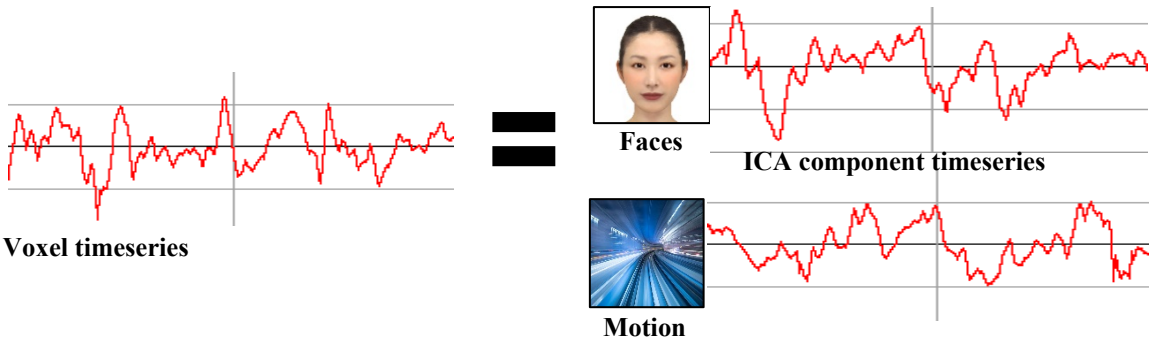

ICA reorganizes the BOLD data from inter-dependent voxel timeseries, to independent functional timeseries driven by specific features in the movie ("source signals"). The ICA algorithm optimizes the independence between these output components (Calhoun et.al., 2013). The number of source signals (N; represented as output components) can automatically be identified by adding components until the variance explained by the new component is not significantly different from zero. N can also be set at a chosen number; in this case the ICA algorithm finds the vectors that describe the data as fully as possible by maximizing the variance and optimizing independence, using the prescribed N dimensions. Following the reduction of dimensions, the variance in the data is normalised in all directions, so the different dimensions (components) are forced to be uncorrelated.

When using functional BOLD or oscillatory data to find functional neural networks across observers, there are two ICA techniques that can be used. The first finds correlations across voxels, but within the same subject. This is used when no temporal structure is assumed across different brains (concatenated ICA; CICA). During rest functional networks have exhibited a high level of coherence that is not stimulus or task driven. This spontaneous activity is used to identify networks using CICA. The second type of ICA correlates timeseries across voxels *and* between participants. This is used when a temporal structure has been applied to the voxel timeseries using a task (tensor ICA; TICA). Both identify functional networks in the brain, but by using the data in slightly different ways.

CICA takes each of the participants' BOLD timeseries at a voxel and concatenates them in time to create a new large "timeseries" (see Figure 1). This new timeseries contains each of the participants' BOLD signal, at that voxel. For example, for 6 participants each with 10 timepoints collected at a voxel, CICA would concatenate the signals so that each voxel was associated with a new timeseries with the first 10

timepoints from participant one, the second 10 timepoints from participant two, etc. Using these new concatenated timeseries, CICA finds voxels of the brain that show a correlation. This does not require any correlation of the BOLD signal between participants, which is why resting state data can be used. The results indicate where in the brain there are networks that show functional connectivity, that are common across subjects. The results do not tell us anything about the correlation of activity between subjects. Using this technique functional networks have been identified that are common across people (Beckmann, DeLuca, Devlin & Smith, 2005).

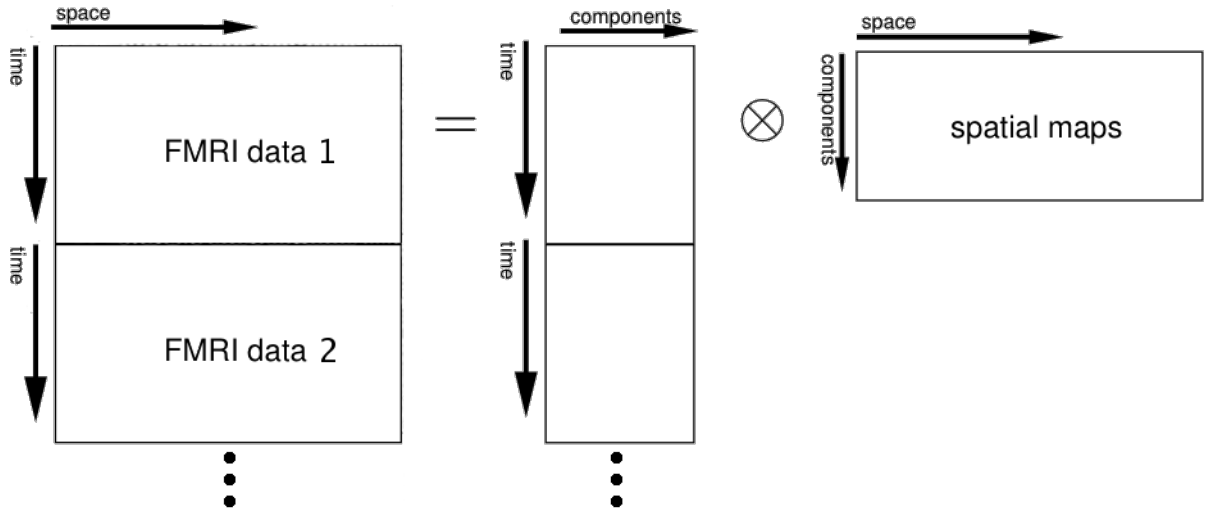

Figure 1. Visual schematic of the CICA process, taken from FSL's MELODIC guidance documents (fsl.fmrib.ox.ac.uk). Data are concatenated along the timeseries before analysis.

Alternatively, TICA does not concatenate subject data but compares the subject timeseries directly, to look for signals that are correlated between participants, and across voxels (see Figure 2). This technique can identify the functional units active across subjects and time-locked to a stimulus. In this thesis I will be applying a temporal structure using a broadband movie stimulus, therefore will be using a TICA analysis.

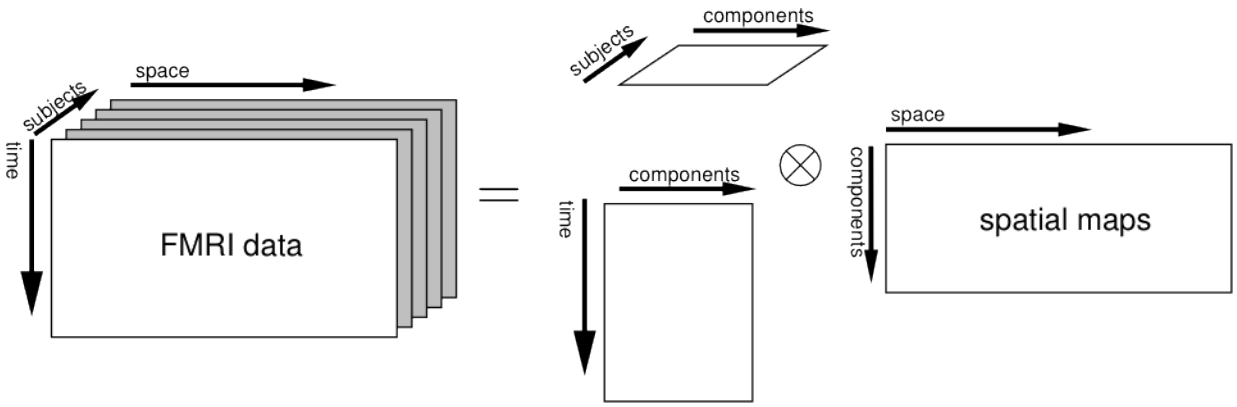

Figure 2. Visual schematic of the TICA process, taken from FSL's MELODIC guidance documents (fsl.fmrib.ox.ac.uk). Data are not concatenated before analysis.

Below, a flow-diagram presents the algorithmic stages of an ICA analysis. For a full technical report and the mathematics underlying these steps, see Beckmann and Smith (2004).

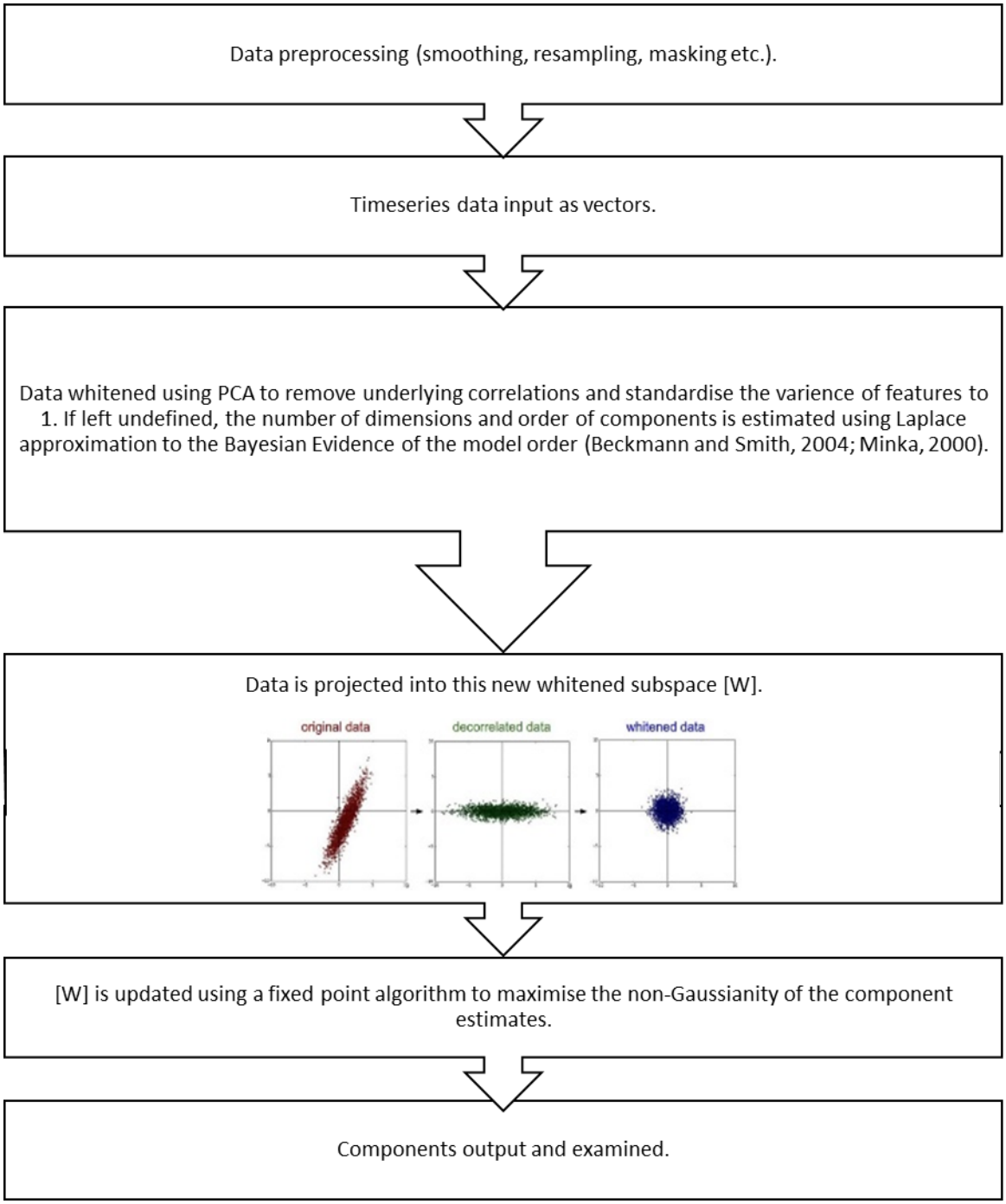

Figure 3. The algorithmic steps executed during an ICA analysis. See Beckmann and Smith (2004) for full technical report.

What is in a TICA output?

TICA organizes the data of all subjects into a 3D matrix (space x time x subject) and decomposes this into its three domains. This means for each component there is a timecourse, a spatial map and a subject/session aspect (amplitude value reflecting the subject contribution to the component). A subject

specific timeseries is estimated as well as the common (or 'average') time-course and the common spatial map for each component.

Four versions of the group level spatial map are output by FSL's MELODIC for each component. Unthresholded maps have a value at each voxel representing the amount that given voxel is modulated by the activation of the component. Another unthresholded map represents the same information but with the values converted into z-score statistics (mean zeroed; McKeown et.al., 1998). Thresholded z-score maps are also produced with any voxel value below a certain threshold zeroed (Beckmann & Smith, 2004; Poppe et.al., 2013). Finally, probabilistic maps are output with each voxel assigned a value between 1 and 0, reflecting the probability of being 'activated' by the component timeseries, rather than background noise.

TICA assumes that the temporal response pattern is the same across the participants and provides a single decomposition for all the original data sets. Components can describe effects common to all or most subjects, or represent effects only demonstrated by a sub-set of subjects. For each component, an estimated effect-size (or 'response amplitude') is reported for each participant describing this representation. Components common across all participants will have a non-zero estimated effect size. Other components will have an effect size around 0 for some subjects and only few high non-zero values. When using TICA the components are output according to the median effect size value, across subjects. The component with the largest median response amplitude across subjects is at the front on the output and these values decrease with each subsequent component. In our dataset components that are visually driven show the largest response amplitudes and therefore tend to be close to the front of the ICA output.

1.1.2 Background: The BOLD signal

Functional magnetic resonance imaging (fMRI) is a dominant means of (indirectly) measuring neural activity in the human brain. Although relatively expensive, it is noninvasive can localize activity to a few millimeters. Increased neuronal firing requires an increased need for energy and oxygen at the cellular level, causing the levels of oxygenated and deoxygenated blood to modulate. fMRI exploits the differential magnetic susceptibility of blood oxygenation levels to identify regions that increase or decrease in activation over time. This is called the blood oxygen-level dependent (BOLD) signal. BOLD signal is understood to reflect local

field potential and neuronal spiking, though this relationship is more complex than a direct correspondence (Ekstrom, 2010) and remains an open and actively researched question.

Usually (and in the case of this thesis), neuronal activity in response to a stimulus or behavior is of interest. However, as well as neuronal activity, the BOLD signal is confounded by other sources of noise such as head movement, respiratory activity, heartbeat and underlying noise generated by the scanner itself. The magnitude of this contributing signals is often comparable or even greater than the signal of interest. It is impossible to eradicate all noise however efforts are made to reduce their influence on the BOLD signal.

1.1.3 Background: Roles of MEG frequency bands in the brain

Using MEG, the activity of populations of neurons in the brain can be measured. Neurons communicate with the use of neurotransmitters, the release of which are modulated by electrical impulses in the neuron. With each electrical impulse there is an associated magnetic field, orthogonal to the direction of the signal. MEG scanners can record the magnetic fields arising from bulk synchronous activity in the aligned dendrites of neurons (called pyramidal cells). When this activity exhibits rhythmic or repetitive patterns, it is categorized within a band of oscillatory frequencies. For example, if activity modulates every 0.1 seconds it would be in the alpha frequency range (8-12Hz), firing at 10Hz.

Neuronal oscillations range from between 1Hz and up to ~250Hz (Wang, 2010) and have been increasingly recognized as playing important and distinct roles in the mechanisms underlying neural processing. Functional networks in the brain are often modulated across several frequency bands, with frequency depending on the brain region and cognitive demands applied by the environment (e.g. see Muller, Chavane, Reynolds & Sejnowski, 2018). For example, theta activity recorded in fronto-medial regions is thought to play an important part in attentional control and working memory (Clayton, Yeung & Kadosh, 2015), while gamma-band oscillations in the frontal cortex are understood to be involved in maintaining items in working memory (Roux & Uhlhaas, 2014).

Using a movie stimulus provides the opportunity to investigate different neural oscillations during natural viewing. Recent work has suggested an important role for lower frequency bands in top-down feedback in the visual pathways (delta, theta, alpha and beta), and associates higher gamma oscillations with

bottom up processing (30-120Hz; Palva & Palva, 2017). This has been demonstrated in the visual cortex of monkeys (Jensen et.al., 2017) and in humans between V1 and V4 (Michalareas et.al., 2016). Certain frequencies have also been reported to be modulated in response to visual stimulus (or lack of). Alpha band activity in sensory cortices has been identified as important in the facilitation of sensory processing by inhibiting irrelevant stimuli (e.g. Mazaheri et.al., 2014). Gamma oscillations have been associated with multiple perceptual and cognitive processes including sensory representation (Ribary 2005), visual spatial attention (Magazzini & Singh, 2018), sensorimotor integration (Sanes and Donoghue 1993) and memory (Herrmann, Munk & Engel, 2004).

1.1.4 Cross frequency coupling

Synchronous oscillatory rhythms across different frequency bands are understood to coordinate neural activity and integrate functionality across the brain (e.g. Wang, 2010). However, the complexities of these interactions are not fully understood, and continued investigation is needed into cross-frequency coupling (CFC; Jensen & Colgin, 2007). Coupling between frequency bands means that the power, frequency or phase in one frequency band is modulated with respect to the power or phase of another frequency band (see Figure 4). CFC is documented across the sensory regions and networks (e.g. Riecke, Sack & Schroeder, 2015). Tasks have been shown to modulate the coupling pattern between frequency bands, for example sensorimotor working memory tasks alter the integration between theta and high-gamma oscillations (Canolty et.al., 2006).

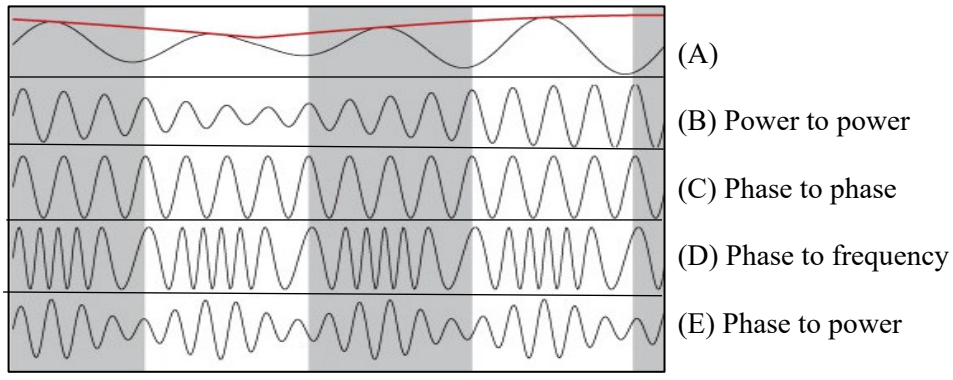

Figure 4. Adapted from Jensen & Colgin (2007). The four types of cross-frequency coupling. (A) A low frequency wavelength (LFW) showing power (amplitude) changes over time (B) A higher frequency wavelength (HFW) with amplitude modulated in coherence with the LFW amplitude. (C) Phase of the HFW is 'locked' to the LFW, at a ratio of four to one. (D) The frequency of the HFW changes in sync with the phase of the LFW. (E) The power of the HFW changes in sync with the phase of the LFW.

CFC is reported to be involved in the transfer of information across the brain. It is accepted that neurons exploit the different frequency channels to communicate both locally and distally (e.g. Bonnefond, Kastner & Jensen, 2017). A recent review proposes that CFC connects fast and slow oscillatory networks to integrate distributed cognitive functions, such as representation of low-level sensory information with high-level attentional and executive functions (Palva & Palva, 2017).

In visual processing, CFC has been suggested as being an important mechanism for integrating information across different neural regions. The research suggests that integration of information across the brain involves multiple frequency bands. During visual processing gamma frequencies are thought modulate activity over smaller spatial regions in the occipital lobe, while lower frequency bands synchronize processing over larger ranges, across occipital, temporal, parietal and frontal regions (e.g. Von Stein & Sarnthein, 2000).

1.1.5 Background: MEG – MRI coupling

Most ICA studies have used BOLD fMRI data, which measures the oxygenation level of blood across the brain. This is an indirect measure of neuronal function, with the increase in the volume oxygenated blood used to infer increased metabolism and activity in neurons. However, it is oversimplified to say that local blood flow is controlled directly by metabolic activity due to neuronal firing (e.g. Raichle & Mintun, 2006; Girouard & Iadecola, 2006), and studies have shown a non-linearity between oscillatory activity and blood flow (e.g. Devonshire et al., 2012; Hewson-Stoate, Jones, Martindale, Berwick, & Mayhew, 2005; Sheth et al., 2004). There is also evidence of individual differences in neurovascular coupling across people due (e.g. Fabiani et.al., 2014) . The better we can understand the relationship between BOLD and neuronal activity the better placed we are to interpret BOLD data. The comparison of MEG and fMRI activity is one method of examining the relationship between oxygenated blood flow and the activity of neurons.

The BOLD signal has been shown to have a complicated relationship with oscillatory activity recorded using local field potentials (LFPs; e.g. Logothetis et.al., 2001). LFPs are recorded using an electrode inserted into the neural tissue, electrical potentials are recorded from surrounding neurons. Using LFP recordings in sensory regions during sensory input, a negative correlation between the BOLD response and

low-frequency oscillations and a positive relationship at high-frequency oscillations has been reported (Yuan, Perdoni, Yang, & He, 2011; Mukamel et.al., 2005; see Figure 5). Dependent on task and brain region this relationship is altered, for example positive correlations have been reported across the brain between the BOLD signal and both low and high frequencies during rest, in the macaque brain (Schölvinck et.al., 2010).

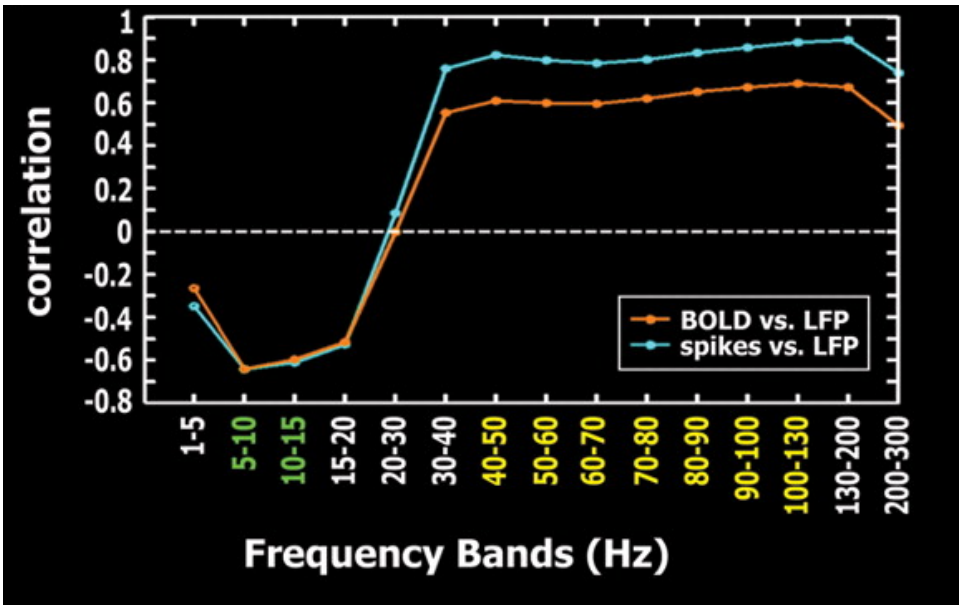

Figure 5. Adapted from Mukamel et.al., 2005. Correlation between the BOLD timeseries and local field-potential (LFP) recordings at Heschl's gyrus in the auditory cortex. Strong negative correlations are seen between the BOLD activation and the low-frequency LFPs (5 to 15 Hz) and the strong positive correlation with the high-frequency LFPs (40 to 130 Hz)

1.2 Overview of Thesis

Section 1 – ICA and movies with fMRI BOLD data

Before movies and ICA can be used as a tool to identify multiple visual regions, it is first necessary to assess and optimize the reliability of the technique. This has not been done systematically before, therefore in Chapter 2 I thoroughly investigate the sensitivity of TICA to pre-processing options to (i) establish how robust the results will be that that I will be working with in following chapters, and (ii) optimize the analysis pipeline to obtain the most robust results. Findings show that TICA is sensitive to various common pre-processing parameters however, components in visually driven regions are relatively robust. Based on the findings of this chapter a pipeline is identified to provide more robust components for further analysis across the following chapters.

In Chapter 3, I check the reliability of the TICA output across different groups and movie clips. Results show that components in visual regions are stable across samples. The peak voxels of these components are robust across different groups and movie clips, supporting the use of this technique. Components representing functional networks are also robust across different movie clips and samples, and in Chapter 4, I compare these network components to established resting state networks. The effect of changing dimensionality also begins to be explored. Results show that using movies and TICA allows for established resting state networks to be identified and show splitting of components as dimensionality is increased.

In Chapter 5, the reliable components generated using the movie data and group TICA at a high dimensionality are compared to regions of interest in the motion pathway; a network expected to be active during movie watching. Reliable components are found to represent multiple visual regions across this network in the occipital and parietal lobe. Based on these findings it is concluded that using movie watching and TICA could be a valid way to identify multiple regions of interest in the visual processing pathways of the brain.

Being able to reliably identify visual regions at the group level is very useful, but it would be ideal to be able to identify these regions and networks reliably in the individual brain. In Chapter 6 I introduce single subject ICA and investigate the reliability of visually driven components across subjects. Components show reliability across subjects for identification of resting state networks and visual regions.

Section 2 – Exploring oscillatory activity during natural viewing and cross modality coupling

In the first section I thoroughly and systematically investigated the components identified using TICA with BOLD data, based on work by Bartels and Zeki (2004). In this second section I introduce a novel technique using spatially concatenated MEG data in a TICA that should allow investigation of correlated activity across oscillatory frequencies, during natural viewing. In Chapter 7, I address some prerequisites to using this technique. I find that reliable visually driven components can be identified in the MEG frequency bands, and that the frequencies show different cross-band relationships in different visual regions. These findings encourage the application of this novel technique and the reliable components identified in a combined-frequency analysis are presented in Chapter 8. Based on the success of identifying cross-frequency components, Chapter 9 uses the same technique as a novel way to investigate coupling across the BOLD timeseries and oscillatory activity. Results show correlation between theta and gamma frequencies with BOLD in primary visual regions and between gamma and BOLD in extrastriate regions, supporting previous research (e.g. Engel, Kreiter, König & Singer, 1991; Kayser, Kim, Ugurbil, Kim & König, 2004). This technique is offered as a promising new way to combine MEG and fMRI data in neuroscientific work.

Section 3 – Exploring the functional hierarchies of natural viewing using ICA and movies

In Chapter 10 a novel technique for mapping the functional hierarchy of visual regions is explored, which exploits the generation of components in ICA across different dimensionalities. Based on initial analyses, this offers a potentially interesting way to map the functional hierarchy of the visual system.

1.3 Methods report

Throughout this thesis the data explored was collected during movie watching. This section will describe the methods used, and unless stated otherwise these are relevant to the data discussed in the rest of the thesis. Data were collected both in the MEG and the MRI scanner, therefore this methods report describes both. Participants watched the same movie clip in both scanners, described below.

MRI data were used in Sections 1, 2 and 3 of this thesis (Chapters 2-6; Chapter 9 and Chapter 10).

MEG data were used in Section 3 of this thesis (Chapters 7-9).

Both MEG and MRI data were used in Chapter 9.

1.2.1 Movie stimuli

In both scanners, all participants watched the same 19 minutes and 40 seconds movie clip, taken from the opening sequence of the James Bond film Skyfall (not including soundtrack; MGM & Columbia Pictures). The choice of film followed Bartels and Zeki (2004); it included a range of social interactions, scenes and actions including close-ups on faces and of hands while manipulating objects, biological motion, outdoor and indoor scenes containing objects and text (from credits). The clip also contained prolonged periods of global image motion (optic flow) caused by panning or zooming of the camera. The movie clip was also selected due to its high action, character driven content and high-resolution image, making it as engaging as possible for the participants to maximise the neural synchronicity between observers (Dmochowski et.al., 2014). Subjects were told to watch the movie ‘naturally, as they would when sat at home watching TV, therefore there were no restrictions on fixation.

1.2.1 MRI data collection

1.2.1.1 Participants

22 participants with normal or corrected vision were recruited as a volunteer sample from Cardiff University, for money or course credits (7 female/9 male). None of the subjects were under the age of restriction for the movie clip (12A), the mean age was 27 years, range: 21-40. All subjects gave informed consent to take part in the study and ethical approval was granted by Cardiff University School of Psychology Ethics Committee.

Each participant took part in one or more scanning sessions, which included obtaining a high-resolution anatomical image of the brain. Functional localisers and retinotopic stimuli were also shown to a sub-set of the participants. Half of the subjects had watched the same movie clip within the MEG scanner, before watching it within the MR scanner in the past 5 months.

1.2.1.2 Equipment

Images were generated by an LCD Canon XEED SX60 Projector at a resolution of 1400 x 1050 pixels, at 60Hz. The images were viewed while the subjects lay on their back in the scanner. Visual stimuli were rear projected onto a screen located within the bore of the scanner. The screen was placed behind the head of the subject and viewed through a mirror located above the head coil. The screen viewing distance was approximately 57 cm. The viewable image was 35cm in width (~35degrees).

At the edges of the screen (+/- 17.5 degrees laterally) the corners of the image were slightly clipped, due to the MR bore obstructing the view. Therefore, the maximum height at the centre of the stimulus was 30 degrees and at the edge was 23 degrees. The occlusions at the corners of the screen were did not affect the movie viewing.

1.2.1.3 Data acquisition

While the participants watched the movie clip their BOLD signal was acquired using fMRI. BOLD responses were acquired using a 3T General Electric (GE) Signa 3T HDxt Scanner (General Electric,

Milwaukee, Wisconsin), equipped with echo-speed gradient coil and amplifier hardware using a GE 8 channel receiver RF coil. Activation images were acquired using echo-planar imaging (EPI) with a TR of 2 seconds, TE of 30ms and flip angle of 76 degrees (Ernst angle calculated).

At every TR a volume of 37 contiguous slices was acquired to cover the whole brain. Slices were aligned to the anterior-posterior line of the participants' corpus-callosum. Four dummy volumes were taken at the beginning of each run to allow the signal to stabilise, which were removed before analysis. Voxels were 3mm x 3mm x 3mm in size.

1.2.1.3 FSPGR

High-resolution anatomical scans were collected for each participant (resolution $1mm^3$), using a fast-spoiled gradient echo scan sequence (FSPGR).

1.2.1.4 Data processing

Unless otherwise indicated, pre-processing of the fMRI data for input into MELODIC was performed in FSL FEAT using default settings: data were smoothed at 5mm and resampled to 4mm3; data were motion corrected using FSL's McFlirt motion correction software; highpass temporal filtering at 100Hz was also used to remove low frequency temporal drifts.

As part of the group ICA each subject's EPI data were registered to their own FSPGR using FMRIB's Linear Image Registration Tool (FLIRT). Each participant's registration was checked manually to make sure the most accurate registration possible was used. For 19 of the participants the best registration was acquired using boundary-based registration (BBR), for the other 5 participants using 6 degrees of freedom provided a more accurate registration of the EPI and FSPGR images. After the functional data were registered to their own structural image, the FSPGR was registered to standard space (MNI152) using FNIRT, FMRIB's Non-linear Image Registration Tool (something about the parameters). Functional data could then be registered into standard space. Registration to the 2mm MNI standard brain was performed using the FSL '*applywarp*' command.

Pre-processed data were then analysed using the command line version of FSL's MELODIC tool (http://www.fmrib.ox.ac.uk/fsl/). Probabilistic group tensor ICA (TICA; Beckmann & Smith, 2004; 2005) was performed on the fMRI data, using FSL's MELODIC (Jenkinson et.al., 2012), version 3.0.

1.2.2 MEG data collection

1.2.2.1 Participants

16 participants (female=7, average age = 27) who had taken part in the MRI move scan were also scanned in the MEG scanner, while watching the movie clip. Half of the subjects had watched the movie clip in the MEG scanner before the MRI scan. All had normal or corrected vision were recruited as a volunteer sample from Cardiff University, for money or course credits. No subjects had any history of neurological or psychiatric illness.

1.2.2.2 Equipment

Visual stimuli were front projected onto a screen located in front of the participant when sat in the MEG scanner. Using a CTF Omega 275-channel MEG system whole head recordings were taken as part of a continuous 20-minute dataset, with the start synchronized to the beginning of the movie clip. Recordings were sampled at 1200Hz and analysed as synthetic third-order gradiometers.

1.2.2.3 Data acquisition

Whole head MR structural scans were co-registered to the head continuously during MEG recording using the localization of electromagnetic coils placed at fixed positions relative to anatomical landmarks (10mm anterior to left and right tragus, 10mm superior to nasion). Fiduciary locations were manually marked onto the anatomical MRI after the scanning session.

1.2.2.4 Data processing

Offline, data were down-sampled to 600Hz. To ensure quality of data recordings were manually inspected. Predefined frequency bands were used to filter the raw data: delta (1-4Hz), theta (4-8Hz), alpha (8-13Hz), beta (13-30Hz), low-gamma (40-60Hz), high-gamma (60-140Hz) and very-high-gamma (140-200Hz). Data at each frequency band were source localized using an LCMV beamformer (SAM). This provided us with virtual timeseries at each voxel in the brain, for the whole of the 20-minute recording. These timeseries were then reconstructed to the MNI-template space at a resolution of 6mm. Using the Hilbert Transform and analytic function, timeseries were converted to an amplitude envelope which was despiked and high-pass filtered at >0.01Hz, removing drift.

The processed MEG data were down-sampled to 0.5 seconds and convolved with the canonical HRF from SPM to match the expected BOLD response. This was performed to allow a direct comparison between the MEG and MR data collected during the movie watching.

Chapter 2: A sensitivity analysis of independent component analysis (ICA)

2.1 Introduction

ICA is a statistical technique widely used in neuroscience for the analysis and segmentation of brain activity into its functional parts. Using fMRI and MEG/EEG data, ICA provides a potentially powerful data-driven method for further understanding the mechanisms underlying neural networks (e.g. Beckmann, Mackay, Filippini & Smith, 2009; Brookes et.al., 2011). Break-through work using ICA first identified functional networks in the brain, based on spontaneous signals recorded during rest (Biswal, Kylen & Hyde, 1997). Since then, ICA has been used to understand changes in functional networks across different clinical and non-clinical groups (e.g. Wang et.al., 2007; Gu et.al., 2010; Rilling et.al., 2007), and across different tasks (e.g. Calhoun, Adali, Hansen, Larsen & Pekar, 2003).

When applying ICA to neurological data there are many pre-processing options, for example the level of smoothing and resampling applied to the data. A pipeline for the analysis must also be selected, with options such whether to remove non-grey matter voxels or how to account for participant motion. Despite the exciting potential and broad usage of ICA, its sensitivity to these common analysis parameters is poorly understood. Differences in the pre-processing and pipeline used could reduce, or indeed improve, the robustness of ICA results. If these analysis choices have an impact on the reliability and validity of the ICA results, then this needs to be understood and considered when using ICA in neuroscientific research.

One previously reported (but little appreciated) sensitivity of ICA using resting state data is the order of brains input into a group analysis, which causes variability in the outputs (e.g. Poppe, 2013; Zhang et.al., 2010). Valuable work in the field using fMRI and MEG/EEG has shown that reliable ICA components can be identified using meta-analyses, resampling and multiple ICA testing (e.g. Zhang et.al., 2010; Meinecke, Ziehe, Kawanabe & Müller, 2002; Ylipaavalniemi and Vigario, 2007; Artoni, Menicucci, Delorme, Makeig & Micera, 2014). However, neuroimaging research using ICA typically only uses a single analysis, and based on previous research (e.g. Poppe, 2013), the results may not be as reliable as they could be, depending on the order of the input data. The scale of the impact of brain order is unknown and it is

not understood whether particular "spots" in the input order are more important than others, e.g. first brain, last brain etc. This is concerning as it means that the robustness of any singular ICA results drawn from these data is unclear.

As well as brain order, the sensitivity of ICA to other analysis parameters is also of high importance as sensitivities may mean results vary depending on the pipeline used. It may also be the case that components in different brain regions show varying robustness across different parameters and during different tasks. To address these concerns, in this chapter I will systematically examine and document the reliability of the tensor ICA (TICA) output as a function of the processing and input parameters available, using data collected during natural vision. First, the effect of the order of brains in the group TICA input will be investigated. Based on previous research it is expected that changing the input order will cause variation in the TICA output (e.g. Poppe, 2013). Next, I will investigate the sensitivity of TICA to motion correction and grey matter masking and then to the resampling and smoothing of data. This will inform my work during this thesis to ensure that I am using the most robust group components possible. Results will also have implication for future research in the broader neuroscientific community, to understand any potential effects of these data pre-processing stages and highlight which appear to be consequential in the TICA pipeline.

The aims of this chapter are to:

a) systematically investigate the sensitivity of ICA to pre-processing options;
b) establish how robust the ICA results are that I will be working with in this thesis
c) optimise the analysis pipeline to obtain the most robust results using our dataset.

22 participants watched the same movie clip in an fMRI scanner, providing a temporal structure which can be exploited for identification of visually responsive regions at the group level, using TICA. Results of thorough analysis showed sensitivity of TICA to brain input order, the smoothing and resampling of data, motion correction (using ICA's AROMA) and grey matter masking. The sensitivity to these pre-processing parameters should be carefully considered when using BOLD data and TICA. Based on our results AROMA has the largest impact on the components generated by TICA and brain order has the smallest effect. Grey-

matter masking is advised and when used with FSL MELODIC's default parameter settings, robust components can be identified.

2.1 Cross subject correlation

Previous work has demonstrated that the BOLD timeseries is correlated across subjects while watching the same movie, suggesting that activity is timelocked to the stimulus (Hasson, Malach & Heeger, 2010). As TICA assumes a temporal structure has been applied across participants, the first step was to try to replicate these findings using our movie clip.

2.1.1 Methods

fMRI BOLD data were collected during movie watching, as described in the methods section of Chapter 1 (section 1.3). The BOLD data collected for each subject during movie watching was correlated in a pairwise voxel-by-voxel analysis. At each voxel the timeseries for all subjects were cross-correlated in a pairwise linear analysis using MATLAB's '*corr*' function. The average correlation coefficient across the pairwise comparisons was calculated at each voxel. The results of this analysis will tell us where voxel activity was driven the movie stimulus, across subjects. It was expected that correlations would be seen across subjects in visually responsive and attentional regions (Hasson et.al., 2010). Significance of correlations ($p<0.05$) was calculated using randomization testing across participants to build a null distribution (omnibus corrected).

2.1.2 Results

A pairwise correlation analysis using BOLD data collected during movie shows high and significant cross-subject correlation in occipital and parietal regions ($p<0.05$, corrected for multiple comparisons), while frontal regions show non-significant low correlation (see Figure 6). This supports previous work that shows correlated activity across subjects during naturalistic viewing (Hasson et.al., 2010). This correlation means cross-subject components in visually responsive regions should be identifiable using TICA.

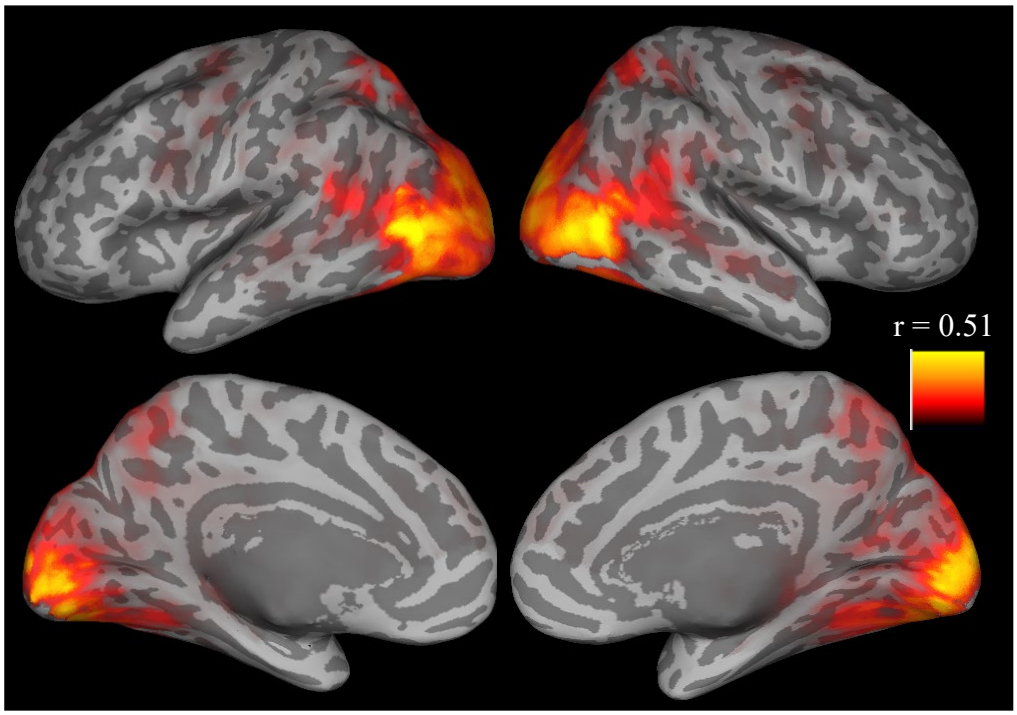

Figure 6. Significant correlation across subjects when watching the movie clip was measured in occipital, temporal and parietal regions (significance threshold r=0.12, p<0.0.5). Linear correlations were performed in matlab using the 'corr' function and r-values are displayed on the surface of the brain. This supports similar findings in previous research using movie watching (e.g. Hasson et.al., 2010)

2.2 ICA: the brain order effect

Previous work investigating the effect of brain order on the ICA output has focused on temporally concatenated ICA (CICA), using resting state data (e.g. Poppe, 2013). In this thesis I am interested in the benefits of using a movie stimulus for the identification of functional, visually responsive regions in the brain. A benefit of using a movie clip is the increase of signal to noise in regions processing the stimulus, as signals are no longer spontaneous, but are responding to features in the movie. This means components should be identified in these visually responsive regions, across subjects (Bartels & Zeki, 2004). Therefore, this thesis will concentrate on the TICA technique, using a movie stimulus to apply temporal structure to the brain (Hasson et.al., 2010).

2.2.1 Methods

2.2.1.1 Data input

Changing the order of the ICA input lists has been demonstrated in previous research to affect the ICA output, when using CICA and resting state data (Zhang et.al., 2010). Pilot analysis using my movie datasets suggested that the same occurs in my data, using TICA. Therefore, I systematically changed the input order of my data to generate and quantify this variability.

The BOLD data collected during movie watching was entered into multiple runs of TICA. As a first step the 22 subject datasets were permuted to give twenty random subject orders to be put into separate TICA analyses. An indication of component validity is to examine the reliability of the components by running multiple ICAs using the same data: if a component is real, then it is likely to appear in different ICAs.

2.2.1.2 Assessing the ICA outputs

When the dimensionality of ICA outputs is identified by MELODIC (see Chapter 1, section 1.1.1 for background of this process) rather than restricted by the researcher, a simple measurement of output consistency is the variability in the number of components generated. If this is not stable across outputs, then it logically follows that different components are being generated by different permutations.

The similarity between outputs can also be assessed by comparing the components directly, rather than just the dimensionality (e.g. Du, Ma, Fu, Calhoun & Adali, 2014). If an ICA output is 'representative', then it contains components that are like those produced by other ICA outputs that use the same input data. To calculate a measure of 'representativeness' for each ICA outputs we can look at the similarity of spatial and temporal features of the components across the different permutations. By generating a measure of representativeness, it is possible to quantify the sensitivity of TICA to the parameters tested in this chapter. If outputs show a change in representativeness when using certain pre-processing parameters, then TICA is sensitive to this parameter. The reliability of the MELODIC ICA when the same data is input can also be quantified (with respect to this dataset).

A pipeline was developed for assessing the similarity of the components across different permutation outputs. Each component has an associated timeseries and spatial map. First, all component timeseries and

maps were cross-correlated across all other ICA outputs. The Pearson's linear correlation coefficient ('Tcorr') between the components' timeseries was calculated using MATLAB's 'corr' function. The Pearson's cross-correlation coefficient was calculated between component spatial maps ('Scorr'), using the '*fslcc'* command, developed by FSL.

The spatial and the temporal correlations were then multiplied to create a similarity metric (overall correlation, 'Ocorr'). Ocorr assigns a value to the spatio-temporal similarity of all pairs of components:

$$Ocorr = Tcorr \times Scorr$$

For example, when comparing two ICA outputs with 20 components in each, there would be 400 (20 x 20) Ocorrs calculated. When running 20 permutations there are 190 pairwise comparisons with 20x20 components compared in each one (190 x 400 Ocorr values are calculated). These Ocorr values quantify how similar components are across space and time.

As described in Chapter 1 (section 1.1.1), the ICA outputs contained four different spatial representations of each component; the unthresholded independent component maps (IC maps), unthresholded z-statistic maps, thresholded z-statistic maps and probabilistic maps. Each of the maps was compared to assess whether the choice affected the representativeness analysis and output. The choice of the map had no discernible effect on the output values, therefore the unthresholded IC maps were used for the rest of the analyses.

Ocorr values can be used to quantify how similar the ICA outputs are to each other, overall. By scanning the Ocorrs the best matched components can be identified across the TICA outputs. How good these matches are across all outputs gives an indication of how well components are represented across input permutations. The pipeline for calculating this measure of representativeness is detailed in Figure 7.

1	2	3	4	5
Two ICA outputs are cross correlated: all components are compared (Ocorrs).	Scan all Ocorrs to find the maximum i.e. the "best matched" across the outputs.	Remove these matched components and search again for the maximum Ocorr.	Repeat until all components from one output have been matched.	Average the Ocorr values in 'groups'. e.g. the top 1-5 Ocorr, top 6-10 Ocorr etc.

Figure 7. Ocorr values (component spatio-temporal cross correlations) were used to calculate how well each of the ICA outputs represented the others.

To provide a full picture of the similarity of the matched pairs of components between each of the outputs, the highest five Ocorr were averaged, followed by consecutive groups of metrics in order: 1-5; 6-10; 11–15; 16-20; 21-30; 31-40; 41-50; 51-75; 76-100; 101-150; 151-200. The number of matches was constrained to the number of components in the output with lowest dimensionality.

2.2.2 Effect of brain order: Random permutations

The number of components was not stable across the twenty TICA outputs generated using the same dataset but randomly ordered subject inputs (mean = 268, range = 154). This indicates that TICA shows sensitivity to brain order. When components were compared directly across outputs, they showed spatio-temporal variation across the twenty permutations (see Figure 8 for Ocorr values averaged across matched components). The top 5 best matched components across outputs show similarity scores around 0.85. This demonstrates some consistency across the outputs, as should be expected. However, when matching across all components, the similarity reduces; components ranked 101-150 in similarity across permutations have an average representativeness value of less than 0.4.

The most representative permutation is identified as the output that has the highest mean Ocorr values across the grouped component matches. In these twenty random permutations, output three was the most representative output and permutation fifteen is the least representative output (see Figure 8). If permutation fifteen had been run on its own by chance as part of an experiment, the results would not have been as representative or generalizable as they could be using a different order of input.

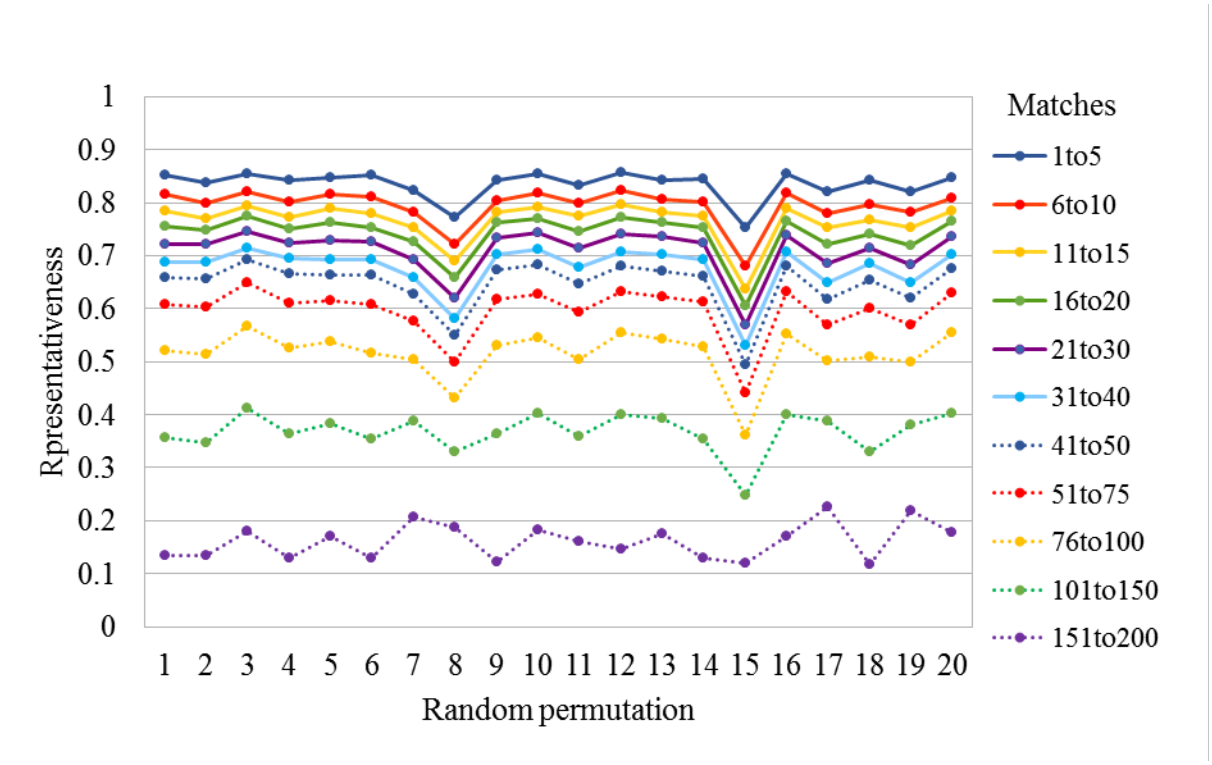

Figure 8. The representativeness of twenty ICA outputs using random permutations of 22 subject fMRI data sets. Results demonstrate the reliability changing based on subject order, even though the same dataset was used in all analyses.

To investigate whether the component timeseries or spatial maps were driving the differences between outputs, I examined the spatial and temporal correspondence between components separately. The matched components show a high correspondence between the timeseries and show less spatial correspondence (see Figure 9 for averages across permutations. Spatial and temporal representativeness values for each permutation can be found in Appendix 2.1a and b). Permutations 8 and 15 show lowered spatial representativeness for up to 150 components, as was seen in the Ocorr analysis (Figure 8). This demonstrates that variability in spatial maps drives representativeness patterns across permutations, rather than differences in component timeseries. The temporal correlations also showed less variability around the mean across permutations (standard deviations shown in Figure 9). These findings indicate that the ICA is picking up the same functional components at the group level, but that these components show some differences in the spatial maps depending on the order of brains.

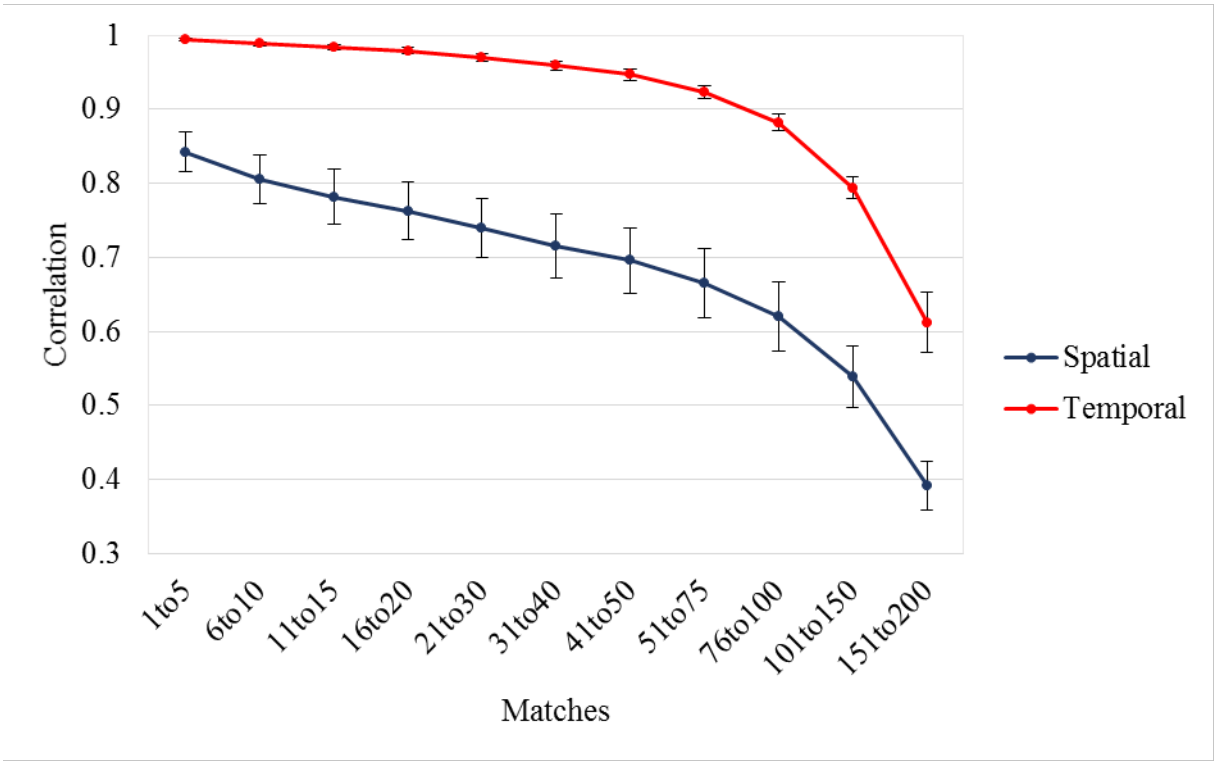

Figure 9. On average, temporal correlations between the best matched components are higher than the spatial correlation values. This may reflect the temporal binding of the neural function to the movie, across subjects.

2.2.3 What is driving the brain order effect?

To investigate what is driving the effect of brain order on the TICA output, systematic changes were made to the order the data were input into MELODIC. This examined whether specific brains, such as the initial brain in the input list, drive these changes in the TICA output, or whether all brain positions contribute equally.

2.2.3.1 First brain swapped

The most representative permutation from the randomized analysis was chosen to investigate the significance of the first brain. To start, the first brain in the input list was swapped with each of the other brains in the list in turn (see Figure 10). This created 22 new permutations, due to there being 22 participants. Excluding the one brain swapped into first position, all other brains remained in the same order. This investigates the effect of the first brain on the output generated by MELODIC.

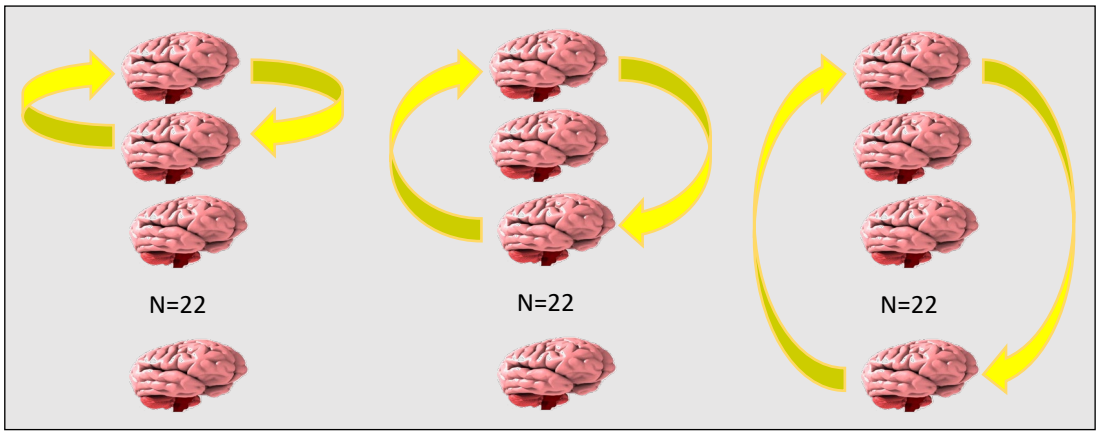

Figure 10. Each brain in the input list was swapped into the 'first' position. 22 input lists were generated for comparison.

2.2.3.2 Results: first brain swapped (unrestricted components)

When the first brain was swapped, the dimensionality was not consistent across the outputs (mean = 262, range = 379-222). It follows that different components are being generated by swapping the first brain. The range of dimensionality was similar to when random permutations were used (range =157 versus 154) suggesting that the changing the first brain may be the primary driver of differences across input permutations. By eye the representativeness levels across permutations look very similar to when random permutations are used (Figure 11). Indeed, if the representativeness values are collapsed across all the matched components, the difference in mean representativeness between the random and the first brain swapped permutations is marginal (difference does not rise above 0.02). These findings suggest that:

a) Swapping the 1st brain only results in significant changes to the ICA output.
b) The differences are almost as big as those you get from randomly swapping all the brains between permutations.
c) The 1st brain is a, or potentially the, major contributor to the brain order effect.

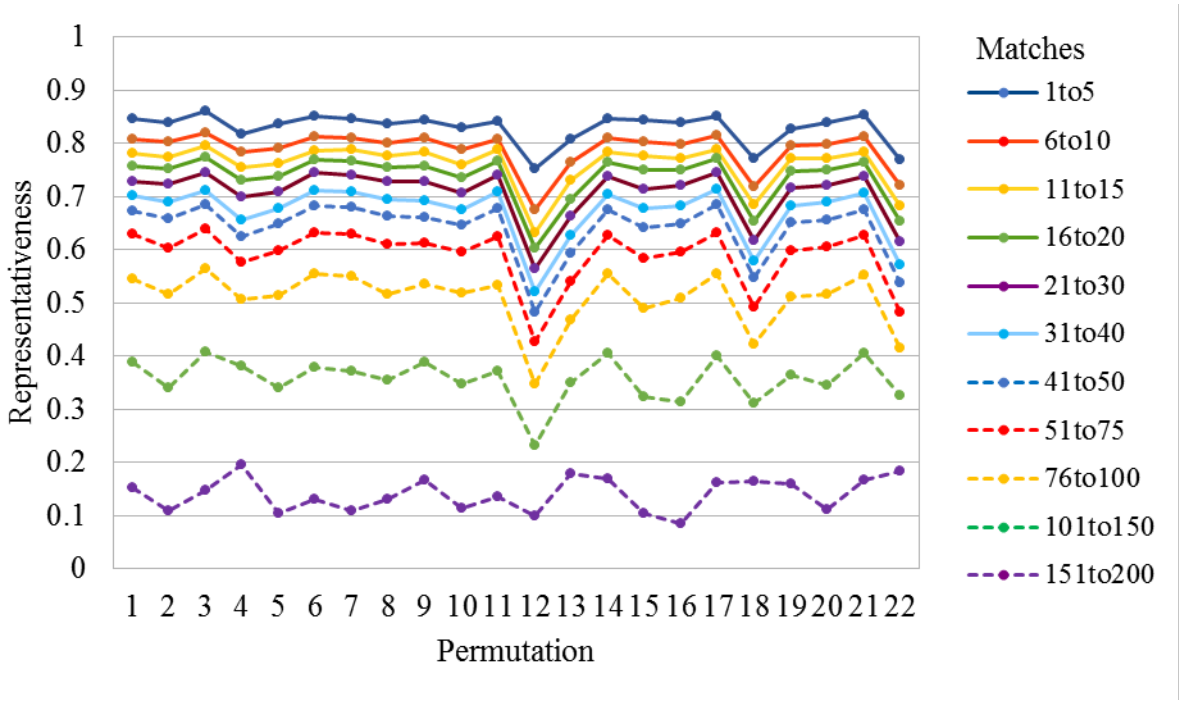

Figure 11. The representativeness of 22 ICA outputs each with a different first brain show variability in the spatial-temporal features of the components. Spatio-temporal correlations >0.17 were in the 99th percentile across all component comparisons.

2.2.3.3 Fifth or second brain swapped

With the representativeness of these outputs looking so similar in value to the fully permuted TICAs, it was then asked what the effect of swapping brains further down the input list would be. It could be the case that changing the position of any two brains generates the same amount of variability as random permutations. This would mean there is no cumulative effect of increasing the number of brains that are swapped across positions, but that any change in the order has the same effect on output variability. Another possibility is that changing the first brain accounts for most of the variability of the random permutations and changing positions of other brains has negligible effect on the ICA output. To check this, the same swapping principle applied with the fifth and second brains in the input list. Each brain was swapped with the fifth brain in the list, so the fifth brain was different on each permutation and all others remained the same. The same was conducted with the second brain, in a separate analysis.

When the fifth or second brain was swapped the number of components was stable (mean = 252, range =0). The representativeness values of the outputs were also stable at 1. This suggests that differences at

the second or fifth brain does not contribute to differences in ICA outputs. These findings support the assertion that only the first brain influences the number of components generated by the ICA[1].

2.2.4 Representativeness and the number of components

One feature of the TICA outputs was that the number of components differed when the first brain was swapped. By eye it looked as though permutations with relatively high or low dimensionalities, compared to the other outputs, showed lowered representativeness. To investigate this, the unsigned difference in dimensionality from the mean number of components was calculated for each output. These values were then correlated with the representativeness of that output, across the top 100 component matches. There was a strong negative correlation between these factors. -0.8143 (see Figure 12).

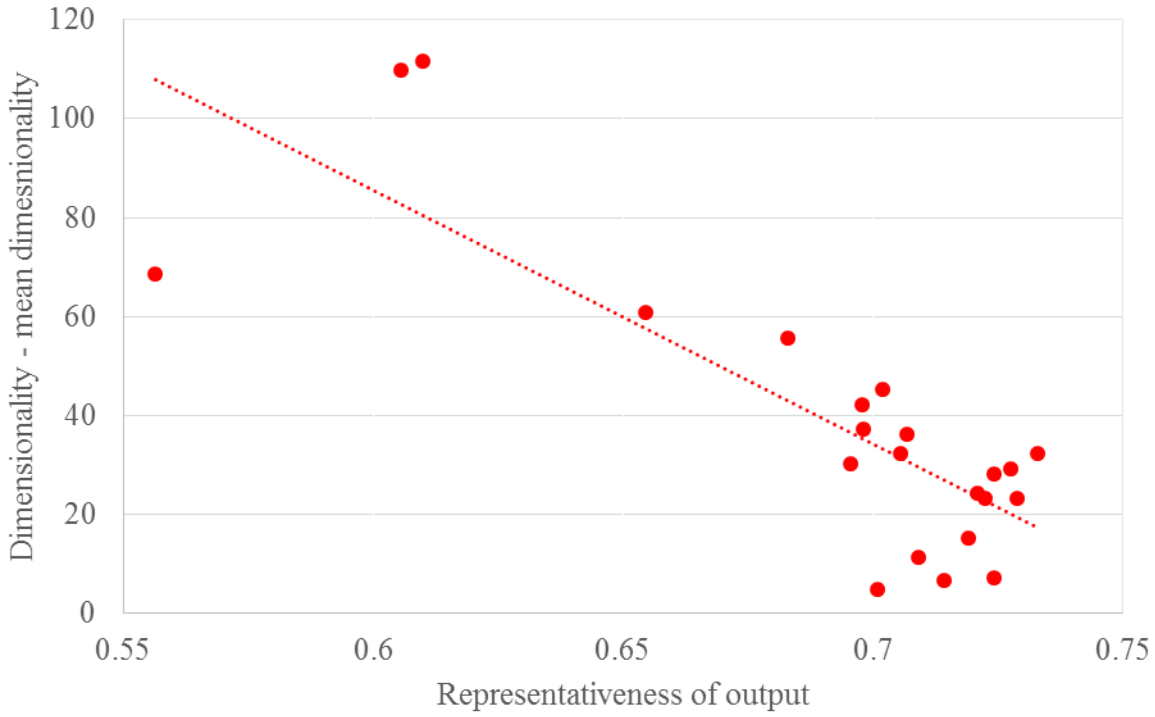

Figure 12. There is a strong negative correlation between the distance from the mean dimensionality (y-axis) across permutations and the representativeness of an output.

[1] With the average subject fMRI brain (voxel timeseries averaged across all 22 subjects) placed at the front of the ICA input the representativeness was moderately good (see Appendix 2.2). This could be further investigated as a means of producing a relatively robust ICA output for a particular sample.

This correlation indicates a quick way of identifying a relatively robust permutation output. It also suggests that a simple method for deciding on a dimensionality would be to run multiple ICAs with the first brain swapped and choose the mean dimensionality of the outputs. A key question is whether fixing the dimensionality improves reliability across outputs. This will be investigated later in the chapter.

It should be noted, that the output with the number of components closest to the mean is not necessarily the *most* representative, however it will show at least relatively good representativeness, compared to other outputs.

2.2.5 Number of brains in the ICA

Systematic analysis of the effect of brain position has shown that the first brain drives differences in the number and nature of TICA components. Given that, the obvious question to ask is how the other brains contribute to the ICA output. Do all subsequent brains make an equal contribution to the final output?

To test this the most representative output from the TICA first brain swapped analysis was used to investigate the systematic removal of brains from the ICA input (permutation 3; see Figure 6). The last brain was removed recursively from the list, until only one brain remained. Each of the input lists was put through MELODIC, resulting in 21 ICA outputs to compare with the original output, which had used all 22 brains. The same representativeness analysis was used (described in section 2.2.3.2, page 32), but this time each of the 21 outputs was compared only with the 22 brain-ICA output. This meant that the effect of losing a brain in a consecutive manner was investigated.

Figure 13A plots the similarity between each of the reduced list ICA outputs, and the 22 brain ICA output. As more brains were included in the analysis, the best matched components became more similar. These figures suggest that although the first brain may drive the number and nature of components, the final form that the components take is influenced by each of the subjects.

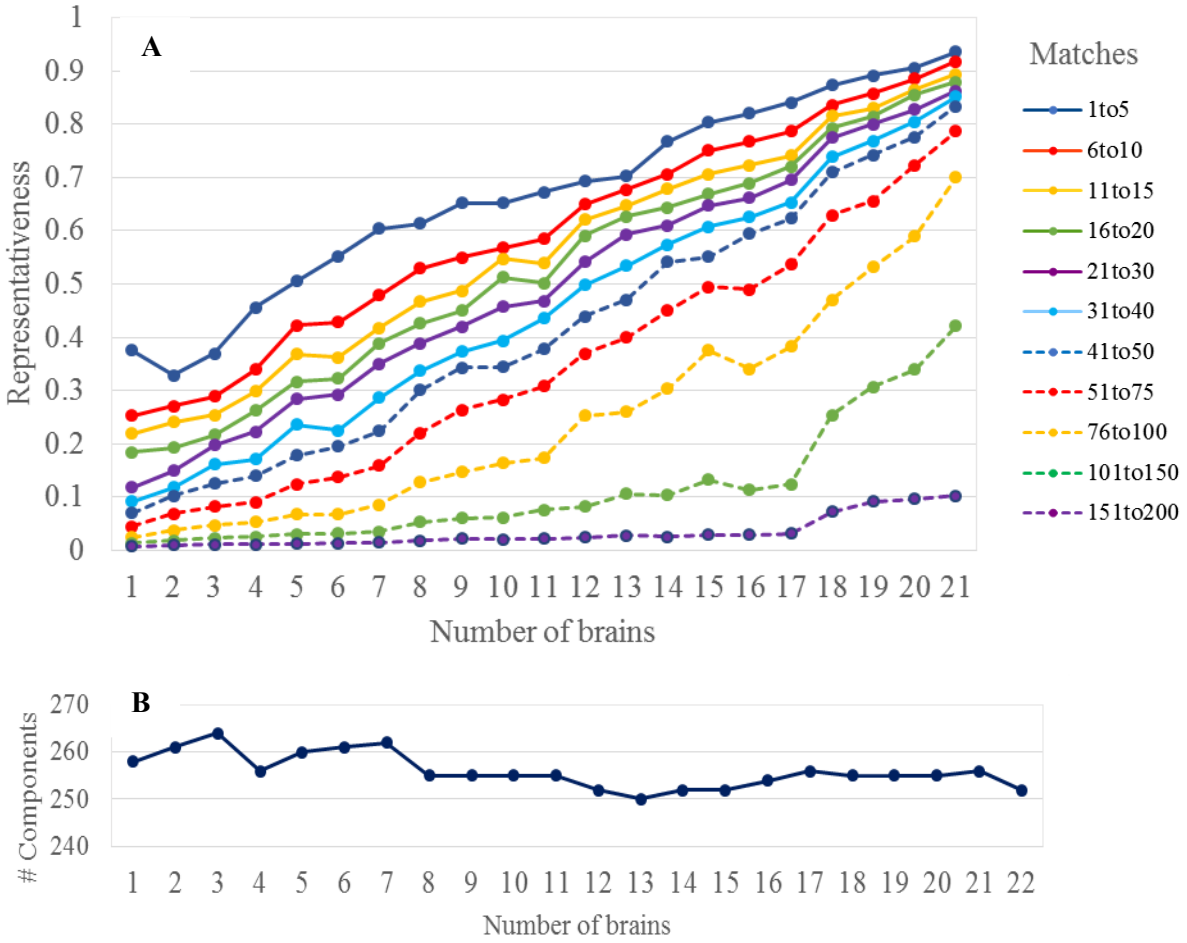

Figure 13. (A) The similarity of ICA outputs when reduced number of brains were used in the group analysis. All outputs were compared to the original ICA output which had 22 brain input. (B) The number of components is relatively stable across the pulled brains outputs.

In these 21 outputs with reduced brains the range of the dimensionality was lower (range = 14 [264-250]; see Figure 13B) than when the first brain is swapped (range= 157 [379-222]). This was expected as the same first brain is being used and supports the suggestion that the first brain drives the similarity between outputs. The number of components did not increase with the number of subjects but oscillated slightly before reaching the value generated by the full list of subjects (252); with only one brain the number of components was 258.

The spatial and temporal similarity of components was examined separately to gain further insight into the influence of additional brains in a group TICA. Figure 14 plots the spatial correspondence between components as brains are systematically removed from the analysis. This shows a steady change in the

components as more participants are included reflecting the incorporation of individual anatomical variation into the final component map.

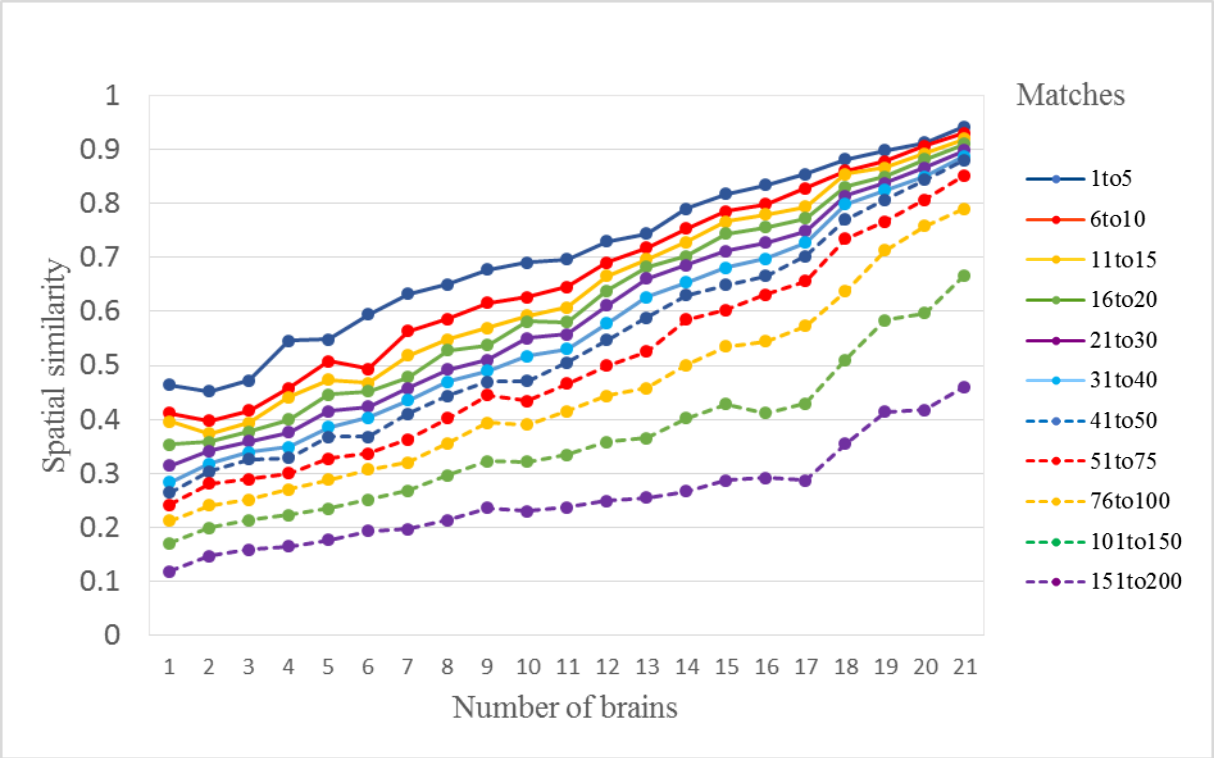

Figure 14. Spatial correspondence (Pearson's R) between the ICA components generated using the full group of participants, and group ICAs with brains systematically removed from the analysis.

Figure 15 demonstrates that the component timeseries remain more stable as brains are removed from the analysis. This supports the findings of by Hasson et.al. (2010) showing that when watching a movie extended regions of the brain are timelocked to the stimulus and show correlation across observers. My analyses have also demonstrated significant cross-subject BOLD timeseries correlation in occipital and parietal areas at the voxel level (section 2.3.1, Figure 4, page 31), and across group component timeseries using different permutations (section 2.3.2, Figure 6, page 36). However, the correlation between subjects was not perfect, and slope of the lines indicate that this temporal variation is incorporated into the final timeseries as more brains are added.

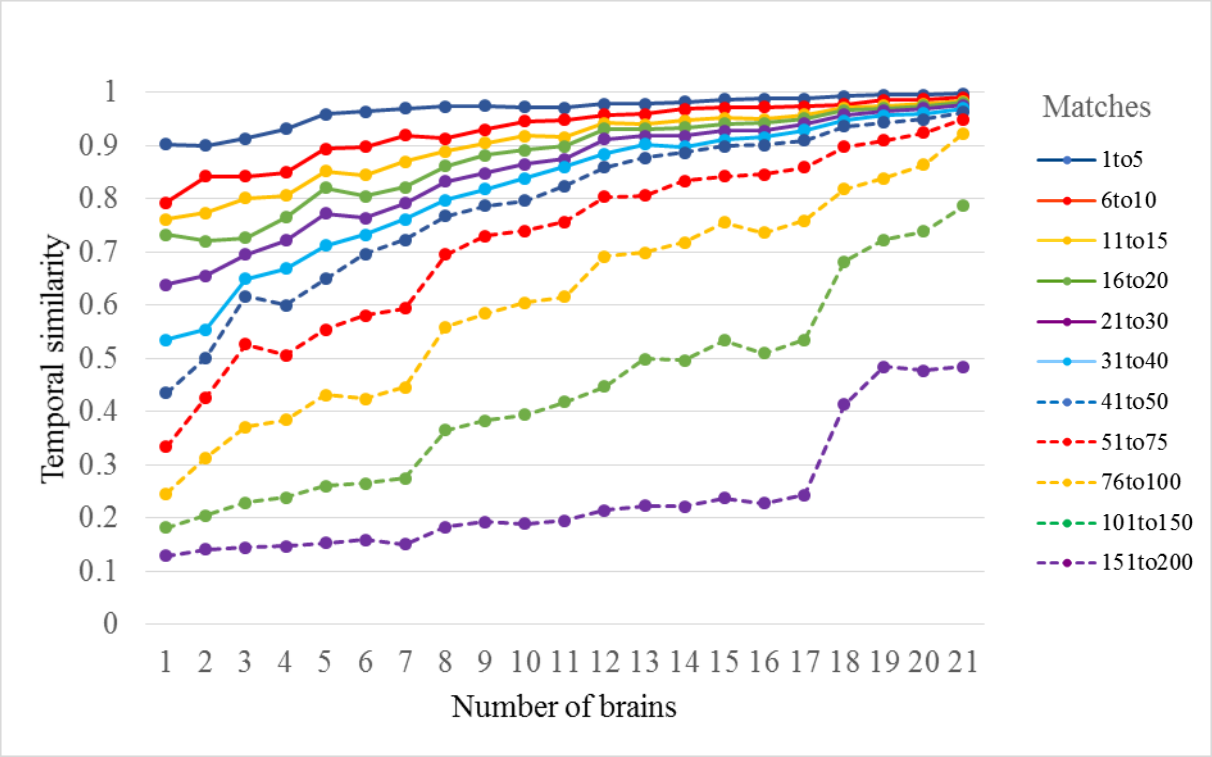

Figure 15. Mean correlation (Pearson's R) between the component timeseries generated with a full group of participants, and GICAs with brains systematically removed from the analysis.

2.3 Exploiting the ICA variation caused by switching the first brain

When the first brain is swapped there are changes in the reliability of the ICA output. This variability across ICA outputs can be exploited to examine whether certain regions in the brain elicit more reliable components than others, based on movie watching. It is expected that reliable components correspond with regions of high cross-subject correlation in the occipital and parietal lobes i.e. the visually responsive areas of the cortex.

To understand where the more reliable components lie in the brain, a heat map of reliability was generated. To create this map, all the thresholded components from the most representative output ("rep-comps") were converted into binary maps. Then, the best matched component in each of the other outputs was found for each rep-comp. The binary mask was multiplied by the spatio-temporal correlation that had been calculated between these two components. For each component there were 21 metric weighted masks; one

match from each output. These weighted masks were then collapsed and averaged to show where the most reliable components were in the brain across the ICA outputs.

The map shows that the most reliable components lie in occipital and parietal regions (see Figure 16). This corresponds with regions showing the highest cross-participant correlation (Figure 6; Hasson, Malach & Heeger, 2010), as expected based on the TICA methodology.

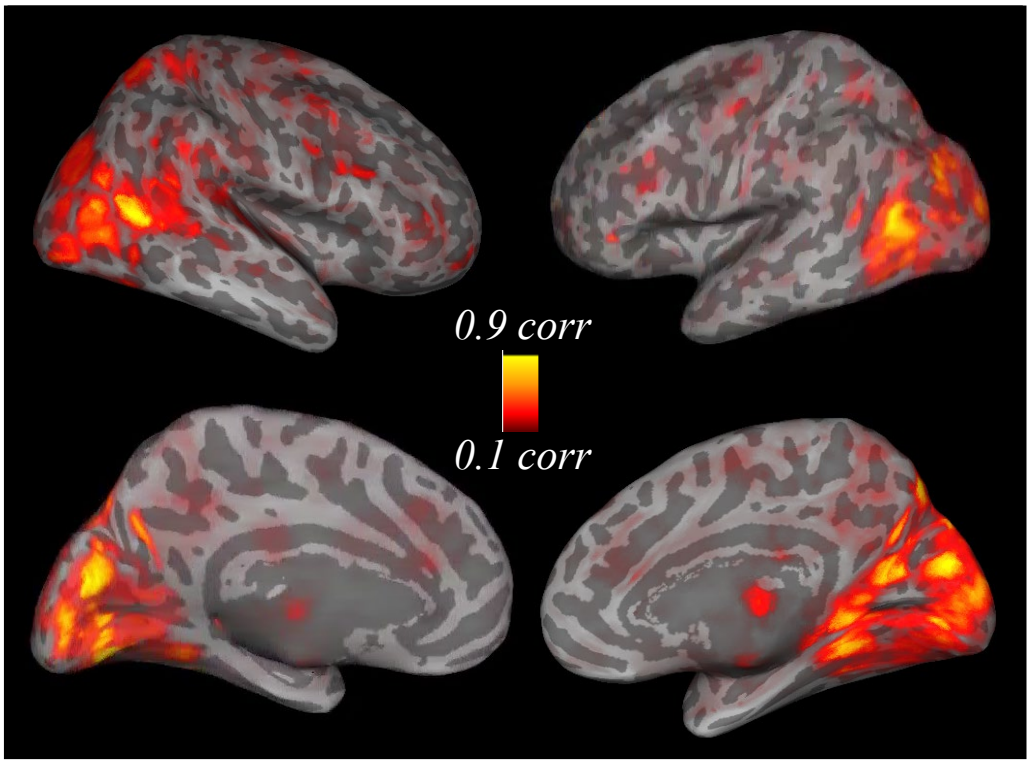

Figure 16. A heat map of where the most reliable components were in the most representative ICA output shows highest reliability in occipital regions, as expected. The left hemisphere represents the activation seen in both hemispheres.

The variability of component robustness across permutations can also be used to examine the sensitivity of TICA to different pre-processing parameters. The next sections explore the effects of data processing on the reliability of TICA outputs across permutations with the first brain swapped. In future discussions TICA outputs based on the default parameters (as described in methods section 1.3) will be called 'Vanilla'.

2.3.1 Removal of motion

One source of noise in the BOLD output is due to head movement in the scanner (e.g. Van Dijk, Sabuncu & Buckner, 2012). Head motion during scanning for this project was minimized as far as possible by ensuring that the participant was comfortable and with firm stabilization of the head using foam padding. There is some evidence that movie watching can reduce head movement during an fMRI scan (Greene et.al., 2018), however some head motion can often not be avoided. Based on literature recommendations none of the 22 subjects scanned during movie watching showed excessive head motion (movement >1.5mm in any plane, between volumes; Poldrack, Mumford & Nichols, 2011).

While watching the movie the subjects showed some movement across the length of the scan, as expected. Movement is not likely to be correlated between participants and therefore it is unlikely a TICA will be able to remove it. To address this problem, software has been developed to correct for head motion in the scanner. Before the movie data were put through the TICA it was pre-processed in FSL's FEAT (see Chapter 1, methods section 1.3), which uses McFlirt motion processing to align volumes and remove some of the effects of subject movement in the scanner. Another data driven technique for removing motion at the subject level employed by FSL is ICA-based Automatic Removal Of Motion Artifacts (AROMA; Pruim et.al., 2015). AROMA uses ICA to identify components generated by head motion and automatically remove them from the data. The algorithm is trained to identify spatial maps with the characteristics of motion (e.g. ringing around the edge of the brain (Griffanti et..al., 2018)). The timeseries of these components can then be regressed from the BOLD activation across the brain, to remove this noise element within the BOLD signal. These motion components are also identified in regular ICA, however, must be identified manually. By removing motion components and then running the ICA for a second time, you are running ICA on this 'cleaned data' and therefore the same motion components should not be identified.

The effect on the other components generated has not bee systematically examined. Using AROMA to remove noise caused by head motion was investigated to understand its effects on the reliability of the ICA output. AROMA was applied to each of the subject's data after recommended pre-processing[2]. Once AROMA had been completed for each participant the AROMA corrected brains were input into MELODIC. The order

[2] Motion correction using McFlirt, 4D mean intensity normalization and spatial smoothing at 6mm FWHM. The AROMA manual can be found at https://github.com/maartenmennes/ICA-AROMA/blob/master/Manual.pdf.

of input matched the first-brain swapped lists used in section 2.3.3.1 to allow for a direct comparison of outputs.

2.3.1.1 Number of components: using AROMA

When using unrestricted ICA, treating data with AROMA reduced the number of components in the outputs. This was expected as the removal of subject-level head motion should reduce the number of noise components and hence the overall number of components. Interestingly, much of the overall pattern of dimensionality in the ICA outputs is preserved (see Figure 17). This suggests that the AROMA is skimming a proportion of components from the outputs. Analysis showed that at least 1 component and up to 150 components were removed from any one of the group outputs. This variance in the number of components removed reflects the reliance on the first brain for generating the seed components, as the first brain is the only one systematically being changed in the input lists.

It may be expected that the TICA permutations that had first brains showing the highest motion during the scan would have the highest reduction in components when using AROMA. However, this did not necessarily occur. Permutations with subjects who had the largest degrees of motion as the first brain are highlighted in Figure 17. Although there is a relationship, it does not explain all the effect.

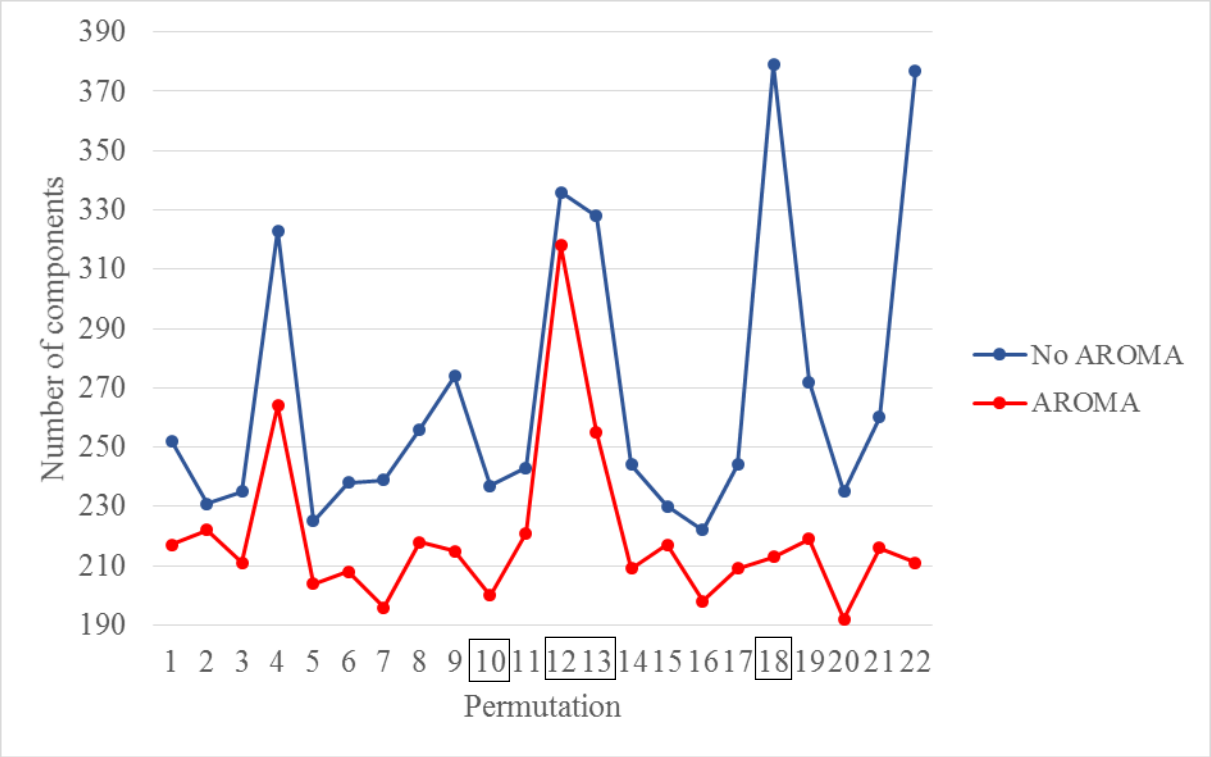

Figure 17. The number of components in unrestricted ICA outputs when FSL's McFlirt motion correction was used, compared to when AROMA was used. The four permutations with the first brain showing high levels of movement are highlighted with black boxes. AROMA can be seen to remove a large proportion of components in some high-motion first brain permutations (e.g. 18, 13) but this was not the case for all (e.g. 12 shows a small decrease in the number of components with AROMA).

2.3.1.2 Representativeness: Using AROMA

Initially the unrestricted AROMA outputs were assessed for similarity. As the number of components differed across outputs (see previous section) it was expected that the components would show tempero-spatial variation when compared directly. This expectation was supported: AROMA outputs showed a similar pattern of variable representativeness across permutations to the Vanilla outputs described in section 2.3.3 (see Appendix 2.3 for AROMA representativeness). For example, permutation 12 was still clearly the least representative output (Figure 11). The first brain in this permutation had the largest amount of overall motion

during the movie watching. Therefore, using AROMA did not improve the representativeness of this output by correcting for this motion.

To directly compare TICA outputs across AROMA and Vanilla data, I ran TICAs restricted to 200 components. There was a slight difference between the levels of reliability, with the Vanilla ICA outputs tending to be a little more reliable for most components (see Figure 18).

Figure 18. When ICA outputs are compared between AROMA and Vanilla data (both restricted at 200 components), there is slightly higher reliability when AROMA is not used, and McFlirt is used instead, during pre-processing.

Despite only slight differences in the reliability of the outputs across permutations, the components generated with and without AROMA show some spatial and temporal differences. Figure 19 plots the temporal and spatial correspondence between the most representative AROMA and Vanilla outputs. This demonstrates how changing the pre-processing stages used can change the components that are identified. The sensitivity of ICA to these pre-processing parameters could affect the usefulness of movies and ICA for identifying visual regions if it reduces the reliability of visually driven components. To address this concern, the spatial distribution of component correspondence between the Vanilla and Aroma outputs was

investigated. It was anticipated that components in visually responsive regions would be robust across techniques.

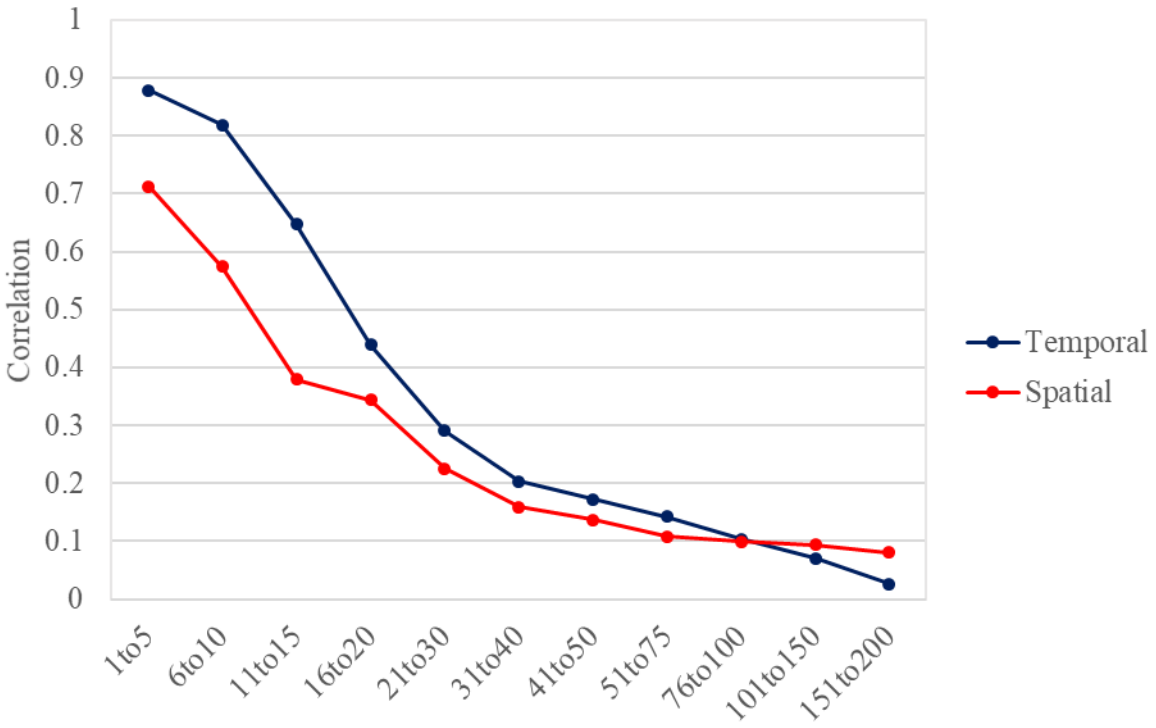

Figure 19. The average correspondence between matched components across ICA outputs with and without the use of AROMA for motion correction. Any spatio-temporal metrics over 0.04 were in the 99th percentile ($p<0.01$) across all component comparisons (200x200).

AROMA components that showed good spatio-temporal correlation with the Vanilla output were all matched to components in the first fifty of the Vanilla output (see Appendix 2.5b). It is expected that components early in the output are visually driven as responses to the movie will account for most of the variance in correlated activity across subjects. A heat map of the spatio-temporal correspondence supports this being the case as it shows robust components identified across techniques in the occipital lobe and parietal

lobes, associated with visual processing (Figure 20). This is reassuring as it means that components in key regions of interest should be comparable despite the pre-processing differences.

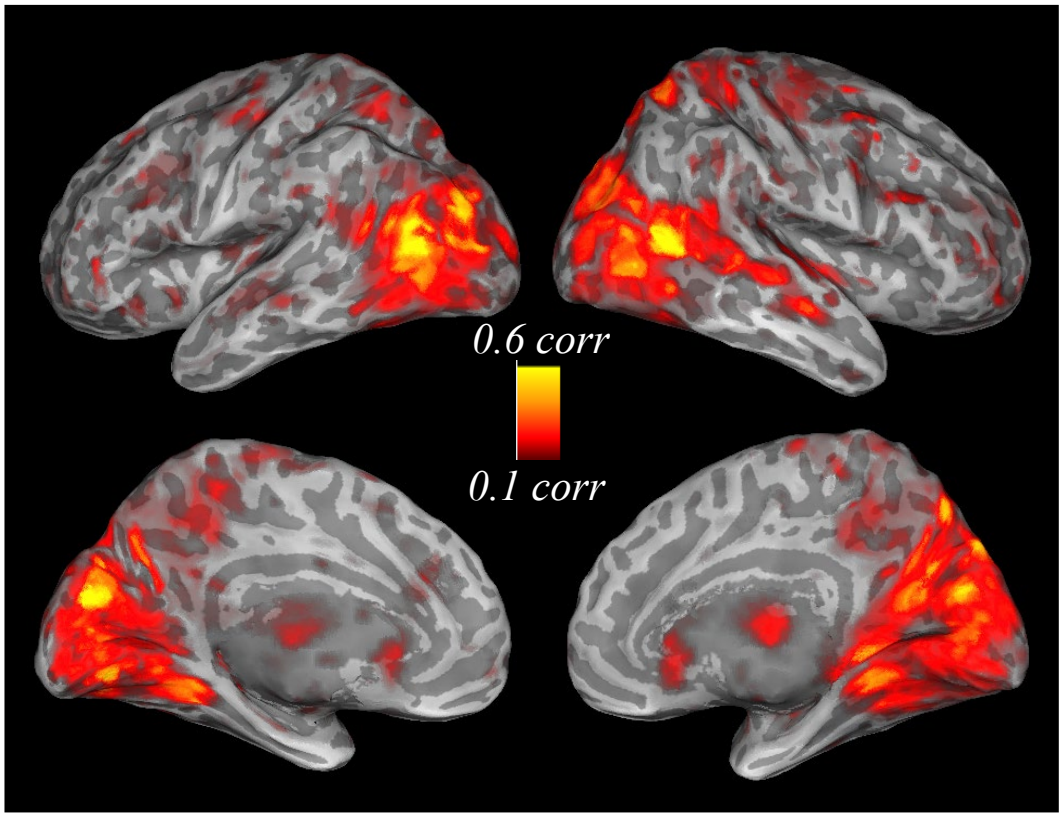

Figure 20. The regions of spatio-temporal correlation between Vanilla and AROMA ICA components are focussed at occipital - parietal regions and extend into temporal and dorsal areas (r-value). This suggests a robustness of components in visually responsive regions across motion correction techniques.

2.3.2 Grey matter masking

Another way to potentially increase the effectiveness of identifying functionally specific signal components the brain is to use a grey matter mask (e.g. Formisano, Esposito, Di Salle & Goebel, 2004; Goebel, Esposito & Formisano, 2006). A mask will focus the analysis on the grey matter, where the signals are of interest. Grey matter masking was performed on each of the subject datasets. The mask was created by segmenting the MNI standard brain using FSL FAST, into white matter, grey matter and CSF. The mask was unthresholded meaning a voxel containing any proportion of grey matter was included in the analysis. Using the MNI grey matter mask rather than individual's own meant that there were not any voxels that only occurred in individual brains. However, by using the MNI brain mask there is a risk of losing some of the grey

matter voxels in atypical brains. Both techniques had advantages and disadvantages; MNI masking was favoured due to individual subject TICAs showing increased reliability across subjects when the MNI mask was used, compared to individual masks.

Three small spheres were created; one in the white matter, one in CSF and one externally to the head. These were combined with the grey matter mask and applied to each of the subjects' data. Spheres were added to account for global noise signals (e.g. Jo, Saad, Simmons, Milbury & Cox, 2010). Each of the subjects' brains was then registered to the MNI brain and the grey matter mask was applied.

TICA analyses were performed using the same 22 first-brain swapped permutations previously used in AROMA treated and Vanilla analyses. This allowed us to compare outputs directly between masked and unmasked data. As done previously, first an unrestricted set of TICAs was run to see the effect of the parameter change on the dimensionality as calculated by MELODIC. Counterintuitively, with grey matter masking the average number of components was higher than without masking (mean = 310 compared to 267). The range was very similar to Vanilla and AROMA outputs. Representativeness across the outputs was also similar to the unmasked Vanilla, with the average similarity slightly increased between permutation outputs compared to the Vanilla. The pattern of spatial and temporal representation across the permutations was altered compared to the Vanilla outputs, with different permutations being identified as the least and most representative (see Appendix 2.4a).

With dimensionality restricted at 200 components, the representativeness of grey matter masked output was very high for the first 150 out of 200 components (see Figure 21, top). These values were markedly higher than restricted Vanilla permutation outputs across all components (see Figure 21, bottom) . These findings suggest that grey matter masking fMRI data can greatly improve the reliability of a TICA output, when the number of components is defined.

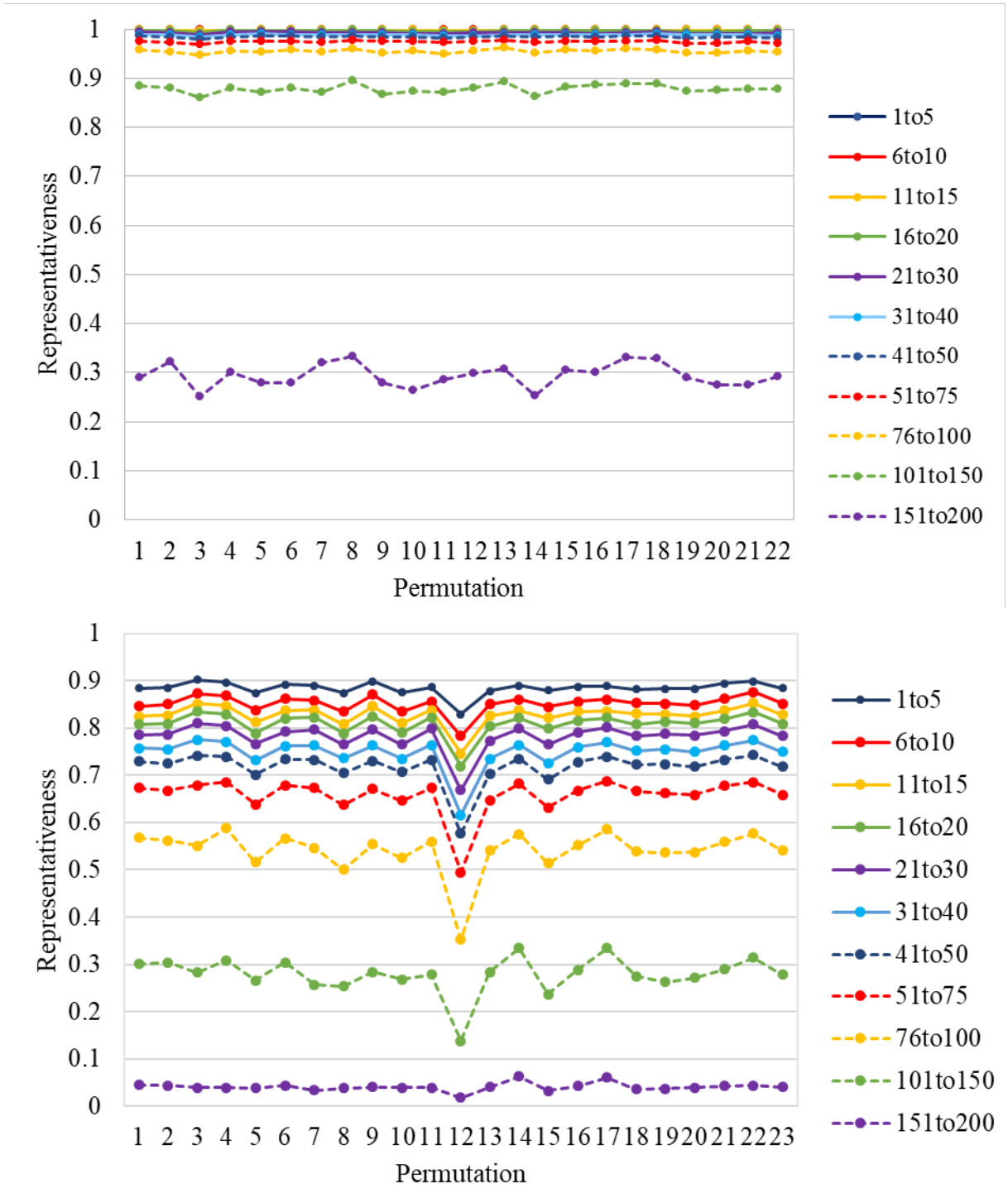

Figure 21. Top The representativeness of ICA outputs using grey matter masked data, restricted at 200 components is very high across permutations for the best matched 150 components. R-values over 0.35 are in the 99th percentile across all spatio-temporal component comparisons. *Bottom* The representativeness values of ICA outputs using non-masked data, also restricted to 200 does not show the same increase in component similarity.

Masking the Vanilla output

My results support the hypothesis that grey matter masking improves the reliability of the ICA output. One initial check as to why this may be was to assess whether spurious voxels included in the component maps that lie outside of the grey matter pull down the correlations in the unmasked Vanilla results. Analysis showed that most of the component activation lay in the grey matter (100%-80%, dependent on component) however the remainder of activation lay in CSF, white matter or non-brain regions. A grey matter mask was applied to the Vanilla ICA output components to remove the non-grey matter voxels that may be pulling the correlation down, and the representativeness of the outputs was recalculated.

Masking the Vanilla outputs did not increase the representativeness of the components by more than a fraction compared to the unmasked Vanilla outputs. This suggests that for the Vanilla ICAs, variability in the output does not originate from white matter or CSF spurious voxels. Instead, the noise removed with grey-matter masking seems to increase the overall reliability of the ICA.

Comparing Vanilla and Grey-matter masked ICA outputs

Analysis so far has shown that grey matter masking data changes in the number of components generated automatically by TICA and the changes in the representativeness profiles of outputs, compared to Vanilla analyses. The next step is to understand how the components are changing when a grey matter mask is applied. Does applying a grey matter mask fundamentally change how the data is being decomposed, or are the same regions being identified with similar temporal source signals?

The temporal and spatial similarity of components was examined separately to understand how the components differed with grey matter masking. Figure 22 shows the correlations between the best matched components. Components show high temporal similarity with and without grey matter masking for most of the components. Spatial correlations are lower, reflecting changes as CSF and white matter is removed with masking. Grey matter masked data produces components that are more spatially and temporally similar to vanilla data than when using AROMA motion correction (see Figure 19 for comparison with Figure 22).

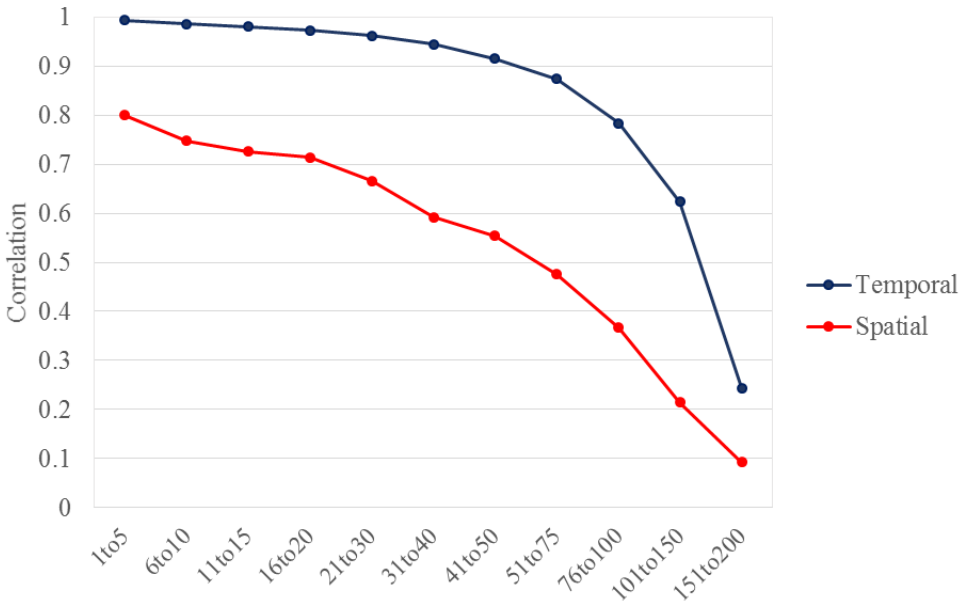

Figure 22. The spatial and temporal similarity between components generated using movies, with and without pre-ICA grey matter masking of the data.

A heat map of component reliability (temporal x spatial similarity) across masking and non-masking shows good correspondence across the medial and lateral occipital lobe (see Figure 23), the same regions showing significant between subject voxel correlations (section 2.3.1, Figure 6, page 31). Some correpondence extends into the temporal and parietal lobes including the pre-motor and motor cortices. Matched components showed high correspondence in component number for the first ~sixty components, while later components show little or no correlation in component number across the outputs (see Appendix 2.4a). Analysis also showed that the earlier components were more reliable across masking and no-masking (see Appendix 2.4b). These analyses together suggest that components earlier in the output are more likely to be visually driven (this is further explored in Chapter 5).

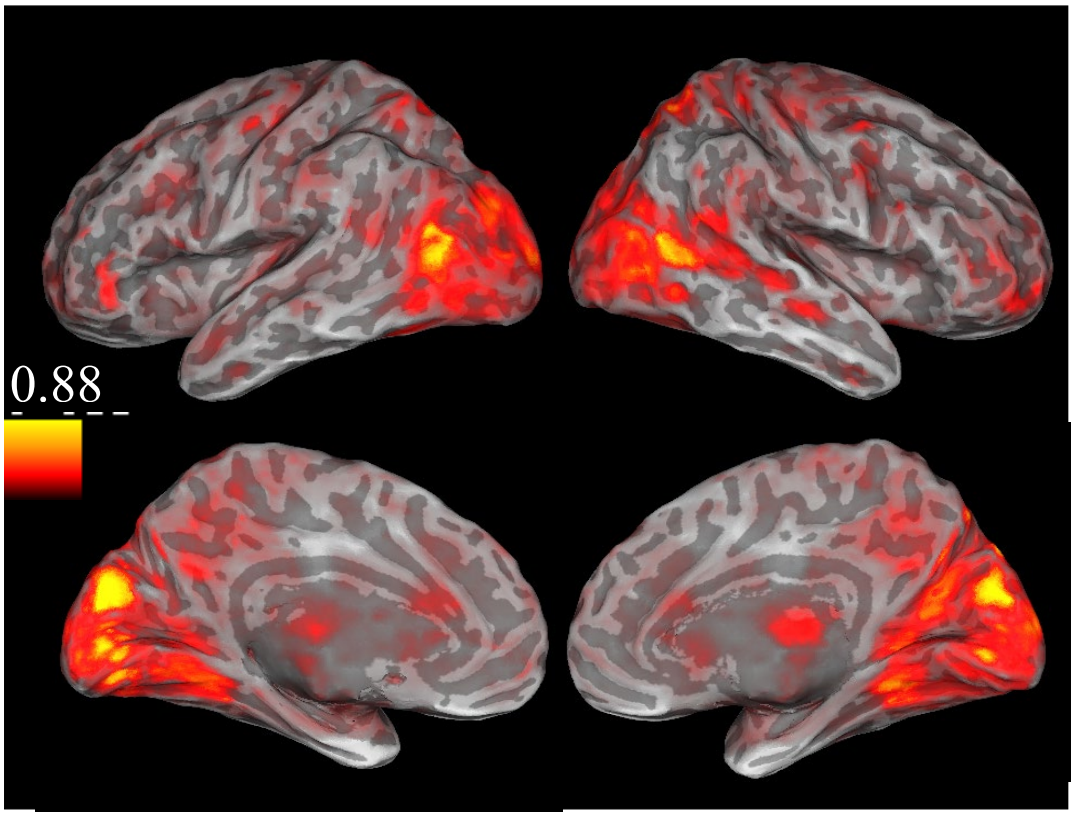

Figure 23. A heat map of correspondence between components in the most representative Vanilla output and the most representative grey matter masked output. Significant component spatio-temporal correspondence is seen in the occipital and parietal lobe as expected and some components were also well matched in frontal regions ($r>0.21$, $p<0.01$).

Despite differences in the data input and some variation in the TICA outputs, reliable components are identified in the visually responsive regions. These data tell us that earlier components, which are more likely to be in the occipital cortex and task driven, are most robust across masking pre-processing techniques.

2.3.3 Comparing ICA outputs across analysis pipelines

The most representative ICA output was taken from (a) "Vanilla" data (no masking or AROMA); (b) the AROMA treated data; (c) the grey matter masked data and (d) AROMA treated and grey matter masked data, for comparison. The most representative Vanilla output was also masked with the grey matter mask, for comparison with these four outputs.

Spatio-temporal correlations (see Table 1) show that using AROMA changes the components that are produced using TICA more than grey matter masking the data, when compared to the Vanilla output. This

change is identified most clearly in the component timeseries (as per Figure 19 where functional similarity drops compared to grey matter and Vanilla component matches, see Figure 22).

Table 1. The spatio-temporal correlation between ICA outputs using data treated with different pre-processes.

Manipulations	Vanilla	Vanilla (masked)	AROMA	GMMasked	GMMasked + AROMA
Vanilla		0.92	0.37	0.73	0.40
Vanilla masked (postICA)	0.92		0.36	0.81	0.44
AROMA	0.37	0.36		0.38	0.66
GMMasked	0.73	0.81	0.38		0.47
GMMasked + AROMA	0.40	0.44	0.66	0.47	

2.3.4 Changing ICA parameters

So far in this chapter I have established that TICA is sensitive to motion correction techniques and grey matter masking, producing different components depending on the pre-processing stages used. However, robust components can be identified across outputs in visually responsive regions. Next, I will explore the sensitivity of TICA to smoothing and resampling options, for a thorough analysis of the reliability of this technique.

2.3.4.1 Smoothing

The amount of smoothing used varies across studies and it is hard to determine the optimum amount of smoothing for a dataset. Smoothing aims to increase the ratio of signal to noise and the amount of smoothing to be used will be dependent on the type of information you want to glean from your data (Griffanti et.al. 2017). It is important to choose a level of smoothing appropriate for the research question you have and the regions of interest (ROI): the anatomical variability in the location of ROI between participant brains should be considered as well as the size of the ROI.

Different levels of smoothing can have different benefits and costs. When using ICA, using less smoothing may help to identifying the true size of your ROI, however may mean that scattered signal is more

likely in a component map meaning it is wrongly classified as noise (Griffanti et.al. 2017). On the other hand, if a high level of smoothing is applied then discrete regions of noise can appear as a larger cluster, which may be mistaken as a region of functional signal (Griffanti et.al. 2017). Additionally, when smoothing to higher levels there may be smaller visually responsive regions of interest that cannot be segregated by ICA as they are 'smoothed out'. Using higher levels of smoothing may also make it more difficult to localize the activation to within the grey matter. It could also be the case that as smoothing is increased, noise signals are more likely to be incorporated into signal components, corrupting the component timecourse. The amount of smoothing chosen by a researcher is therefore decided on discretion based on these considerations. The question we address here is how smoothing impacts the reliability of components.

The default smoothing level in FEAT of 5mm Full Width at Half Maximum (FWHM) may be observed as relatively high when applying ICA (Griffanti et.al., 2018). To investigate the effect of smoothing the data, the data were smoothed to 0mm, 3mm and 8mm to be compared to the 5mm default smoothing in FEAT. It should be kept in mind that the acquired resolution of the data was $3mm^3$, therefore results are in to be understood within this context. Smoothing effects may interact with the native resolution of the data.

Results showed that different levels of smoothing changed the number of components produced in an automated TICA. The average number of components across permutations was reduced to 150 when smoothing was set at 0mm and the number of components in the outputs increased with the introduction of smoothing, until a level of 8mm FWHM, when the average number of components levels out at just under 250. Variability in the number of components across permutation also changed across different smoothing levels. Middling smoothing levels of 3mm and 5mm FWHM demonstrate the highest variability in component number compared to higher and lower resolutions. Smoothing therefore does not only produce components with different sized clusters, but also can have an impact on the number of components.

To compare the reliability of components directly at each smoothing level, ICAs were restricted to 200 components. The reliability of the components within each smoothing level was not greatly altered by the amount of smoothing of the data (see Figure 24). There was a slight, improvement in reliability for matches 20 to 150 with 0mm smoothing. This is surprising given that smoothing is supposed to increase the ratio of signal to noise. The standard deviation from the mean representativeness was similar across all levels of smoothing.

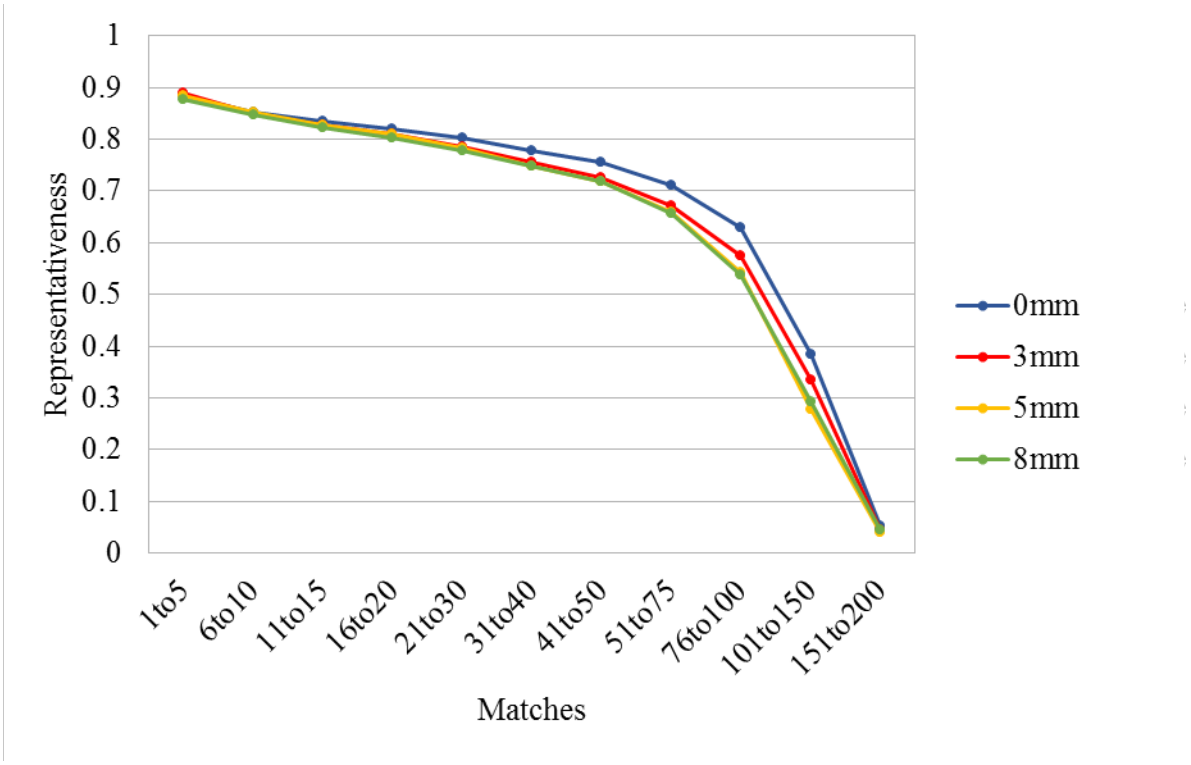

Figure 24. The mean reliability of ICA outputs across the different metric groupings show a very slight improvement for lower levels of smoothing or none, compared to higher. Spatio-temporal correlations were in the 99th percentile when the r value was over 0.26 (0mm, 8mm), 0.25 (5mm) or 0.24 (3mm).

The temporal and spatial similarity between components at different smoothing levels was investigated using correlations. The average correlations of the best matched components across the smoothing levels demonstrated default smoothing of 5mm was the most representative output (see Table 2). This means outputs from 5mm smoothed data best represented the components generated across the different smoothing levels. Therefore, for this dataset (acquired resolution 3mm^3), although lower smoothing has slightly better representativeness within smoothing level, a 5mm kernel generates components that best represent across smoothing levels.

Table 2. Smoothing at the FSL default 5mm showed the best spatio-temporal correlations across smoothing levels. Correlation values here are averaged across the twenty best matches for each output comparison.

Smoothing	0mm	3mm	5mm	8mm

0mm		0.73	0.82	0.69
3mm	0.73		0.78	0.75
5mm	0.82	0.78		0.87
8mm	0.69	0.75	0.87	

2.3.4.2 Resampling

Before performing ICA, data can be resampled to a different resolution, usually for efficiency. Resampling the data means re-slicing the data into smaller or larger voxels. The process allows either a finer grained or coarser resolution to the data. Higher resolution allows for small regions of interest to be identified however may increase the presence of scattered signal in the spatial map. It also increases the processing power needed for analysis to levels which may be impractical due to time or technological constraints. Reducing the resolution solves these problems but does not allow for finer grained analysis meaning smaller regions of interest may be missed. As with the question of smoothing – the resampling rate you choose may depend on your research question and your regions of interest.

The sampling rate used for MELODIC ICA was set at a default of $4mm^3$. I resampled the movie data to 2mm and 6mm, for comparison. Counterintuitively, when dimensionality of the ICAs was not restricted there was a negative correlation between the number of components and the resolution of the data i.e. as the resolution was increased from 6mm to 2mm, less components were identified by MELODIC. Each resolution produced different numbers of components across the first-brain swapped permutations, meaning the sensitivity to first brain was not ameliorated at any of the resolutions. As the case with smoothing effects, the acquired resolution of the data may interact with resampling effects. Therefore, results are in to be understood within the context of the data's native resolution being $3mm^3$.

ICAs were then restricted to 200 components to directly compare results without having differences in component number confound the results. Analysis revealed a marginal increase in the reliability of all components when data were sampled at the higher resolution of 2mm, compared to the default of 4mm (see Figure 25). When data were resampled at 6mm the reliability of the components in ICA outputs was reduced. This suggests that using the higher resolution is better, although does raise constraints in terms of memory needed for the analysis.

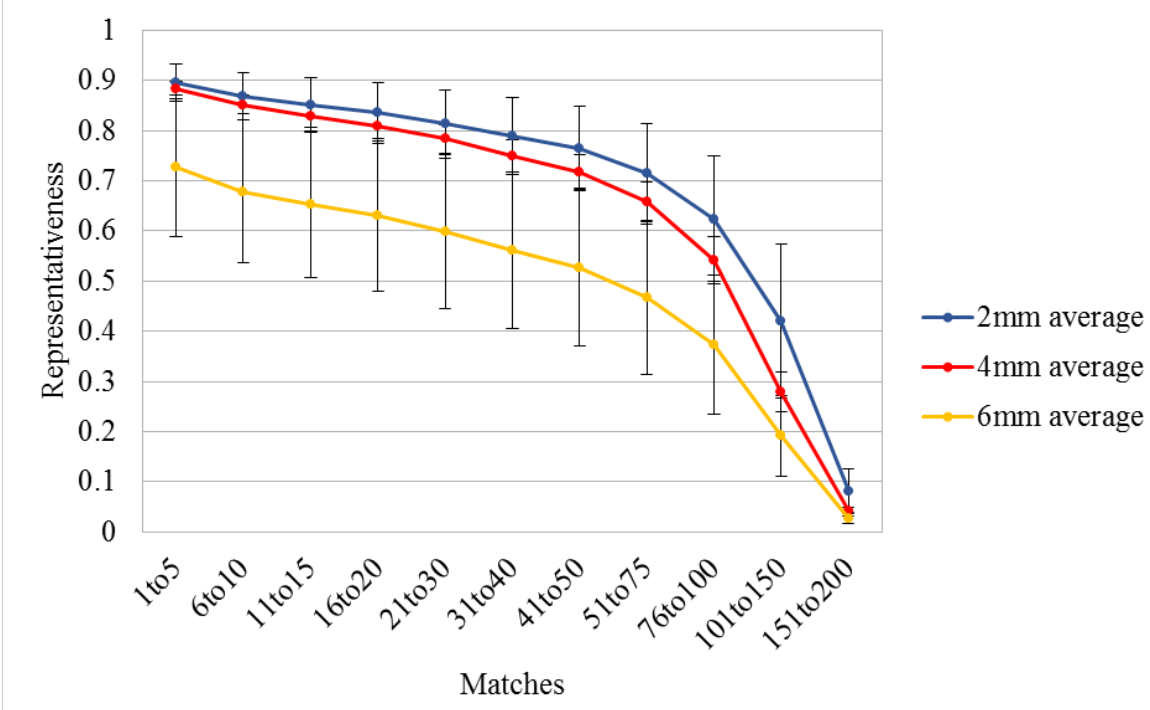

Figure 25. Using input data of a lower resolution will reduce the reliability of outputs. A higher resolution is recommended for increasing the reliability of your output. The standard deviation from the mean of the representativeness was also increased at a lower resolution (see error bars).

These reliability findings may be relative to the native resolution of the dataset, with lower resolutions causing less reliable outputs. As part of our movie study, functional data were collected at $3mm^3$, further research is needed with functional data collected at a different resolution to test whether the reliability of ICA outputs is relative to the native resolution

A cross-correlation comparison showed highest similarity across resolutions for the default 4mm (see Table 3). This means outputs at this resolution best represented the components identified across different

resampling levels. Using this resolution may allow for better reliability across different experiments, however other resolutions should be tested as you may expect the middle value to be the most similar to the other two.

Table 3. A resolution at the FSL default 4mm showed the best spatio-temporal correlations across smoothing levels. Correlation values here are averaged across the twenty best matches for each output comparison.

Resolution	2mm	4mm	6mm
2mm		0.79	0.61
4mm	0.79		0.74
6mm	0.61	0.74	

2.3.5 Comparing the magnitude of effect across data manipulations

Results have demonstrated that data TICA is sensitive to different pre-processing parameters causing differences in the output depending on the pipeline used. However, components in visually responsive regions show robustness across manipulations. The magnitude of each of the pre-processing options was assessed by comparing each of the manipulation outputs to the default pipeline. Apart from when comparing the effects of the first brain being swapped, the same permutation (first brain permutation) was used for comparison. All outputs were restricted to 200 components for comparison. Results show that the effect of swapping the first brain has least impact on the output, though the magnitude of the effect is variable dependent on which first brain is used in the input (see Figure 26). AROMA has the largest effect on the TICA output, while grey matter masking, resampling and smoothing have an intermediate effect.

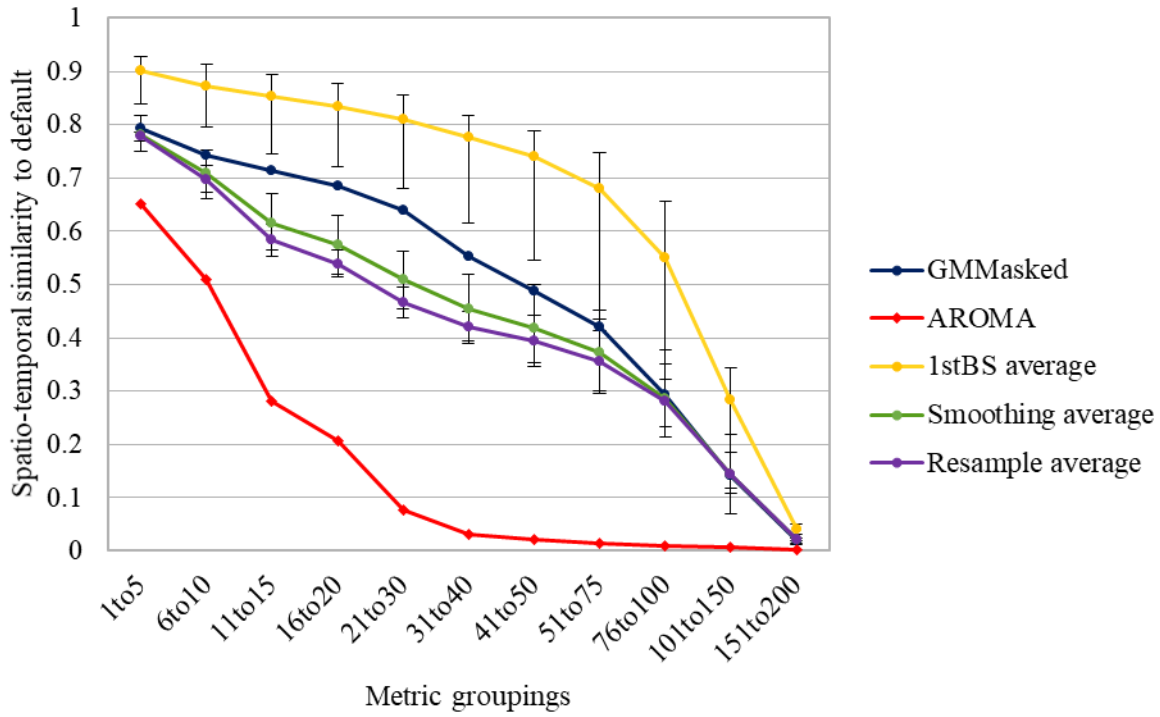

Figure 26. The magnitude of parameter effects was compared by assessing the spatio-temporal similarity of components generated to the default output. Apart from the first brain swapped (1stBS) manipulation, the same permutation was used for analysis of the effect of each manipulation. Error bars represent the maximum and minimum across different outputs compared to the default (1stBS = across 21 different first brains; Smoothing = 0mm, 3mm and 8mm; Resampling = 2mm and 6mm). Swapping the first brain has the least impact on the TICA output, though the magnitude of the effect was dependent on which first brain was swapped in (see error bars on 1stBS average line). Using AROMA had the largest impact on the TICA output.

2.4 Summary of parameter effects

In this chapter I have used first brain effects to quantify reliability and have identified that using a grey matter mask markedly improves the reliability of an ICA output. It is possible that other techniques such as jackknifing, or resampling would show something different, but unlikely. This chapter has also systematically reviewed the sensitivity of TICA to pre-processing such as motion correction techniques, smoothing and resampling resolution. FSL's AROMA changes the output components compared to Vanilla data to a larger degree than grey matter masking. Sensitivity to ICA's AROMA is therefore high and can produce quite different components without greatly improving the reliability of the outputs. Reassuringly, components in the occipital and parietal lobes show consistency across motion correction and masking techniques. This is likely due to the use of a movie stimulus applying temporal structure to BOLD activity across subjects that is preserved across techniques.

Choosing a lower resampling resolution than the 4mm default reduced the reliability of components in this dataset. Therefore, based on the research so far it would be advised that a resolution higher than the default be chosen, subject to processing power. Although there was a slight trend towards lower reliability with increased smoothing, this was less notable effect. Therefore, smoothing levels should be influenced by the research question.

2.4.1 Combining optimal parameters

Each of the parameters have been examined individually to understand their effect, however they have not yet been tested in conjunction. Therefore, the next step was to run permutations of the ICA using the parameters that were identified as being optimal when run alongside the other default settings. It may be the case that when the optimal parameters are combined they interact to produce suboptimal outputs. 22 ICAs were conducted using the same 1st brain swapped permutations as used previously, with dimensionality restricted at 200 components. Based on the findings above optimal parameters chosen were grey matter masked data, resampled at 2mm and with no smoothing.

Results showed that using these optimal parameters reduced the representativeness overall when compared to default smoothing and resampling. This suggests that combining the resampling and smoothing parameters does not benefit the reliability across all components.

Analyses were also re-run with data sampled at 2mm and with grey matter masking, but with default smoothing (5mm). This was due to 0mm smoothing having only a slight advantage over the default smoothing level. The representativeness results from these ICA outputs are very similar to the grey mater masked data sampled at 4mm (see Figure 21).

2.5 Restricting the number of components

So far, we have been using ICA with unrestricted dimensionality for investigation of the effect of different pre-filtering on ICA outputs. In addition, a dimensionality of 200 components has been employed to compare ICA outputs directly. In this final section, the next question to be asked; what happens to the reliability of the outputs and components if we restrict the analyses to having a certain dimensionality?

Based on previous work (e.g. Smith et.al. 2009) and an aim to systematically assess the effect of changing the dimensionality, ICA runs were run restricted to 20, 50, 70, 100, 150 and 200 components. The nature and reliability of components at different dimensionalities will be investigated. For each level of dimensionality, the 22 permutations generated by swapping the first brain were used. For each of the dimensionalities a representativeness plot was generated across the permutations to assess how reliable the components were across the outputs.

As the dimensionality is increased, the proportion of reliable components stays relatively similar. This means there are more reliable components at higher dimensionalities as there is no obvious trade-off using a higher dimensionality. It could be argued that rather than restricting an ICA to the number of components you would like, it may be better to use a higher dimensionality and then take the subset of reliable components. Heat maps of the reliable components showed that across all dimensionalities the most reliable components remain stable in the occipital lode, extending into regions of interest in the parietal lobe. This is the same pattern as when dimensionality was unrestricted (see Figure 16) and covers the regions of significant subject voxel correlation. This means at a higher dimensionality you will have access to more reliable and visually driven functional components. As dimensionality increases, it is expected that the components in these regions will change as the data is split and reorganized in different ways. The effect of dimensionality on the components identified and the visual regions they represent is examined in Chapter 4.

As expected, when the ICAs were restricted, the 22 permutations provide more consistently similar outputs than when the ICAs are unrestricted. This means that it may be preferable to restrict an ICA to a certain number of components when trying to replicate findings, as it allows for easier replication of methodology as well as comparison across datasets.

To quantify the changes to outputs across the different dimensionalities, component spatial maps and timecourses were compared at each dimensionality with the most representative unrestricted output (which had 235 components). As expected the outputs with a more similar number of components had more similar components maps (see Figure 27 and Figure 28). The timeseries of components showed better correspondence than the spatial maps across dimensionalities (Figure 27). The temporal correlation of components remained very high for the best five component matches across all the ICA outputs (Figure 28).

This suggests that the same functional processes are being identified but that splitting of component into functional subregions occurs at higher dimensionalities. This is explored further in Chapters 5 and 7.

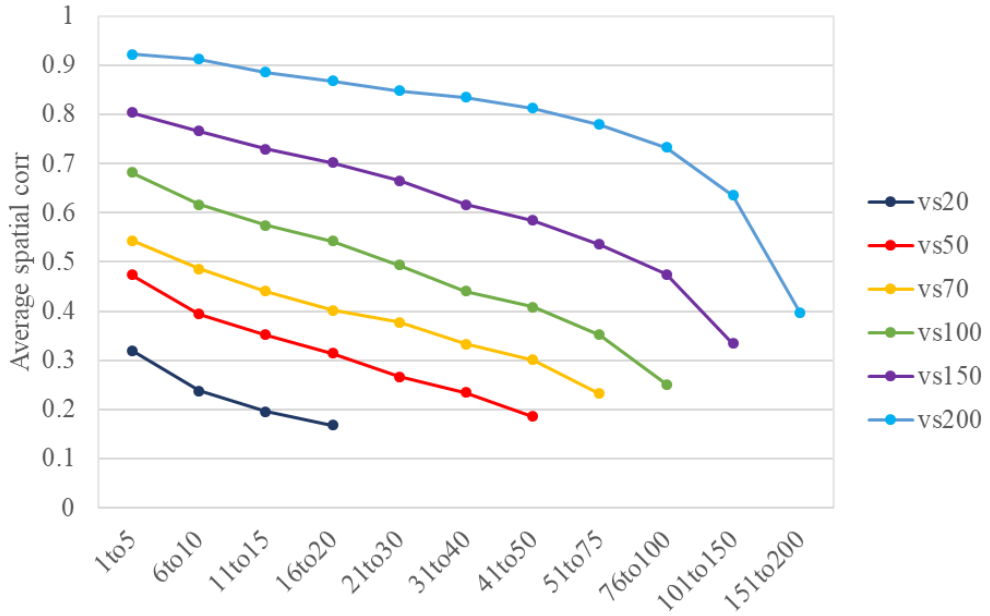

Figure 27. The correlation of the best matched spatial maps across the most representative unrestricted output (235 components) and restricted ICAs at dimensionalities 20, 50, 70, 100, 150 and 200. Dimensionalities closer to the unrestricted are more similar. Spatial maps change as dimesnsionlaity is altered.

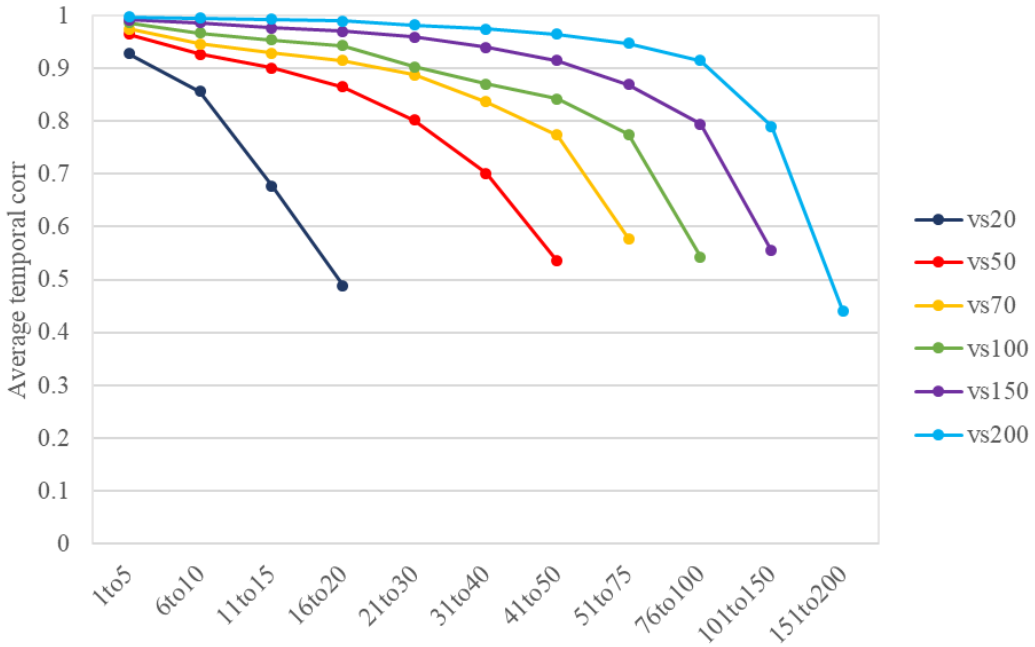

Figure 28. The temporal correlation between components in the most representative unrestricted output and restricted ICAs shows good correspondence between component timeseries, even when dimensionality is much lower. This suggests the ICAs are identifying the same functional processes at different dimensionalities.

2.5.1 How do you choose the number of components to use?

It is more useful to select a higher number of components (or leave the number unrestricted), and then take a subset of the reliable signal components within the regions of interest, to increase the reliability of your results. Using a higher number of components will mean that on average more reliable components are produced. There is no obvious cost to running a TICA with more components, if the dimensionality is kept below that identified in automatic dimensionality calculation by MELODIC. The effect of changing the dimensionality is addressed in Chapter 5.

The optimum number of components calculated by melodic alters when different lengths of movies are presented. Shorter movie clips generate fewer components; a twenty-minute clip using grey matter masked data gave an average of 312, while a five-minute clip with grey matter masked data gave an average of 36 components. A longer movie clip will therefore allow for greater flexibility in the generation of a higher number of components, allowing for selection of a reliable subset. The effect of the length of the movie clip on the components identified is examined in Chapter 4.

To select the number of components most suitable for an analysis, it is useful to run multiple unrestricted permutations of a data set. The mean value of the dimensionalities of the outputs can then act as a guide for restricting dimensionality. This will allow data to be more replicable using further testing and allow for more direct comparisons between different participant groups.

2.6 Chapter summary

In this chapter, I have thoroughly and systematically investigated the sensitivity of TICA to pre-processing parameters, to establish a pipeline for generating robust components that can be used in the rest of this thesis. This systematic review can also inform future work using ICA, which has exciting potential in neuroscientific research. The technique is widely used in neuroscientific research and previously the impact of common pre-processing parameters was unknown.

Results have shown that TICA is sensitive to smoothing and resampling, motion correction techniques and grey matter masking. TICA can also show relatively high variability in output, even when the same data is used as input. This is driven primarily by the first brain input into the analysis, which establishes the

component map and timeseries. Despite this sensitivity, the components obtained using a broadband movie stimulus and TICA show relative *insensitivity* at visually driven regions. This supports the potential use of TICA and movies in future research. In the next chapter I will investigate the reliable signal components generated using the movie dataset and compare them to an established functional network.

Based on the findings in this chapter, BOLD data input into TICAs in the rest of this thesis will be grey matter masked, as it was shown that this increases the reliability of components in the output. Smoothing will be set at the FSL MELODIC defaults of smoothing to 5mm FHWM and resampling the data to 4mm.

Chapter 3: The reliability of ICA results across different samples and movie clips.

3.1 Introduction

In Chapter 2 I identified the optimal analysis parameters to produce robust components using BOLD data collected during movie watching. Grey matter masking helped to improve the reliability of group TICA components and resampling to a resolution of $4mm^3$ and smoothing at a level of 5mm FWHM provided the most representative components across different pre-processing parameters. This supports the use of the default MELODIC settings when using BOLD data (collected at a resolution of $3mm^3$). However, the results have only been examined within one dataset. To address this, the aim of this third chapter is to assess how robust the components are across different samples and different movie clips.

Different people show correlated neural responses when watching the same film clip (see Chapter 2, section 2.3.1; Bartels & Zeki, 2004; Hasson, 2010). Therefore, if we compare the components we obtain with one group of participants to the components we obtain with a different group of participants, the components should be the same and not be dependent on the specific members of the group. It is anticipated that the same functional ROI can be identified across different samples.

When comparing across different movie clips it is also expected that the same functional regions active during natural viewing, will be identified. The assumption that underpins the use of movie clips and TICA is that the brain is organized into a series of functionally specialised anatomical areas. Different features within the film will stimulate different areas at different times, e.g. faces will stimulate a face sensitive area whenever they appear in the film. Different film clips have features occurring at different times, e.g. the times at which faces occur in one clip are very unlikely to be the same times that faces occur in a different clip. However, the specific timings should have no impact on the segmentation that occurs. The only difference between clips that would be consequential is if as feature was present in one clip but not another, e.g. if there were no faces in a second clip.

In this chapter I test these two predictions – that the components obtained will be similar across different clips and across different groups of observers. I do this by (i) breaking the 20 min clip into two halves and running separate TICAs and by (ii) breaking the group of participants into two groups of 11 and

running separate TICAs. Results show that although spatial maps of components show some variability, the peak voxels of components are very stable across different samples and movie clips. This supports the robustness of the technique in identifying the locations of multiple regions of interest in different samples and using naturalistic movie stimuli.

3.2 General Methods

BOLD data were collected as described in Chapter 1 (methods section 1.3). Based on my results in Chapter 2, a grey matter mask was applied to each of the 22 subjects pre-processed dataset. The mask was generated by segmenting the MNI152 standard brain into grey matter, white matter and CSF and used to restrict analyses to the grey matter of the subject data.

A pipeline for assessing the similarity of the components across different permutation outputs was described in Chapter 2, the same pipeline was applied here. This pipeline was used to assess the similarity of across the different subject groups and across each of the movie clips. It was also used for comparing the similarity of components across different subject groups and when different movie clips were also used.

3.3 Across different movie clips

3.3.1 Methods

To test the reliability of the TICA output across different movie clips, the functional BOLD data for each participant was split into two halves to be used in separate TICAs. Movie clip one was the data recorded during the first 9 minutes and 50 seconds of the James Bond Skyfall film. Movie clip two was the data recording during the second 9 minutes and 50 seconds. All participants had watched the full movie clip, so when data from the two halves were compared it was a within subject comparison.

To compare the components generated using the two movie clips, the input list was permuted so that each subject brain was at the front, for input into the ICA. The rest of the input list remained the same across permutations, so only the first brain was swapped each time. This gave 44 outputs (22 for each movie clip).

Previous research has demonstrated that changing the first brain alters the ICA output (see Chapter 2). This variability was exploited to investigate the reliability of ICA components across samples.

The analyses using the shorter movie clips were restricted to 88 components, based on the number of components generated when dimensionality was left unrestricted. Before comparing across different movie clips the reliability of components using the shorter clip (half the movie) and smaller sample size (11) was checked.

3.3.2 Within-clip reliability (half the movie length)

A similarity analysis across permuted TICA outputs show that good retest reliability of components is seen with a shorter movie clip (~ ten minutes; see Figure 29). This pattern of representativeness is similar to when using the original twenty-minute movie clip (see Chapter 2, Figure 18, page 58). This, along with further analysis using movie clips only five minutes long (documented later in the chapter), provide evidence that using a movie clip as short as five minutes in length does significantly not reduce the re-test reliability of TICA outputs.

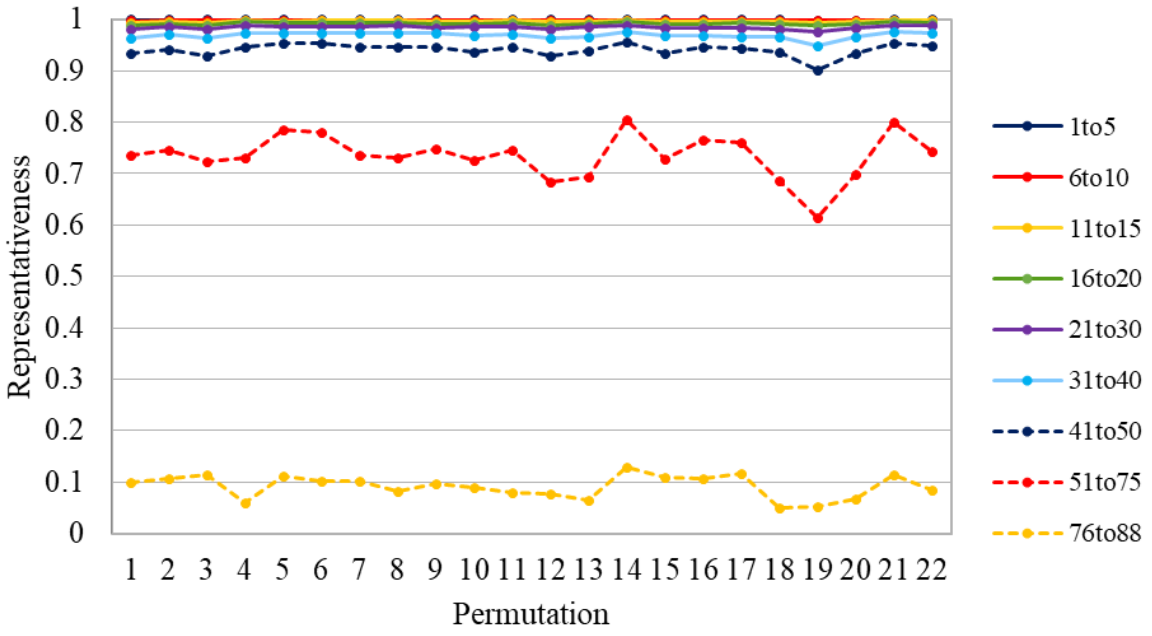

Figure 29. The reliability of ICA outputs when using a ten minute movie clip. Spatial correlation is high for 75 of the components from each of the permutations. This pattern was also seen for the other ten minute movie clip (see Appendix 4.1).

The most representative ICA output was identified for the first movie clip and the second movie clip. These outputs were used to compare the outputs across the different clips. The spatial maps of the components from the two most representative outputs were then compared. Each component in one output was compared with each component in the other and the best matches were identified for each component, in a waterfall analysis.

3.3.3 Different movie clips

Spatial correlation of matched components

When comparing between the two movie clips spatial correlation was compared only. Temporal correlation was not compared as the two different stimuli were expected to elicit different responses, timelocked to the movie clip. I was interested in whether the same functional components were being identified across outputs despite differences in the clip and timeseries.

Figure 30 shows that the best matched 20 components had a similarity metric of over 0.5. The 75 best matches had a metric of over 0.25. Smith et.al. (2009) used a Pearson's r correlation value of over 0.25 to indicate a spatial match between ICA ($p<10^{-5}$, corrected for multiple and for spatial smoothness). Therefore, a rho-metric of 0.25 signifies a spatial map within this remit. All the top matches showed correlations over 0.02, which was the threshold for the 99th percentile of matches, calculated across all component comparisons[3].

[3] As these shorter clips showed good spatial reliability across outputs, outputs generated using two different five-minute movie clips were also compared, out of interest. For both masked and unmasked data, there was good spatial correspondence between components (outputs were restricted to dimensionality of 20; see Appendix 4.3).

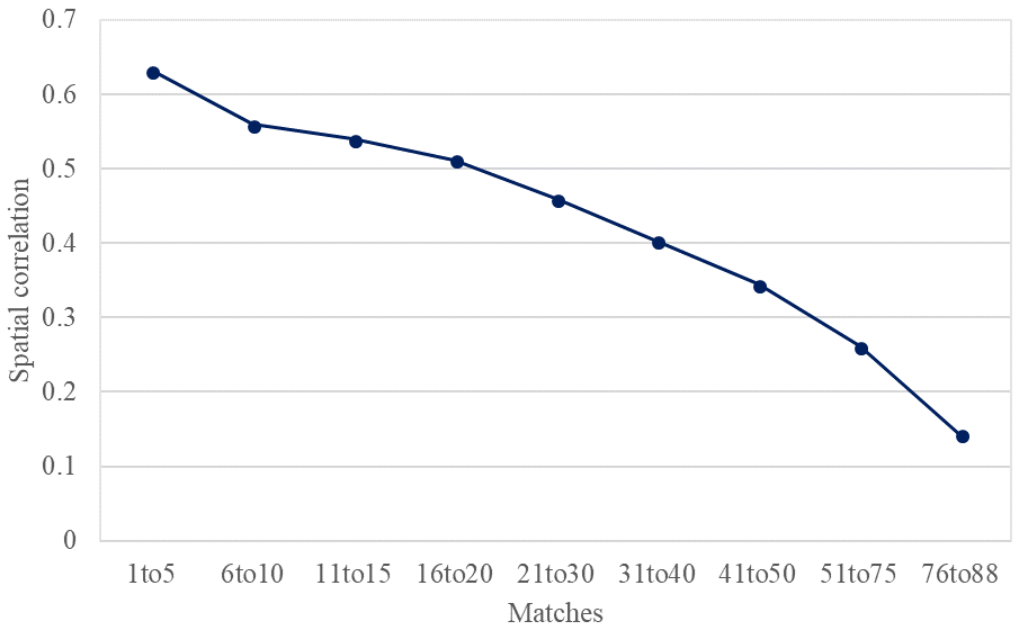

Figure 30. ICA outputs from different ten-minute movie clips show good spatial correspondence for up to 75 components. Any correlation over 0.02 was in the 99th percentile of matches, calculated across all component comparisons

A plot of the matched correlation value for each of the component generated by the first movie clip showed that very early components tended to show the highest spatial matching across outputs, and the first ~20 components tended to show good matches, relative to the rest of the output. However, overall there was no further discernable relationship between component placement and spatial matching between outputs (see Figure 31).

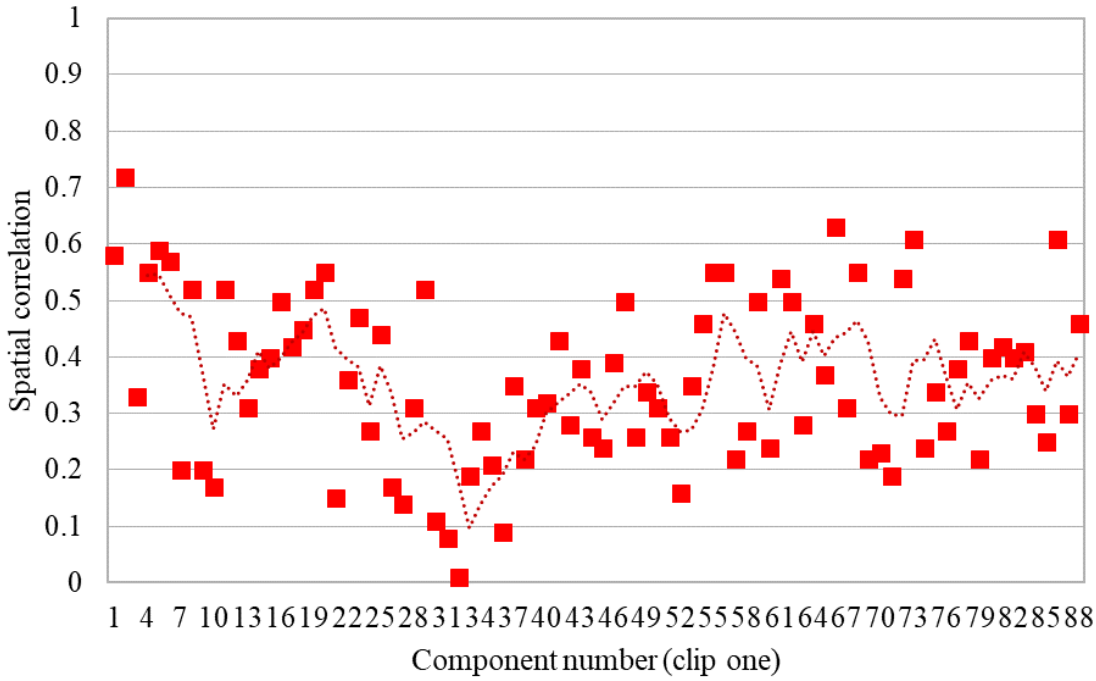

Figure 31. The first 20 components from movie clip A tended to have a well-matched spatial correlation with components in the movie clip B output (> 0.25). After this there was no correlation between component number and the matched spatial correspondence value. Dotted line = windowed mean line (4 per move).

So far it looks as though there is some spatial reliability of components generated using different movie clips, with early components looking like they tend to show slightly better robustness. A moderate positive correlation between the placement of components matched across outputs was also observed for the first 20 components in the outputs (see Figure 32). After this there was no correlation between the matched component number. In Chapter 2 it was suggested, in line with expectation, that the earlier components were more likely to be in visually responsive regions. Therefore, the matching of these early component numbers suggests that the same visual regions may be being identified across movie clips. Interestingly it also suggests that the variance explained in the data by the different functional regions/networks shows some similarity across different movie clips.

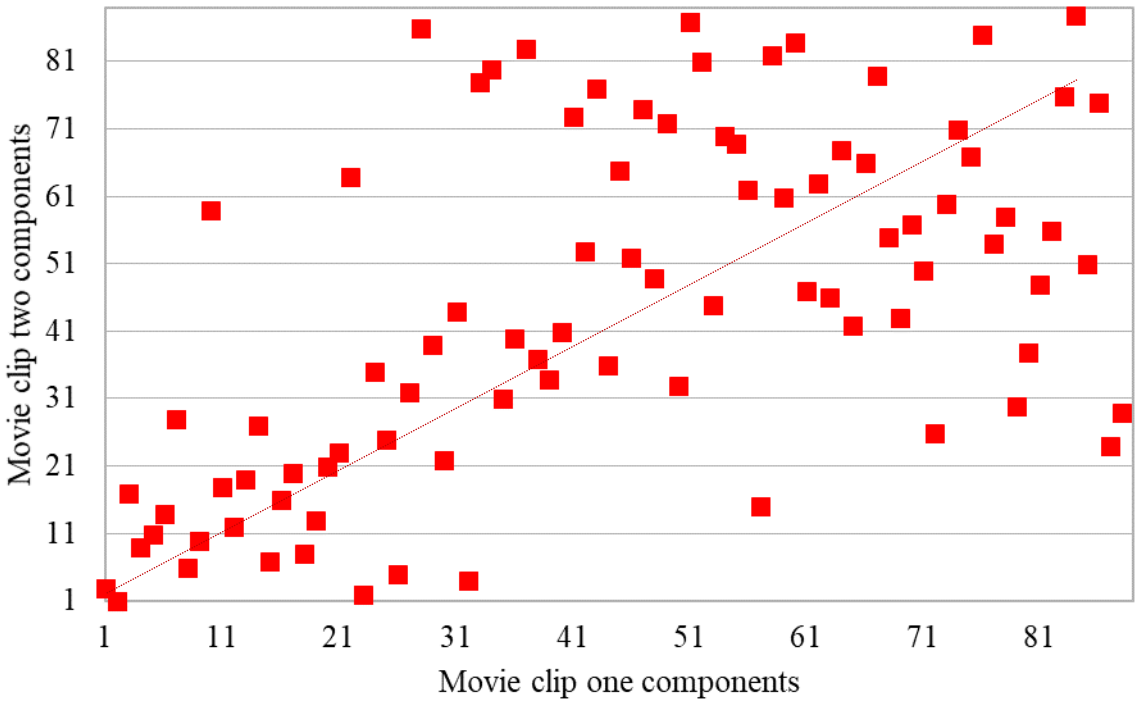

Figure 32. When the best spatially matched components were analysed in terms of component position in the TICA output, there was a good correspondence to around 40 components. After this there was no correlation between the component numbers across the outputs. Dotted line = trend line for early components matched by number.

A spatial heat map showed that components in the occipital lobe and parieto-temporal regions showed the best correspondence across the TICA outputs generated using two different movie clips (see Figure 33), as expected. There is also some evidence of reliability in more anterior regions, though as these were outside the regions of significant cross-subject BOLD correlation they will not be investigated further in this chapter. These results so far suggest that visually responsive components can be reliably identified across different movie clips, within the same sample.

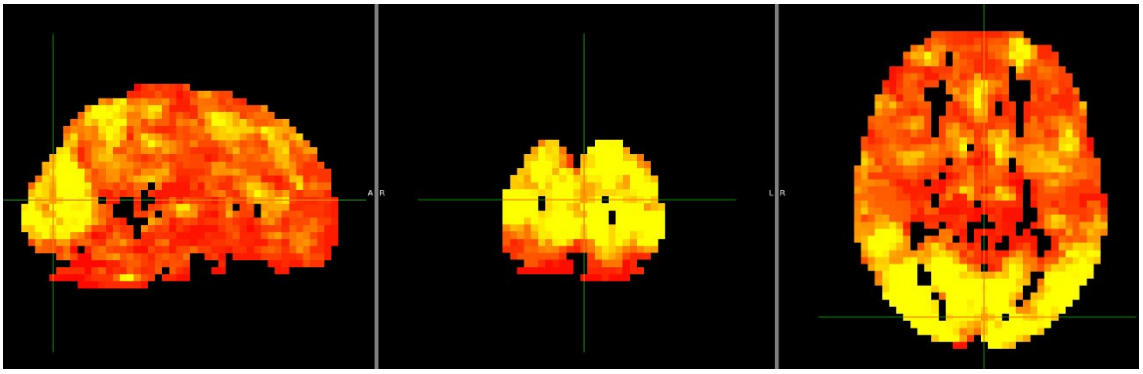

Figure 33. The regions of best spatial correspondence between the components generated by the two movie clips is focussed in the occipital lobe, moving into parietal and temporal with some correspondence in dorsolateral prefrontal cortex.

Peak voxel location

Rather than using the whole active region of the component map, the peak voxel of components could also be investigated as an alternative measure of stability across samples. The peak voxel provides a more discrete location of interest to investigate across outputs. This was investigated to further understand how the components represented each other spatially across different movie clips. The peak voxel was found for each of the components and compared across spatially matched components generated by the different movie clips (see scatterplots in Figure 34)[4]. Coordinates showed a high positive correlation between matched components across the three dimensionalities demonstrating that the peak voxels of matched components were similar, as well as the spatial correlation overall.

[4] During these analyses x-coordinates were reflected into one hemisphere (flipping the sign of the x-coordinate), as it was recognised that that that the hemisphere of the peak voxel was arbitrary in bilateral components that were matched based on high spatial correlation. This meant that deceptively large peak voxel distances across hemispheres were removed. This did not affect the unilateral component matches as components in opposite hemispheres would not have been matched using the spatial correlation values.

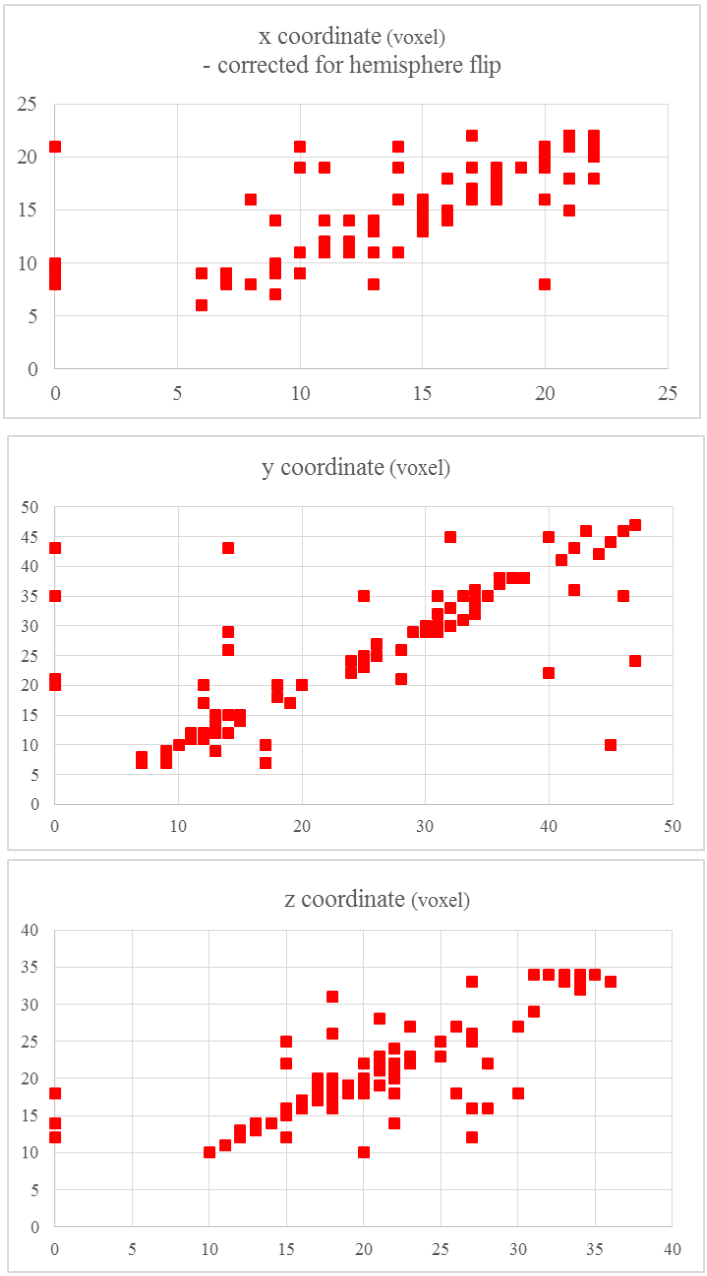

Figure 34. The coordinates of matched components across two different movie clips show strong positive correlations. The x-coordinate was corrected for hemisphere caused by bilateral component matches. Coordinates are in voxel space (resolution $4mm^3$).

The Euclidean distance between matched components was calculated and showed a distance of less than 5 $voxels^3$ (=$20mm^3$) for up to ~60 components matched across the TICAs (see Figure 35). This demonstrates a high correspondence of components across the outputs based on the peak voxels.

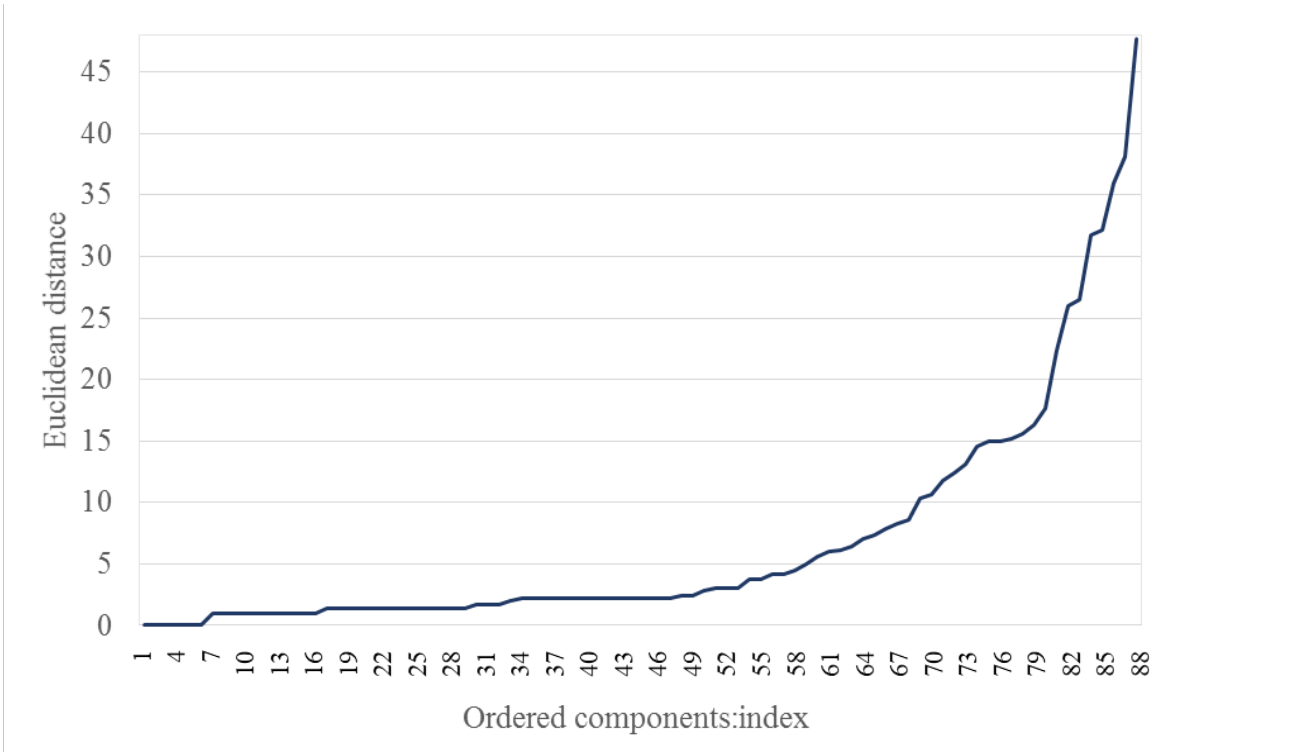

Figure 35. The Euclidean distances (units = 4mm voxels) between matched components when the same sample is used but different movie clips are watched. Distances are ordered from smallest to largest.

When the Euclidean distance between matches is plotted not in descending order but according to the component number of one of the ICA outputs, it is not the case that component number is highly correlated with matched distance; the best matches at peak voxel are distributed throughout the ICA outputs. The largest distances are not seen in the earlier components, though this may not be generalizable across datasets. Components at regions of interest including early visual regions, MT+ and V3A showed good correspondence. This was expected based on the hypothesis of functional specialization during movie watching (see Figure 36 for example matches).

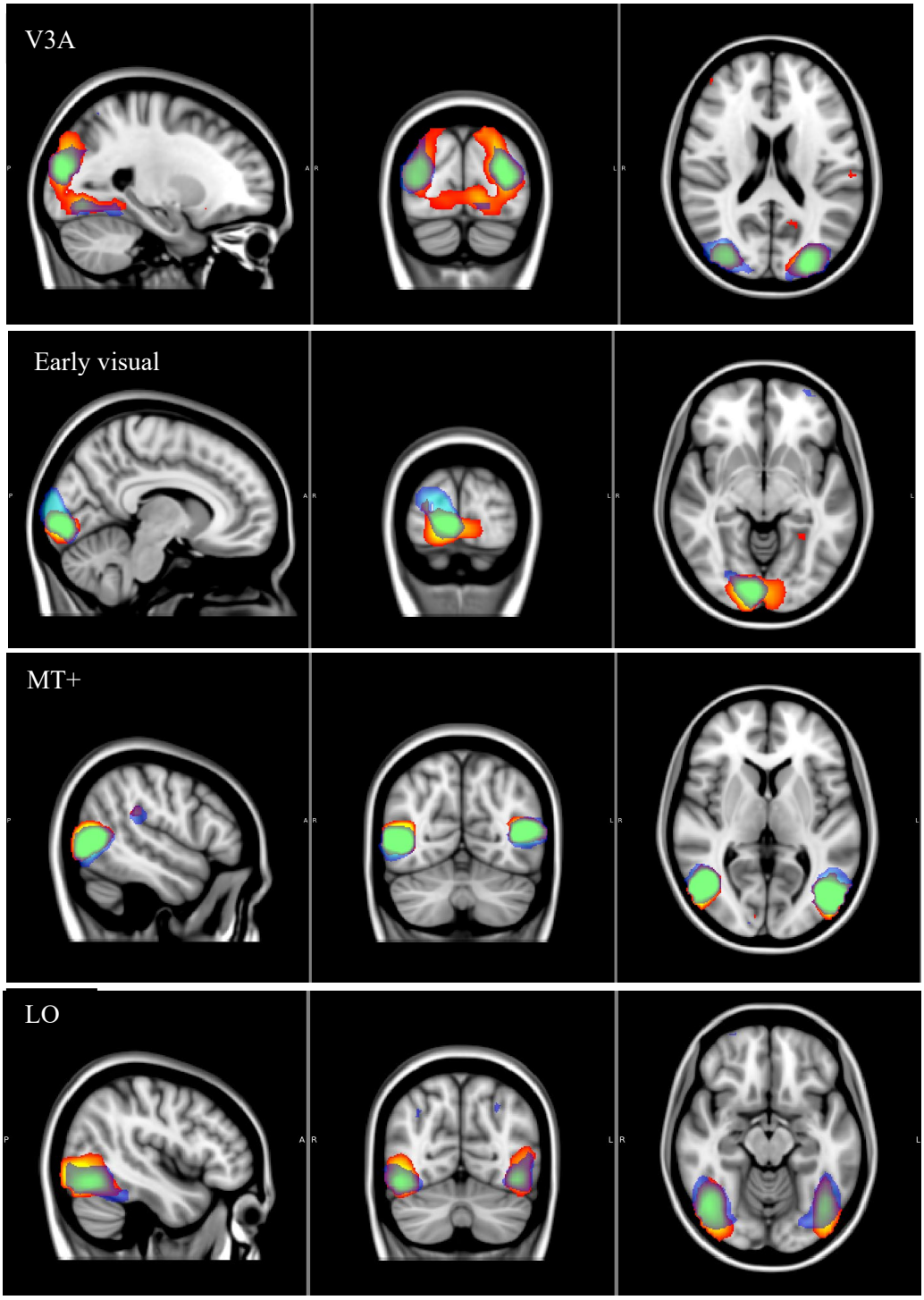

Figure 36. Four examples of matched components with good correspondence across movie clip. Orange = component from movie clip A, Blue = matched component from movie clip B, overlaid to show overlap.

3.4 Across samples

3.4.1 Methods

To investigate the sensitivity of ICA outputs to input data (different samples), the original group of 22 participants was randomly permuted and the first eleven participants formed one sample and the second eleven formed another sample. Using this method, no participants were included in both groups. This method of splitting the 22 participants was repeated ten times, resulting in ten pairs of groups, with eleven participants in each group. Each of the ten pairs could be compared for between subject differences in the TICA output.

3.4.2 Within-sample reliability (smaller sample of 11 participants)

To test the sensitivity of ICA to different input samples an original participant group of 22 was split into groups of eleven. As research in this thesis so far has examined the reliability of group ICA outputs with the whole 22 participants as the input, the re-test reliability of the smaller sample group was tested. The dimensionality of the outputs was restricted at 200. The within sample representativeness can be used as a 'baseline' for understanding the sensitivity of ICA to different samples.

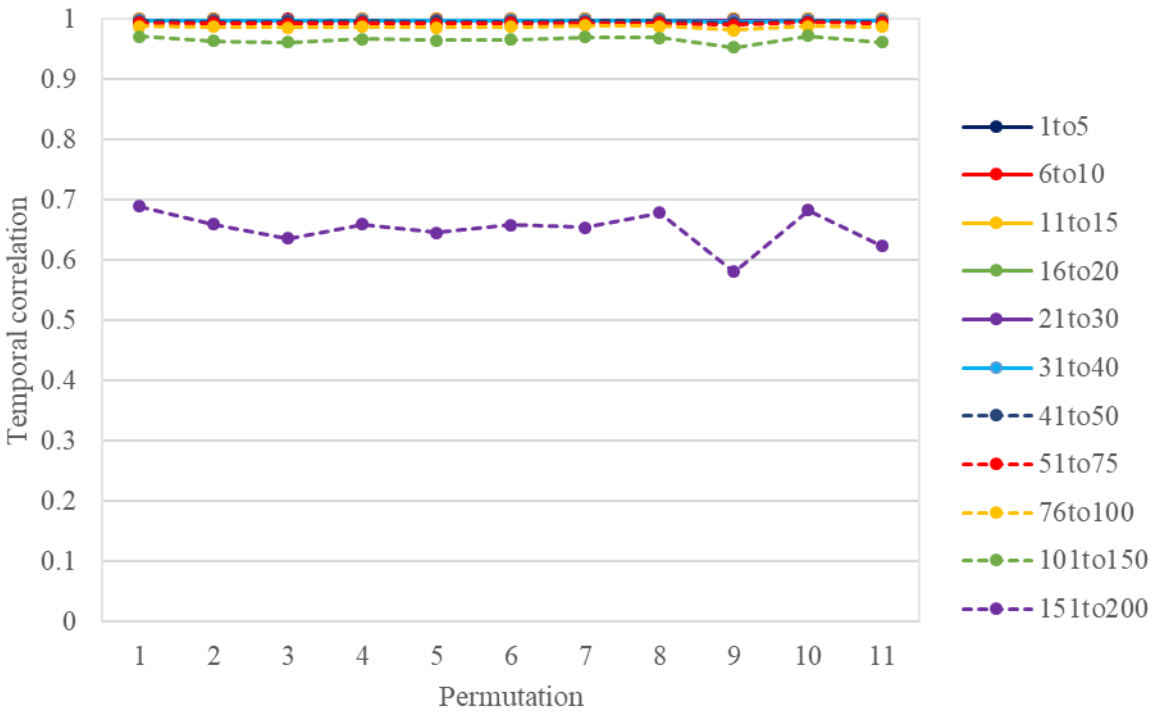

Figure 37. The representativeness of ICA analyses with 11 subjects, permutated so each input had a different first brain. Analysis shows good temporal correspondence between outputs with the use of a grey matter mask. Spatial correlations show a very similar pattern, see Appendix 4.2.

Representativeness across the outputs showed high temporal and spatial reliability for up to 150/200 components (see Figure 37 for temporal correlations). Spatial correlations showed a very similar pattern, see Appendix 4.2). This provides evidence that the reliability of group ICA does not reduce as the number of subjects in the input is reduced.

3.4.4 Different samples

Spatio-temporal correlation of matched components

Representativeness analyses show that for this twenty-minute movie clip group TICA results from different samples show a lower spatial and temporal similarity compared to a within subject comparison, as expected (compare Figure 38, Figure 39 and Figure 37). Figure 38 plots the average spatial correlation between component matches between each of the subject group comparison pairs. These data show that for the best matched 50 components there is spatial correlation of over 0.25 and over 0.2 for the best matched100

components. This is again lowered representativeness compared to the within subject group comparison (see Appendix 2).

Across different samples the temporal correlation between matched components is much higher (see Figure 39), supporting the finding that there is a temporal locking of the BOLD signal to the movie stimulus (Hasson et.al., 2010). This also supports the hypothesis that due to the functional specificity of the visually responsive regions during natural viewing, comparable components can be identified across subject groups. Lowered correlations in the spatial aspect of the components reflects individual differences that may exist between the groups.

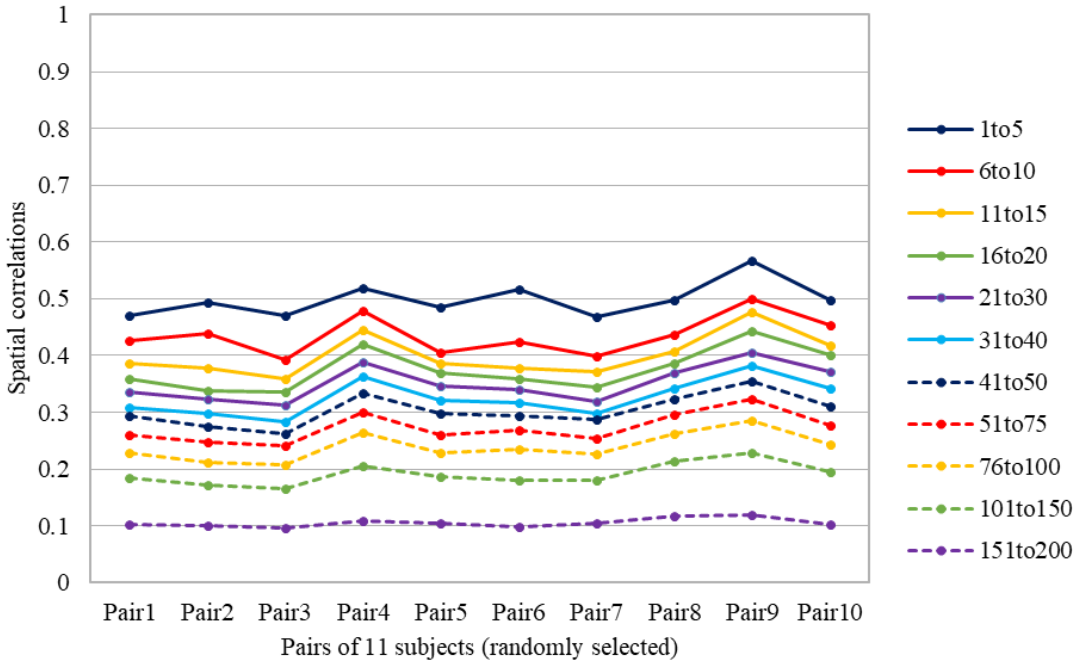

Figure 38. Spatial correspondence between different sample pairs demonstrated that up to 50 components showed a linear correlation of r> 0.25 (used as a matching threshold based on work by Smith et.al., 2009). Any spatial correlations with r>0.07 were in the top 99th percentile across all component comparisons.

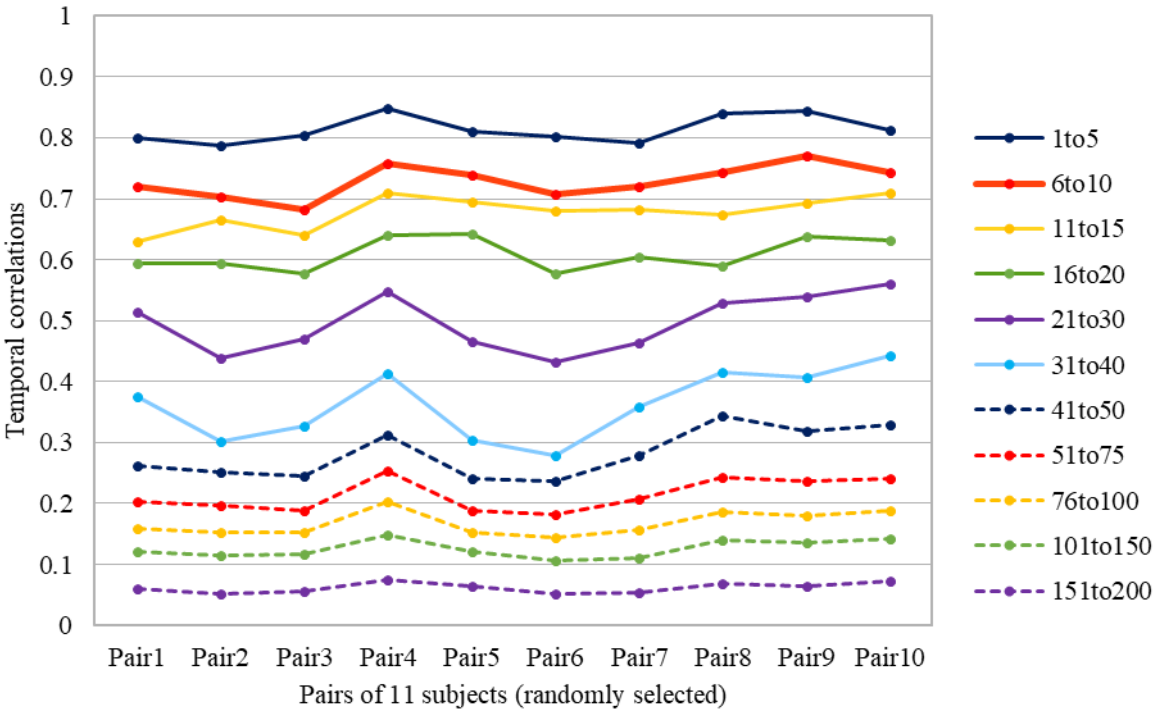

Figure 39. The temporal correlation of components across different sample pairs show temporal matches in the top 99th percentile across all correlations for up to 100 matches (r>0.15).

The similarity between the ICA outputs is again improved with the data grey matter masked than when left without masking. Representativeness is also improved when the dimensionality is restricted, compared to when it is left unrestricted. This supports a conclusion that using a grey matter mask and restricted dimensionality not only improved within sample re-test reliability, but also reliability across samples.

For each of the sample pairs a heat map of component spatio-temporal correspondence was produced to see where components correlated best across the samples. By combining the heat maps generated by matching within each pair, an overall map of probabilistic correspondence between ICAs from different samples is produced (see Figure 40). Correlated activation can be seen in early visual regions V1 – V3 in the medial occipital lobe as well as at lateral occipital regions including MT+, bilaterally (circled). Each of the pairs analyzed individually showed a distribution of increased correspondence between the components at the occipital lobe, medially and laterally.

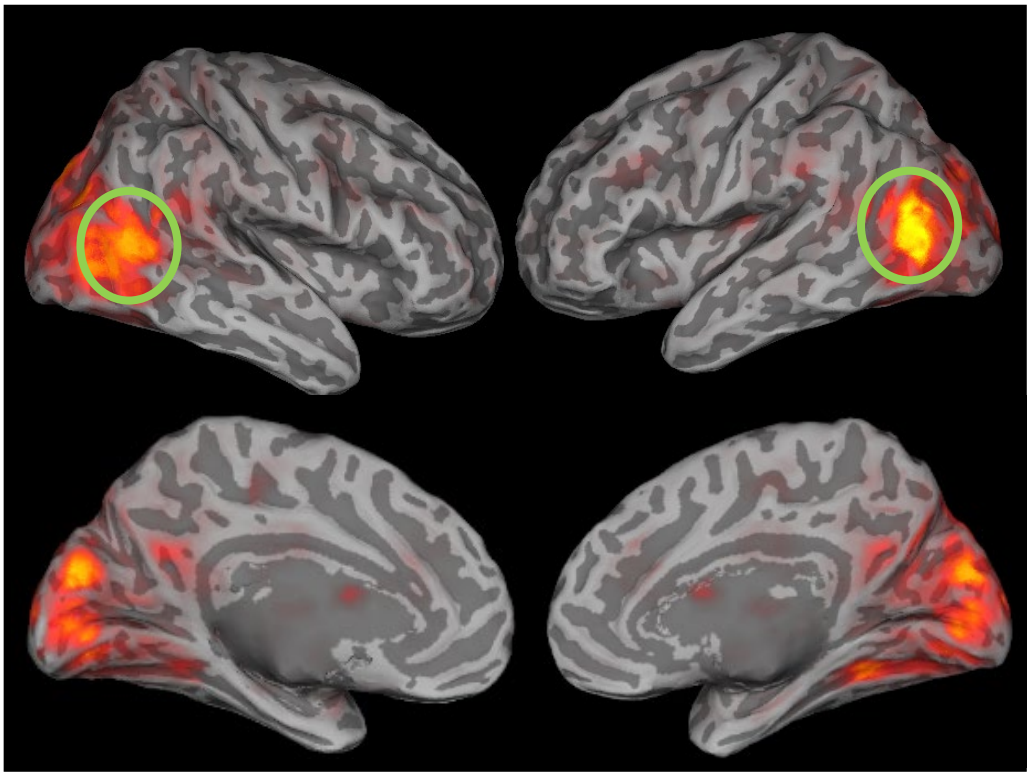

Figure 40. When all the sample pair correspondence is summed, it shows that there is increased correlation in early visual areas and lateral occipital regions, including MT compared to other regions of the cortex.

Peak voxel location

For further analysis across different samples, the peak voxels of components were compared. The peak voxel was identified for each of the components in the ICA outputs generated using the different sample groups. Components were matched across the ICA outputs for each randomized pair, based on spatial correlation and the Euclidean distance between component peaks was calculated for each matched component

pair. Figure 41 plots the average Euclidean distances between each of the 200 matched components, across each pair of between subject samples. The distances are ordered from smallest to largest distance and show that for all pairs the Euclidean distance was less than 5 voxels (units = 4mm) for up to ~170 components when the same twenty-minute movie clip was used.

As an additional comparison I also calculated the stability of peak voxels using data from two different samples *and* different movie clips. The same groups of eleven subjects were used, with pairs of subject groups having no subject overlap. One of the groups was input into TICA using the first half of the movie clip, while the other used the second half of the movie clip. This ensured that different data and subjects were generating the TICA outputs. The components resulting from different samples and different movie clips were compared within each pair. The distance between the peak voxels for each matched component was then averaged across the between subject sample pairs. Up to ~125 matched components had a Euclidean distance of less than 5 voxels^3 (units = 4mm^3; see Figure 41). This is less well matched than when the same movie clip is used, but still shows good spatial correspondence between most matched components.

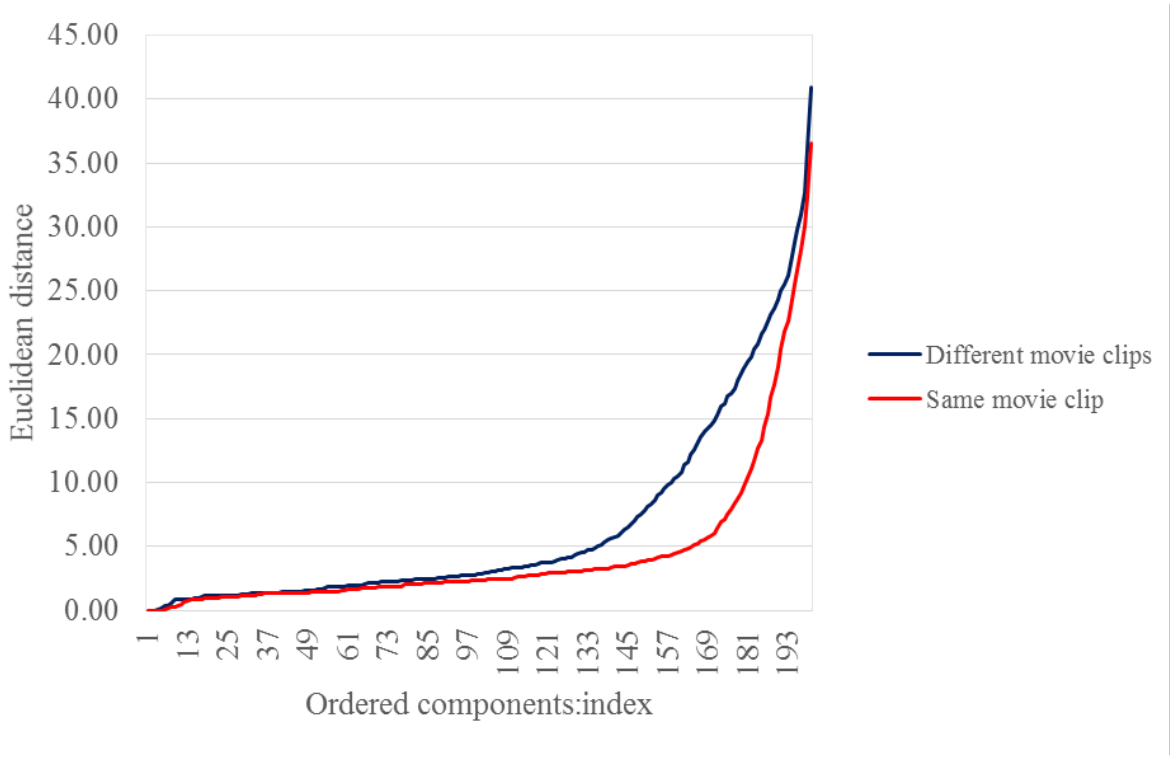

Figure 41. The Euclidean distances (units=voxels) between each of the matched components, the average across each pair of participant groups is plotted. The matched components (200 matches) are ordered from smallest to largest distance.

3.4.5 Summary

The similarity analyses in this chapter have shown that when different samples and movie clips are used, most components identified by TICA have very similar peak coordinates when matched across outputs. This demonstrates a reliability of using movies and ICA to identify regions of interest. Spatial correspondence between components is highest at visually responsive regions in the occipital lobe, across movie clips and between subject samples. Based on these findings the use of movie stimulus and TICA for identifying visual regions is supported.

So far, the components generated using smaller groups and shorter movie clips have not been compared directly. In Chapter 6 I examine the components generated using single subjects, suffice to say that ROI and networks identified at the group level can also be identified at the individual level. Therefore, it is inferred from this that components in visual ROI are also identifiable in a group of eleven participants. The next stage of this chapter will document the networks and regions of interest that can be identified in different lengths of movie clip (5, 10 and 20 minutes), and their reliability across clips. This was to add context to our results and understand how the components may differ based on different movie clip length.

3.5 Length of movie clip

3.5.1 Methods

Data from five-, ten- and twenty- minute clips of the original movie were pre-filtered as described in the methods section in Chapter 1 (section 1.3). Permutations with the first brain swapped (as per Chapter 2) were run using each of the movie lengths. In each analysis all 22 observers were included.

3.5.2 ICA outputs: spatial correspondence

When five-minute clips were used the number of components automatically generated was reduced compared to longer clips, as expected (mean with grey matter mask = 34, mean without mask = 36). For comparison of components across the different movie clip lengths, group ICA analyses were restricted at a dimensionality of 20. Reliability of components was improved across all movie clip lengths with the use of a grey matter mask (see Figure 42). Re-test reliability scores showed that on average shorter movie clips (down

to five minutes) generated more reliable components across permutations, with dimensionality set to 20 (Figure 42). However, this is likely not to hold if the movie clip was even shorter e.g. 60 seconds, due to there being not enough data.

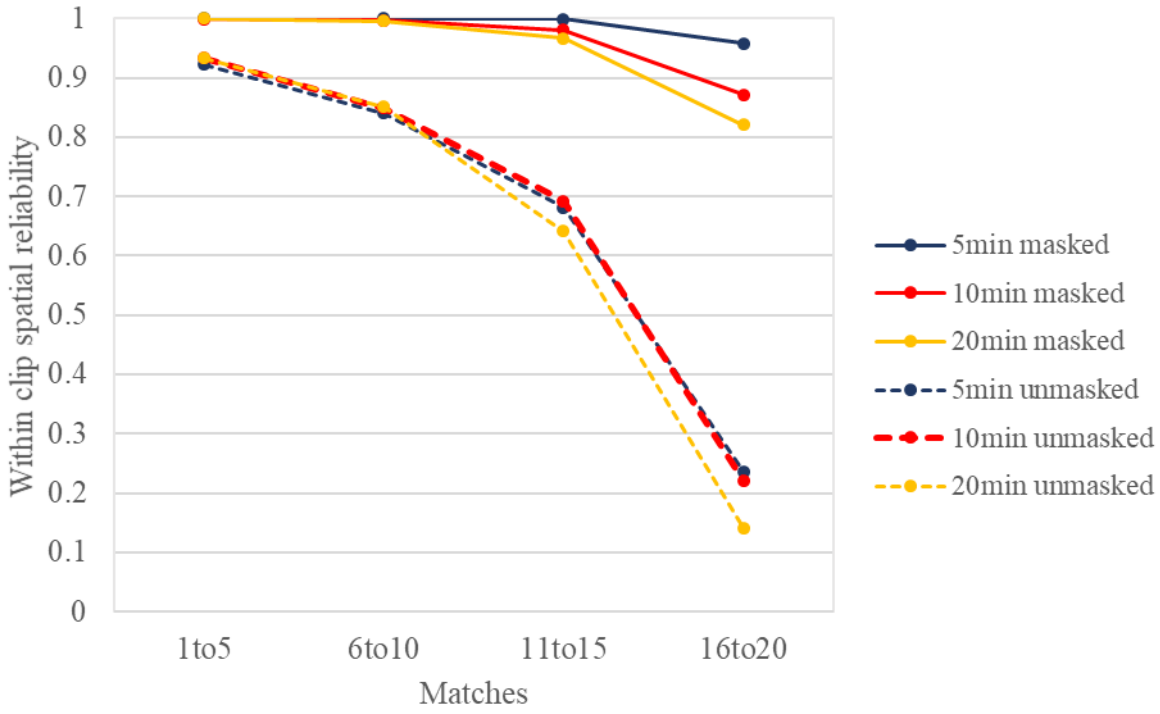

Figure 42. Across all the different length movie clips, using a grey matter mask improved the reliability of the component spatial maps. Five-minute movie clips showed slightly improved reliability with dimensionality restricted at 20.

The spatial correspondence between components generated using different length movie clips was also examined. Overall, ten and twenty-minute movie clips generated the most similar ICA components (see Figure 43). This was expected as the twenty-minute movie clip contained the ten-minute movie clip, and the five-minute movie clip (the first five-minutes and the first ten-minutes were used in the comparison). With the ten-minute movie clip being longer the similarity of the two clips is increased. All length movie clips generated similar components at a dimensionality of 20.

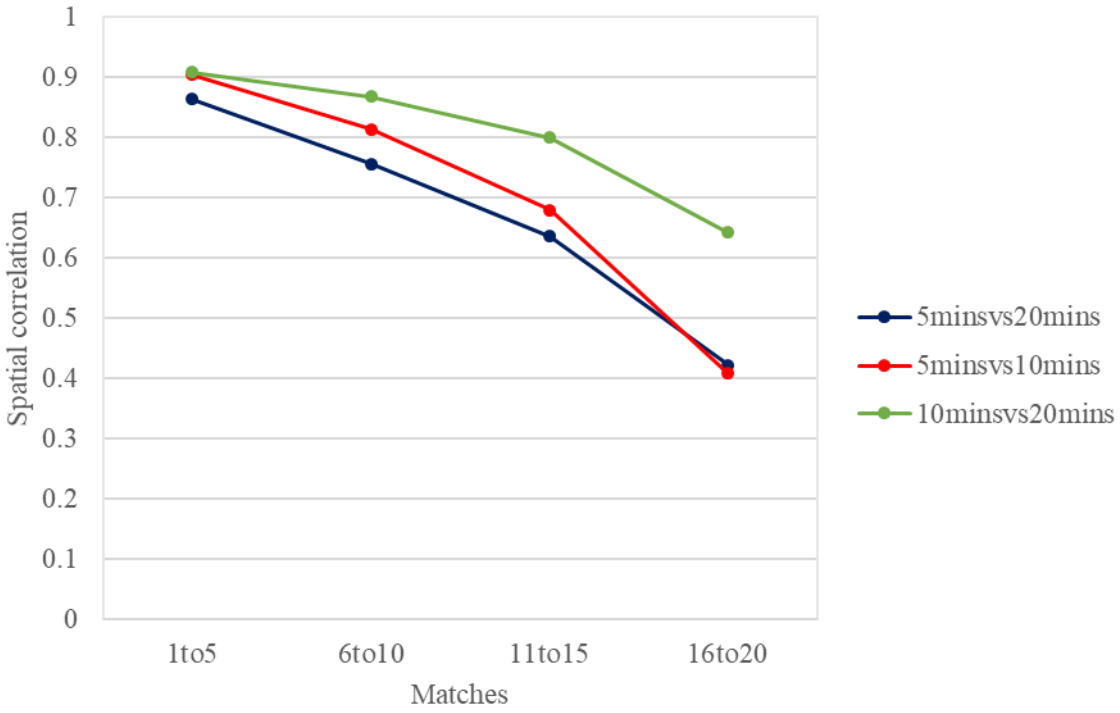

Figure 43. The spatial correspondence between components identified using different lengths of movie clip show similarity. The first five-minutes and the first ten-minutes were used for this comparison and data were grey matter masked.

It is worth noting that when eleven subjects are used with the full-length movie clip, the spatial similarity between components is slightly lower than when half the movie clip is used with all the 22 observers contributing (see Figure 44). As this is the same amount of data, this suggests that the number of observers has a larger impact on the components generated than the length of the movie clip.

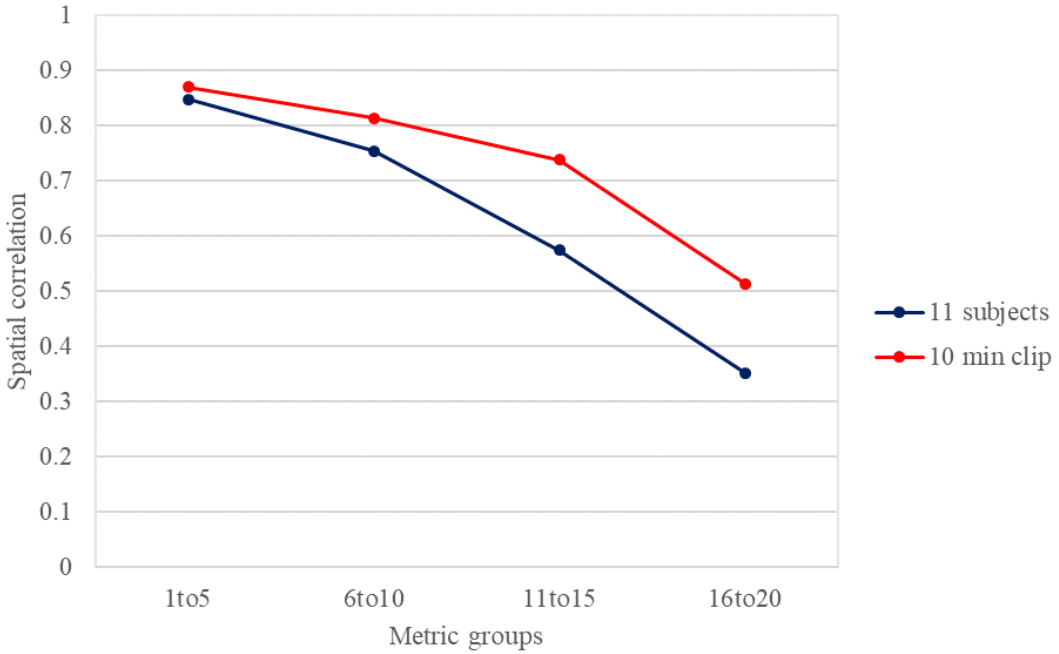

Figure 44. The spatial maps of components in most representative output using eleven participants (whole movie clip) and half of the movie clip (eleven participants) was compared to when the full movie clip and all the participants (22) were used. This was the same amount of data but showed that having fewer participants had a larger impact on the similarity of component maps.

Summary

So far, results suggest that there are robust components being identified across TICAs using different lengths of movie clip. Using a shorter movie clip has less of an effect of the component maps produced than using a lower number of participants (if the amount of data input is equivalent). Next, components were matched across the five- ten- and twenty- minute TICA outputs, based on peak voxel and spatial map correlations. Dimensionality was kept at 20. Matched components were examined to assess whether regions and networks of interest are being identified using different lengths of movie clips. Results suggest that networks of interest can be identified using movie clips down to five minutes in length.

3.5.3 Networks identified across movie lengths

Matched components across the TICA outputs using different lengths of movie clip showed clear spatial correspondence and represented a range of functional networks across the brain. Only one signal component was identified in the five-minute clip that did not show good correspondence across the different

outputs. This showed activity in the auditory cortex (peak voxels ~MNI[+/-54, -14, 12]) for the five-minute movie clip. At longer movie clips the activity in the auditory cortex was greatly reduced. It may be that the auditory cortex was initially active during the scan due to the noise of the scanner in the MRI bore. It is likely that at the beginning of the movie session, the subjects' auditory cortex was processing this noise, before habituation as the scan continued (Thompson & Spencer, 1966). The noise caused by the scanner is rhythmic with the TR (we used a TR of 2 seconds, so sounds will have been at ~0.5Hz), therefore this may have caused some correlated activity in the auditory system, across subjects.

Networks that were matched across movie clip lengths are documented below and presented in Figure 45 -Figure 49. An example of the high spatial correspondence of network components generated using different length movie clips can be seen in Figure 45B, where the network components from ten- and twenty-minute movie clips are overlaid. Other networks showed a similar level of correspondence in their spatial maps, therefore only the components generated by the five-minute clips are presented for the other networks. All the matched signal components are presented. In the next chapter (4), I compare the networks found using movie data to established functional networks found during resting state. The remaining components in the TICA outputs were noise components.

MT+, V3A and post central sulcus

The first network identified across movie clip lengths at dimensionality 20 has activation at MT+ and the post-central sulcus (Figure 45). This is a network showing functional connectivity across meta-analyses (Yeo et.al., 2011), and is thought to represent a motion processing pathway (Culham, He, Dukelow & Verstraten, 2001).

MT+, V3A and post-central sulcus

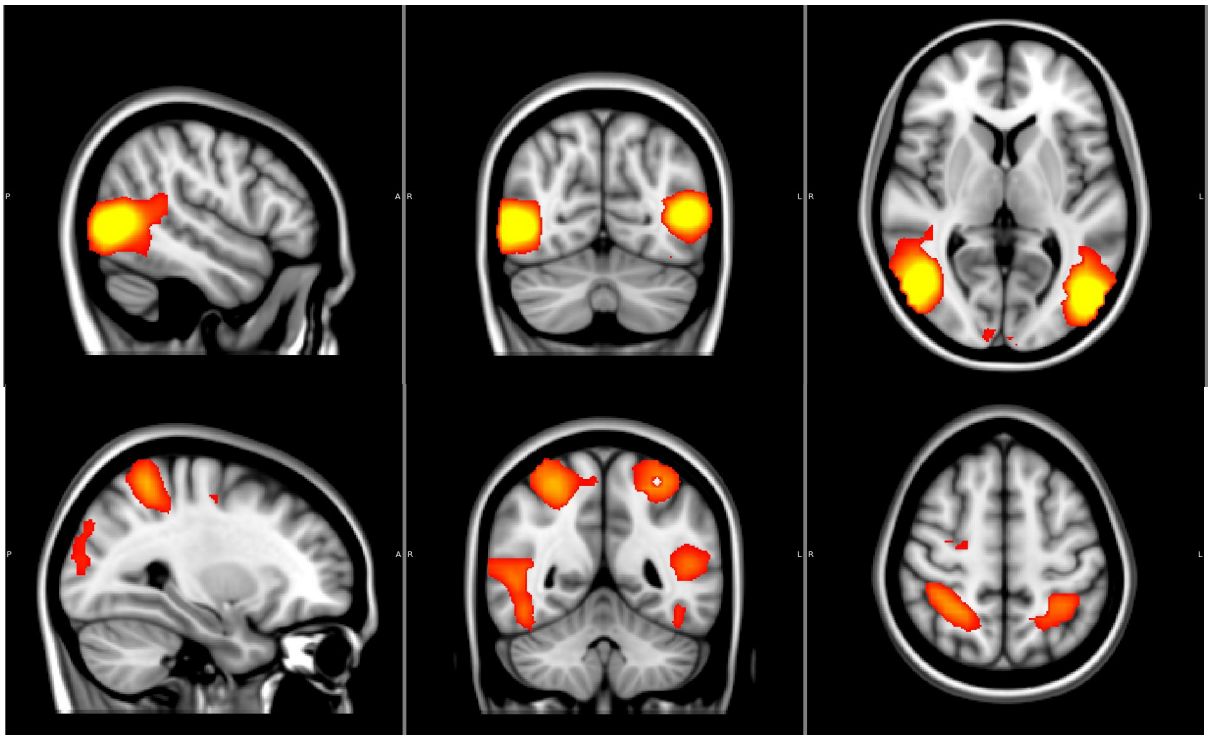

Motion Network: Overlaid different movie clip lengths

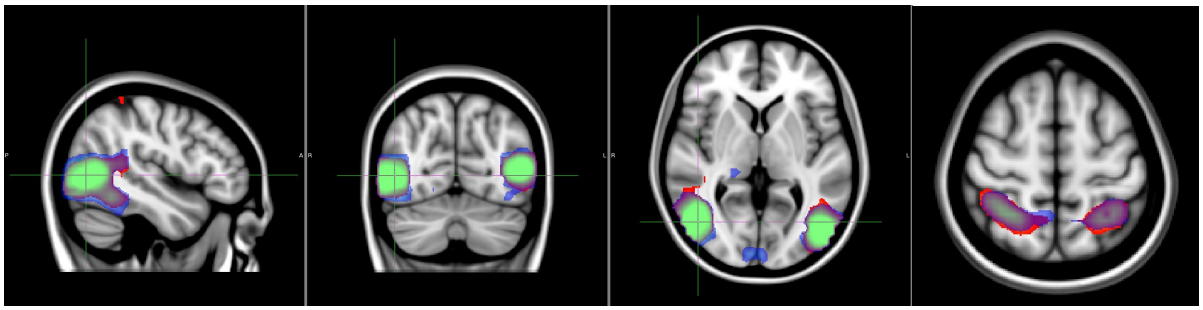

Figure 45. (A) A network including MT+ and the postcentral gyrus bilaterally was identified for all of the movie clip lengths, showing good correspondence when different length clips were used (see B). These regions have shown functional connectivity in large meta-analyses (e.g. Yeo et.al., 2009) and are understood to constitute an action and motion pathway (Culham et.al., 2001).

V3A, V6 and inferior occipital

A second network covered motion region V3A, extending bilaterally to dorsal regions V6 and towards the post central sulcus (Figure 46). As part of this network bilateral regions were active in the inferior medial occipital lobe (putative V4). This was a network that lay at the front of the TICA outputs, and therefore

described most varience in the data. This network may represent functional connectivity during natural viewing, processing complex scenes across regions with different functional specificity. Research has suggested different but parrallel roles for motion regions MT and V6 (Pitzalis et.al., 2013), with V6 receiving information from area V3A. This network supports this view as it does not include MT+ regions but demonstrates functional connectivity between motion responsive V6 and V3A. The inclusion of V4 regions in this network may be due to colour-luminance changes at the edge of moving objects (Vinberg & Grill-Spector, 2008). This network organisation suggests a closer functional relationship between V4 to motion areas V3A and V6 during natural viewing, supporting findings that V4 has low direct anatomical connections with MT+ (Prados & Deriche-Olivier, 2007). The activity in this inferior occipital region should be further validated to rule out the potentially modulating effect of venous eclipse (Winawer, Horiguchi, Sayres, Amano & Wandell, 2010).

V3A, V6 and inferior occipital network

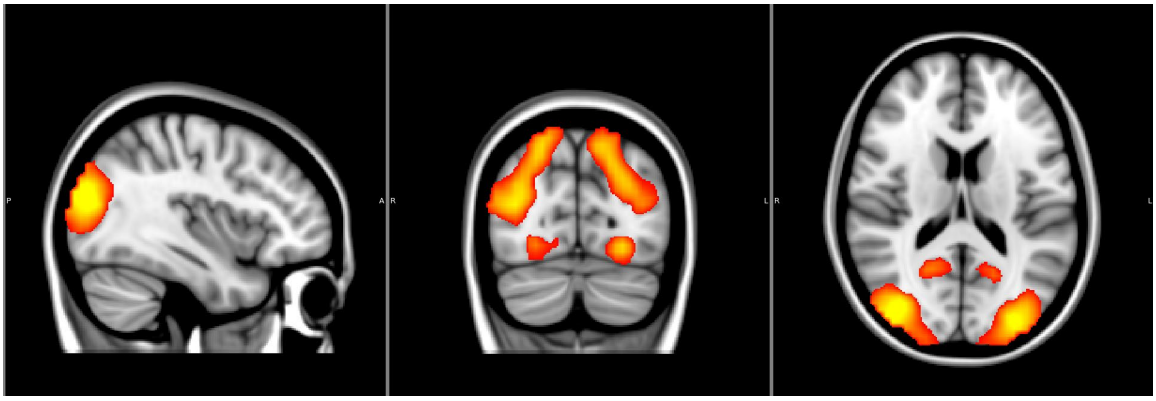

Figure 46. Activity in occipital lobe extending parietally past V3A and V6 regions show anti-correlated activity with lateral occipital-temporal regions.

Default mode network (DMN)

A network representing the DMN was identified in the five-minute movie clip, with the activity at medial parietal lobe, the lateral parietal lobes and the medial prefrontal cortex (Figure 47). The identification of the default mode is interesting as TICA finds regions that show timesereies correaltion across subjects. The DMN was not identified in longer movie clips, as a whole network. The mPFC and medial parietal regions were identified within two separate components in the twenty minute clip, for example. Previous research has

shown reliable responses to naturalistic stimulation in regions of the DMN (e.g. Jääskeläinen et.al., 2008; Hasson et.al., 2008). This could be further investigated using movies and TICA as there has been much speculation abut the possible functionas of the DMN and these findings dispute other research in the field showing low / below baseline responses in the DMN during natural viewing (e.g Golland et.al., 2006).

Default mode network

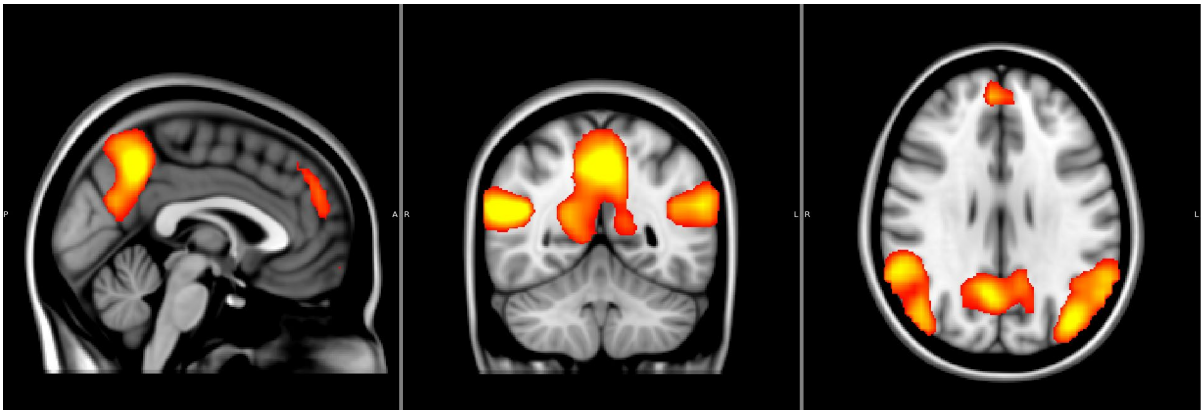

Figure 47. Activity corresponding to the default mode network were identified across movie lengths. Anti-correlated activity was seen at the post-central sulcus.

A component was also identified showing anti-correlated activity between the medial parietal portion of the DMN and MT+ regions, bilaterally (Figure 48). This is interesting as it suggests that the activity in the DMN may be functionally responsive to regions processing the movie. This may be a reason why activity is correlated across subjects in DMN regions; the acitivity may be a biproduct of cross-subject visually responsive activity. However, significant cross-subject correlations were not identified in DMN regions in a voxel-by-voxel correlation (see Chapter 2, section 2.3.1, page 31), which was calculated across a five-minute clip. This suggests that the identification of source signals in the data using TICA can pull out anti-correlations across DMN and visual regions, which that BOLD timeseries correlations are not sensitive enough to find.

Anti-correlated MT+ and medial parietal DMN

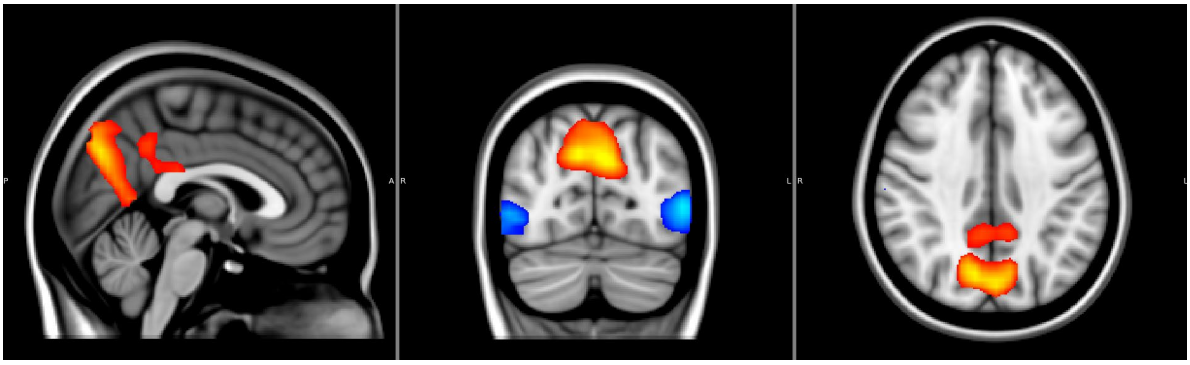

Figure 48. A network had activation in the medial parietal portion of the DMN, that was anti-correlated with the MT+ areas, bilaterally.

Somatosensory

A network was identified with activstion covering the central sulcus bilaterally, the supplemetary motor area, sensory motor cortex and medial regions. The central sulcus separates the primary motor cortex at the pre-central gyrus and the somatosensory cortex at the post-central gyrus. Activity here was not significantly correlated across subjects (see Chapter 2, section) or in previous research using movie stimuli (Hasson, Malach & Heeger, 2010). This functional network has been associated with action perception and execution and proprioceptive processing (Skipper, Goldin-Meadow, Nusbaum & Small, 2009; Smith et.al, 2009).

Somatosensory network

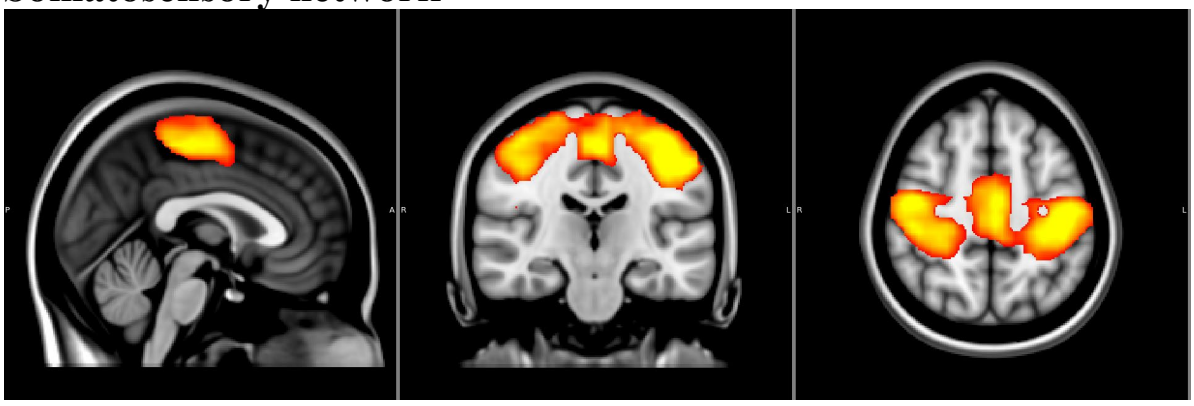

Figure 49. A network focussed at the central sulcus was identified across the different length movie clips, with the dimensionality set at 20.

Interestingly, another component had activation bilaterally at the post-central gyrus associated with somatosensory processing (MNI ~[+-58, -38, 36]; Iwamura, 1998).). The component also showed activation

and lateral occipital regions at expected MT+ (MNI[-/+54, -66, 0]). These regions are known to be functionally connected based on meta-analyses (e.g. Yeo et.al., 2011; Choi, Yeo, & Buckner, 2012). Research in the monkey literature has also found that the inferior parietal gyrus has connections to region MST (Boussaoud, Ungerleider & Desimone, 1990). Using naturalistic movies, activity at the post-central sulcus was associated with delicate human movements, suggesting a role for the region in action perception (Hasson et.al., 2004).

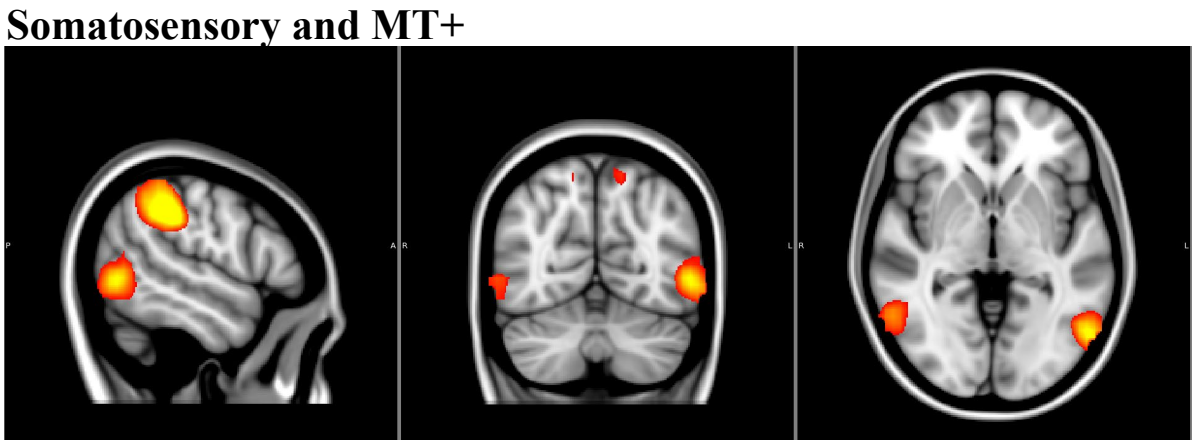

Figure 50. (A) A network showing activity at anterior MT+ regions (potentially MST) was identified, with activity at the post-central gyrus. This functional network may play a role in action perception during natural viewing

Occipital networks

Two occipital components were identified across movie clips. The first lay in medial regions, covering early visual regions V1, V2 and V3 (Figure 51). The second component covered extrastriate regions at more posterior locations of the occipital lobe (Figure 52). Both components look like visual networks identified by Smith et.al., (2009), using resting state data. The next chapter will compare components generated by the movie with these established resting state networks.

Medial occipital network

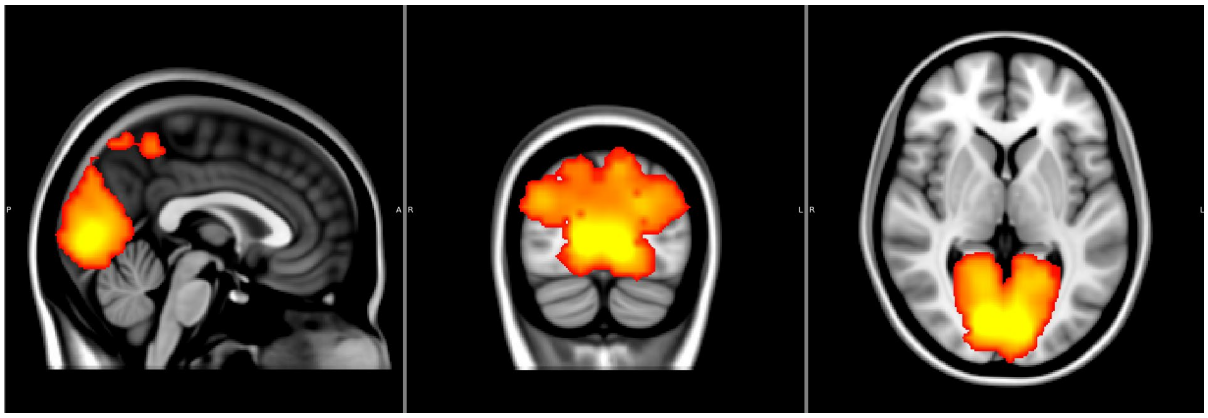

Figure 51. A network with activity in early occipital regions was identified. Interestingly this shows anti-correlated activity at MT+ regions. Peak voxels lie at the calcrine sulcus bilaterally, and activity extends anteriorly in the medial occipital lobe towards V4 regions

Posterior occipital network

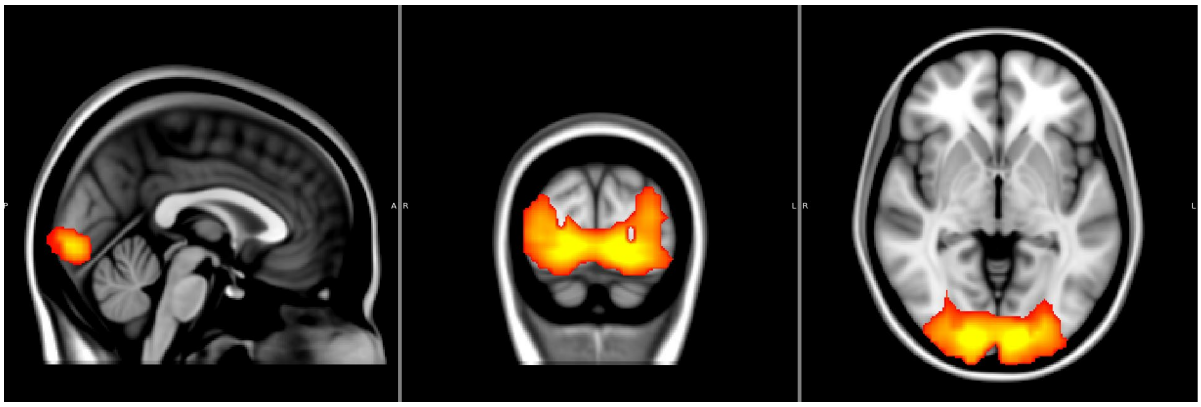

Figure 52. A visual network focussed at the posterior occipital lobe was identified across the different length clips.

Lateralised fronto-parietal

Lateralised activity was seen across movie clips (Figure 53) in the parietal and frontal lobes. These are networks that has been identified in resting state studies (e.g. Smith et.al., 2009, discussed in next chapter (5). They have been associated with several cognition and language processes including memory and semantics. There was no speech audiable in the movie clip we showed to the subjects, therefore any language processing will have been caused by visual cues, such as the actors mouths moving and body language cues. The neural response to language cues (mouth movements and gestures) has been localised to motor cortices (Skipper

et.al., 2009), restricted to ROI; this could be further investigated with natural stimuli and a whole brain analysis.

Lateralised networks

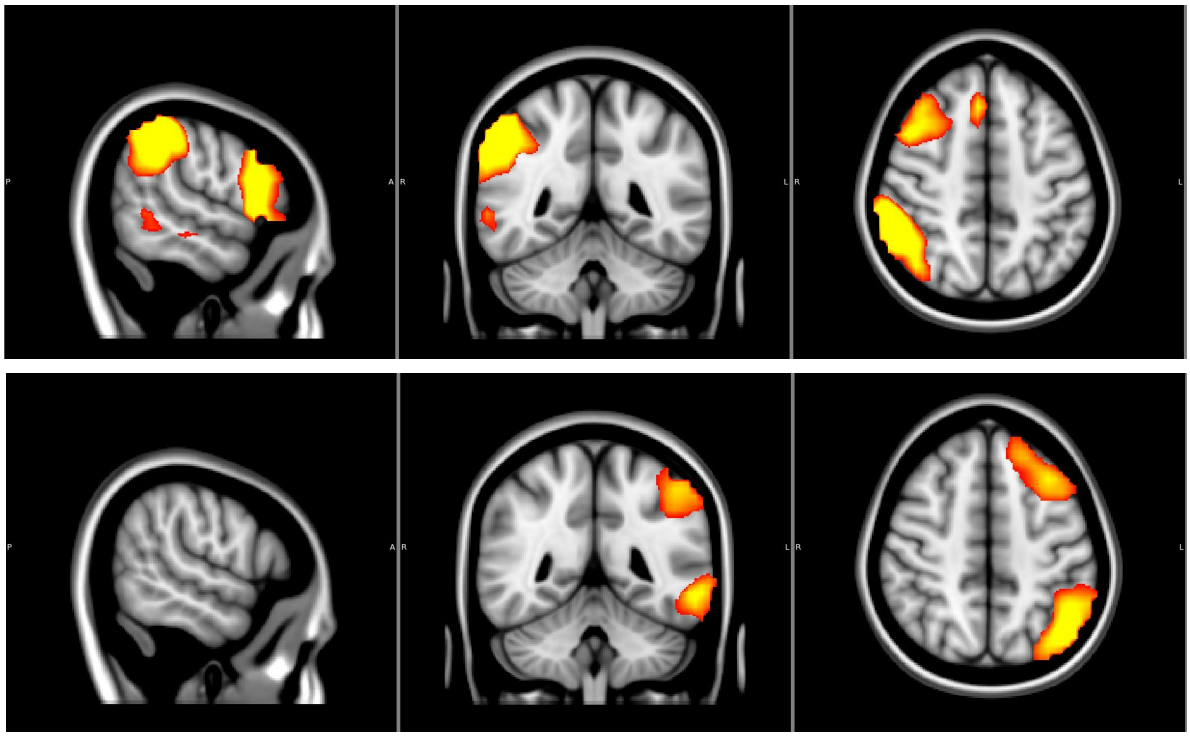

Figure 53. Two of the networks were lateralised, showing activity at left/right parietal, occipital-temporal and frontal areas.

Temporal and frontal regions

The final component matched across subjects showed activation at the posterior temporal lobe (MNI ~[+/- 58, -50, 4]) and in the inferior frontal cortex (DLPFC; MNI ~[+/-50, 10, 28]). These regions have been associated with semantic processing (e.g. Manenti, Cappa, Rossini & Miniussi, 2008; Whitney, Kirk, O'Sullivan, Lambon Ralph & Jefferies 2010).

Temporal and frontal network

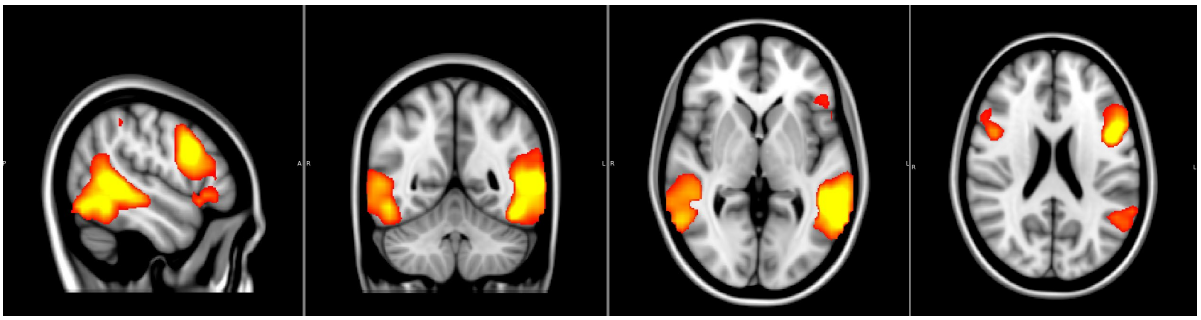

Figure 54. A network showed posterior temporal activity with the inferior frontal cortex, bilaterally. It is speculated that this network could have a role in semantic processing during movie watching.

3.6 Summary: Chapter 3

These results show that similar components can be identified across different movie clips and different samples. Reliable components are focused in visually responsive regions in the occipital lobe, medially and extending laterally and temporally. Matches across outputs using different samples show good correspondence at these regions of interest. These findings support the findings of Bartels and Zeki (e.g. 2004) and the theory that functional specialization persists during natural viewing of complex stimuli.

Using different length movie clips, a range of neural networks can also be reliably identified. Although different movie clips can produce similar components, what is still not understood is how the components generated by watching a movie correspond with established networks identified using resting state. Therefore, in the next chapter I compare my results to networks identified by Smith et.al., (2009), which represent known functional networks in the human brain. If these networks can be identified, this is another benefit of the technique as it means visual regions and functional networks in the brain can be identified using one movie clip.

Chapter 4: Comparing group ICA components to established resting state networks

4.1 Introduction

In Chapter 2 a thorough investigation into the sensitivity of TICA to analysis parameters showed some sensitivity to analysis parameters, but stability of components in visual regions across pre-processing options. Based on the findings a pipeline was developed with the aim of maximizing the reliability of ICA outputs using functional MRI data recording during movie watching. In Chapter 3 the stability of results was assessed across different samples and movie clips was confirmed. Components identified across samples showed stability in peak voxel and spatial correspondence, especially in occipital regions. In Chapter 3 components that are reliable across different movie clips look as though they represent a range of neural networks.

Although having a technique that produces reliable results is important for direct comparison across datasets, this does not mean the output is valid or useful. Unreliable techniques implicitly demonstrate that not all the produced data can be valid, however reliable results may be based on a consistent, yet invalid measurement pipeline. Unsupervised machine learning (i.e. here, ICA) classifies the data without a validation of class/cluster labels. Therefore, the most reliable components in the ICA outputs need to be examined to see if they represent known visual regions and networks of interest.

This chapter will compare the TICA components generated using movie stimuli with functional networks identified using RS data, specifically those documented by Smith et.al. (2009). Smith identified ten functional networks thought to represent different neural pathways processing visual, somatosensory and auditory information as well as higher executive functions and default mode systems. These networks were very similar to those found by other research groups using the ICA and RS (Beckmann, DeLuca, Devlin & Smith, 2005; Damoiseaux et.al., 2006) and therefore can be used as examples of established RSN.

Functional networks in the brain are usually identified based on spontaneous neural signals recorded during resting state (RS; e.g. Damoiseaux et.al., 2006; Lowe, Dzemidzic, Lurito, Mathews & Phillips, 2000; Brookes et.al., 2011). If the components generated using a movie stimulus are comparable to established RS

networks (RSN), this both validates the components identified using movies and provides an opportunity to examine the functional organization of these networks during natural viewing.

ICA analyses using RS data cannot assume temporal similarity across subjects in functional networks. This means components represent networks of neural regions that show functional correlation for each participant, however they do not represent any correlation across subjects. When watching a movie stimulus there is evidence of temporal locking across participants (e.g. see Chapter Two; Hasson et.al., 2010) and components identified using TICA represent functional correlation within each subject brain and across subjects. If the functional networks usually identified using RS can also identified using a TICA analysis it will suggest that these networks are timelocked across subjects during natural viewing.

The first aim of this chapter was to determine whether any of the functional networks identified using resting state can be identified across subjects during natural viewing. Results show good correspondence between all cerebral RSN and the movie components. This gives us some insight into the functional correspondence in regions across subjects during natural viewing, as well as the functional organization of the cortex. It also opens the opportunity for using movie watching as an alternative to RS that may be a preferential scanning experience for participants.

Smith et.al.'s paper also found that as dimensionality was increased from 20 to70, networks showed some 'splitting', with components representing sub-regions of networks identified at dimensionality 20. To build on these findings, the second aim of this chapter was to start to investigate and document how components identified at a low dimensionality split as dimensionality is increased. Results show that components split to represent sub-regions of the original component, as dimensionality is increased. However, this process is not neat but shows oscillation across similar dimensionalities.

4.2 Methods

Smith's resting state networks were initially identified at dimensionality 20, therefore ICAs using the movie data were conducted at the same dimensionality for a direct comparison. Subject data were grey matter masked, based on findings in Chapter 2. Data were smoothed at FWHM 5mm (MELODIC default), the same resolution used by Smith et.al (2009), who's component maps were used in comparison analyses.

Spatial correlation values were calculated between the unthresholded images of the movie ICA components and nine of Smith's networks (the cerebellar network not included as outside of the grey matter mask). A threshold of r = 0.25 (Pearson; $P<10^{-5}$,corrected for multiple comparisons; Worsley, Marrett, Neelin & Evans, 1992) was used as the minimum correlation when defining matches between Smith's maps and the movie data (Marrett, Neelin & Evans, 1992). As another complimentary analysis, component maps were thresholded at z-score of 3 and the overlap between components and Smith's networks was calculated.

To investigate the effect of dimensionality on the components, TICAs were conducted at increasing dimensionalities (from 20 to 100). The spatial correlation between the components at dimensionality 20 and components generated at each of the dimensionalities was calculated directly. The best correlated components across dimensionalities were examined to compare (a) The location of the peak voxel of activity (b) The component spatial map.

If the location of peak activation remains stable across the dimensionalities between matched components, this suggests that similar components are being identified across dimensionalities. If the peak activation changes it suggests that a reorganization of components is taking place, with different sub-regions being identified with different peak voxels. A size comparison of the spatial maps of components matched across dimensionalities was also conducted. It was expected that as dimensionality was increased the size of components will reduce overall, as the TICA splits the data into smaller functional parts.

4.3 Results

Spatial correlations with a movie component over the significance threshold of r = 0.25 were found for each of the nine networks identified by Smith et.al. The spatial correlations of the best matched components at dimensionality 20 are presented in Table 4. The three networks best represented in the movie data were two visual networks and a sensory-motor network. The three networks showing the best spatial correlation with movie components at a dimensionality of 20 also showed the most overlap (63%, 61% and 55% of Smith's network was overlapped by the matched component, respectively). When overlap was examined at dimensionality seventy, there was most overlap (%) for the three visual networks (60%, 53% and 52%, respectively).

Table 4. The correlation between the best matched component from the Movie ICA outputs and Smith et.al.'s network using RSN data. Networks are ordered in descending order of correlation values (r).

Correlation of top movie component match (r; Dimensionality 20)	**Association**
0.71	VISUAL (1)
0.68	VISUAL (2)
0.53	SENSORIMOTOR
0.51	FRONTOPARIETAL (LH)
0.48	FRONTOPARIETAL (RH)
0.46	VISUAL (3)
0.38	AUDITORY
0.38	EXECUTIVE FUNCTION
0.37	DMN
N/A (grey matter masked)	CEREBELLUM

Both the percentage overlap and the spatial correlation demonstrate that visual and sensorimotor networks are well represented in the movie ICA outputs. All networks show component matches over the correlation threshold. Grey matter masking improved the spatial matching overall when compared with component matches from unmasked ICAs (average across all networks r = 0.5 for masked data and 0.46 for unmasked; average correlation with visual networks was r = 0.62 for masked data, and 0.56 for unmasked). This supports the earlier conclusion that grey matter masking is beneficial when using ICA and movies for identifying networks and regions of interest reliably. Although TICA showed significant spatial correlations with the networks, using a CICA produced components that showed a higher correlation overall with Smith's networks (average across all networks with masked data r = 0.64, compared with 0.5). This was expected as Smith also used a CICA analysis, which does not assume temporal correlations across subjects.

The best matched component to each network from the grey matter masked TICA output at dimensionality twenty is displayed below. Results show how movies can be used to identify the same networks of interest as resting state.

A size analysis of components matched across dimensionalities confirmed a negative correlation between component size and dimensionalities, with higher dimensionalities producing smaller components overall. However, the size of the matched components oscillated across dimensionalities (see Appendix 4.1 for size plotted for components matched by highest spatial correlation to the three visual networks), suggesting that components are not remaining stable nor are splitting neatly at a certain dimensionality, but are showing some variation in the organization of components identified across different dimensionalities. The size oscillations are particularly present when the peak voxel of spatially matched components shows movement, demonstrating that components are reorganizing with different dimensionalities.

4.3.1 Visual network 1

Smith's first visual network covers medial regions of the occipital lobe, including the primary visual cortex (Figure 55, top). It is well represented in the movie data output (Figure 55, bottom).

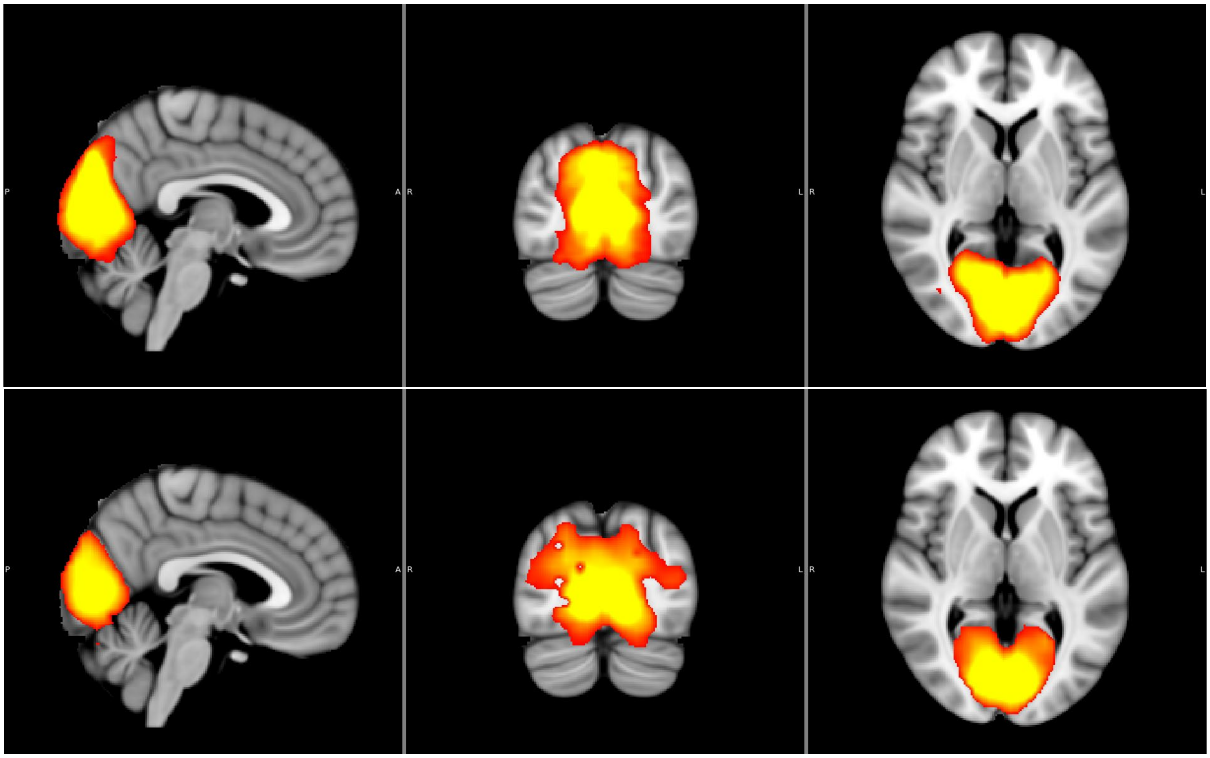

Figure 55. Smith et.al.'s first visual network (top) and the matched component from a TICA using functional data collected during natural viewing (bottom). The spatial correlation between these components is 0.71 (r).

The peak voxels of the network component were at medial regions MNI [5, -78, 0] in the right hemisphere and MNI [-11, -78, 4] in the left. Across dimensionalities the spatially matched components showed some movement of the peak voxel after dimensionality 44 (see Figure 56 for a plot of peak voxel position; lateralized peak voxels were used in the hemisphere that had the highest peak in the seed component). This suggests that components are altering their organization as dimensionality increases and the best matches are representing different regions of the original component.

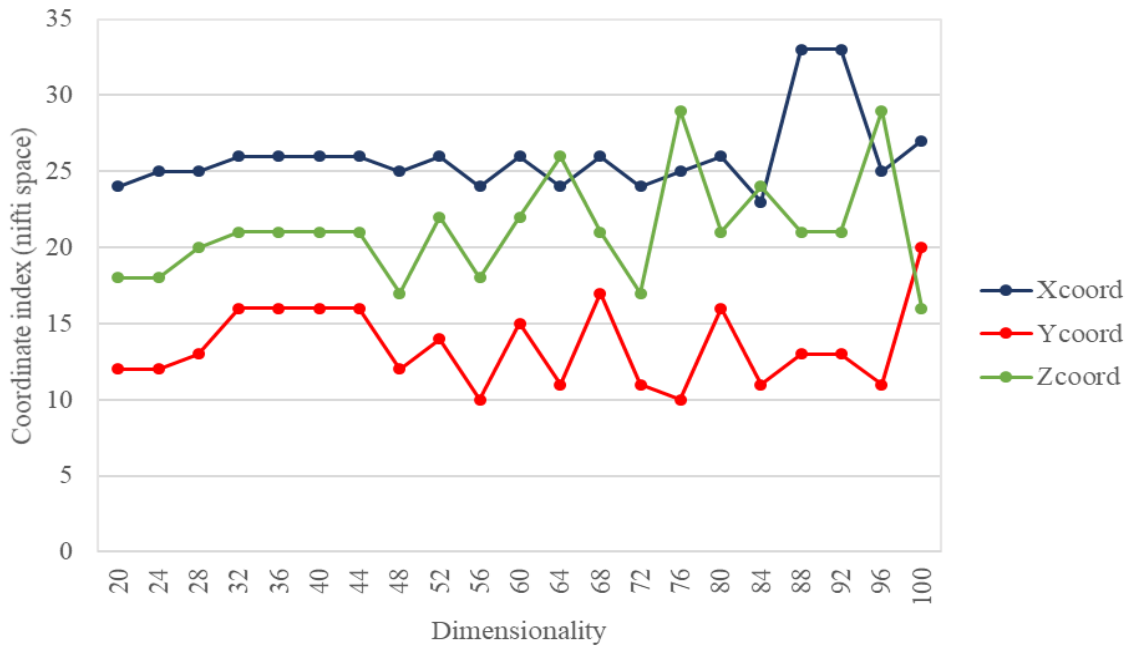

Figure 56. The peak voxel of components best matched by spatial map showed some movement, indicating that components are moving or splitting as dimensionality increases. Nifti space has a resolution of $4mm^3$.

The best matched component by spatial map at dimensionality 100 shows activation in a sub-region of the original component at anterior medial regions of Brodmann Area 19 (see Figure 57, top), with peak voxels at MNI [22, -46, -8] in the right hemisphere and MNI [-23, -50, -8] in the left. Activation extends dorsally towards the retrosplenial cortex, covering some anterior extrastriate regions between the occipital-parietal lobes. Functional connectivity showing this pattern and connectivity with early visual regions is observed using large meta-analyses of functional data (Yeo et.al., 2011).

The two next closest matches by spatial map also show activation in subregions of the original network (Figure 57, centre and bottom). The first shows more dorsal activation at occipital-parietal areas and is driven by lateral regions around the expected location of MT+ at MNI [41, -70, 8] and MNI [-47, -74, 8]. The second is a lateralized component at the primary visual cortex (peak MNI coordinates [14, -82, 4]).

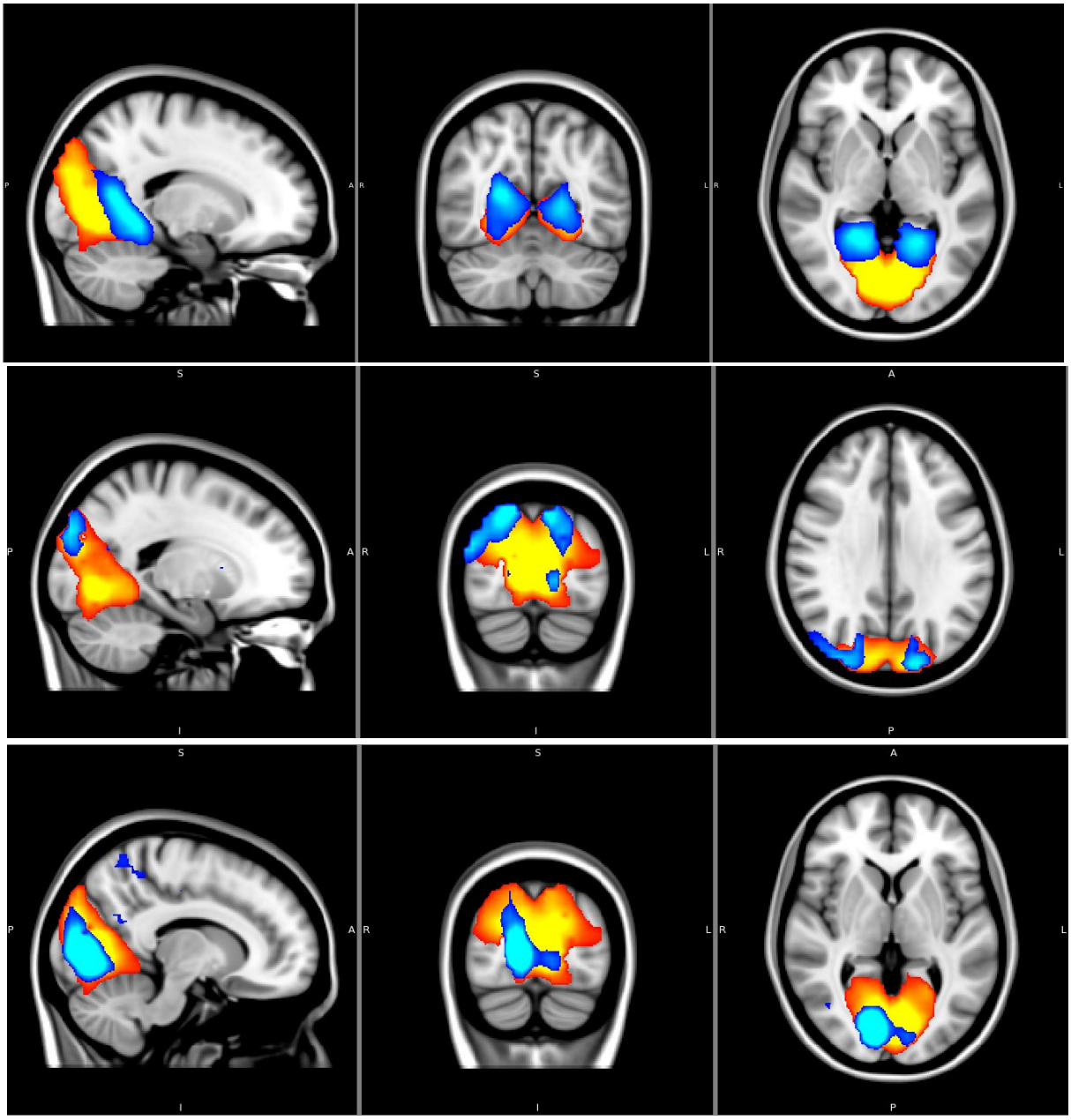

Figure 57. The three best matched components to the first visual network (orange) at dimensionality 100 show sub-regions of activity at the anterior medial occipital lobe (blue). Subregions are represented at the fusiform gyrus extending dorsally (top), the dorsal occipital pathway (middle) and the primary occipital region, lateralised to the right hemisphere (bottom)

Given that three components matched with the visual network component and each represented different regions of the spatial map (Figure 57), this supports the hypothesis that the splitting of components as dimensionality increases reveals subregions within the networks. The components with the closest peak voxel to the seed network component showed stability across dimensionalities (see Figure 58).

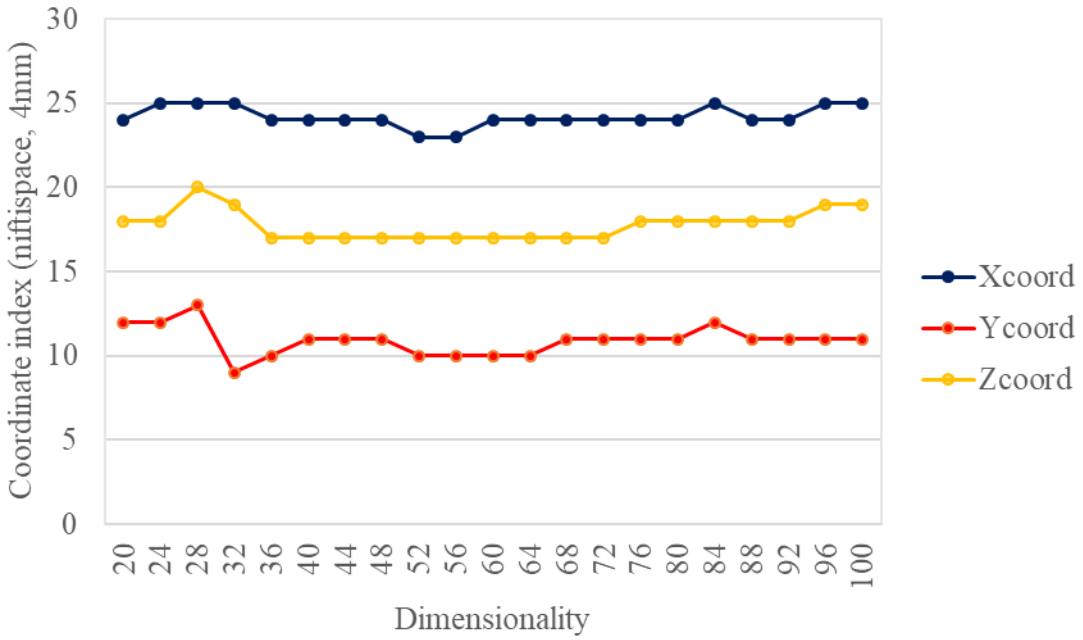

Figure 58. Visual network 1, V1 driven component. The component with the closest peak voxel to the seed visual network was found at each dimensionality. The peak voxel shows stability at the primary visual region. This suggests that the seed peak voxel is being represented through the dimensionality even though the spatial maps are altering and the components are reorganising.

4.3.2 Visual Network 2

The second network was also based in the occipital lobe, covering extrastriate regions in the ventrolateral visual regions (Figure 59, top). Overlap with the first visual network is seen at the posterior primary cortex centered at MNI [1, -91, 0] but the overlap region is small as the first visual network extends dorsally and the second laterally. These two networks are thought to represent separate dorsal and ventral streams of the visual processing pathway (Goodale & Milner, 1992; Milner & Goodale, 2008; Valyear, Culham, Sharif, Westwood & Goodale, 2006).

This second ventral visual network was well matched in the movie data ICA output (Figure 59, bottom). The peak voxels for this matched network lay in a posterior occipital location, at MNI [-15, -98, 0] in the left hemisphere and MNI [5 -94, 0] in the right.

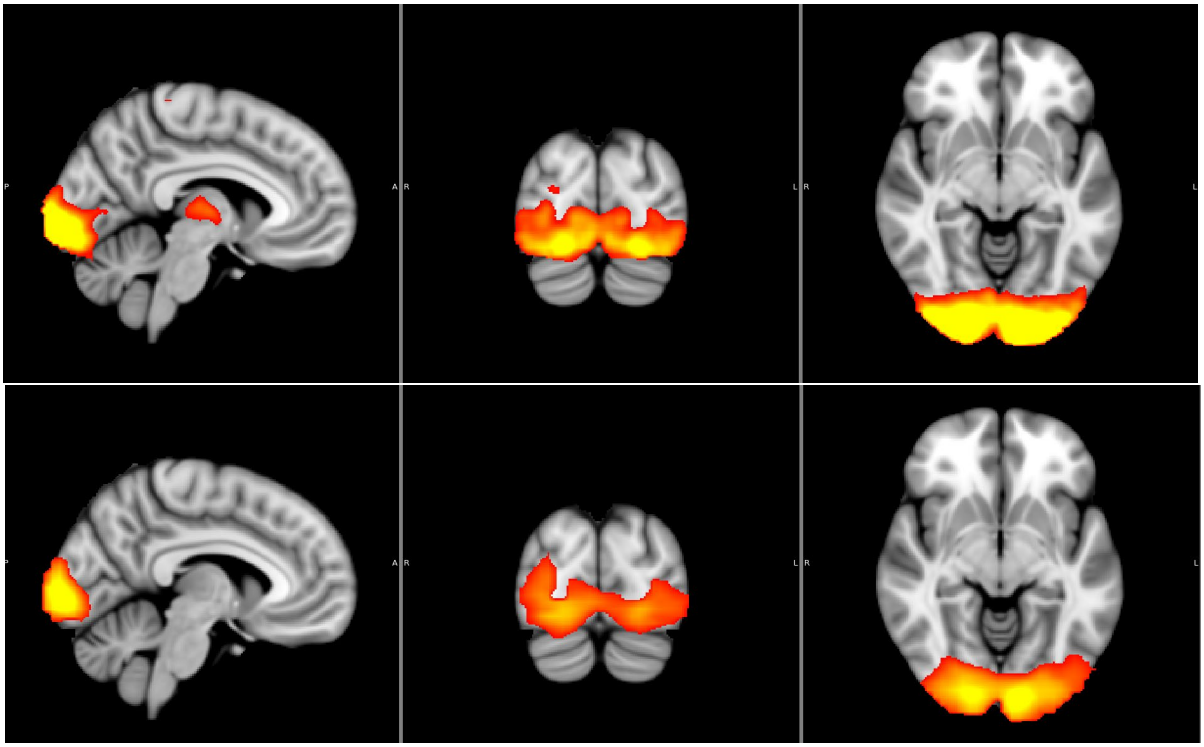

Figure 59. Smith et.al.'s second visual network (top) and the matched component from a TICA using functional data collected during natural viewing (bottom). The spatial correlation between these components is 0.68 (r).

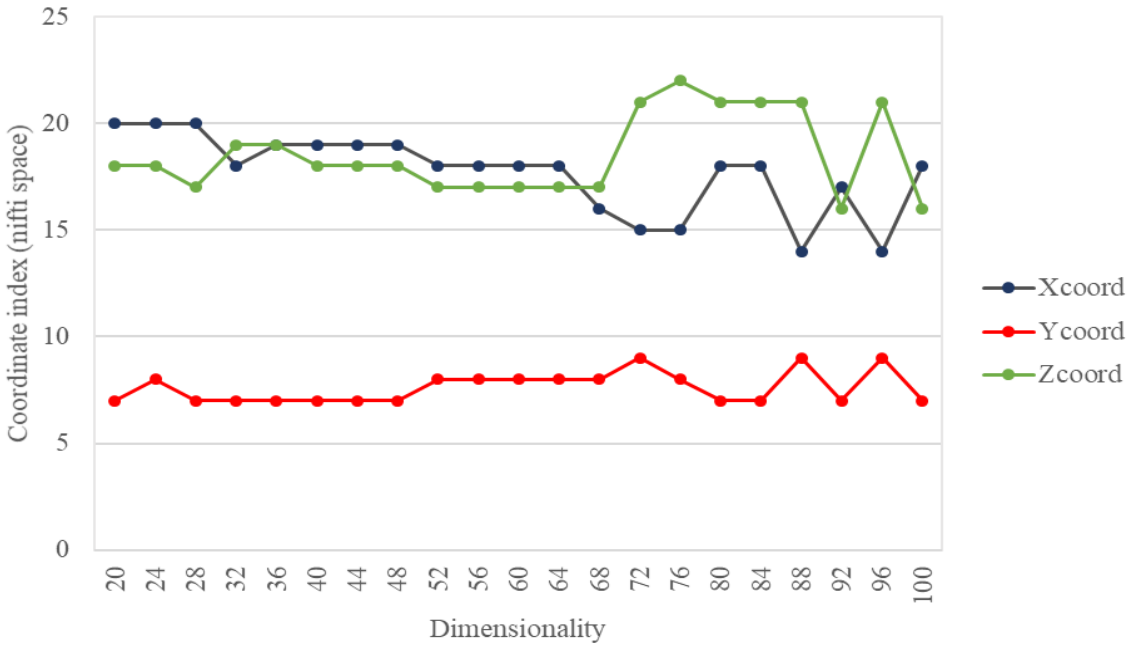

Figure 60. The second visual network again shows some movement around the peak voxels of components that have the most similar spatial map suggesting some splitting of the components as dimensionality is increased. Nifti space has a resolution of 4mm

At a higher dimensionality (100) the best matched component covers part of the original network (Figure 61). Like the first visual network, the movement of peak voxels of the matched components across dimensionalities suggests reorganization of the functional splits as dimensionality is increased (Figure 60). The peaks show stability until dimensionality 64, indicating components may be stable until this point.

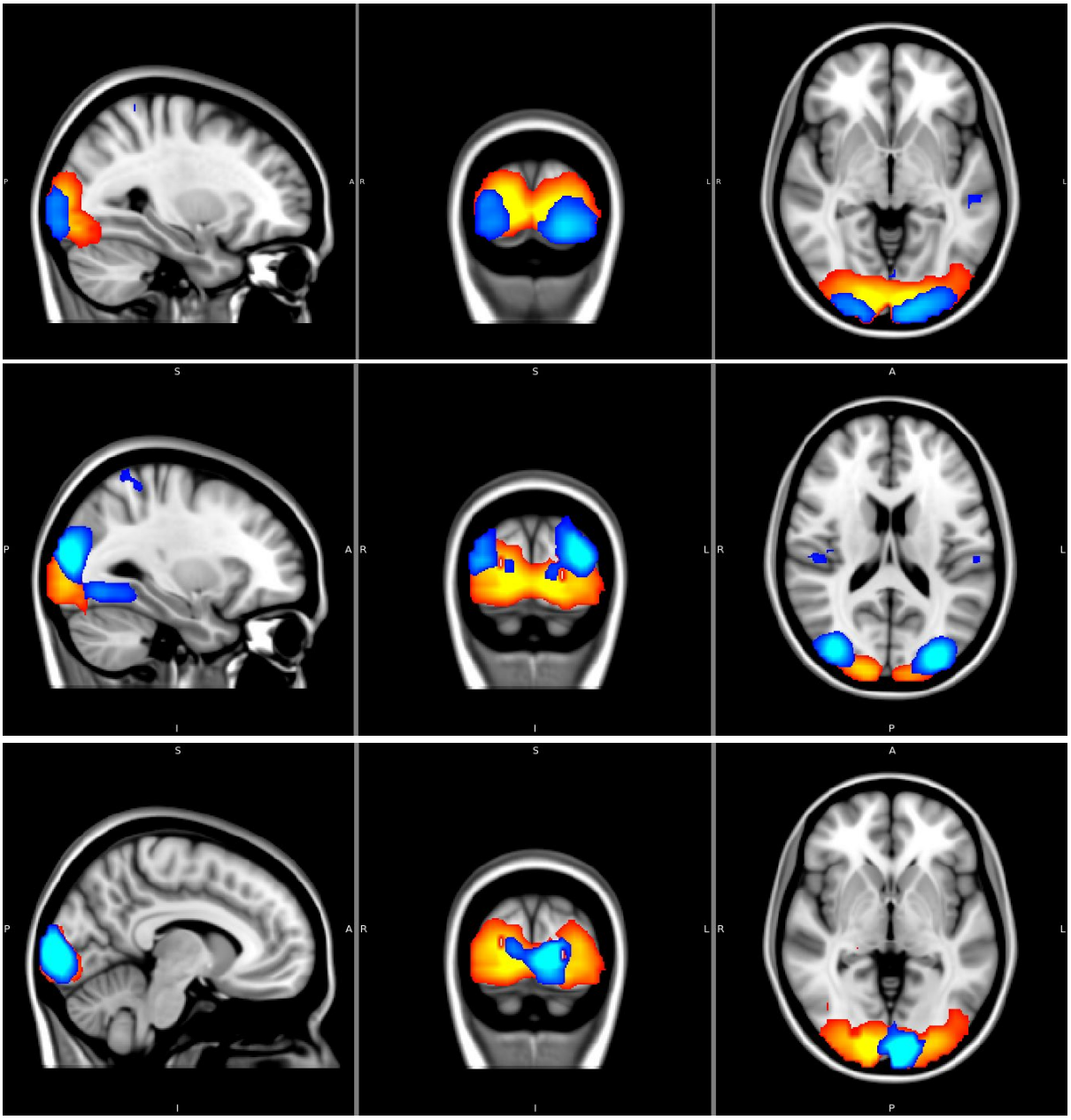

Figure 61. The three best matched components at dimensionality 100 show smaller sub-regions of activation (blue) compared to the component at dimensionality 20 (orange).

Also, like the first visual network, the matched components at dimensionality 100 covered different sub-regions of the original activation (see Figure 61, blue regions are components at dimensionality 100). The first matched component had peak voxels in at MNI [-23, -98, -8] in the left hemisphere and at the occipital

pole, MNI [13, -102, 4] in the right (Figure 61, top). The second showed peak voxels bilaterally at MNI [-39, -90, 16] and MNI [29, -82, 12] (Figure 61, centre), located at lateral regions of BA19. These peak voxels lie in a dorsal region of the occipital lobe and overlap with the original component at the location of the peak voxel before moving dorsally, as well at inferior occipital regions of BA19. This component therefore supports a functional segregation of BA19 matching the cytoarchitectural segregation by which it was originally identified (Brodmann, 1909). The third matched component at dimensionality 100 was lateralized to the left hemisphere covering posterior primary visual cortex with peak coordinates at MNI [-6, -98, 0] (Figure 61, bottom). Again, the pattern of component splitting as dimensionality is increased suggests that functional sub-regions of the network are being identified.

The component with the closest peak voxel to the original component network was identified across dimensionalities and showed stability (see Figure 62). This suggests that although the spatial maps of components are reorganizing, the functional activity of the network, focused at this peak voxel of activation, is still being represented.

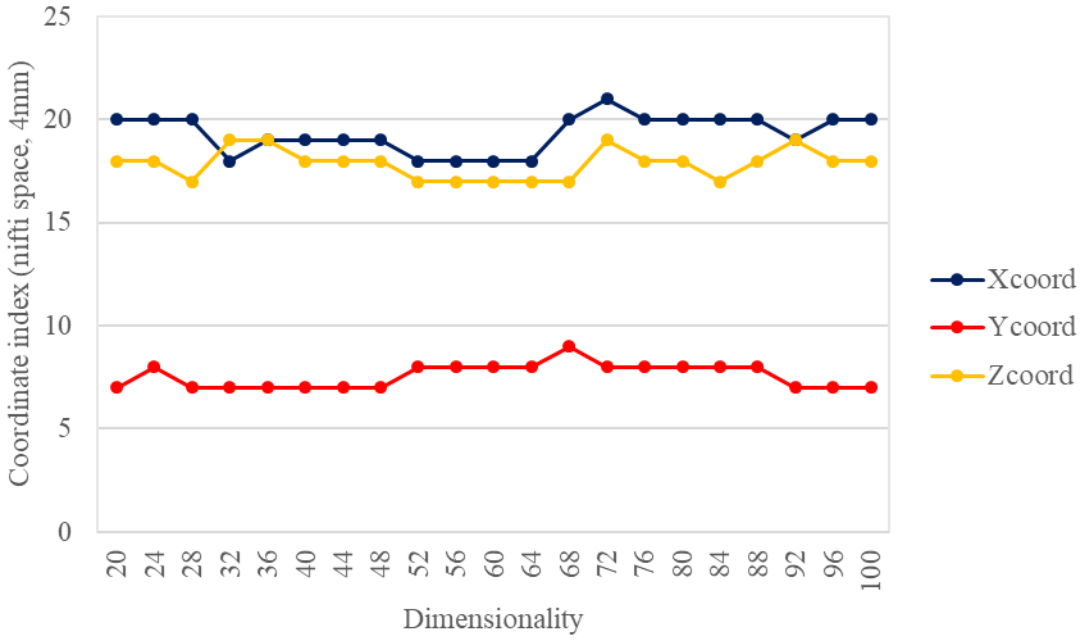

Figure 62. The component with the closest peak voxel to the seed network at dimenionality 20 was identified across the ICA outputs. There are very similar peak voxels of components across dimensionalities, suggesting that this seed of activity is being represented across dimensionalities, even though the spatial map has altered and components are reorganising.

4.3.3 Visual Network 3

The third visual is a visual network covering lateral occipital regions, including MT and extended dorsally past regions V3A (Figure 63, top). Two components from the movie data were similarly matched at r = 0.46 and r = 0.42, therefore both were examined. The best matched represented regions MT+ bilaterally (Figure 63, centre) with a peak voxel at MNI [49, -66, 0] and MNI [-51, -74 8]. The other showed activation in the more dorsal region V3A bilaterally with peak voxels MNI [-31, -86, 24] and MNI [25, -82, 24] (Figure 63, bottom).

The two different representations of this visual network may be due to the functional reorganization of neural activity during naturalistic viewing (which includes motion stimuli), compared to resting state. The separation of the network into one driven by motion region MT+ and another driven by motion region V3A suggests different functional roles of the regions during natural viewing. Both regions respond strongly to motion (e.g. Pitzalis et.al., 2013b) and pursuit eye movements tracking a moving object (Galletti, Battaglini & Fattori, 1990; Komatsu & Wurtz, 1988). However, research has identified some processing differences such as evidence that region V3A may process local processing while parallel processes at MT+ can distinguish global motion patterns (e.g. Cai, Chen, Zhou, Thompson & Fang, 2014; Pitzalis, et.al., 2013a, 2013b; Duffy & Wurtz, 1991).

Interestingly the component driven by activation at V3A (Figure 63 and Figure 64, bottom) shows activation at the intraparietal sulcus (IPS), while the component driven by MT+ does not (Figure 63 and Figure 64, centre). Research has suggested that a hierarchical relationship may exist in this dorsal network, with local and global motion information processed in MT+ and V3A being combined at IPS (Cai et.al., 2014). The components identified using ICA during movie watching suggest that there is a closer correspondence between activity in the IPS with V3A than with MT+ during natural viewing. The relationship between regions in this pathway needs further examination.

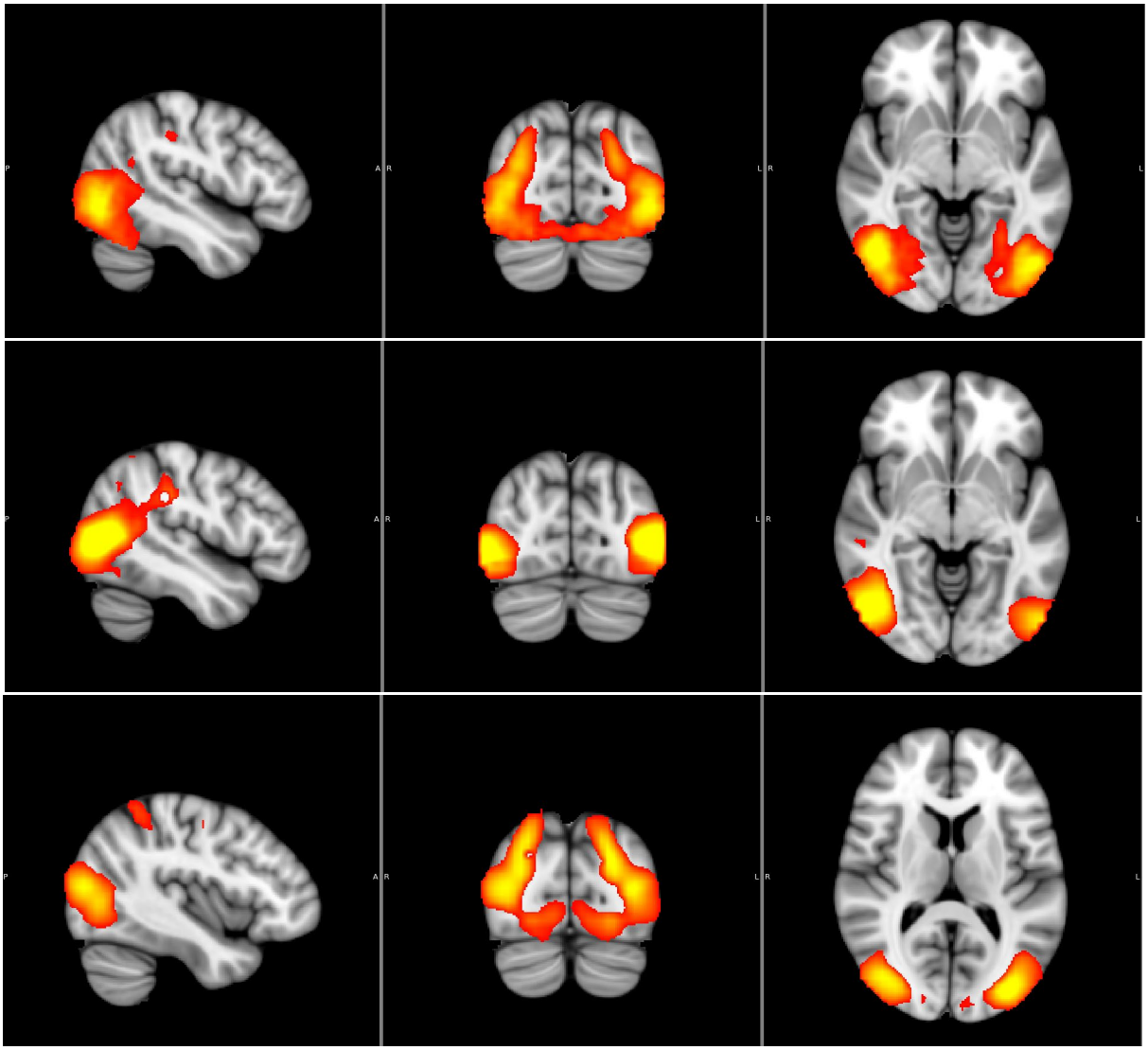

Figure 63. Smith et.al.'s third visual network covering MT+ regions (top) and the bets matched component from a TICA using functional data collected during natural viewing (middle). The spatial correlation between these components is 0.46 (r). Another component with a correlation of 0.42 shows activation at the more dorsal visual regions.

Regions of activity were also at the post-central sulcus in Smith's third network (Figure 64, top). Both components identified using movie watching and matched to this network also showed activation at the post-central sulcus bilaterally as well as pre-central sulcus regions (Figure 64, centre and bottom). A meta-analysis of hundreds of resting state studies (Neurosynth, Yeo et.al., 2011) demonstrates functional connectivity between these post-central and pre-central sulci, with MT+ (see Appendix 4.3 for image). Within the pre-central sulcus lies the frontal eye field and inferior frontal eye field (Derrfuss, Vogt, Fiebach, von Cramon & Tittgemeyer, 2012) important in spatial attention (Taylor, Nobre & Rushworth, 2006) and saccade production (Gaymard, Ploner, Rivaud, Vermersch & Pierrot-Deseilligny, 1998; Blanke et.al., 2000). The lack

of pre-central activity in Smith et.al.'s study may be due to reduced power as no visual stimuli was shown to the subjects. Showing a movie to the subjects is likely to increase the frequency of saccades and therefore the activity in these regions, allowing the functional connectivity to be more likely to be identified with lower numbers of subjects. Interestingly, a network for processing the temporal structure of events has been identified as involving MT+, parietal regions (Battelli, Pascual-Leone & Cavanagh, 2007) and pre-central sulcus (Zacks et.al., 2001).

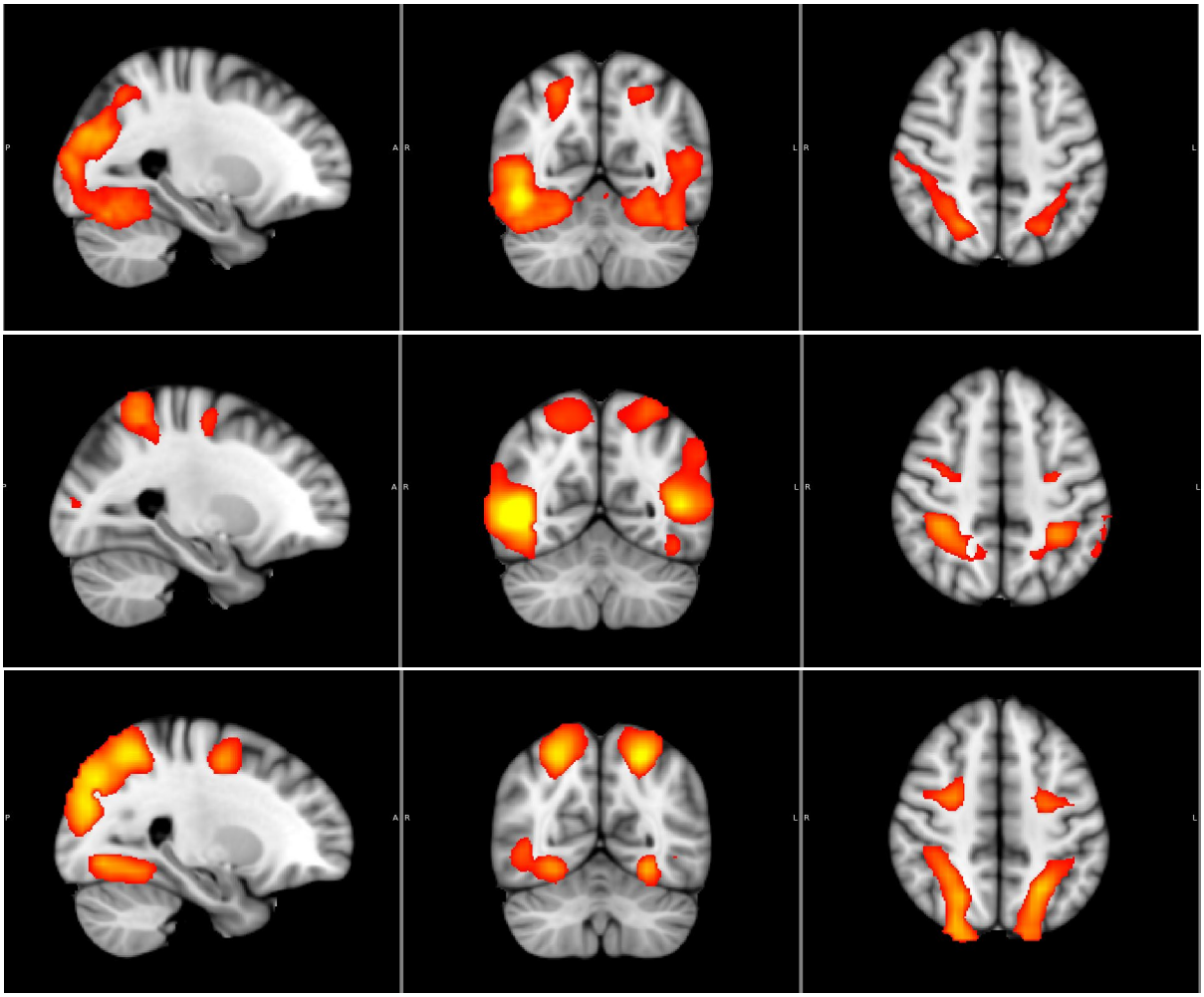

Figure 64. Regions at the post-central sulcus were also identified in Smith et.al.'s third visual network (top). The best matched component (centre) and the second matched component (bottom) from the group movie data ICA output, both showing some pre-central activity.

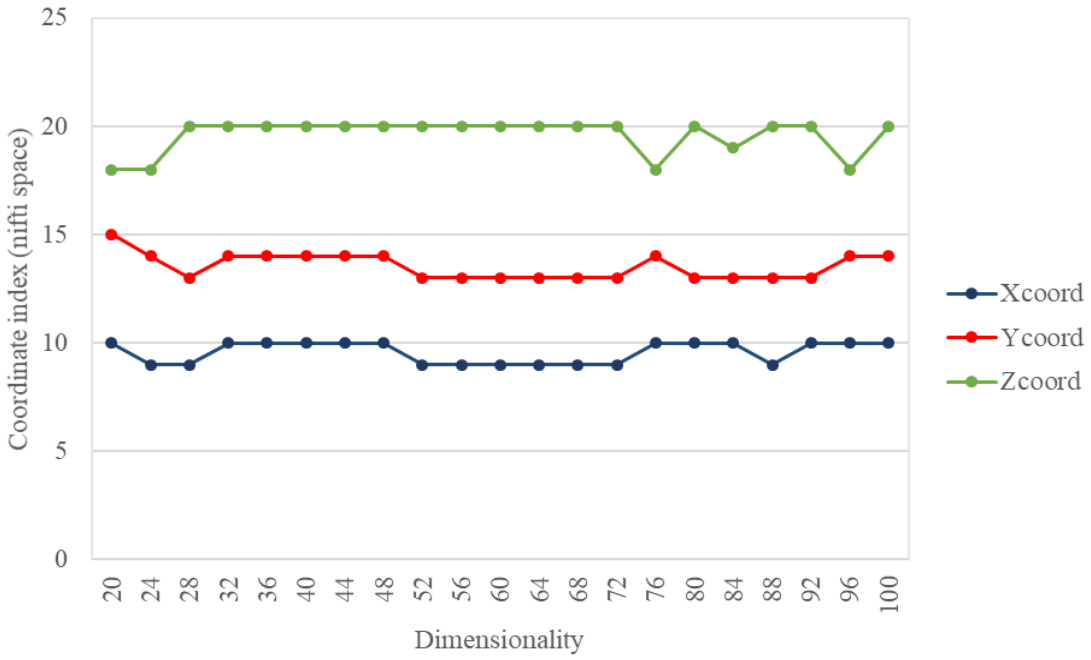

Figure 65. The peak coordinates based at the MT+ region stay stable across dimensionalities. This means the components that are most spatially similar overall show the same peak voxels.

The best matched component across dimensionalities shows better stability for the component with peak activity at the MT+ region. This suggests that these regions may be stable as dimensionality is increased, at least up to a dimensionality of 100. The activity at MT+ is present in the first two components at all dimensionalities suggesting that the power of this activity is high during movie watching and therefore these regions will remain stable and be identified as peak voxels within components containing this region.

When three the components with the highest spatial correlation at dimensionality 100 were examined (see Figure 66), the MT+ regions showed high activation. The best matched component at dimensionality 100 (Figure 66, top) had peak voxels at MT+ in the left hemisphere (MNI [-46, -70,8], as did the second in the right hemisphere (MNI [-45, -70, 0]; Figure 66, centre). Although driven by different hemispheres, both components showed bilateral activation at the MT+ regions. This supports the finding that these regions showed high peak voxel stability across the dimensionalities. It also suggests a lateralization of components as dimensionality is increased. The third matched component showed some activation at MT+ but the peak voxel lay at MNI [62, -26, 32]; a lateral parietal position behind the central gyrus, at regions associated with somatosensory processes in BA40 ((Figure 66, bottom). Meta-analyses have demonstrated a functional connectivity between motion region MT+ and the somatosensory cortex during different tasks (e.g. Yeo et.al.,

2011). The components identified during movie watching suggest that this functional connection is correlated across subjects during natural viewing.

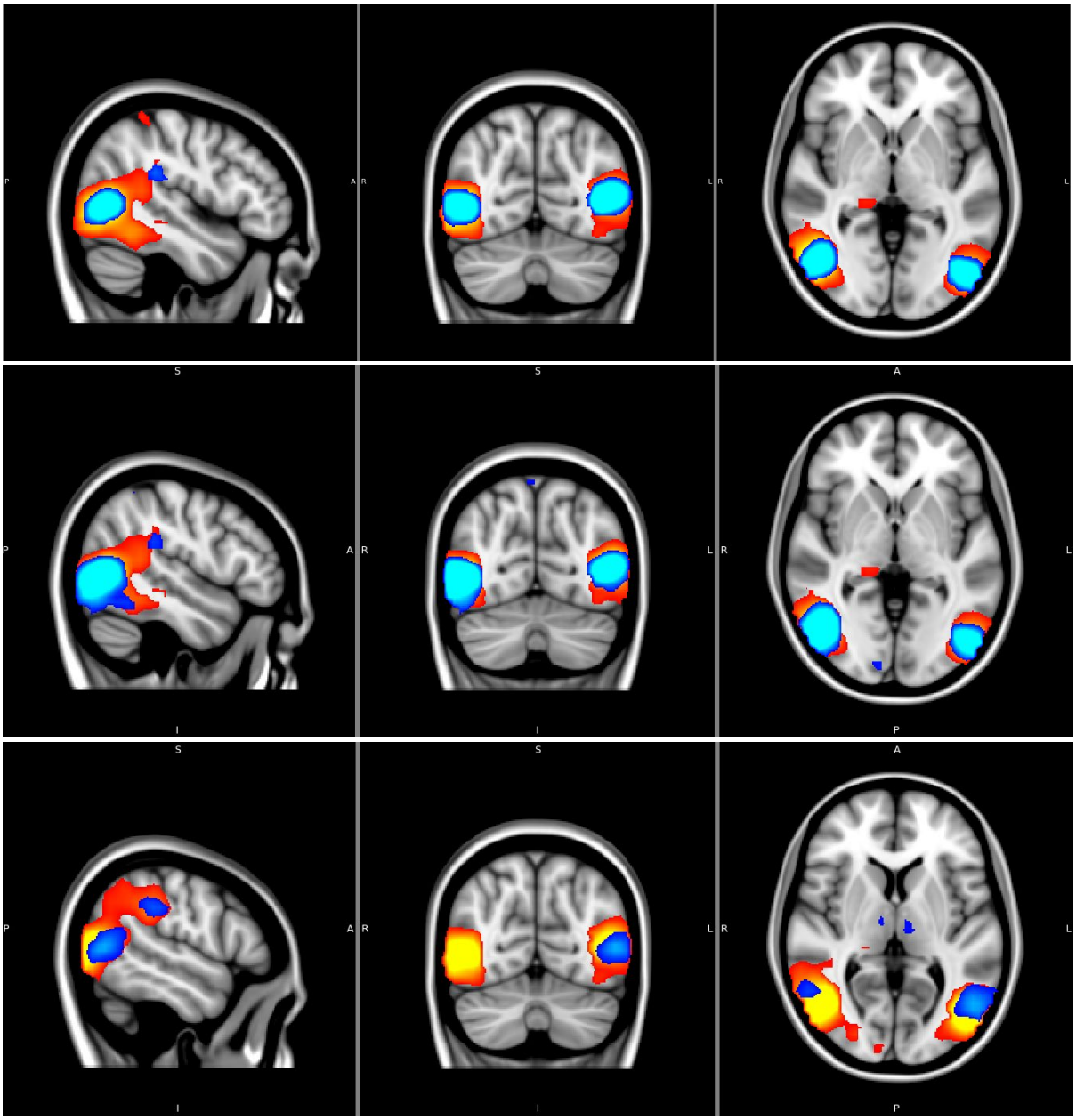

Figure 66. The best matched components at dimensionality 100 (blue) show activation at MT+ regions of the original component (orange).

As with the other visual networks, the peak voxel at of activation at dimensionality 20 was checked at each of the outputs, to see whether this functional activity was still being represented. The peak voxels of components that were closest to the peaks of MT+ were identified and represented components that also had the best spatial correlation to the original MT+ driven network (Figure 65). This suggests that these

component maps and peak voxels remain similar even as dimensionality is increased and the components reorganize. The peak voxels at V3A also showed stability across ICA dimensionalities (Figure 67) however were not the same components that matched with the most similar spatial maps. Therefore, for the V3A region, component spatial maps are altering as dimensionality increases, but the functionality at the peak voxel is still being represented.

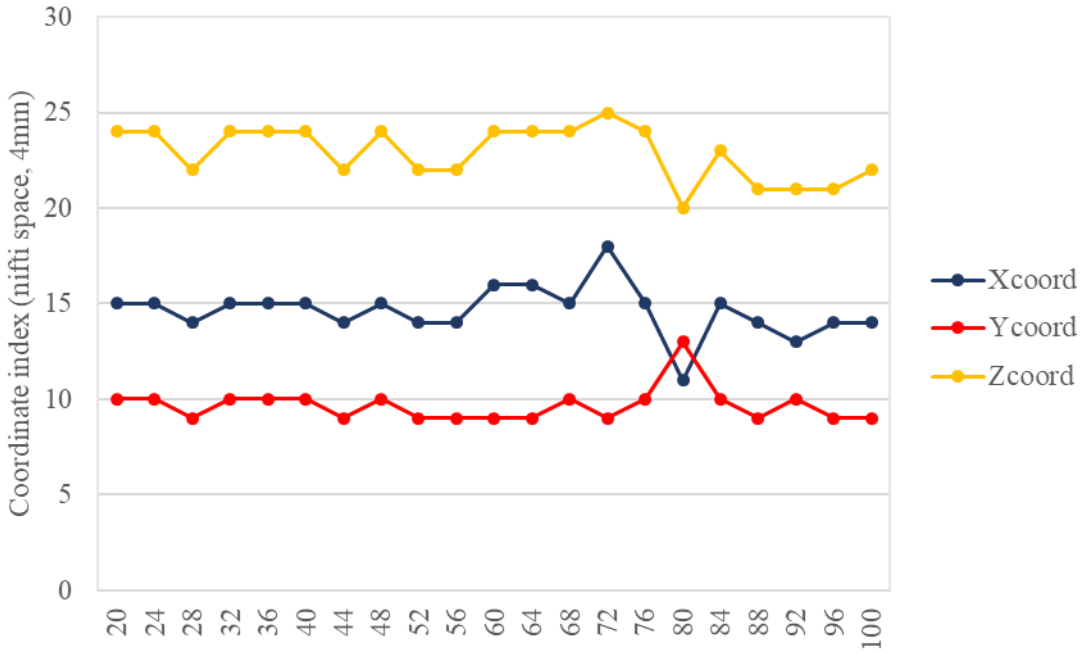

Figure 67. The closest peak voxels of components across dimensionalities shows stability at V3A. These components show a different spatial map to the original network but the peak voxel of functionality is still being represented at most dimensions.

4.3.4 Default mode network

The DMN identified by Smith et.al. showed medial and lateral parietal and mPFC activity (Figure 68, top). The matched DMN from the movie data also showed medial and lateral parietal activity, along with lateral prefrontal regions (Figure 68, bottom). Activity was not seen in the mPFC, suggesting a reorganization of the functionality across this network during movie watching, compared to resting state. This is plausible as the DMN is usually identified as increasing in power when no task is being performed (Raichle, et.al., 2001). As the subjects were watching a movie functional networks involved in processing the visual stimulus may be engaged and the DMN disengaged.

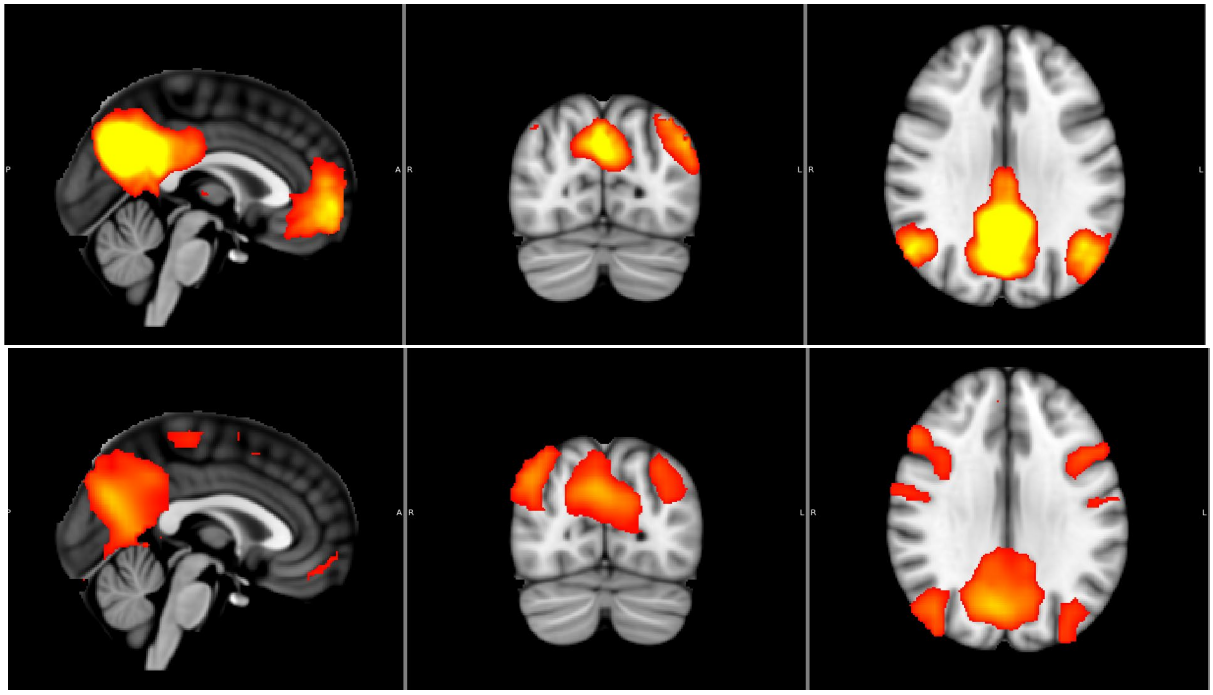

Figure 68. Smith et.al.'s default mode and the matched component from a TICA using functional data collected during natural viewing (bottom). The spatial correlation between these components is 0.37 (r). The mPFC activation is not represented in the movie network in this output.

4.3.5 Sensorimotor

A sensorimotor network identified by Smith et.al. covered dorsal regions of the brain, medially and at the central sulcus (Figure 69, top). Movie data identified similar regions in the brain (Figure 69, bottom). The peak voxel lay in the central sulcus in both hemispheres at MNI [45, -26, 64] and MNI [-43, -30, 60].

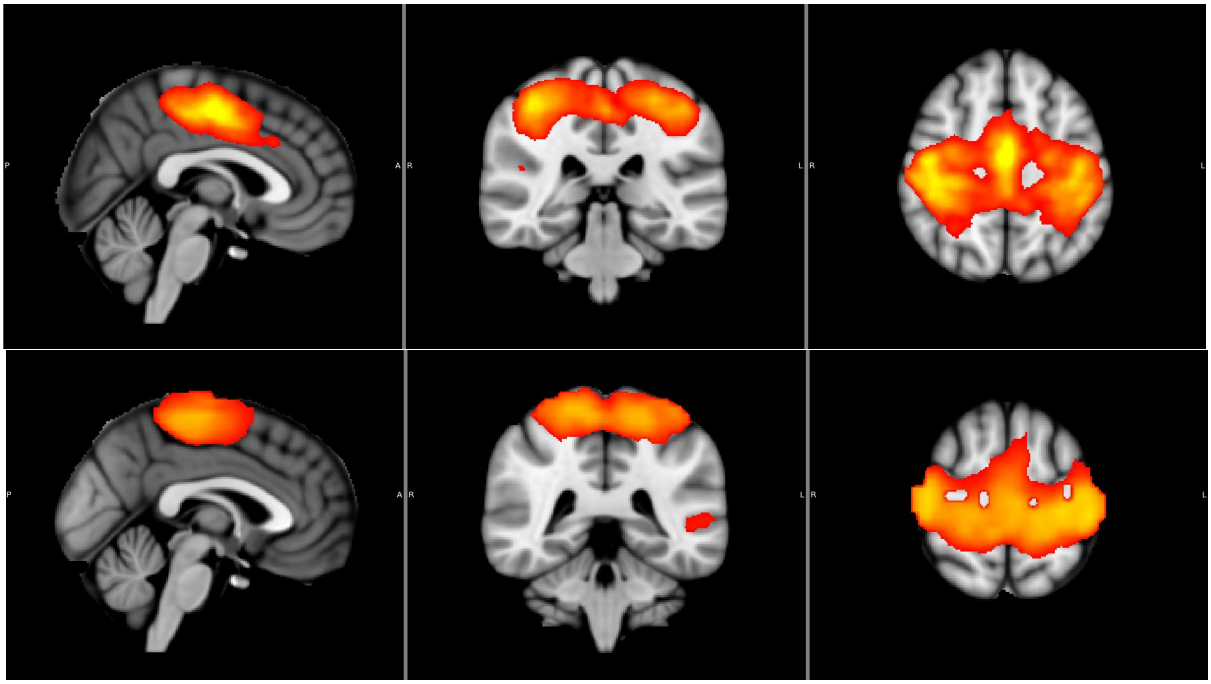

Figure 69. The sensorimotor network identified by Smith et.al. (top) was well represented in the move data (bottom), covering dorsal regions medially and at the central sulcus.

4.3.6 Auditory

The auditory network identified by Smith et.al. (Figure 70, top) was not represented in the movie data. The closest matched component showed activation not at the auditory cortex, but in temporal regions and with activity at the dorsolateral prefrontal cortex (Figure 70, bottom).

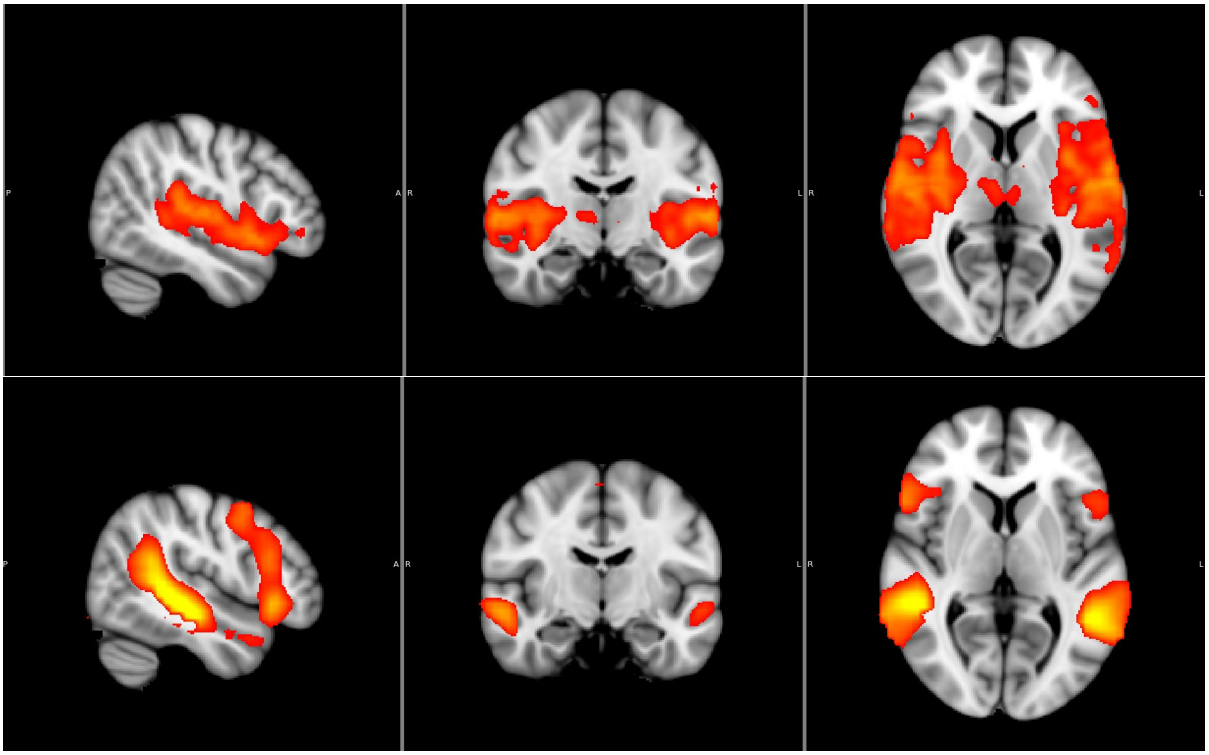

Figure 70. An auditory network identified using resting state data (Smith et.al., 2009; top) was not closely represented during movie watching (bottom). In Chapter 4 I find that auditory regions are represented in a five-minute movie clip, and suggest the lack of activation in the longer clip may be due to habituation to the scanner noise (see section 4.3.3).

A meta-analysis of resting state data shows a functional connectivity network between the regions identified using the movie data, in the temporal lobe and lateral frontal regions (Figure 71). Subjects were asked to watch a movie clip while in the scanner, therefore it is expected that attention to the visual stimulus increased activity in the networks processing this information (e.g. Gandhi, Heeger & Boynton, 1999; Moran & Desimone, 1985). Although the MRI scanner makes a relatively loud noise while the subject is watching the movie, this noise is repetitive, and the subjects are likely to have habituated thus showing reduced power in the auditory network (e.g. Pérez-González, Malmierca & Covey, 2005; Condon & Weinberger, 1991).

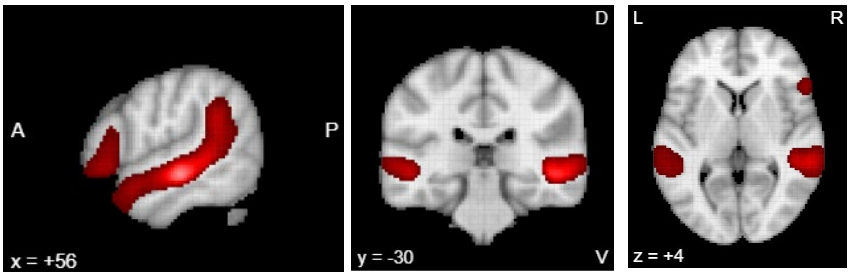

Figure 71. A meta-analysis shows a network matching that found using the movie data.

4.3.7 Executive control

A component in the pre-frontal cortex was identified in both the resting state (Figure 72, top) and the movie data (Figure 72, bottom). The movie data component was based slightly more dorsally than in Smith's networks, with a peak voxel of MNI [-10, 54, 36]. However, when checked against a larger meta-analysis (Yeo et.al., 2011) this location and region is still within the expected prefrontal DMN activity.

Research has shown that increased BOLD response in the mPFC is seen during mind wandering (Christoff, Gordon, Smallwood, Smith & Schooler, 2009) and while engaging with a plot or narrative (Tikka, Kauttonen & Hlushchuk, 2018.).

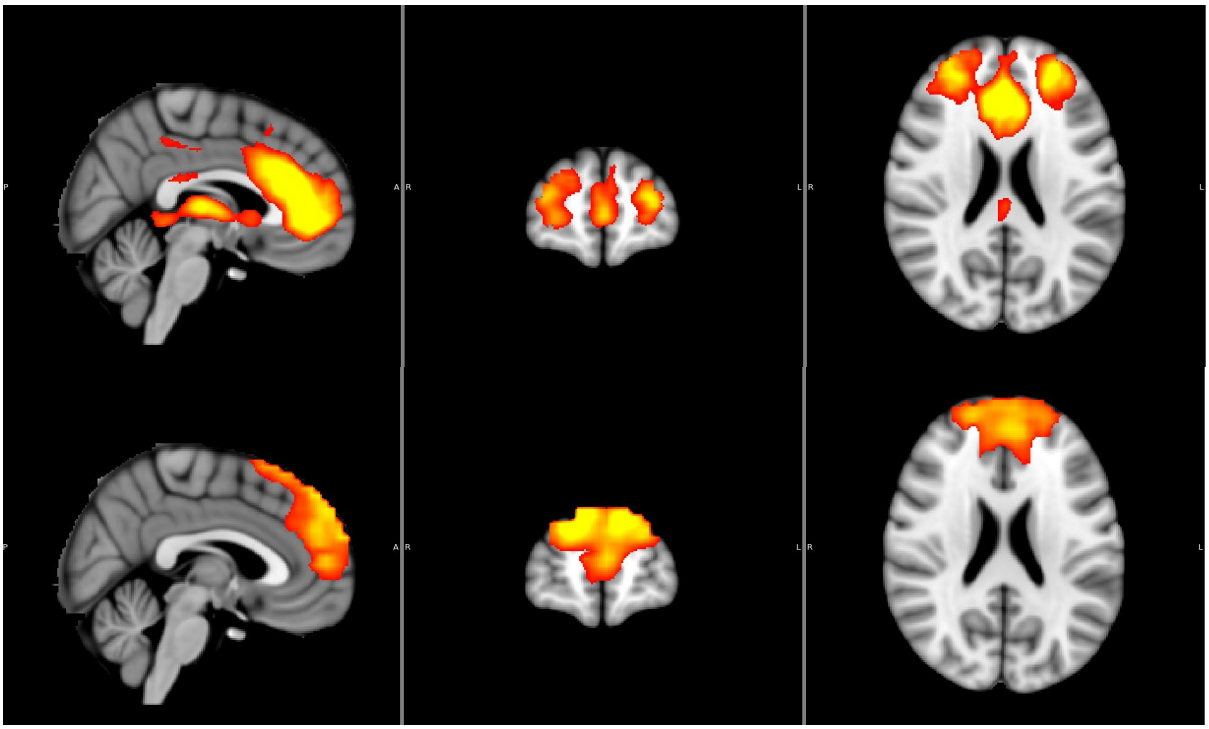

Figure 72. The pre-frontal cortex shows activation in a Smith et.al., network (top) and in the movie data slightly more dorsally (bottom).

4.3.8 Frontoparietal (lateralised)

Lateralized components covering parietal and frontal areas were identified using the resting state and movie data (Figure 74a and Figure 73b). The movie data provided components that were more localized to the peak areas of activity at the dorsolateral prefrontal cortex and the dorsolateral parietal cortex. The highest activation was seen at MNI [-42, 46, 0] and MNI [42, 54, 8] in the dorsolateral prefrontal cortex, respectively.

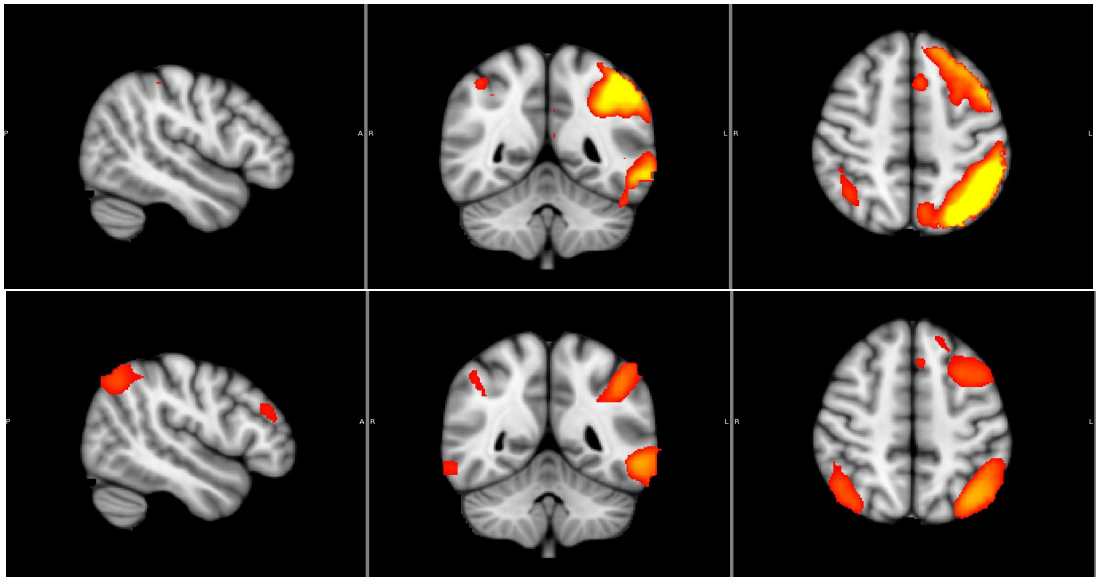

Figure 73a. Lateralised frontal and parietal regions in the right hemisphere (top) were also identified in the movie data (bottom). Again, the activity was less dispersed across the dorsal regions of the cortex and localised to the dorsolateral pre-frontal cortex and dorsal parietal areas.

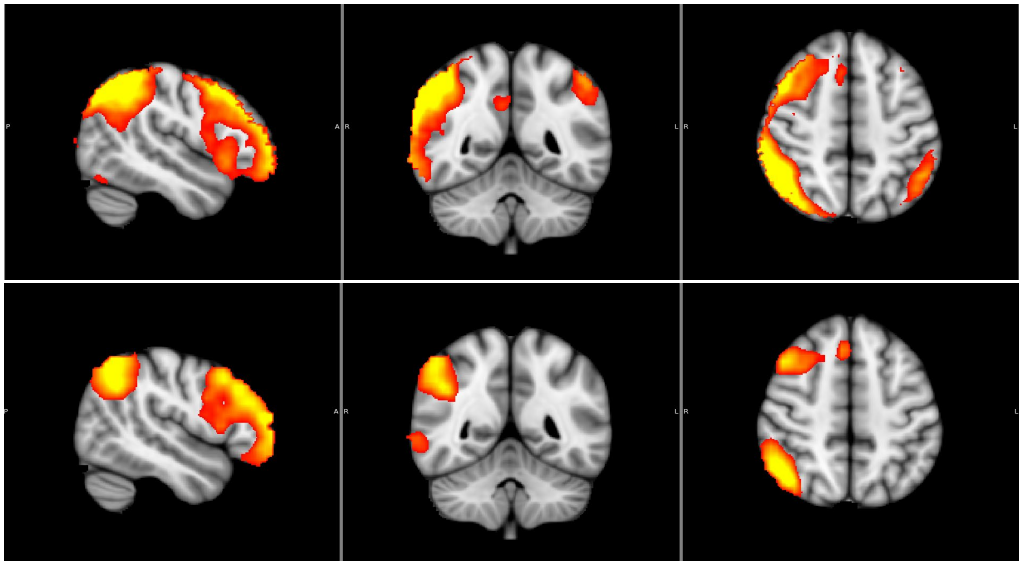

Figure 74b. Lateral frontal and parietal regions in the left hemisphere (top) were identified using the movie data (bottom). The regions were more localised in the movie data, though peaks of activation were in similar positions at the dorsolateral prefrontal cortex and dorsal parietal lobe.

4.4 Summary: Chapter 4

Using naturalistic viewing and TICA the functional networks identified during rest can be identified in the brain. The visual and sensorimotor networks are particularly well represented, while the default mode network and auditory network show less correspondence. This suggests that these visual and sensory motor regions are functionally timelocked to the movie stimulus, across participants. It also suggests that the networks do not reorganize to a large degree during natural viewing. One potential insight into the functional organization of visual networks during natural viewing was that movie stimuli did allow for different motion sensitive visual networks to be identified driven by MT+ and V3A, respectively. Naturalistic viewing provides an alternative method for identifying functional networks of interest in the brain, with improved signal to noise and the opportunity to examine the timelocking of functional networks across participants.

As dimensionality is increased the components become smaller and may represent sub-regions of a component. This does not look to be a particularly neat process but could hold useful information about the connectivity and hierarchy between subregions. Analysis of the peak voxels and correlated components of the visual networks as dimensionality was increased suggests that there is a reorganization of components. The stage at which networks change and reorganize may depend on the strength of connectivity of regions in the

network. Regions that show less shared functionality will split into separate components before others that show a higher functional correlation. If this could be tracked across dimensionalities it would give some insight into the structural hierarchy of functional networks. This idea is explored further using individual ICAs in Chapter 10.

So far in this thesis the robustness of group level components identified using movie stimulus and TICA has been systematically and thoroughly examined. Reliability is seen across different data permutations when a grey matter mask is used, and the same dimensionality is applied to the ICA segmentation. When examined, the components are shown to represent visual regions of interest and components at these points of interest are reliable across different samples and movie clips. Established RS networks are also represented in movie data TICA outputs, when lower dimensionalities are used. This work supports the use of movies and ICA for identification of functional systems in the brain, as a preferable alternative to using resting state or individual localisers.

Chapter 5: The reliable components identified using a movie stimulus and group TICA

5.1 Introduction

In the previous chapters the sensitivity of ICA to pre-processing parameters and across different samples was systematically investigated using data collected during natural viewing. Results showed that regions in visually responsive regions are relatively stable across different pre-processing options and that similar components can be identified across different samples. In the previous chapter components generated using the movie data were compared to resting state networks (Smith et.al., 2009). It was found that established functional networks can be identified at low dimensionalities (20), and that sub-regions of these networks can be found when dimensionality is increased.

Multiple cortical regions processing visual information have been recognized in the primate and human brain (Tootell, Dale, Sereno & Malach, 1996; Desimone & Duncan, 1995). The aim of this chapter is to understand how the reliable components segmenting BOLD data collected during movie watching represent visual regions of interest in the motion processing pathway. Regions in this visual pathway have traditionally been identified using separate localisers (e.g. Huk & Heeger, 2002; Dumoulin & Wandell, 2008; Cardin, Hemsworth & Smith, 2012). If using a movie stimulus and TICA can reliably identify these motion ROI it would be a preferable alternative as using multiple individual localisers can be tiring and uninteresting for an observer causing increased noise in the data. This pathway was selected as it was expected to be active across subjects as throughout the movie clip there were many types of motion (Hasson et.al., 2010).

Comparisons documented in this chapter find that regions and components of highest reliability in the most representative ICA output show correspondence with established regions of interest in the motion processing pathway. This suggests that using ICA to segment BOLD data collected during movie watching is a promising way to identify the motion processing pathway at the group level. The spatial organization of components also provides insight into how the different regions in the pathway are functionally connected.

5.2 Methods

Data were collected as described in Chapter 1 (section 1.3). Data were pre-processed using a grey-matter mask (MNI segmented brain) and MELODIC's default parameters, based on the findings in Chapter 2. As I was interested in finding visual regions of interest, 22 TICAs were conducted at high dimensionality (200), based on the findings in Chapters 3 and 4. The subject order was permuted across the 22 analyses, so the first brain was different in each permutation. All outputs showed high representativeness across permutations, therefore a random permutation output was selected for comparison of reliable components/regions with visually driven regions of interest (the REPRUN).

First, components from REPRUN were categorized as signal or noise based on the guidance provided by Griffanti et.al. (2017). The reliable signal components were identified in the output and compared with known regions of interest in the visual pathway.

Signal and noise components

Sixty-two of the 200 REPRUN components were identified as noise, and the rest were categorized as signal (see Figure 75 for the proportion of signal to noise components; Griffanti et.al., 2017). This proportion was similar across dimensionalities 20, 70, 100 and 200, indicating that as dimensionality is increased the number of signal components increases, with the signal being split to represent different sub-aspects of a functional network.

The proportion of noise to signal components was similar to the number of components that showed lowered reliability across the permutations (spatio-temporal metrics <0.4). Therefore, it was initially hypothesized that the least reliable components were the noise components. To investigate this all the signal and noise components were matched across each of the ICA outputs and the values of similarity (Ocorr) were averaged. This gave a measure of how reliable the noise components were compared to the signal components and the overall average. There was not a significant difference between the mean reliability for signal (M=0.827) and noise (M=0.843) components; $t(61)=-1.54$, $p = 0.129$.Therefore, the noise components were as reliable overall as signal components.

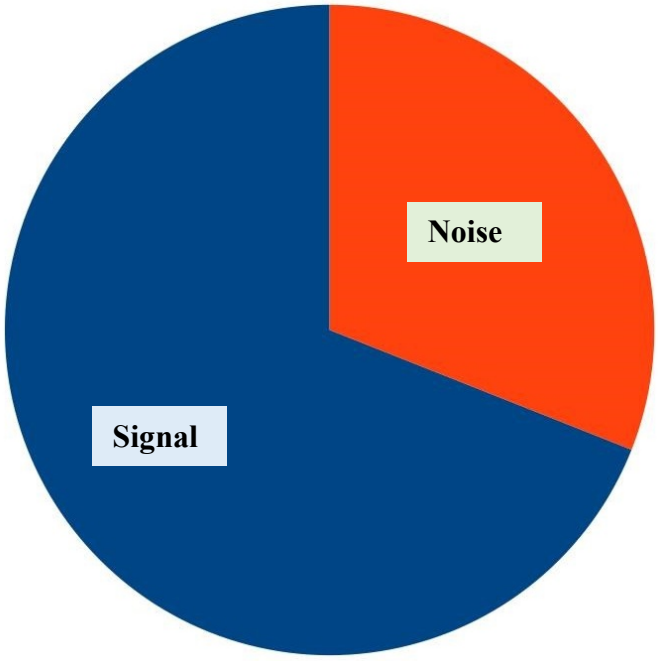

Figure 75. The proportion of signal and noise components in REPRUN resulted in around on third of the components being categorised as noise.

Figure 76 provides a visual schematic of the finding that noise components were relatively evenly distributed in the ICA output, after the first 73 components. The color of the signal lines in this figure gives a measure of reliability for that signal (darker means they are more reliable). The first 73 components were some of the most reliable in the output. Based on these findings, one quick-fire method of identifying reliable signal components may be to exclude components that lie after the 'threshold' at which noise components begin to appear in the output. However, one problem with this is that some reliable signal components that lie after this threshold will be missed.

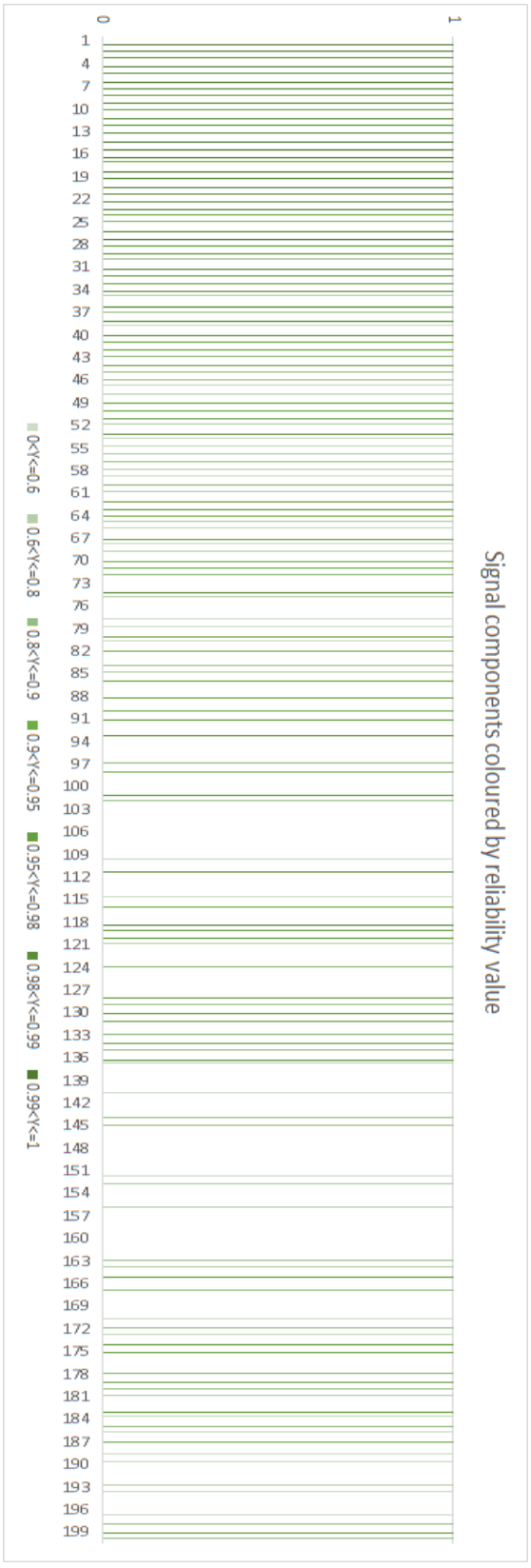

Figure 76. A schematic of where signal components lie within the REPRUN output.

Each line represents a signal component.

The reliability of these components are represented by the saturation of the component signal line.

Darker line = more reliable

To understand the profile of components across the ICA output a map of the distribution of signal components under the 73 “signal threshold” and one for those after the 73-signal threshold, were generated. The maps show the signal components from 1-72 have a reliability focused in the occipital regions of interest (see Figure 77). The signal components appearing after this threshold show reliability in frontal regions of the brain (see Appendix 3.1). Therefore, selecting these earlier signal components is crucial for identifying visually responsive regions and networks when using visually driven stimuli.

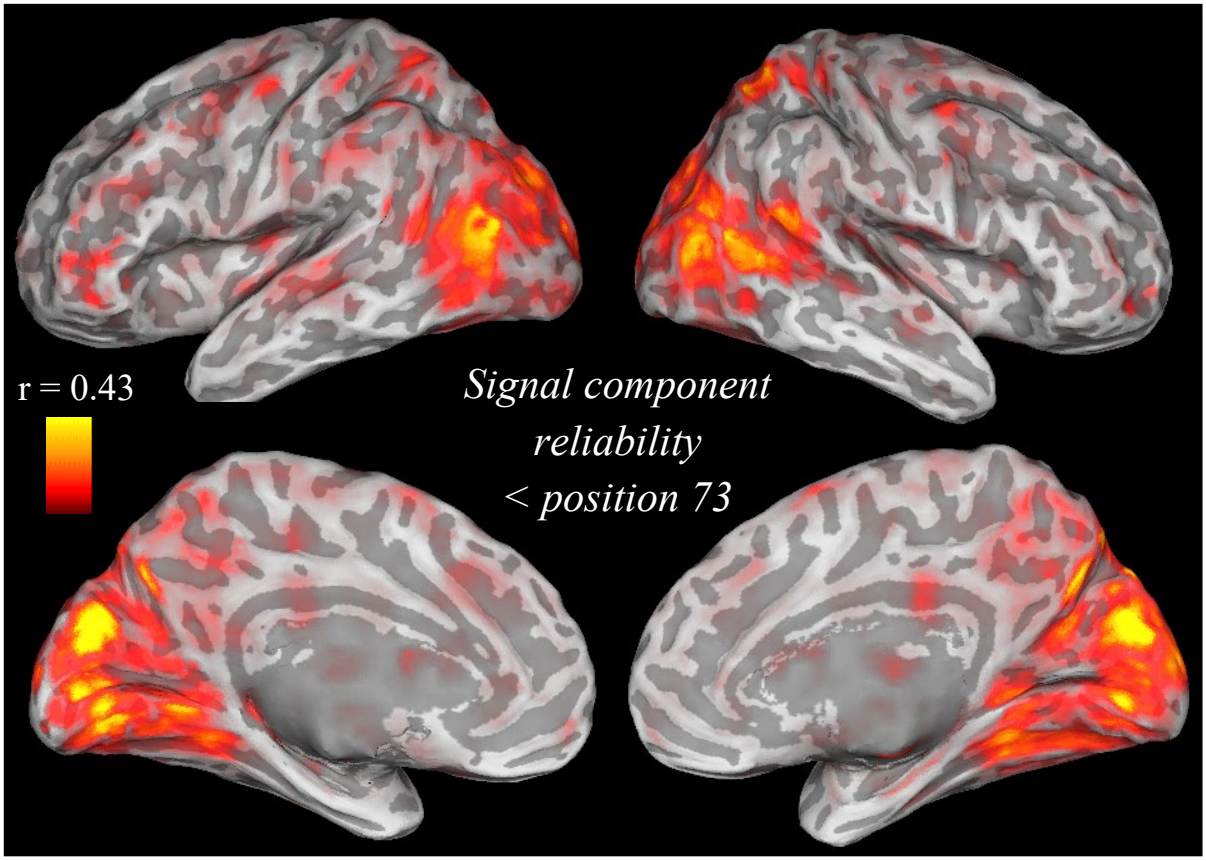

Figure 77. The most reliable signal components across TICA permutations (first brain swapped) lie primarily at the occipital and temporal lobes and are earliest in the ICA output (position <73/200 in the TICA output).

Using the amount of variance explained (output order) as a means of identifying components of interest is often used in the field to quickly identify components of interest. The variance explained by each component is plotted (see Figure 78), and where this is seen to drop off (or reach a certain proportion of variance explained in the data e.g. 80%), components are discarded as being more likely to be noise. Based on our movie data using this cut-off method would cause a bias in the spatial location of components to the

occipital lobe. Therefore, if a visual stimulus is being used a threshold based on variance explained may not be a sensible option if components lying in more anterior regions are of interest. As my aim is to assess the movie technique for identification of visual functional regions, this technique is appropriate for identifying visual components of interest in the REPRUN output.

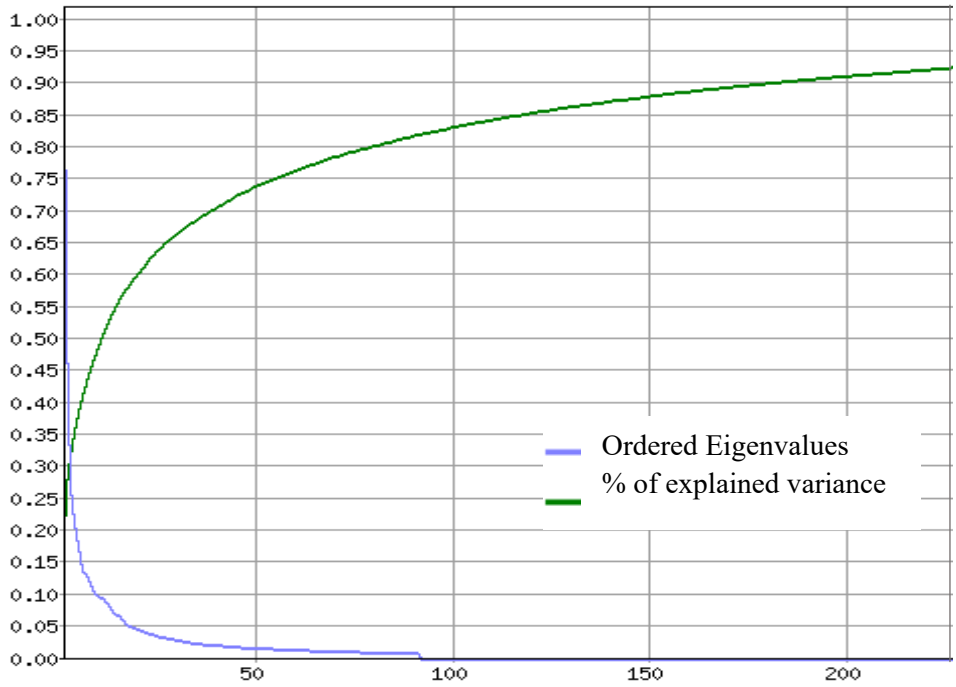

Figure 78. The variance explained by components is plotted in the ICA output. One technique of pulling components that are likely to be signal is to restrict inspection of components up until the gradient of this line is observed to plateau (i.e. the amount of variance explained per component drops off).

Can using this optimal method of ICA and movies identify known visual areas of interest?

The regions of high reliability of early signal components corresponds closely to the voxel-by-voxel correlation of subject activity while watching the movie (see Chapter Two, Figure 2). One network of interest we expect to be active across subjects during movie watching is the motion processing pathway, as the clip contains many types of motion including discrete, global flow patterns and biological motion (Hasson et.al., 2010; Nishimoto & Gallant, 2011; Cardin & Smith, 2009; Grossman & Blake, 2002). Indeed, the signal components showed high reliability across the occipital cortices and parietal regions (Figure 77) where we know regions in this network lie (e.g. Cardin, Sherrington, Hemsworth & Smith, 2012; Huk, Dougherty &

Heeger, 2002; Tootell et.al., 1998). These established regions, previously identified using retinotopic techniques and individual localisers, were compared with reliable components in the ICA output.

Using a heat map of reliability generated REPRUN signal components, the regions of high reliability across the runs can be cross-referenced with the visual regions identified in the literature and associated with motion processing (e.g. Sunaert, Van Hecke, Marchal & Orban, 1999). Reliable signal components were found with activation representing visual regions of interest including the primary visual cortex and early visual regions (V1, V2, V3), and motion sensitive areas V3A, MT+, V6, pVIP and CSv. All the regions identified were also present as regions of highest reliability in unmasked ICA outputs (restricted at 200). This demonstrates that multiple regions of interest can be reliably identified using movies and TICA, supporting work by Bartels & Zeki (2008).

5.3 Regions of interest: motion processing pathway

5.3.1 pVIP

The VIP region has been identified in non-human primates as being involved in self-motion processing (e.g. Bremmer, Klam, Duhamel, Hamed & Graf, 2002). This selective function responds to both vestibular signals and optic flow motion, such as the expansion and contraction or rotational motion on fronto-parrallel planes caused by translational movement. Using a movie stimulus, camera movements simulate self-motion with zooming and panning within scenes. The putative human VIP (pVIP) has been identified in previous research, when contrasting dots simulating self-motion with stationary dots (Arnoldussen, Goossens & van den Berg, 2011) or contrasting self-motion compatible with self-motion noncompatible moving dot arrays (Cardin & Smith, 2009). pVIP lies at BA7, in the parietal lob and shows reliable identification bilaterally in the TICA output, using movie stimulus (MNI coordinates = LH [-24, -61 65]; RH [28 -66 65]; see Figure 79).

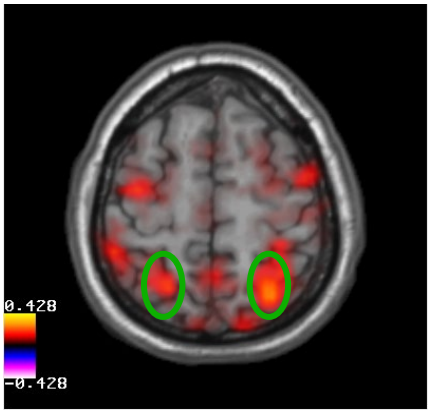

Figure 79. Reliable ICA component(s) at the pVIP (locations circled).

5.3.2 V3A

Neurons in region V3A have been identified as responding strongly to motion, compared to static stimuli (Tootell et.al.,1997). This region has also shown some sensitivity to optic flow structure (Greenlee, 2000) and has been indicated as potentially processing information about heading direction (Cardin, Hemsworth & Smith, 2012). At the region corresponding to V3A, which lies anterior to the dorsal V3 region, high reliability of components was seen across the ICA outputs (MNI coordinates = LH[-17, -92, 25]; RH[17, -92, 25]; Yeo et.al., 2011, see Figure 80).

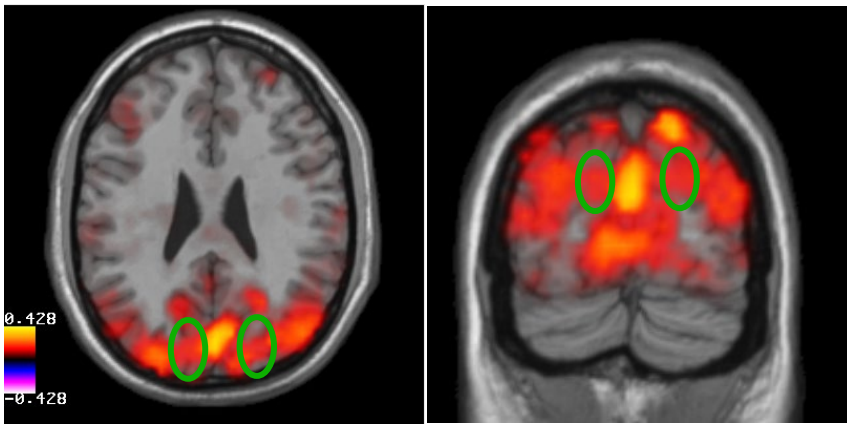

Figure 80. High reliability of components is seen at the bilateral V3A (locations circled).

The first component in the ICA output and therefore describing most of the variance in the data, lay at the MT+ region (see Figure 81A), with some activation extending dorsally to V3A (see Figure 81B and C),

and the somatosensory cortex at the postcentral gyrus (see Figure 81C), in the right hemisphere. V3A and regions at the post-central gyrus have been identified in meta-analyses as functionally connected with MT+ (e.g. Yeo et.al., 2011). Therefore, this component is representing an established motion network.

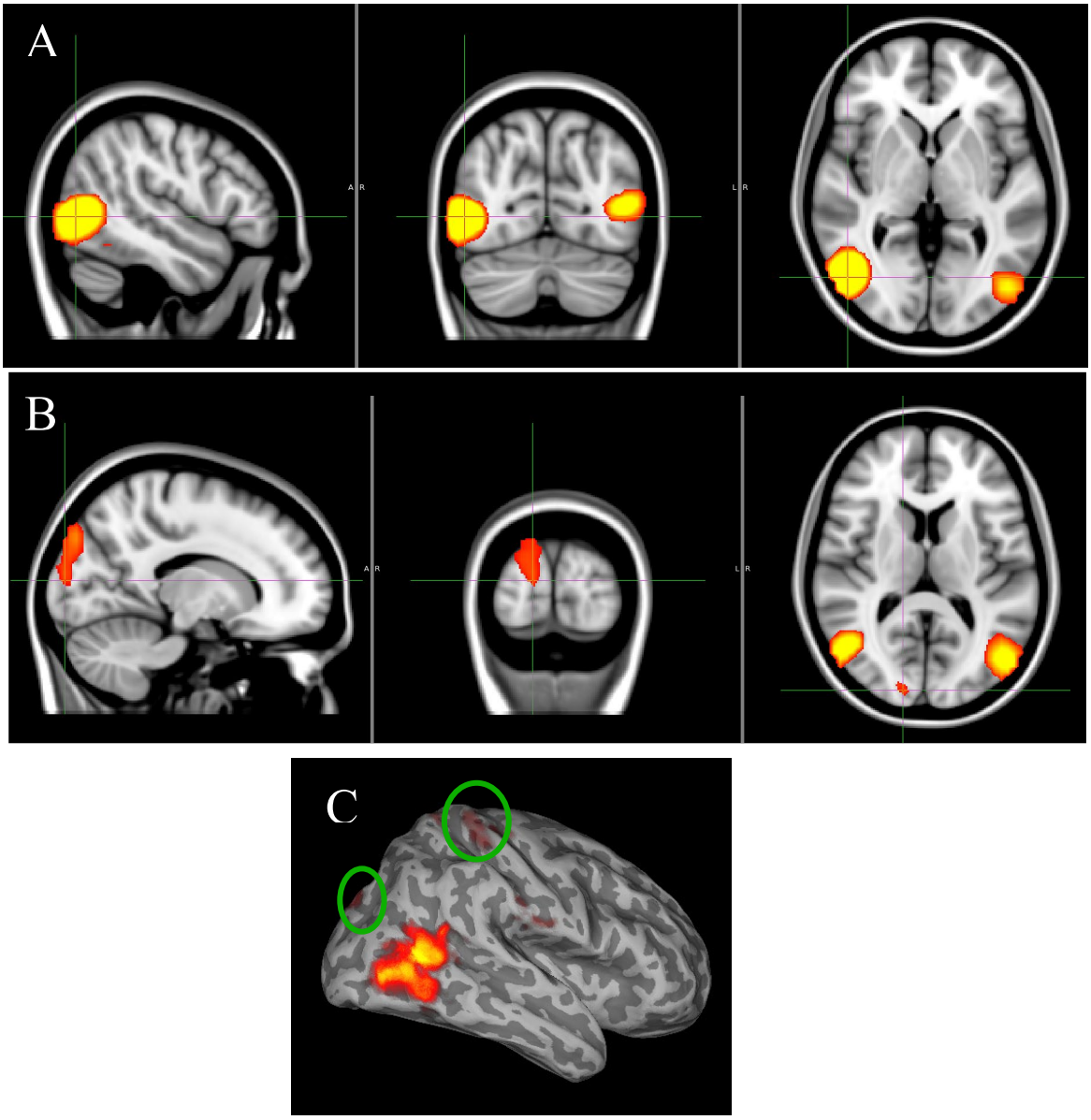

Figure 81. The first MT+ component in the grey matter masked output.

(A) Activation peak at MT+ region and bilateral activation across sites.
(B) Some associated activation extending dorsally towards V3A
(C) Component rendered onto the right hemisphere surface. Some residual activation at V3A and the postcentral gyus (circled).

Other components showing reliable activation at V3A coordinates had activation driven at these regions, in the left and the right hemispheres (see Figure 82). This suggests that V3A can be identified

bilaterally at the group level either as a separate component, or as part of a functional network (at dimensionality 200).

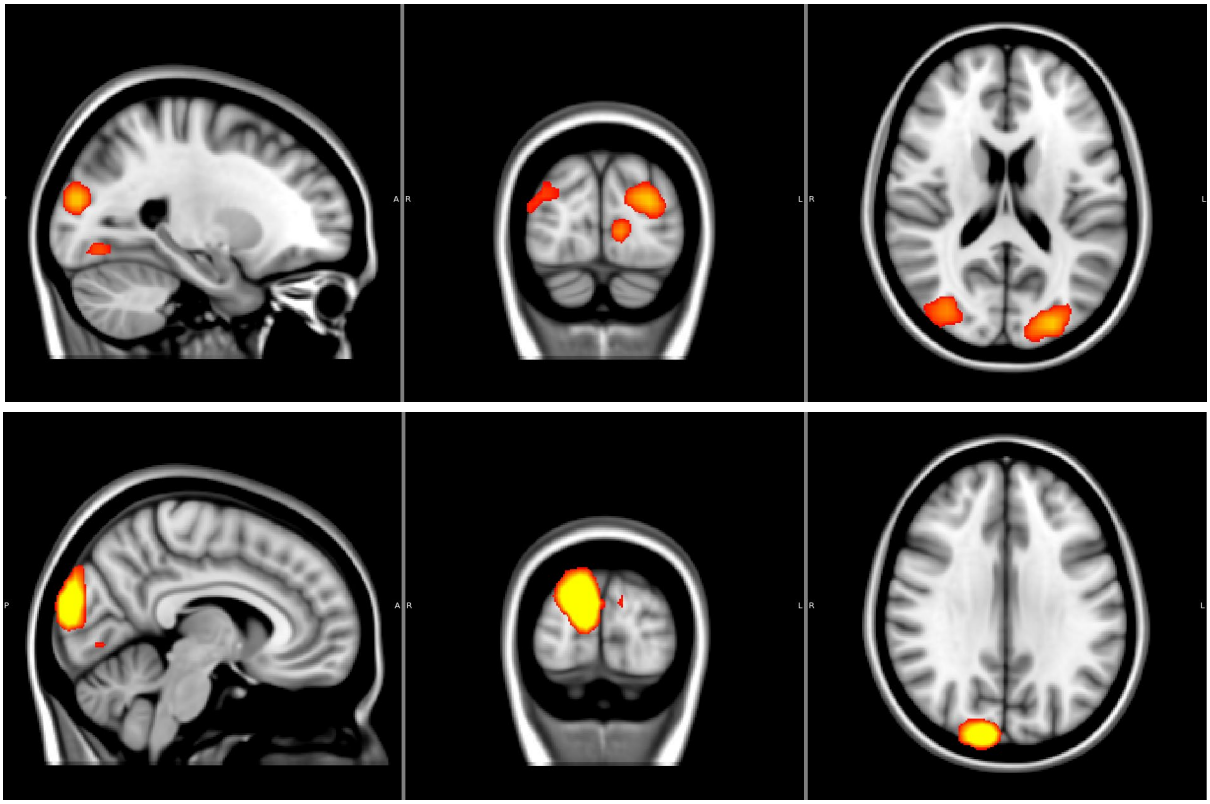

Figure 82. Two components showing activation at expected V3A. These components were driven by activity at V3A, in different hemispheres. These results suggest region V3A can be reliably identified at the group level using movies and TICA.

5.3.3 MT+

MT+ is a highly motion selective region of the human brain (Zeki et.al., 1991). It comprises of posterior and anterior sub-regions which show strong responses to optic flow motion ('MT' and 'MST', respectively; Huk, Dougherty & Heeger, 2002; Smith, Wall, Williams & Singh, 2006). MT and MST have traditionally been inseparable and are typically referred to as the MT complex, MT+ or V5. Within the MST there has been shown to be ipsilateral activation (Smith et.al., 2006) and discrete object motion processing (Recanzone, Wurtz & Schwarz, 1997). Regions MT and MST are sometimes also referred to in the literature as TO-1 and TO-2, respectively. Component activity at the expected MT+ location shows high reliability across the ICA outputs (MNI coordinates = LH[-45, -64, 0]; RH[45, -63, 1]; see Figure 83).

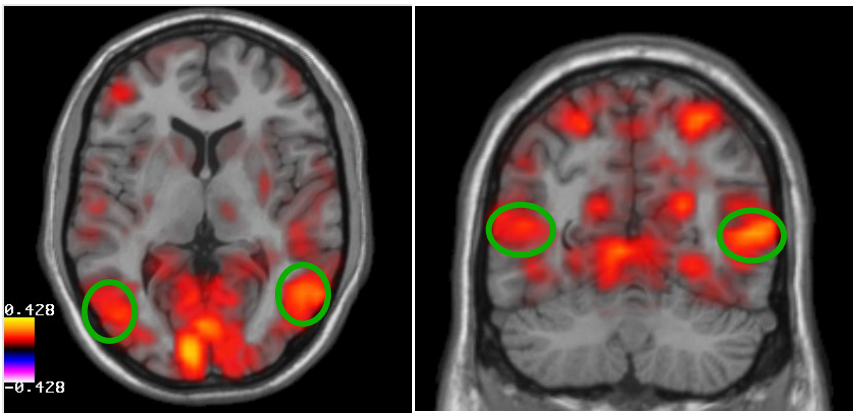

Figure 83. High reliability is seen at MT+ region (regions circled) in the grey matter masked TICA output, using a movie stimulus.

When the components are examined within this region there are three bilateral components that lie at the location identified as MT+. These components are not driven by a sub-set of the participants but have input from all subjects (bar one of the components, which has all but one participant contributing). The first component has already been described above as also showed activation at the V3A region (see section 3.3.2 V3A). Another MT+ component is also early in the ICA output meaning again that it has a relatively high median peak amplitude within the output. This component matches the previous very closely in the right hemisphere but lies more ventrally in the left hemisphere (see orange component Figure 84).

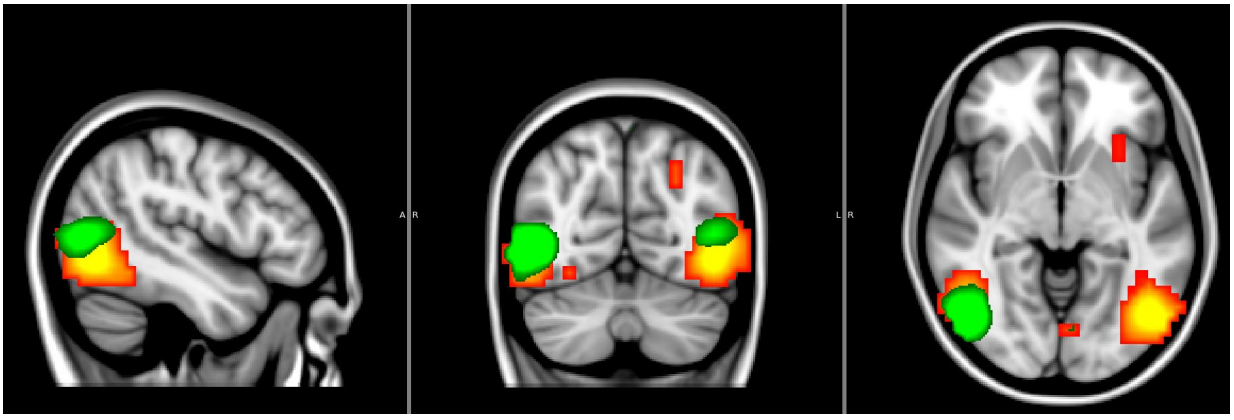

Figure 84. Two components lying at region MT+ could be identified in the ICA output. One is driven by activity in bilateral MT+ showed activation at region V3A in a functional network (yellow/orange). The other is driven by activity in bilateral MT+ (green) and does not show activation at other regions of the motion network.

This second MT component does not show activation around the somatosensory cortex or V3A. Looking at these two components it is not apparent that MT+ region is splitting into MT and MST sub-regions. Another component was identified that may be lying in the anterior portion of the MT+ complex, and therefore potentially MST. This component also had activation in early visual regions, CSv and lateral inferior parietal regions associated with the somatosensory cortex (see Figure 85).

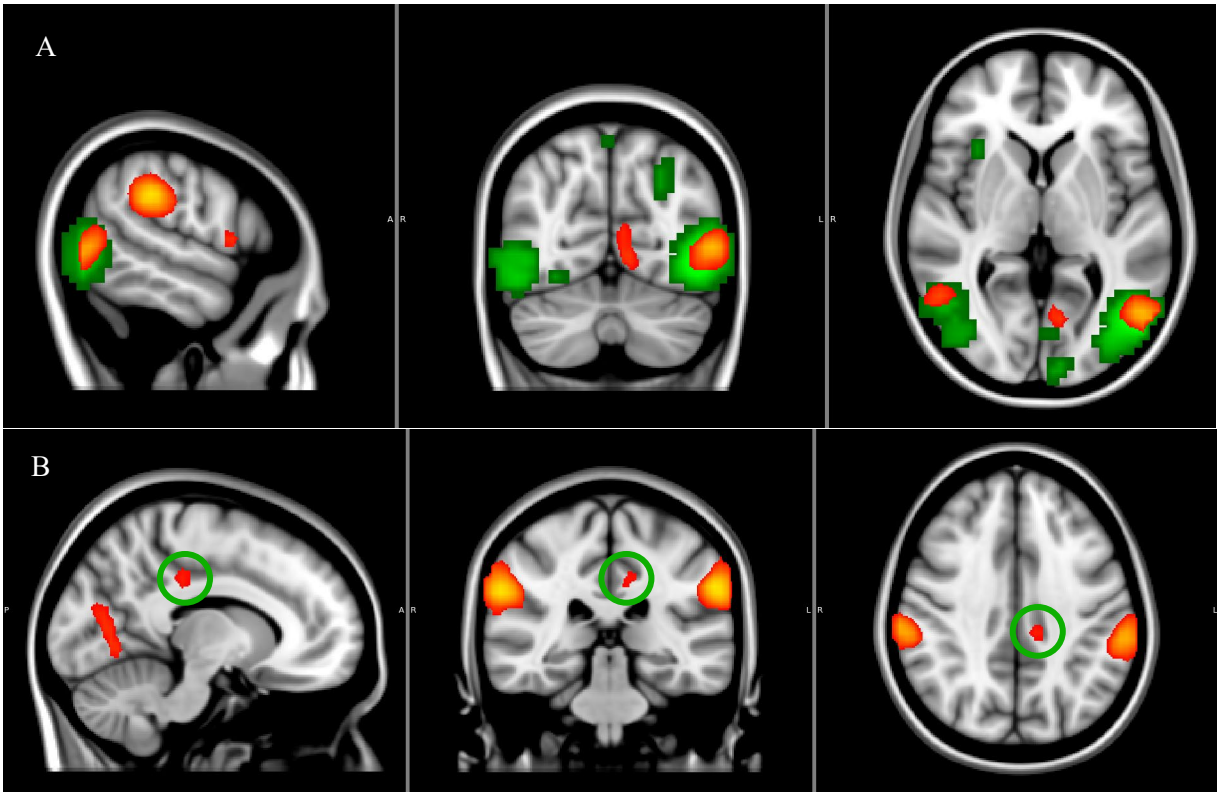

Figure 85. One component shows a network of activation at putative MST, early visual, CSv and somatosensory regions. (A) Green = Component identified as MT; Orange = potential MST aspect of network component. (B) Other regions of activation in the component showing potential MST activation. CSv is circled for reference.

5.3.4 V6

Region V6 lies medially at the parietal occipital sulcus and shows selectivity for optic-flow structures that are compatible with self-motion (e.g. Cardin, Sherrington, Hemsworth & Smith, 2012). In humans, V6 has been associated with head-centered motion perception and perceptual stability during eye movements (e.g. Fischer, Bülthoff, Logothetis & Bartels, 2012). The region is very sensitive to translational motion (Pitzalis,

Fattori & Galletti, 2013) and it is also suggested that V6 may be involved in object recognition during self-motion, due to the presence of real motion cells in the macaque brain (Galletti & Fattori, 2003) (MNI coordinates = LH[-14, -90, 33]; RH[15, -90, 29]). Real motion cells are responsive to an object which moves, even if it is kept stationary on the retina by keeping the object in focus at the fovea. When an object is stationary in the world, but head motion causes it to move on the retina, the 'real motion' cells do not respond.

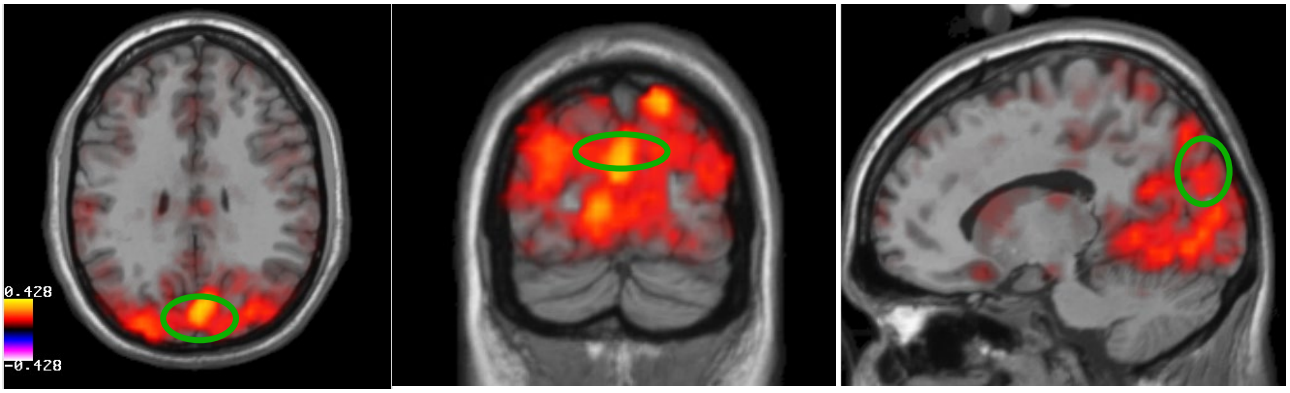

Figure 86. High reliability seen at region V6, associated with sensitivity to optic flow patterns that are compatible with self-motion (Cardin & Smith, 2009).

Bilateral components were matched to the expected location of V6, showing activation at CSv region also associated with self-motion compatible visual processing (see Cardin & Smith, 2009). These regions may represent a functional network active during natural viewing, which contains global patterns of motion simulated in movies with camera panning and zooming. These findings suggest that a movie stimulus could be used rather than traditional dot-array localisers (Cardin & Smith, 2009).

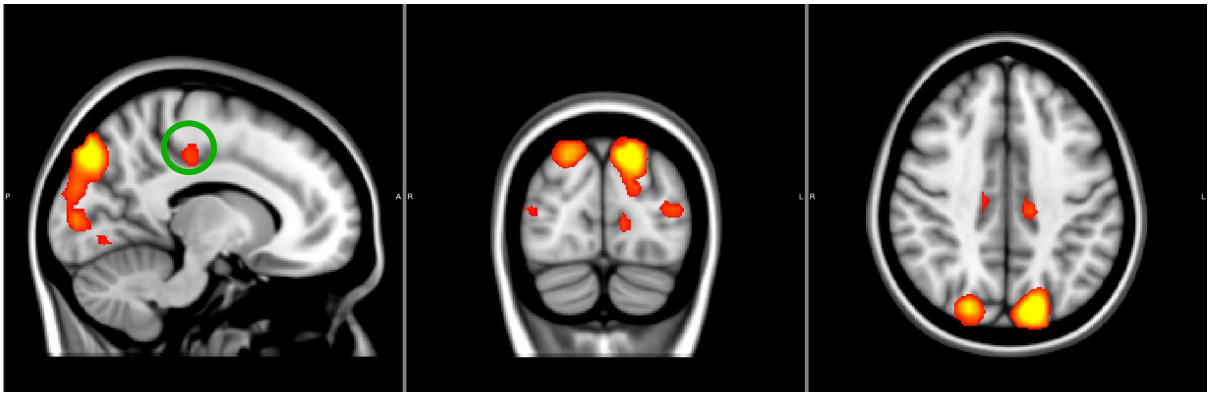

Figure 87. Bilateral activity at region V6 was identified as a reliable component. Region CSv (circled) was also active as part of this funcrional network which is understood to process global patterns of motion in the visual field usually associated with self-movement.

5.3.5 CSv

The CSv region has been identified as responding preferentially to coherent optic flow motion (Pitzalis et.al., 2013) compatible with self-motion (Cardin & Smith, 2010). The reliability map at CSv shows some (though reduced compared to other regions) reliability lateralized to the left hemisphere (MNI coordinates = LH[-12, -26, 51]; see Figure 88).

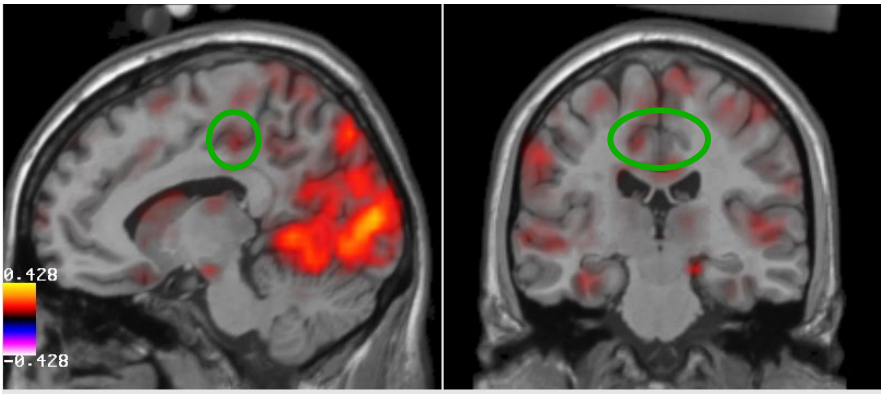

Figure 88. CSv region showed some reliability, but only in the left-hemisphere.

Components identified with activity at CSv show patterns of activation in other regions including an early visual area at anterior V1 and occipital-parietal regions (see Figure 89).

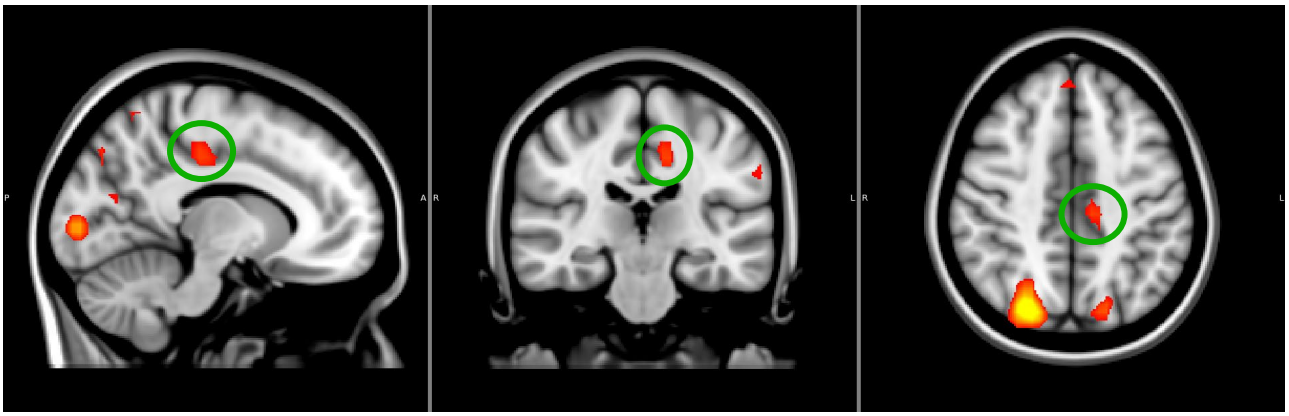

Figure 89. Region CSv was identified as part of a functional network including an early visual region and dorsal occipital-parietal regions, extending past V3A to region V6. CSv is circled for reference.

5.3.6 V1/V2/V3

Early visual regions lying close to the calcarine sulcus in the medial occipital lobe showed high reliability across the TICA outputs (see Figure 90).

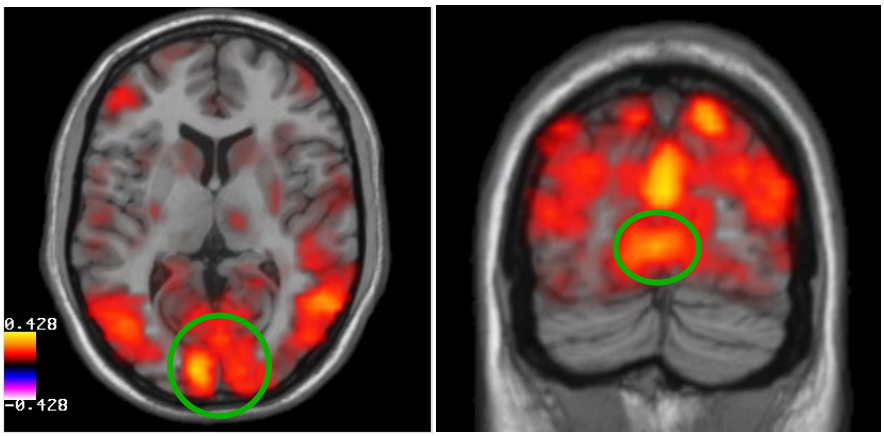

Figure 90. Early visual areas show reliable components at dimensionality 200, across permuted ICAs.

Multiple components in early visual regions were identified by the group ICA. Many had activation localized to striatal regions lateralized to one hemisphere (see Figure 91A-E). These components spanned dorsally and/or ventrally across early visual regions V1, V2 and V3. The position of the component activity did not span the whole of the calcarine sulcus, but instead showed activation at posterior or anterior portions of the early visual regions. This may mean that the TICA is delineating functional activity processing foveal versus peripheral visual field information, rather than differentiating early visual regions V1, V2 and V3. This would make sense as previous research has shown these regions to have high correlation due to processing the visual field topographically in parallel. The peripheral and foveal regions may be architecturally distinct (e.g. Hinds et.al., 2008) but act as a functional unit that cannot be split across the three regions. One bilateral component shows activation concentrated within the calcarine sulcus (see Figure 92B), this being the only exception.

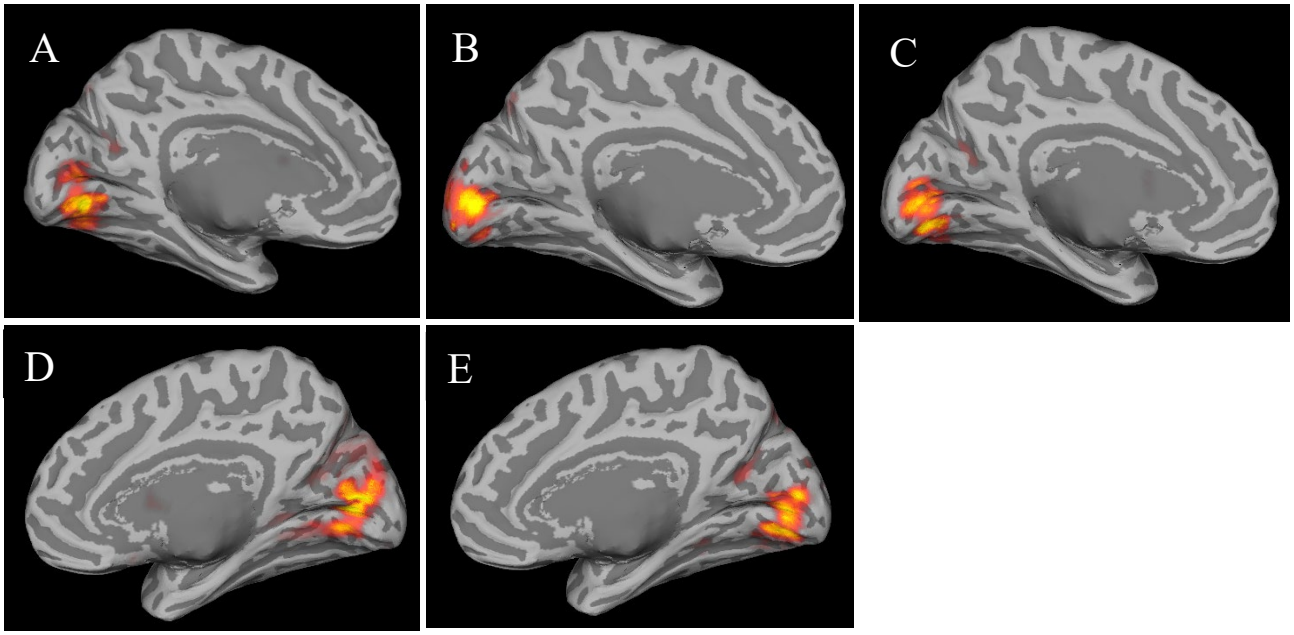

Figure 91. (A-E) Five lateralised components in early visual regions in an ICA restricted at 200. Each of these components was driven by all subjects. (A-C) lay in the left-hemisphere; (D-E) lay in the right-hemisphere.

Other bilateral components showed activity at ventral or dorsal locations around the calcarine sulcus. It may be that TICA can pull apart the dorsal and ventral visual field quadrants, using movie data. Further research using a wider field of view should explore the reliability of this segregation. This would be useful for mapping the early visual regions at the group level. Figure 92A lies at the posterior end of the occipital lobe, dorsal to the calcarine sulcus, while Figure 92C shows activation driven at a location ventral to the calcarine sulcus.

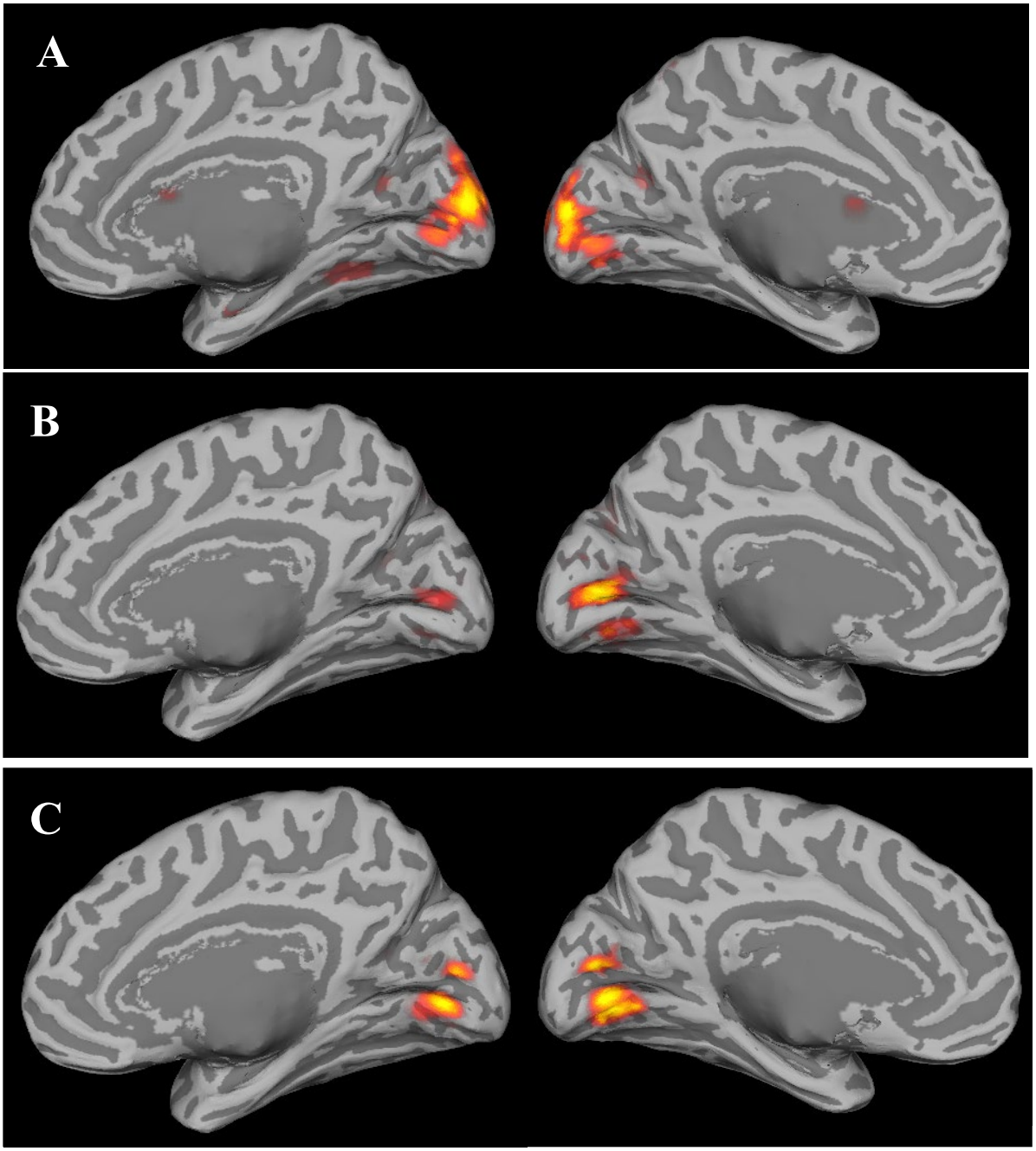

Figure 92. Early visual components with bilateral elements were reliable in the TICA output at dimensionality 200.

Other components showed activation in early visual regions and regions of interest further down the visual processing network (for example of activation with MT+ region see Figure 93). This network with early visual, MT+ and post-central gyrus activation is identified in meta-analyses (e.g. Yeo et.al., 2011). Using a movie stimulus these regions can be reliably identified as a network, or as separate sub-components. This separate identification of network subcomponents may depend on the dimensionality of the ICA output

as components have been identified as 'splitting' as dimensionality is increased (e.g. Smith et.al., 2009). The splitting of components at higher dimensionalities into useful sub-components is addressed in Chapter 5.

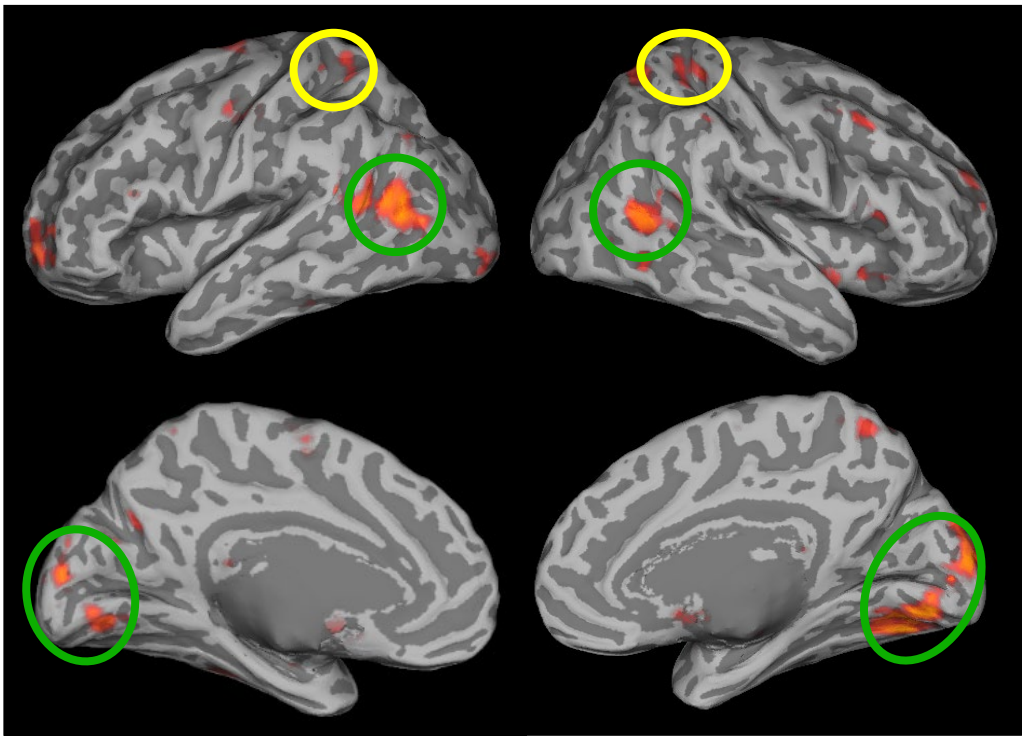

Figure 93. Example component showing activation in early visual regions and other regions in the motion pathway. Here MT+ region is showing bilateral activation. There is also small amounts of activation at the post-central gyrus (circled yellow).

5.4 Summary: Chapter 5

Regions of interest in the motion pathway can be reliably identified at the group level using a complex naturalistic stimulus (here we used a movie clip) and TICA. These regions are activated in response to a rich visual scene containing motion, and time-locked across participants. Regions representing early visual responses to peripheral and central visual field information, MT+, V3A, CSv, pVIP and V6 were identified as components in this REPRUN output. These components represented functional networks containing multiple regions of interest, or subcomponents of these networks.

These results support the use of a movie stimulus for identifying regions and networks of interest within a group, rather than the use of individual localisers. This would have a positive impact on the research community as movies would cut down on scanning time and improve the experience of the observer. The

previous chapter indicated that components within the occipital lobe and parietal lobe were relatively consistent across motion correction and masking techniques. Therefore, it is probable that the regions of interest identified in this chapter may also be observable in these alternative outputs. Further work would be useful to confirm that this is the case.

So far, I have provided evidence that movie stimulus and TICA can be used for identifying regions of interest in the visual pathway within a group. This is a very useful for locating ROI as an alternative to using multiple simple localisers and retinotopy. It would also be beneficial to be able to reliably identify visual ROI at the individual level. In the next chapter I will investigate whether this is possible using a movie stimulus and TICA. Based on previous work by Bartels and Zeki (2004; 2005) it is hypothesized that visual regions can be identified at higher dimensionalities. This will be tested as well as the generated of larger scale networks, expected at lower dimensionalities in line with previous chapters and research in the field (Smith et.al., 2009).

Chapter 6: Single subject ICA and movie stimuli

6.1. Introduction

The previous chapters have examined the robustness of visually driven group TICA components using movie data from twenty-two subjects. The findings demonstrate that reliable components can be identified across different samples, representing multiple visual regions and networks of interest. Although this is very useful, it is also of interest to be able to map visual regions and networks at the individual level. This chapter will examine whether this technique can identify visually driven regions and networks at the single subject level.

One concern is that the reduction in data-points at the individual subject level may reduce the robustness of results, meaning regions cannot be identified reliably in different individuals. Previous work by Bartels and Zeki (2005) demonstrated that visually driven regions of interest could be identified across 8 observers at V1/V2/V3, V5/MT+, regions in in the fusiform gyrus including V4 and sub-regions of the lateral occipital complex, including the FFA. This finding pioneered a potential new method for identifying functional regions in the cortex. The aim of this chapter is to build on the work by Bartels and Zeki and compare a larger sample of individual TICA results to known visual networks (at low dimensionality) and multiple visual regions of interest (at a high dimensionality).

First the spatio-temporal representativeness of components between subjects overall will be calculated. It is expected that there will be some variation in component maps and timeseries, due to individual differences (e.g. anatomical). Next, subject components will be compared with known visual networks (presented with group data in Chapter 4), with the aim of learning whether the same regions and networks can be identified in single subjects. As components at a low dimensionality show correspondence with known visual networks across the subjects, components generated at a higher dimensionality in visually driven regions will be compared across subjects to see how reliably they . This is assessed at dimensionalities of 70 and 200 and results show that visually driven ROI can be reliably identified across individual subjects. It is also shown that even at high dimensionalities some global networks remain in the single subject output. Finally, I test the robustness of the technique by using a “leave-one-out” method of analysis, correlating the

timeseries of components with BOLD activity of subjects who were not included in the TICA. These results are promising, and I generate probabilistic maps using the outputs.

6.2 General Methods

The data of twenty-two participants was collected during movie watching, as described in Chapter 1 (section 1.3). Arguably, smoothing and resampling is not necessary for investigating single subject outputs as part of the reason for this pre-filtering is to deal with anatomical differences between observers (e.g. Van Essen et. al., 2011). However, as we were comparing across subjects for an idea of consistency I wanted to limit the effect of anatomical differences as far as possible.

Three individual ICAs were run for each participant for comparison (a) without grey matter masking, (b) using a grey matter mask generated using segmented regions of the MNI standard brain, using FSL's FMRIB's Automated Segmentation Tool (FAST), and (c) using a grey matter mask generated using the subjects own structural MRI scan.

ICA outputs showed high temporal and spatial similarity across the two different masking techniques (average temporal correlation r = 0.86; average spatial correlation r = 0.65). The components generated using the MNI mask are documented as the similarity of components across subjects was slightly improved, compared to the subject's own mask. Using a grey matter mask improved the similarity between ICA outputs across subjects overall compared to using no mask, but only very marginally; the average correlation improvement across all matched timeseries was 0.002 and for matched spatial maps was 0.02.

6.3 Across subject ICA comparisons

6.3.1. Methods

Initially dimensionality was automatically calculated using MELODIC. Across the subjects the mean component number was 198 (range = 265-169). As previously noted (see Chapter 2), the number of components output using the twenty-minute movie clip is quite a way higher than the dimensionality often used when analyzing resting state data to identify neural networks (e.g. ~20-25; Smith et.al., 2009). The variation in the dimensionalities of the outputs demonstrate that components being identified are different for

each subject. This was expected by on the findings in Chapter 2, where different first brains produce different ICA outputs and some difference is expected due to variances in noise aspects such as motion artefacts across subjects. Despite this variation, it is also expected that functional networks and regions of interest will be matched across subjects due to the functional specificity common across brains and the temporal structure applied to visually responsive and attentional regions by the movie (Hasson et.al., 2010). In Chapters Three and Four my work has demonstrated that key visual areas seem to be identified irrespective of dimensionality.

Dimensionality was restricted at 70 to match for comparison across subjects and with the group network components. The representativeness (similarity) of the outputs between subjects overall was assessed using the same correspondence technique described in Chapter 2; spatial and temporal correlations were calculated between all the components and matched across subjects.

6.3.2. Results

The spatial maps show higher mean correlation values overall (see Figure 94, top) than the temporal correlations (see Figure 94, bottom). This suggests that despite anatomical differences, the location and size of matched components is similar across groups and that it is likely the same regions of interest are being matched across subjects. The similarity of component timeseries here represent the correlation between the underlying functional source signals across participants at these ROI. Work in the previous chapters showed significant correlation of the BOLD timeseries in visual regions across subjects, suggesting that these regions show some timelocking of response to the movie stimulus (Hasson et.al., 2010). Differences in the component timeseries across subjects are expected due to individual differences and noise. The extent to which functional temporal locking occurs in ROI is of interest and could be explored further to build on findings of observer differences in this analysis.

Both the temporal and the spatial similarity are less similar between individual subjects than across different group ICAs with the first brain swapped (see Chapter 2, page 9). This is expected as the same data is included across permuted groups and influences the component output (see Chapter 2), while different participant data is used in each individual ICA. A larger decrease in similarity is seen across the temporal correlations relative to the permuted groups

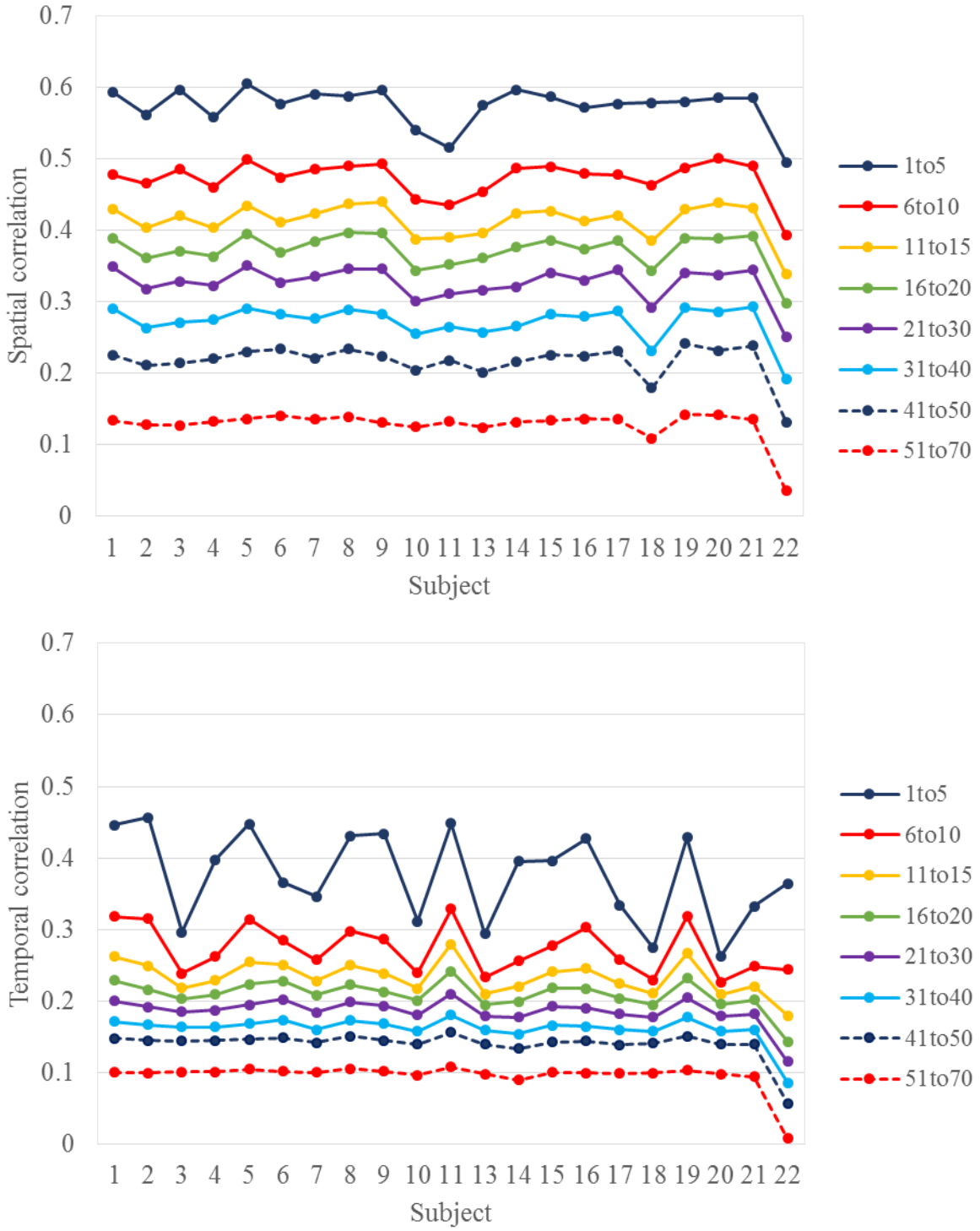

Figure 94. Top: The mean spatial correlations between components in single subject ICAs show some correspondence despite individual anatomical differences. Spatial correlations with an r-value>0.11, are significant $p<0.05$. Bottom: There is some temporal variation between the ICA components across single subjects. The temporal correlation of components is lower than spatial across single subject ICAs. Temporal correlations with an r-value>0.12, and are significant $p<0.05$.

6.4 Single subject networks vs. Known visual networks

6.4.1 Methods

ICAs were run for each subject at dimensionality 20. I compared single subject component maps with known visual networks identified at the group level (see Chapter 3). These were used as a baseline to assess how reliably these established networks were represented at the individual level. The peak voxels of matched components are also discussed, below.

6.4.2 Results

When compared with the three visual network components, the average spatial correlations across subjects were r= 0.58 (SD = 0.12), r= 0.55 (SD = 0.10) and r= 0.47 (SD = 0.11), respectively. The average spatial correlation across the three visual networks for each subject is displayed in Figure 95 and demonstrate that visual networks can be reliably identified using movies and TICA in a single subject.

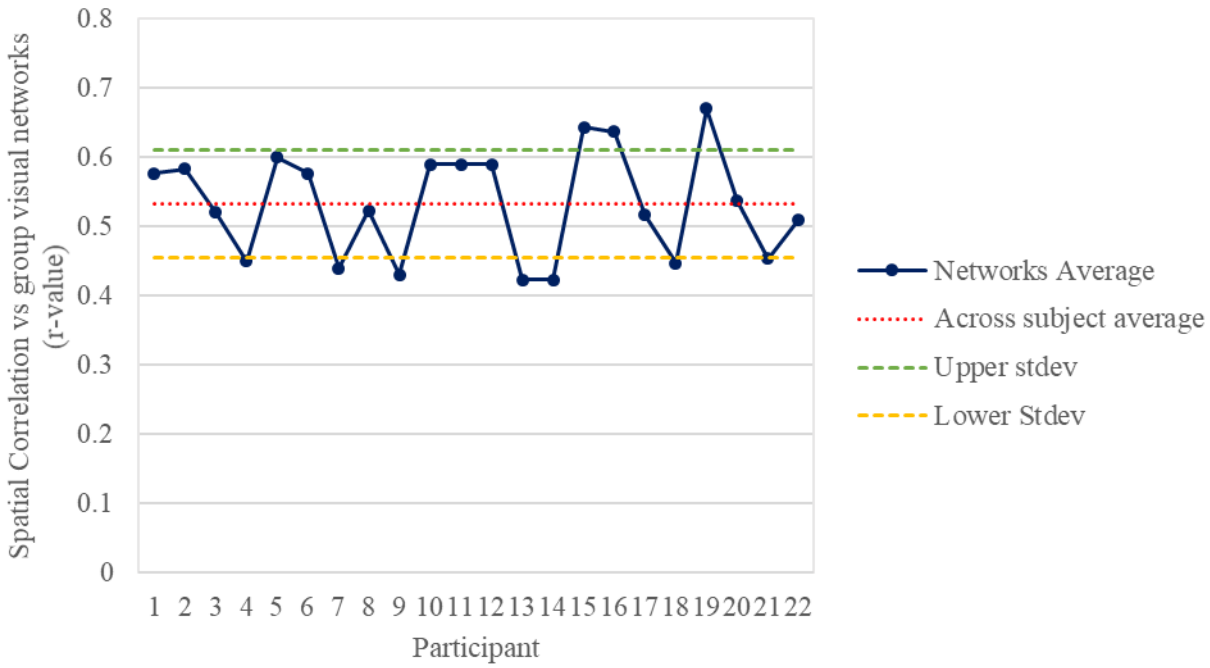

Figure 95. The spatial correlation between single subject components at dimensionality 20 and matched group visual network components, at dimensionality twenty. Correlations are averaged across the three visual networks for each subject. Single subject components were chosen as being the best matched to the group visual network component based on spatial similarity.

The timeseries of the single subject components were also compared to the group timeseries. The average timeseries correlation was also well matched on average for each of the visual network group

components across these single subject components (r = 0.38 (SD = 0.17), 0.49 (SD=0.23) and 0.47 (SD = 0.26), respectively). However, some of the individual timeseries did show low correlation with the group component with the range across subjects 0.67, 0.82 and 0.81 for each of the networks, respectively. When components at the subject level often showed significant temporal correlation across more than one of the group visual networks, indicating some temporal correlation between the visual networks. This is expected if meaningful functional segregation is being achieved by ICA.

The analyses above show significant correlations (r threshold 0.25; Smith et.al., 2009) between the single subject and group subject visual networks, however there are some differences in the component spatial maps. One option when aiming to identify functional regions and networks of interest in a single subject is to run a group tensor ICA and then use the group level spatial maps to locate individual subject regions of interest. Work in Chapter 2 demonstrated that the ICA components incorporate single subject data into the analysis to create robust components. These components provide a reference to compare single subject results. Next, peak voxels of single subject and group components were compared for each of the matched visual networks.

6.3.2.1 Visual network 1

Individual subject components matched to the first group visual network showed peak activation around the primary visual regions (see Figure 96 and Figure 97). Some components showed regions of activation extending laterally and/or dorsally with reduced activation at the calcarine sulcus. These components were averaged spatially and by peak voxel for further comparison with the group component and to understand the variability between subjects.

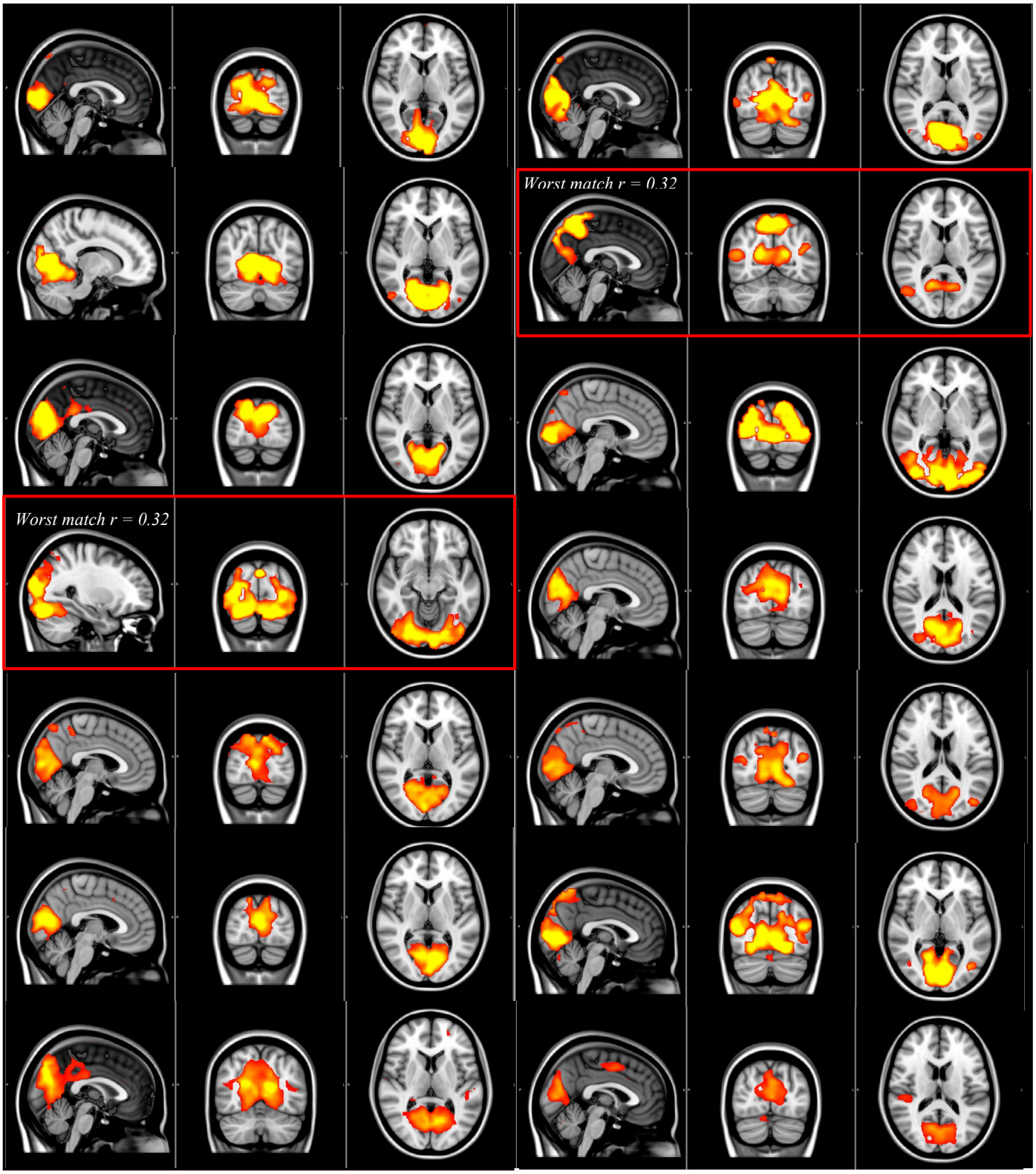

Figure 96. Subjects 1-14 individual ICA components matched to the first group network, covering primary visual regions. Some components show more dorsal and/or lateral activation. The two components with the (joint) lowest spatial correlation to the group component is highlighted (r = 0.32).

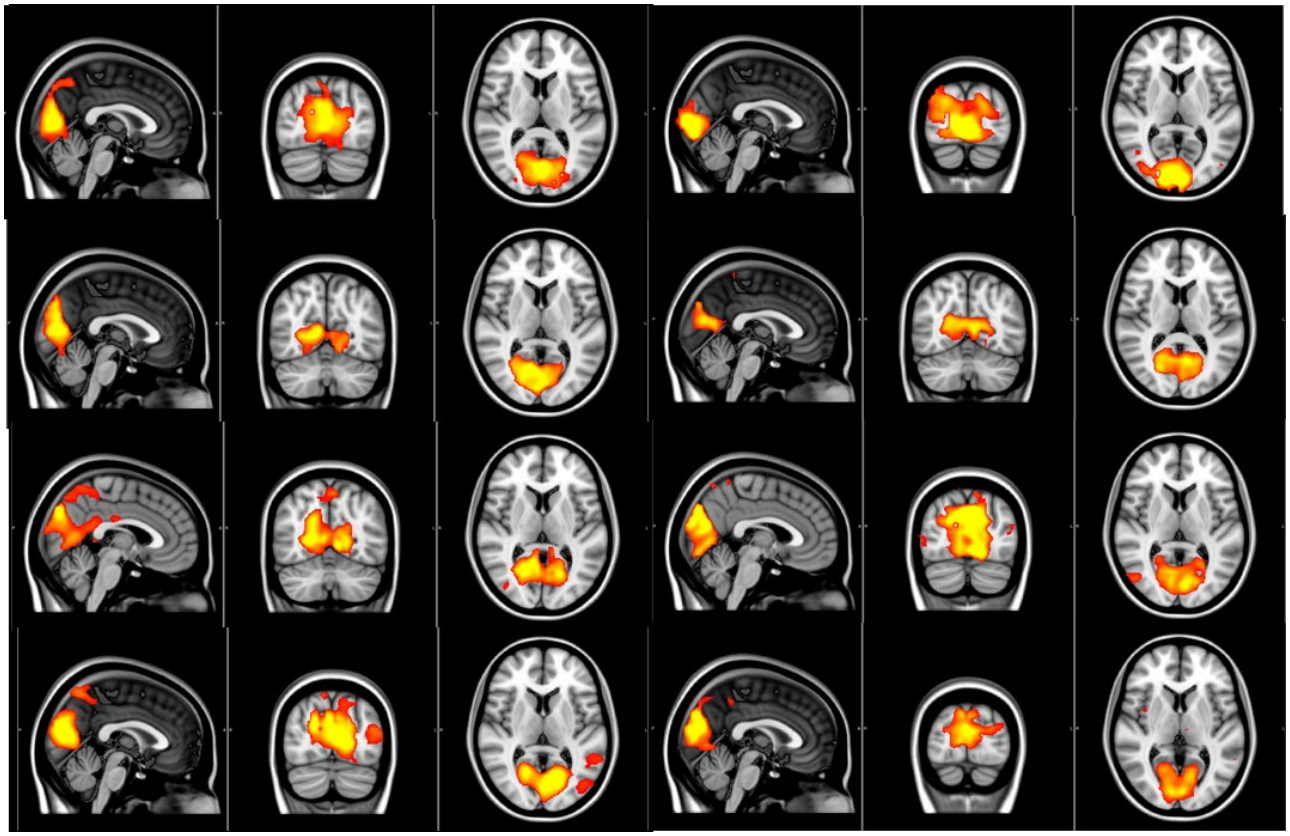

Figure 97. Subjects 15-22 individual ICA components matched to the first group visual component, covering primary visual regions. Most participants show activation focused in medial occipital regions.

The peak voxels of the first group network component were at primary visual regions (MNI coordinates [5, -78, 0] in the right hemisphere and MNI [-11, -78, 4] in the left). The peak voxel in each hemisphere was averaged across the matched single subject components to MNI coordinates [8, -79, 18] in the right hemisphere and [-10, -80, 19] in the left. The standard deviation across single subject components showed some variation in the peak voxel location (left hemisphere standard deviations x = 9mm, y = 10mm, z =16.5mm; right hemisphere standard deviations x = 8mm, y = 10mm, z = 15.5mm), with the largest differences seen on the z-axis (inferior-dorsal).

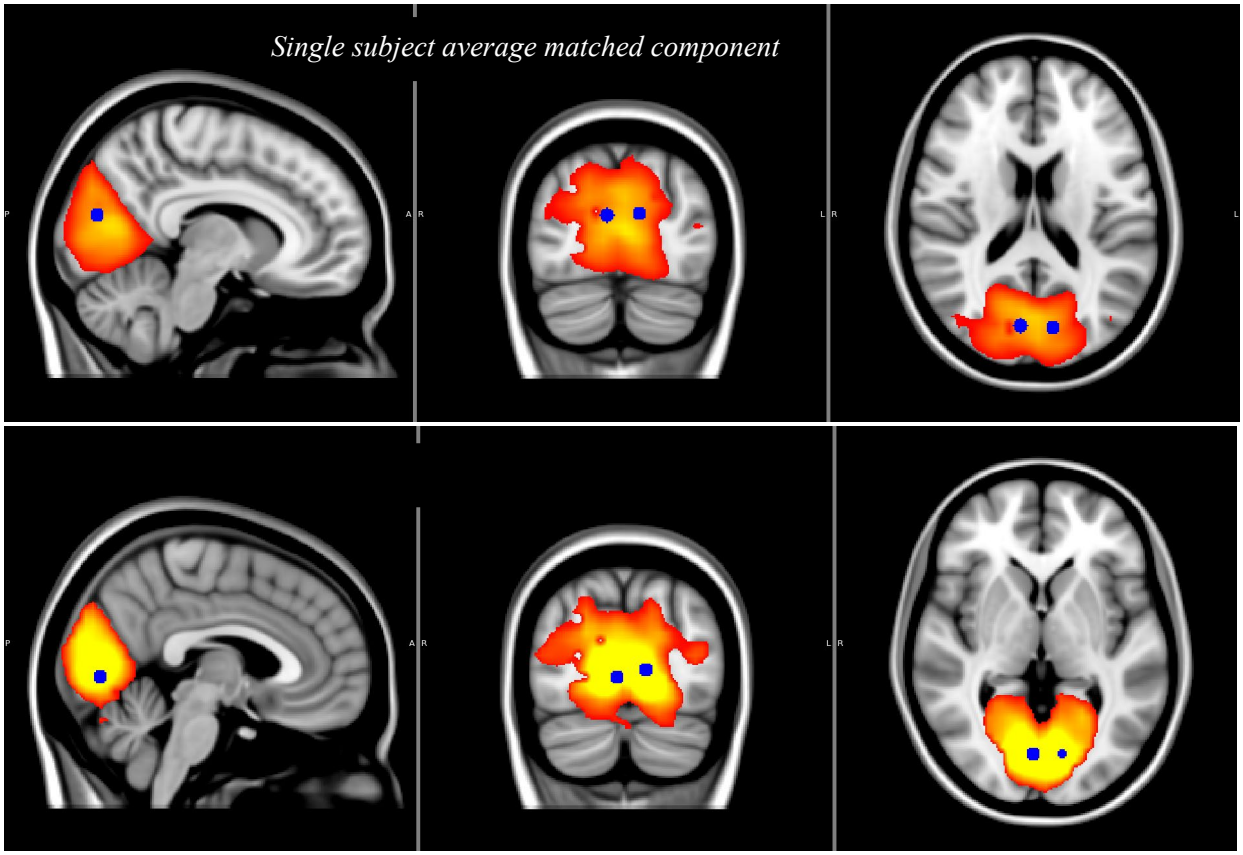

Figure 98. Top: The average of single subject components matching the first visual network (group level ICA). Peak voxels lie in the medial occipital lobe, above the calcrine sulcus and shifted dorsally compared to the group component (bottom). Bottom: The group component representing the visual network covering primary visual regions. The peak voxels are located at the calcrine sulcus in both heispheres, marked with blue spheres.

These mean coordinates show that at the subject level the peak coordinate of coordinates matched by spatial map correlation lay more dorsally within the occipital lobe (see Figure 98). Across subjects the peak voxel was at an average Euclidean distance of 23mm^3 from the group peak voxel in the left hemisphere (range = 59mm^3) and 24mm^3 in the right (range = 56mm^3). Within both hemispheres the average single subject peak voxel was 18mm and 15mm shift on the z (depth) axis, therefore most of this difference was taken up in this dimension, with less variation laterally and on the anterior-posterior axis. Although there were some differences in the location of peak voxel between the group visual network component and the components at the subject level, the average spatial map of matched components was very similar to the group network, as expected (see Figure 98).

6.3.2.2 Visual network 2

The second visual network covered lateral and posterior occipital regions. Individual components show good spatial correlation overall (see Figure 99 and Figure 100). The lowest R-value across a single subject component and the network comparison was 0.35 (indicated in Figure 99).

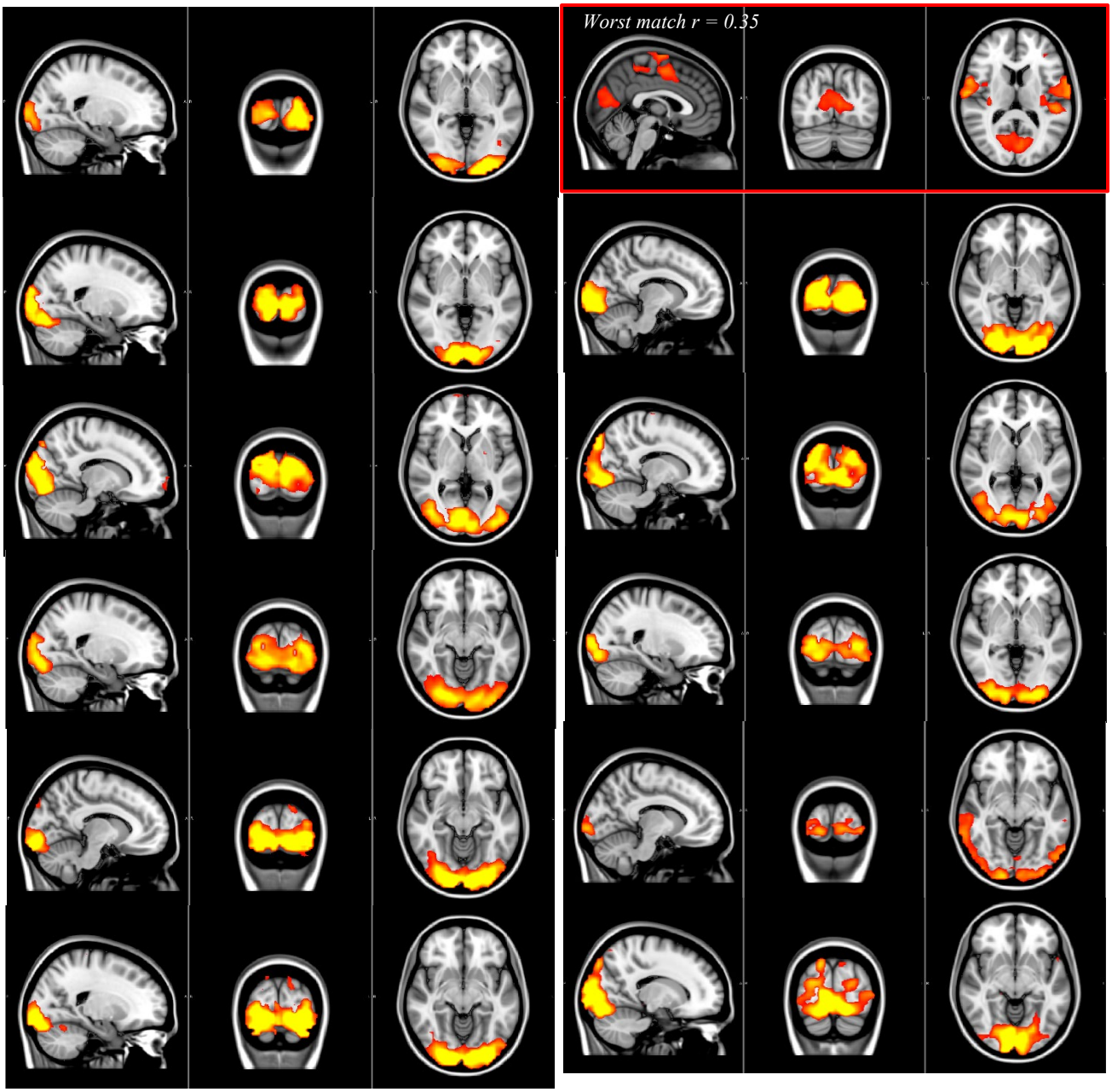

Figure 99. The indivisual subject components (Subjects 1-12) matched to network 2, covering posterior and lateral occipital regions.

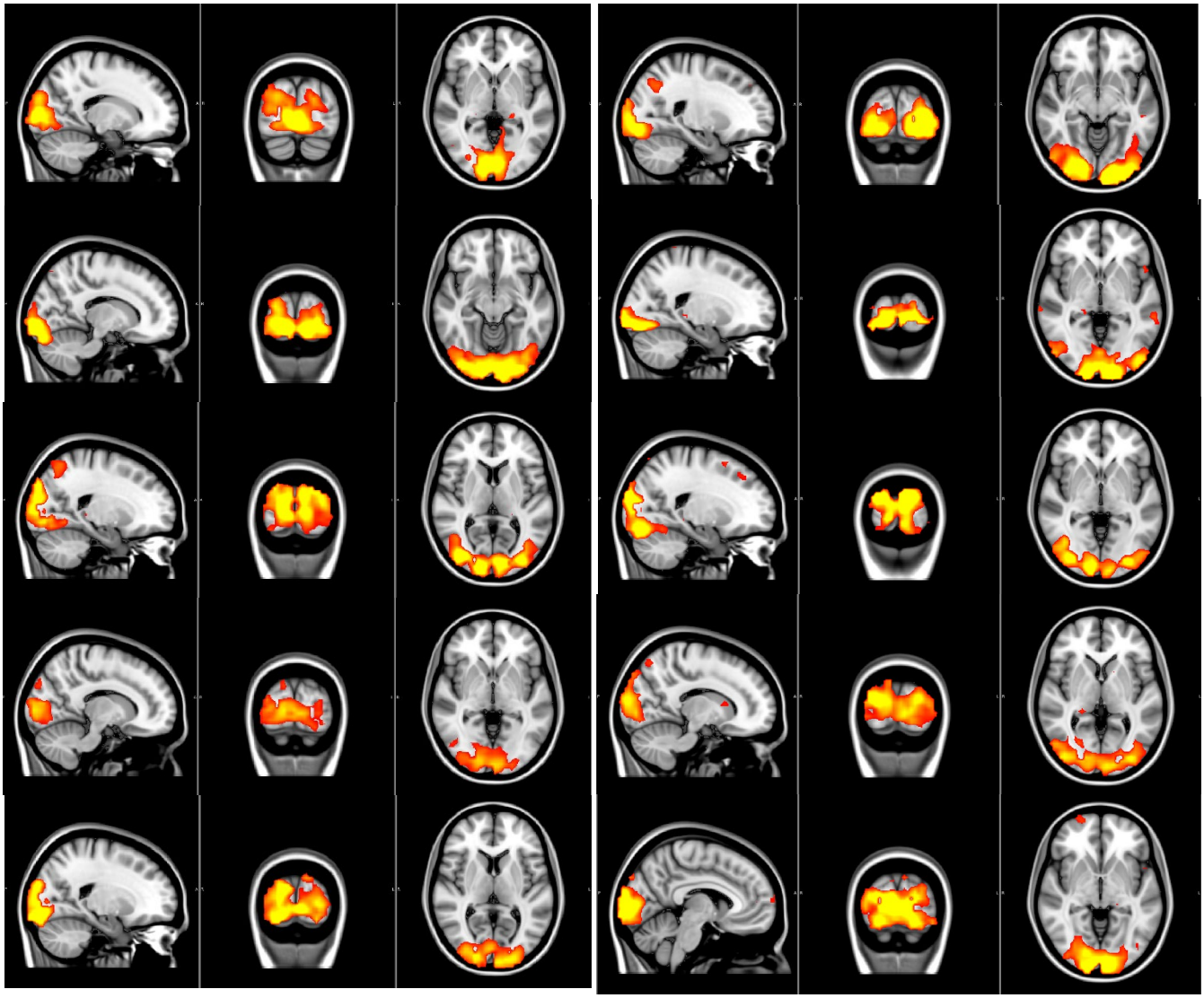

Figure 100. Subjects 13-22 individual components with the best spatial correlation to visual network two in the lateral and posterior occipital lobe.

Again, the average peak voxel and spatial map was generated to compare with the group component. The mean component map across single subject matches showed good spatial correspondence with the group reference component, overall (see Figure 101 comparing average spatial map with the group component). The peak voxel of the group component for visual network two lay in a posterior occipital location, at MNI [-15, -98, 0] in the left hemisphere and MNI [5 -94, 0] in the right. The average peak voxels across subjects showed movement laterally in the occipital lobe, compared to the group component (plotted onto Figure 101).

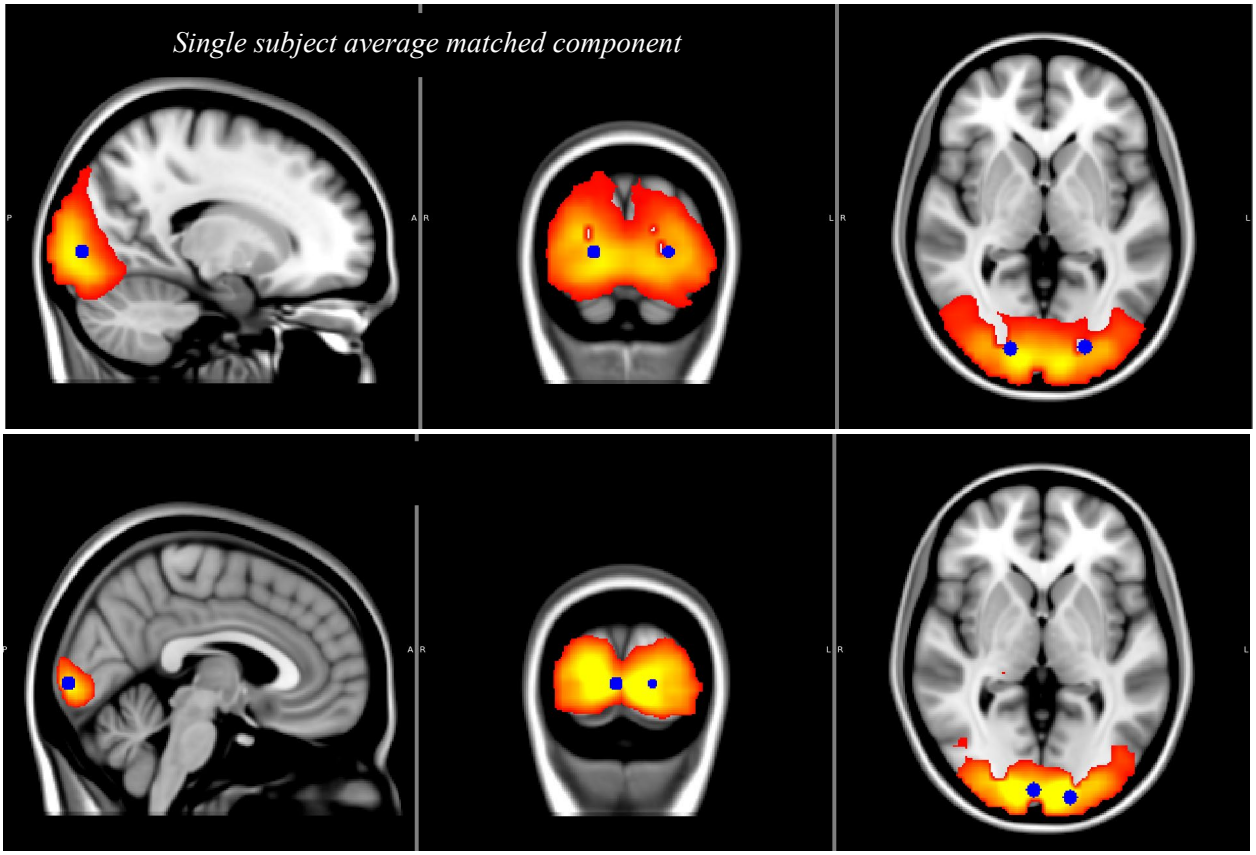

Figure 101. Top: The average of single subject components matching the second visual network (group level ICA). Average peak voxels in each hemisphere are marked with blue spheres. Bottom: The group component used as reference, covering lateral and posterior occipital regions. The peak voxels of this component lie more medially in both hemispheres than the average peak voxels across subjects. The spatial maps are well matched.

The average distance of the peak voxel of matched single subject components was a Euclidean distance of 16mm^3 in the left hemisphere (range = 23mm^{3,} MNI coordinates [-22, -88, 0]) and 20mm^3 in the right (range = 25mm^3, MNI coordinates [19, -89, 0]). The range in peak voxels in the matched single subject components was 14mm in the x-direction, 19.5mm in the y-direction and 13.5mm in the z-direction (see Figure 101 for location of average single subject peak voxels).

6.3.2.3 Visual network 3

The third group component covered the MT+ regions with some activation at V3A and the pre-central gyrus. Subject components matched to this network often showed peak voxels at V3A, rather than MT+. suggesting that this network may be driven by either MT+ or V3A during natural viewing, perhaps dependent on attention, task or individual differences (individual component presented in Figure 12 and Figure 13).

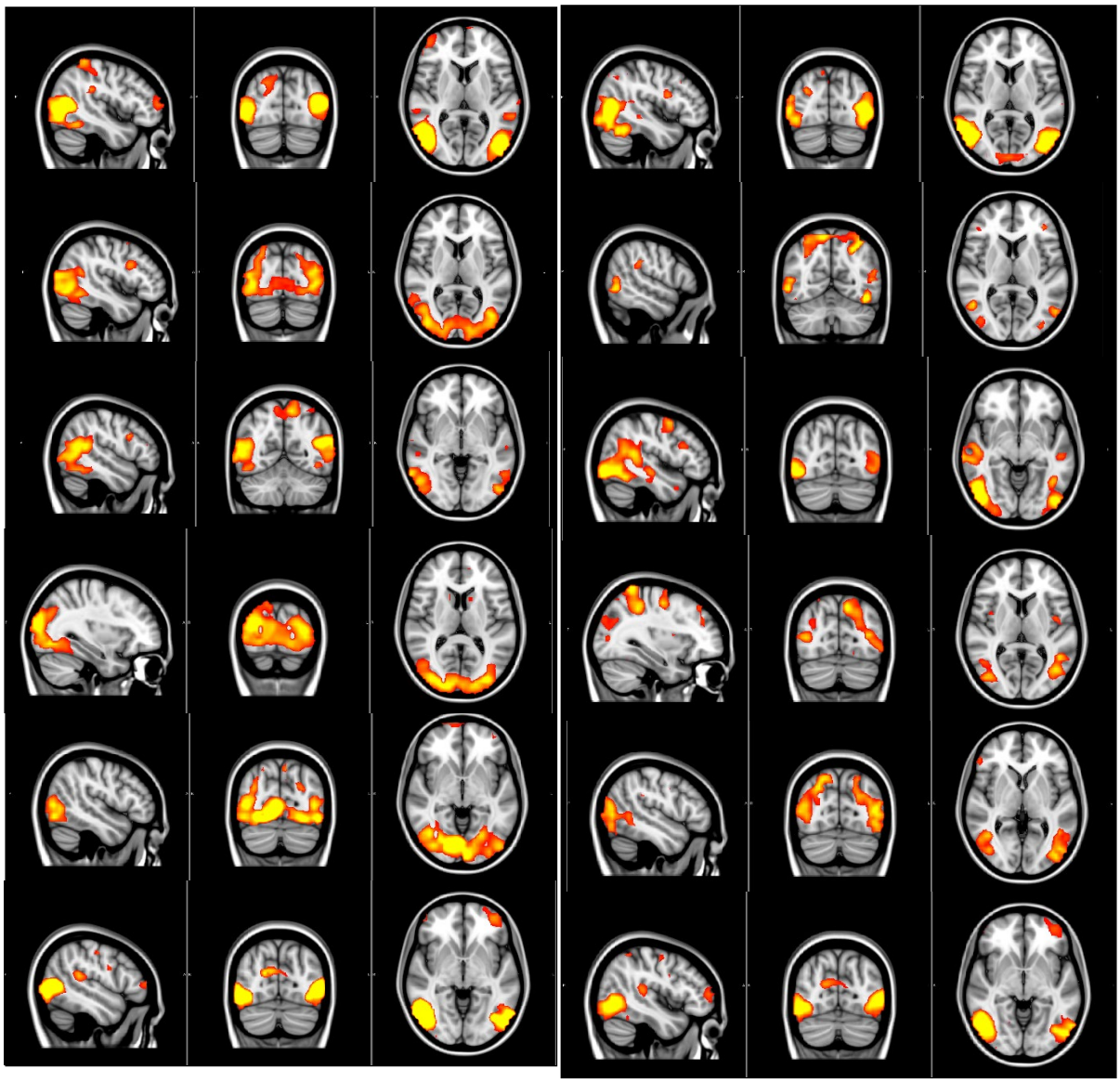

Figure 102. Single subject best matches to the third group visual network which is largely driven by MT+, but shows actication at V3A and pre-central regions to different degrees across the subjects.

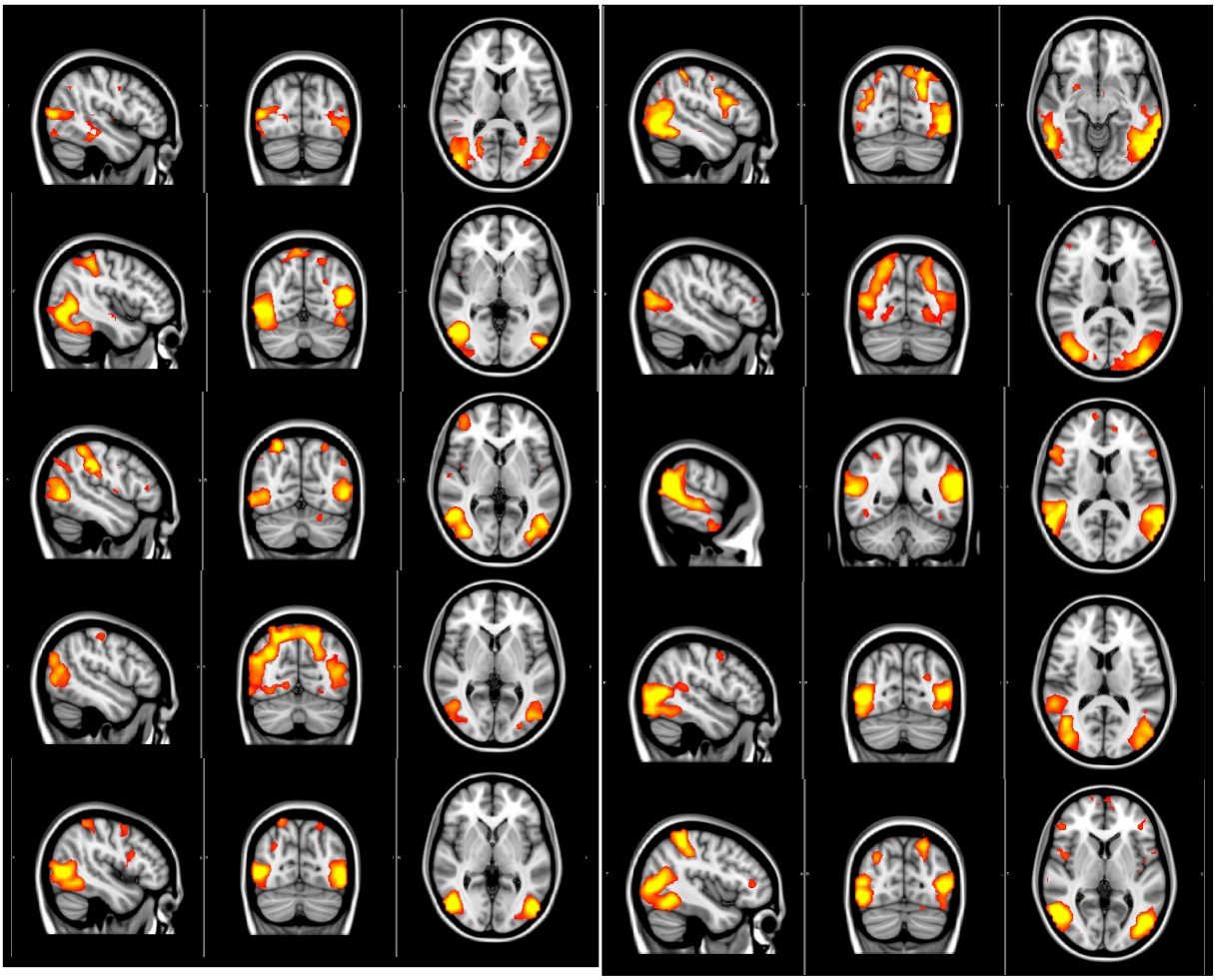

Figure 103. Subjects 12-20 individual components matched to the third visual network covering lateral occipital regions MT+ and some dorsal areas including V3A.

The peak voxels of the group component for visual network three lay in the lateral occipital regions at MNI [-51, -74, 8] and MNI [49, -66, 0]. The average distance of the peak voxel for the matched single subject components was a Euclidean distance of 26.5mm^3 in the left hemisphere (10mm in the x, y and z dimensions, range = 59mm^3) and 29mm^3 in the right (11.5mm in the x y and z dimensions, range = 62mm^3). This component was the least well represented of the three network components. The mean peak coordinates across subjects were at MNI [-40, -61, 18] and MNI [36, -55, 19]. The variation of the peak voxel was much higher with this network and the mean peak voxel location is pulled dorsally and anteriorly. Both analysis results are due to some subjects having components matched to this network with peak voxels at region V3A and the pre-central gyrus, rather than at MT+. As this pulled the peak voxel to an intermediate location between MT+ and V3A (see Appendix 6.1), the peak voxels were identified in ventral regions excluding V3A, to check that

these coordinates matched expected MT+. The average peak across subjects lay at expected MT+ MNI [-47, -74, 5] and MNI [47, -70, 0] (see Figure 104, top).

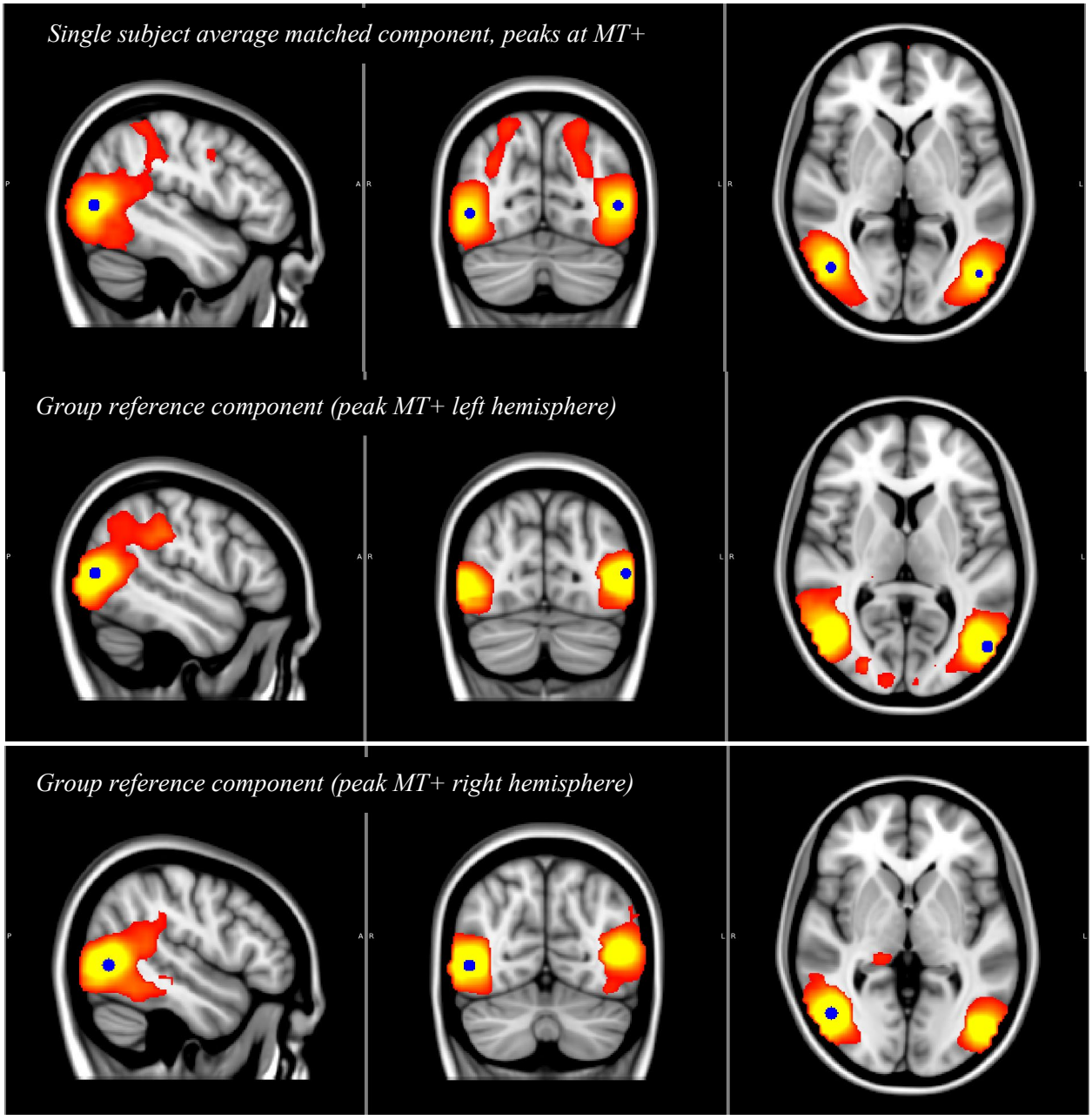

Figure 104. Top: The average of single subject components matched to the third visual networks shows activation at MT and V3A, plus pre-central regions. This has pulled the average peak voxels across subject up towards the V3A regions. The fact that some subjects have peak voxels in MT+ and others at V3A suggests that this network may be driven by either MT+ or V3A during natural viewing, perhaps dependent on attention, task or individual differences. Marked on the maps with a blue sphere is the peak voxel exclusing activation in dorsal regions, which lies at the expected MT+ region MNI [-47, -74, 5] and MNI [47, -70, 0]. *Centre and bottom*: The peak voxels of the group component lay in MT+ regions, bilaterally.

6.3.2.4 Summary

Results show that visual networks are represented at the single subject level, supporting the use of using TICA and data collected during movies for identification of individual visual networks. Visually driven networks show some variation in spatial map and peak voxel across subjects, therefore group level components may not fully represent the networks in individual observers.

In the next section I investigate component reliability at higher dimensionalities. When single subject TICAs were run using the movie data the average dimensionality was ~200 components. Work in the previous chapter at the group level has suggested that as dimensionality increases, the components represent sub-regions of networks. Therefore, it is of interest to investigate the components at higher dimensionality to see whether functional regions of interest can be identified in a single observer.

6.5 Components identified at high dimensionality

6.5.1 Methods

Single subject ICAs were run using unmasked data at dimensionality 200. One concern with implementing a higher dimensionality is that overfitting may cause useful components to be split. However, when single subject ICAs were run with unrestricted dimensionality (i.e. automatic allocation of dimensionality), data provided a minimum of 201 components based on Bayesian PCA analysis (used by FSL's MELODIC for determining dimensionality; Beckmann & Smith, 2004), suggesting that components are meaningful at this dimensionality for a single participant. We found that components at this dimensionality were stable across single subjects, representing visual regions in striatal and extrastriatal areas. If components were being overfitted you would expect the components to become unstable as their splitting would not be based as grounded in functionality, but more arbitrary.

Unmasked data were used as grey matter masking did not affect the between subject similarity and I wanted to investigate the components generated with reduced pre-processing. The peak voxels of the 200 components were compared to nine regions of interest at V1, V2, V3, MT+, V3A, V4 based on spatial maps and seed coordinates generated using large meta-analysis (see Table 4 for coordinates used; Yeo et.al., 2011). Those with the closest peak voxels were identified for each of the ten subjects.

Table 4. The seed coordinates used for matching single subject components to regions of interest. Coordinates were identified based on large meta-analyses (Yeo et.al., 2011).

Region of interest	**MNI coordinate used (x, y, z)**
V1 peripheral dorsal	+/-18, -70, 8
V1 peripheral ventral	+/-8, -63, -6
V1 central dorsal	+/-18, -95, 3
V1 central ventral	+/-8, -92, -5
V2 (dorsal)	+-8, -79, 13
V3 (dorsal)	+-8, -79, 20
MT+ RH	-44, -66, 4
MT+ LH	45, -72, 3
V3A	+/-17, -92, 20
V4 LH	-22, −65, −9
V4 RH	30, -67, -9

6.5.2 Results

Findings showed that V1, V2 and V3 regions were not represented as separate components, instead components represented activity relating to peripheral or central visual field processing *across* these regions (see Figure 105 for schematic of the FOV eccentricity processing, across the medial occipital lobe). This means that although V1, V2 and V3 have been identified using retinotopic techniques to represent the full visual field as "different visual areas" (Wandell, Dumoulin & Brewer, 2007), there is no functional separation between the regions when processing the peripheral or central visual field. This lays example to a benefit of using ICA and movies as method for examining the visual processing networks in the human brain; functional "units" will be identified rather than presumed based on architectural changes across brain regions. Two regions may have distinct architectural differences, but functionally never work without the other and should be understood as a functional 'unit'.

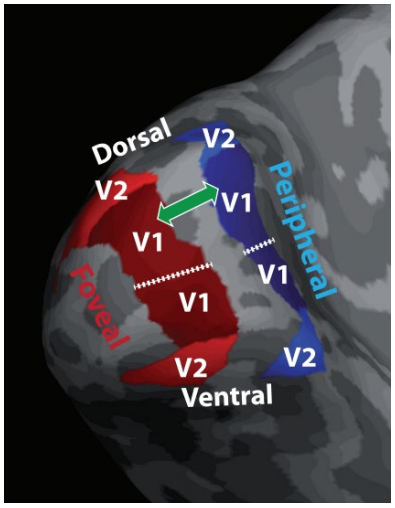

Figure 105. Adapted from Genç et.al. (2016). A schematic of retinotopic eccentricity overlaid onto an inflated subject brain. The foveal (central) visual field is processed towards the occipital pole while peripheral regions are processed in anterior medial regions.

6.5.2.1 V1 peripheral dorsal

Components matched to the peripheral dorsal coordinates of V1 showed clear matches and lateralisation across subjects (see Figure 106). This region covers V1, V2 and V3 regions processing in the anterior medial occipital cortex.

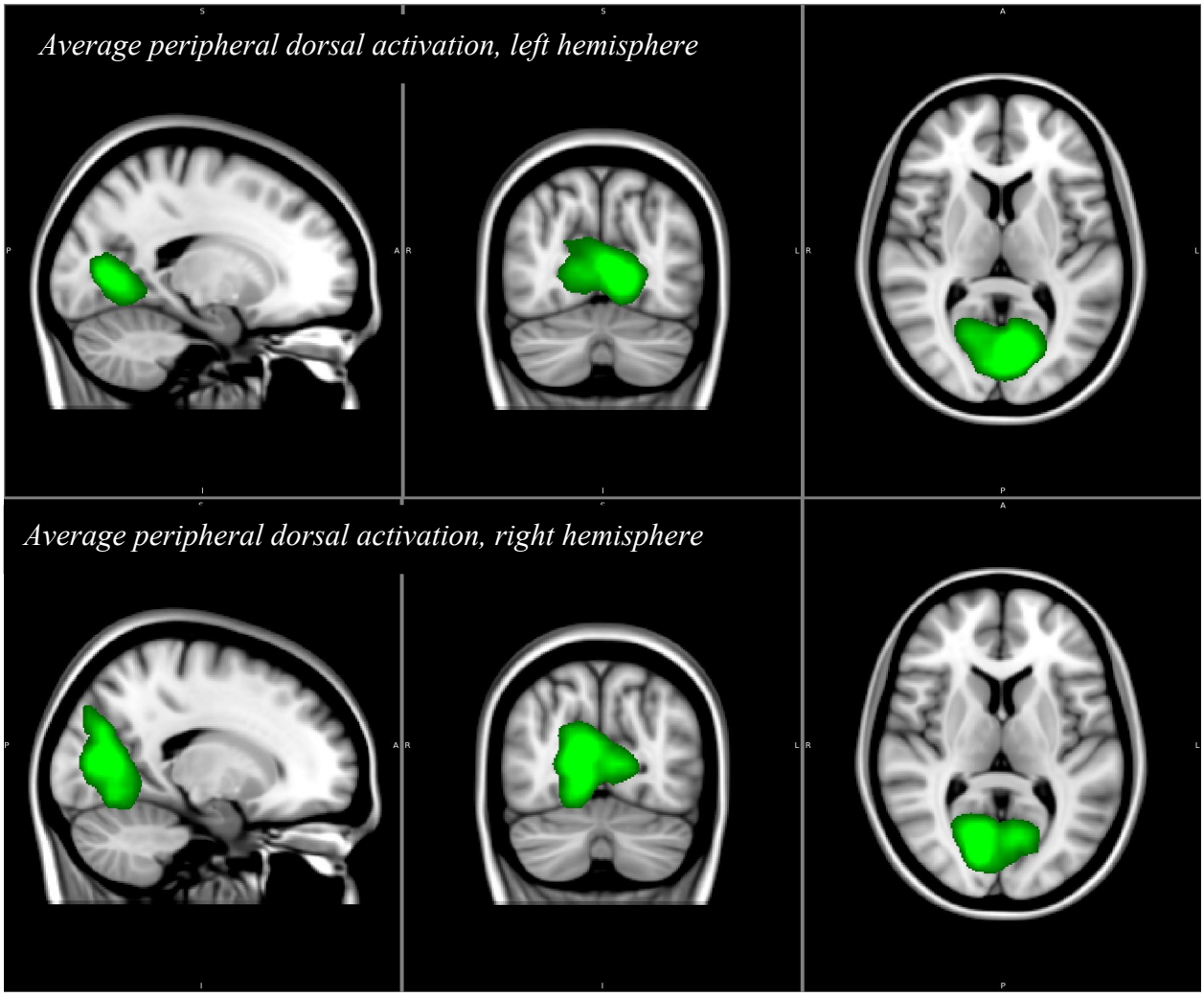

Figure 106. The components matched to peripheral V1 coodinates MNI [+/- 18, -70, 8] showed clear matches across ten subjects. Displayed here are these matched components averaged across the subjects examined.

6.5.2.2 V1 peripheral ventral

Components were matched to the ventral coordinates in the primary visual cortex and showed some lateralisation across subjects. The components matched to the ventral and dorsal coordinates were the same in at least one hemisphere for 7/10 subjects. This meant activation was not limited to the ventral regions below the calcarine sulcus, but on average extended dorsally and ventrally around the calcarine sulcus.

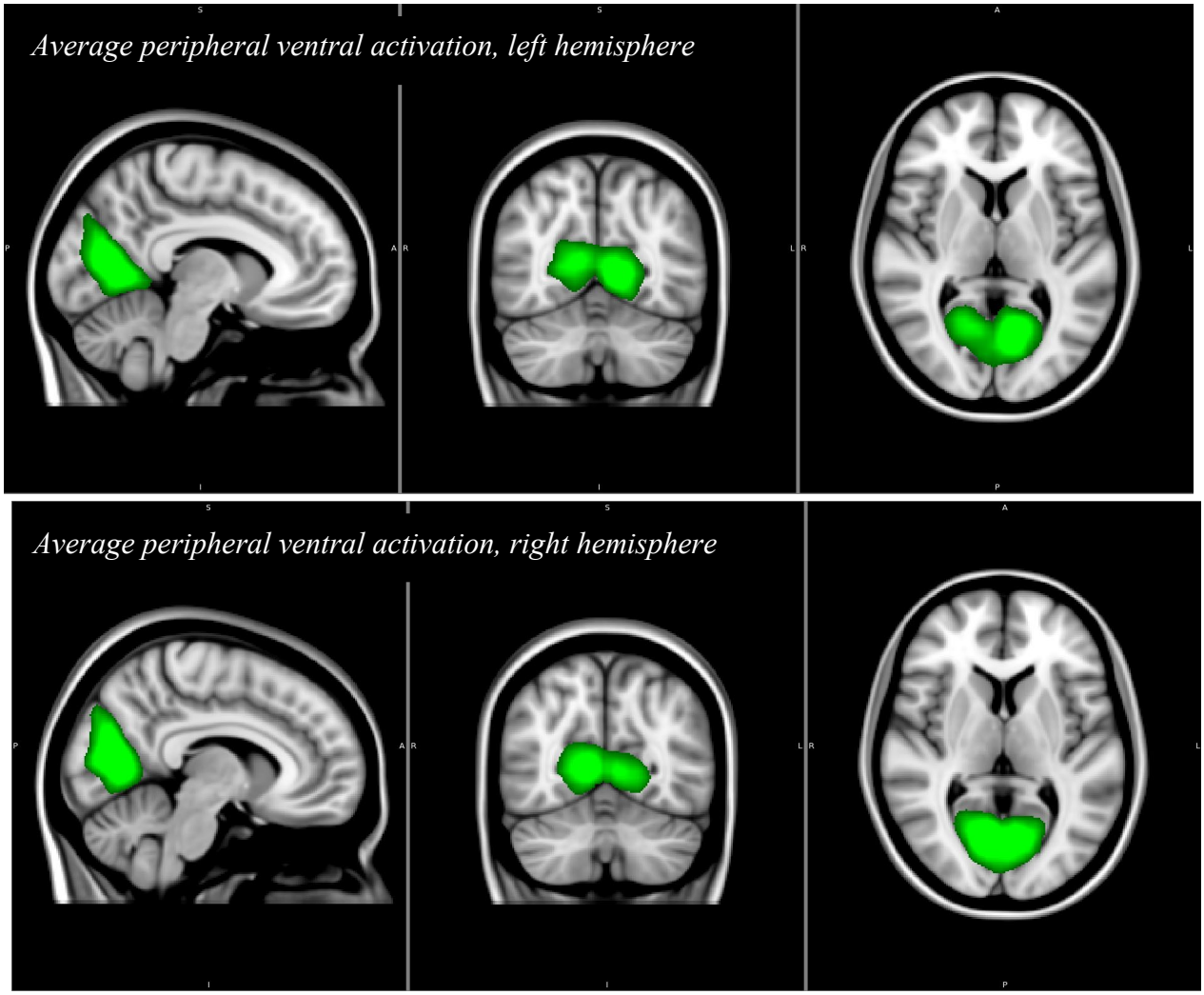

Figure 107. Components matched to regions processing peripheral visual field activation, in the left and right hemispheres (MNI coordinates [+/-8, -63, -6]). Some lateralization in seen on average across subjects. Activity is not limited to ventral regions but is seen above and below the calcarine sulcus.

In this data set the dorsal and ventral early visual, regions which represent upper and lower quadrants of the visual field, respectively, could not be reliably segregated during natural vision at the single subject level using ICA. This may be due to the size of the movie stimulus, which did not span the whole of the visual field. It may be that with a wider field of view the ventral and dorsal regions of early visual regions processing peripheral visual regions can be discerned.

6.5.2.3 V1 central dorsal

In posterior regions of the primary cortex around the occipital pole, central regions of the visual field are processed (e.g. Genç et.al., 2016, Dumoulin & Wandell, 2008). Activation averaged across subjects showed some lateralisation (see Figure 108).

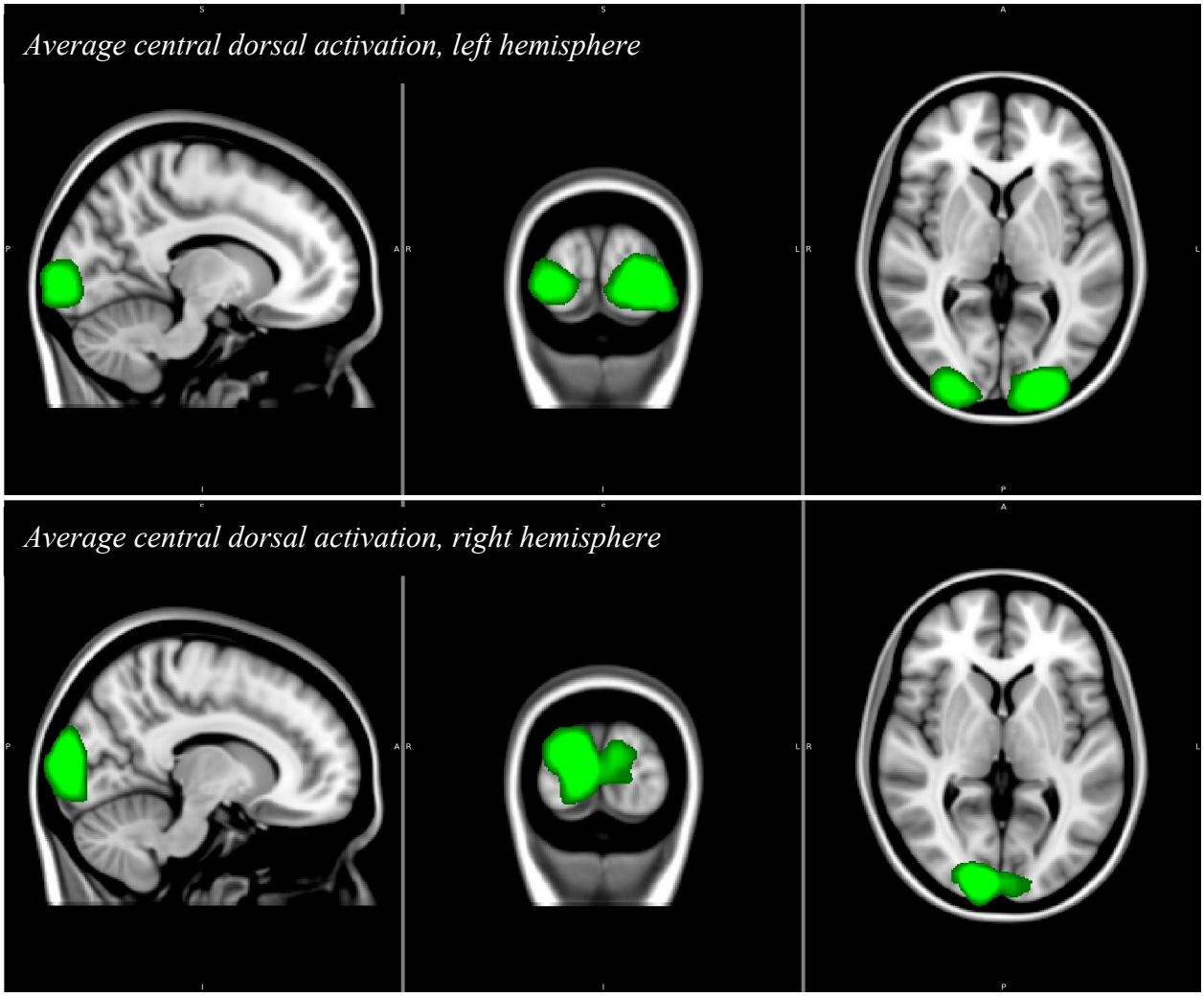

Figure 108. Subject components matched to central dorsal coordinates at V1 (MNI [+/-18, -95, 3]) were averaged. Components showed lateralized activation.

It is worth noting that for 4/10 observers the same component was matched to the V3A coordinates as to the central field dorsal coordinates. This suggests that for these participants the coordinates used were not appropriate for identifying V3A and dorsal visual field maps. In future work I would look to use a comparison algorithm that compared components matched to the different coordinates and scanned for alternatives based on cross-matching and component features (such as location, size etc.).

6.5.2.4 V1 central ventral

Components matched to the central ventral V1 coordinates again showed some evidence of lateralization across subjects (see Figure 109).

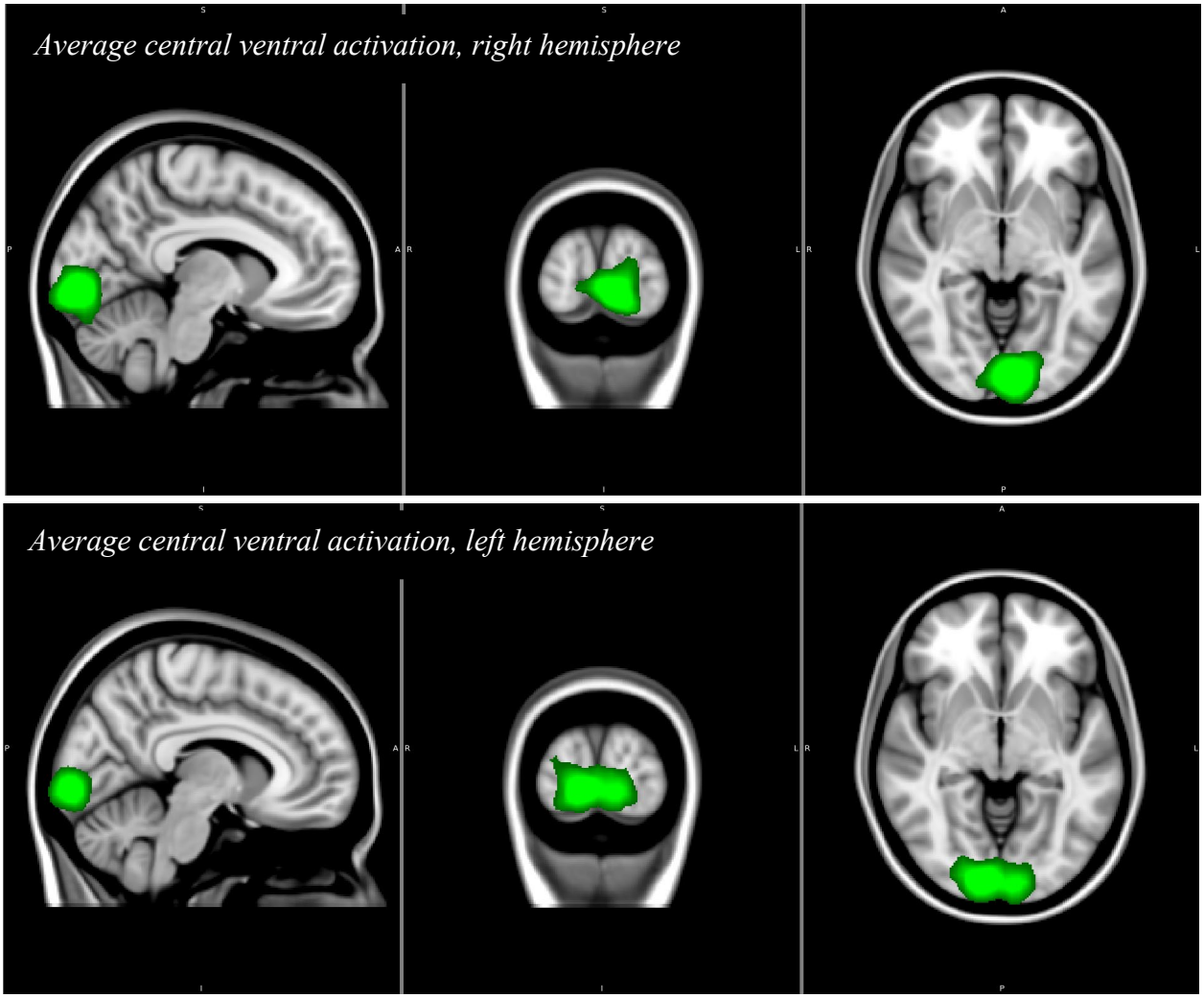

Figure 109. The average components matched to regions processing central (foveal) visual field. Lateralisation is seen on average across subjects and these ventral components lie on average below those matched to the dorsal coordinates.

Unlike the peripheral visual field regions, the averaged dorsal and ventral coordinates showed some differentiation across these central regions. For this region 5/10 of the subjects had the same component matched across ventral and dorsal coordinates, in one hemisphere (2 had the same match in the left hemisphere and 3 in the right hemisphere. These findings suggest that the movie stimulus and ICA used in this thesis (Chapter 1, section 1.3) can segment lateralised central field processing in some participants.

6.5.2.5 MT+

All the ten subjects showed components with activity driven at the left MT+ region. All the subjects bar one showed the highest activity in this region within components restricted at the MT+ bilaterally. One subject showed activity extending into other regions of the motion pathway (V3A).

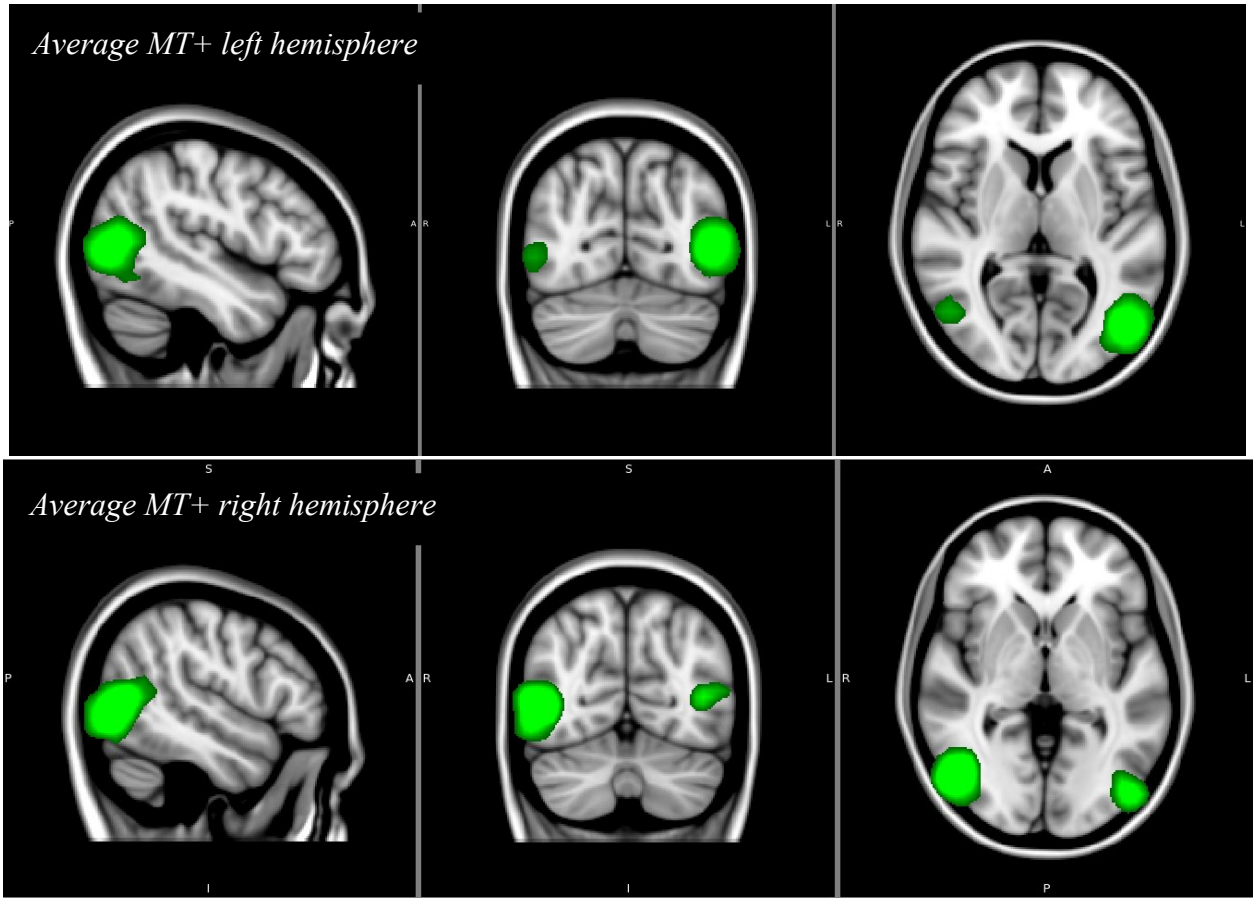

Figure 110. The best matched individual subjects matched to the left and right MT+ regions were averaged to show the MT+ region identified across subjects. These lateralised regions can be reliably identified across subjects, though components can sometimes include other regions of activation in the dorsal motion pathway (e.g. V3A and the pre-central gyrus).

6.5.2.6 V3A

Across subjects, activation at V3A was identified, in the right and left hemispheres. Activation was lateralised, and components found were restricted to the V3A rather than comprising of multiple regions in a functional network.

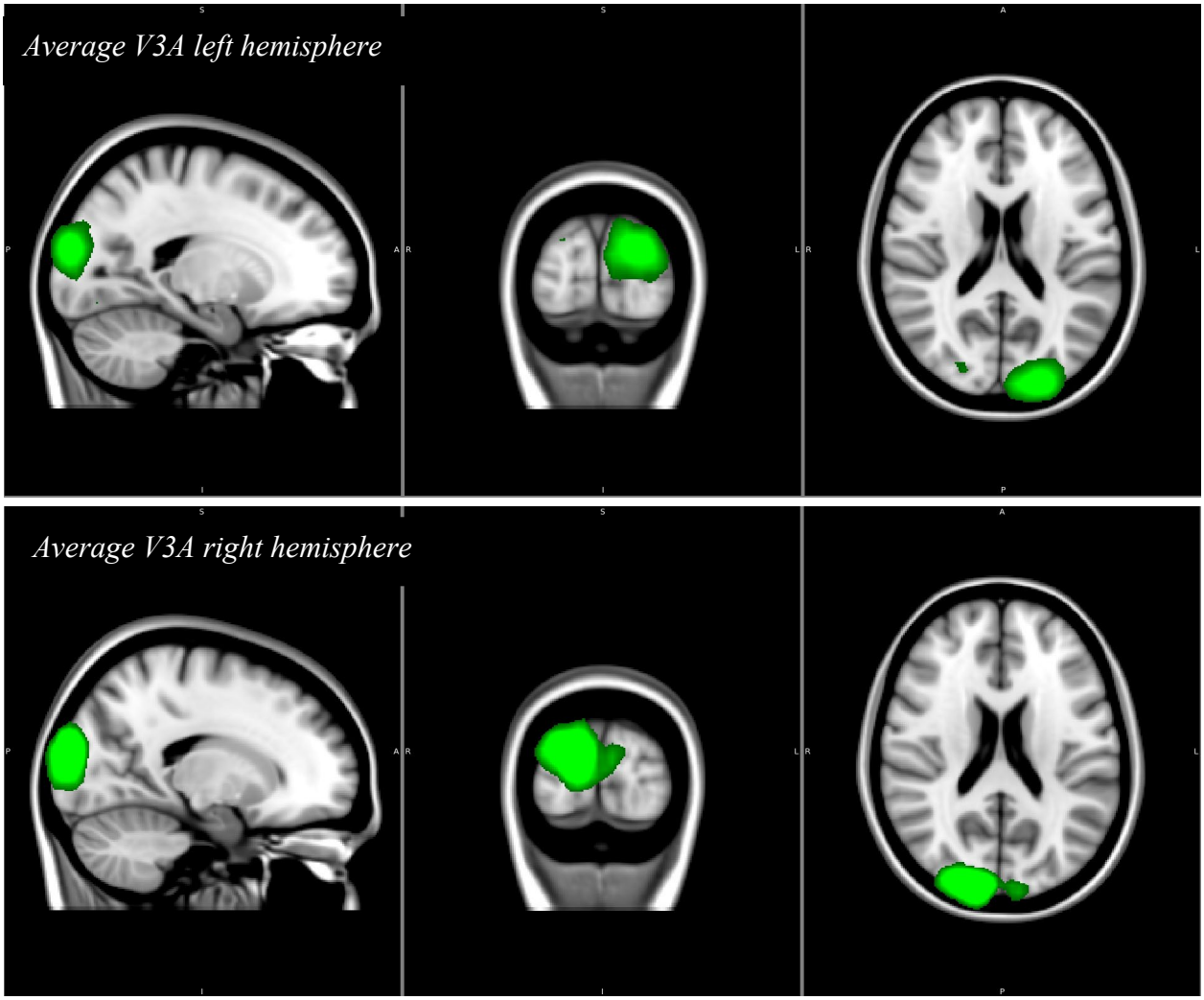

Figure 111. Components matched to V3A coordinates were averaged across subejcts. The V3A region was identified across subjects and showed lateralisation across the hemispheres.

6.5.2.7 V4

Components matched to coordinates at V4 in the fusiform gyrus on average also show activation at dorsal regions towards the intraparietal sulcus (IPS). This suggests a strong functional connectivity between these regions during movie watching. The functional role of V4 is relatively elusive, as it has been associated with a number of diverse processes (Roe et.al., 2008). V4 is best known for its importance in object recognition and colour processing (e.g. Seymour, Clifford, Logothetis & Bartels, 2009). Research has suggested that V4 and regions in the IPS work together during grouping of stimuli based on colour (Zeki & Stutters, 2013). This finding supports a correspondence between these regions that is present when processing rich natural scenes. Large meta-analyses also demonstrate a functional connection between these regions (Neurosynth; Yeo et.al., 2011).

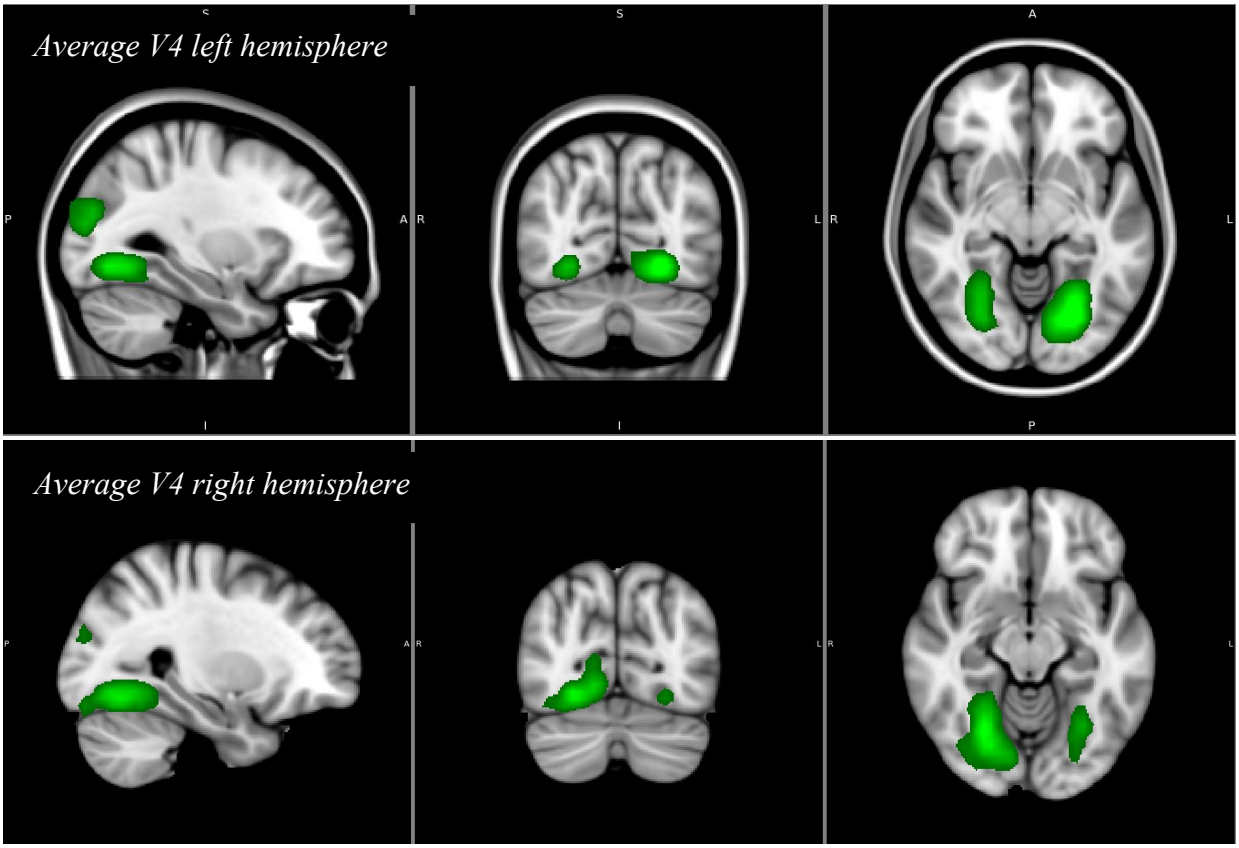

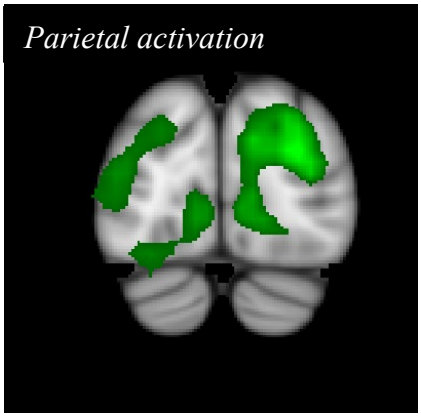

Figure 112. Components matched to the region V4 were averaged across ten subjects at dimensionality 200. The average components showed activity at the fusiform gyrus (V4) and in dorsal regions covering IPS regions (*see bottom panel* ; Peak coordinates in the left-hemisphere = [-27, -85, 23], peak coordinates in the right hemisphere = [22, -88, 26]). This suggests that these regions work in correspondence during natural viewing.

6.5.2. Correlation of component timeseries

Using ICA and a movie stimulus, Bartels and Zeki (2005) found that timeseries of visually driven components at V1, ventral V2/V3, V5/MT+, V4 and lateral occipital (LO) regions were significantly correlated across subjects. Correlations between the components indicate that the same regions of interest are being identified. A cross-correlation analysis for each ROI showed significant average correlations across subjects at these ROI (in the 95th percentile across all possible component comparisons). This supports the assertion that the same functional regions are being identified across subjects.

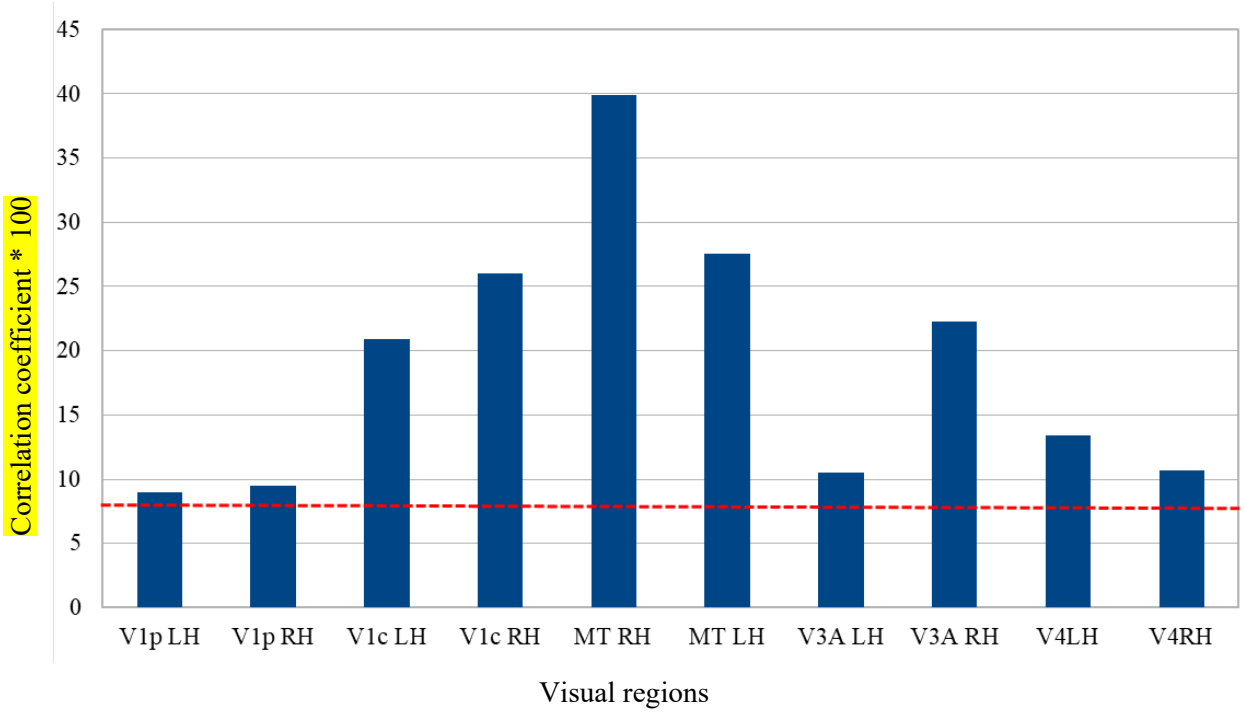

Figure 113. The correlation of component timeseries matched to regions of interest was significant (in the 95th percentile of all comparisons) across subjects. This supports the work by Bartels and Zeki (2005), suggesting that the same functional regions can be identified across observers, using movies and TICA.

6.5.2.9 Networks that remain at a high dimension

It is worth reiterating at this point that although components do show a splitting pattern as dimensionality increases, there are also components at high dimensionalities that represent networks that include multiple regions of interest, which are seen across all observers. These networks include the central executive network (Figure 114) and MT+ with pre- and post -central regions (Figure 115). A functional network that includes bilateral V4 and dorsal regions covering V3A and extending towards the IPS is also present (Figure 116), as demonstrated across subject averages in the previous section (6.3.4.9). These findings suggesting high functional connectivity between these network regions during natural viewing. This may be driven by motion characterized by chromatic differences at the edges of objects moving over a background, in the movie (McKeefry, Burton & Morland, 2010).

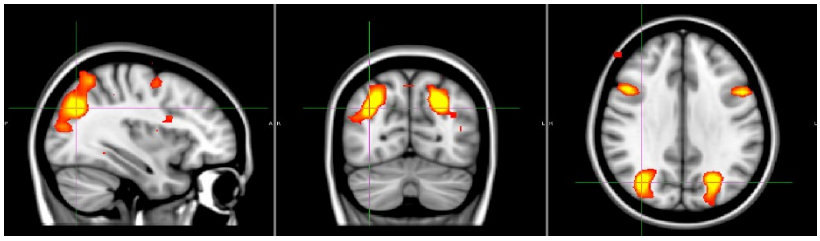

Figure 114. A central executive network is still present at the highest dimensionality (ICA200). These regions are also identified as components representing the sub-regions.

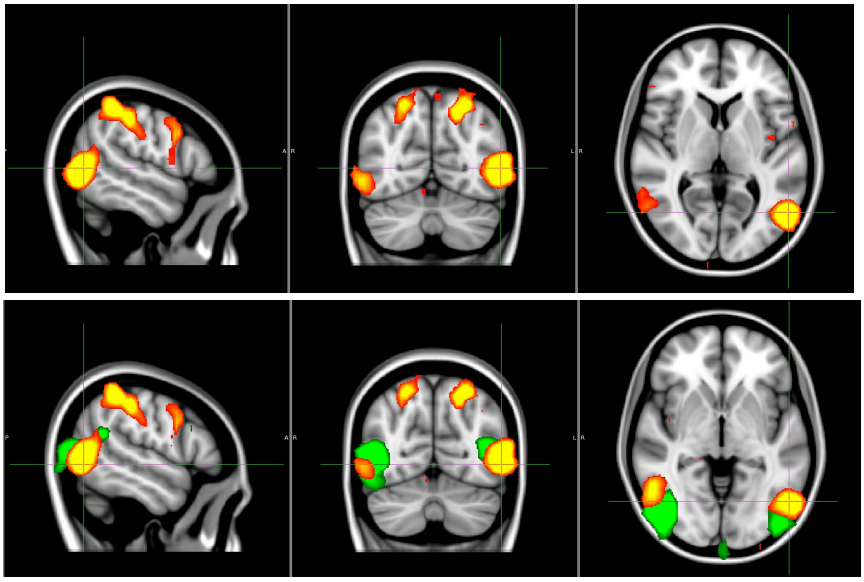

Figure 115. A network including MT+ regions and pre-motor regions an some frontal actvation is still present at high dimensionalities. Sub-regions (such as bilateral MT+) are also identified as separate components (green, overlaid).

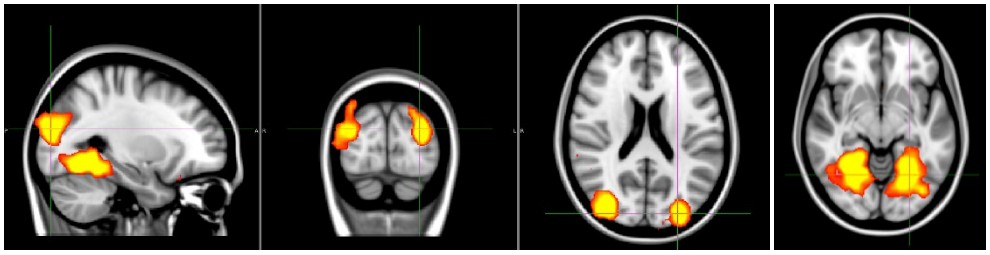

Figure 116. Activity at the fusiform gyrus (putative V4) and dorsal regions near the IPS remains as a network at high dimensionalities and seen reliably across subjects.

6.5.2.9 Summary

The analyses in this section demonstrate that visually driven regions of interest can be reliably identified across subjects, using TICA and a movie stimulus. This supports the work by Bartels and Zeki (2004), and the proposal that this may be a useful technique for mapping visual regions in individuals.

6.7 Summary: Chapter 6

This chapter has investigated the components generated at the single subject level, using a movie stimulus and ICA. Individual ICAs show variation in the components that they produce, however robust components were found in visual areas.

At low dimensionalities (20) components were identified representing functional activity at V1, MT+, V3A and pre-central locations across at least 21/22 subjects. Analyses of single subject components at a high dimensionality (200) demonstrate that multiple visual regions of interest can be reliably identified across individuals. Interestingly in this dataset, V1, V2 and V3 could not be delineated functionally. Instead, TICA identified separate functional units representing central visual field processing and peripheral processing, across primary and extrastriate regions V1, V2 and V3. This highlights an important benefit of ICA, as it can pull out functional units of activity in the brain that may be missed if looking only at architectural or retinotopic features. This finding suggests that the central and peripheral activity in V1, V2 and V3 cannot be separated functionally and is best understood as their own respective functional units. At dimensionality 200 MT+, V3A and V4 can be identified as individual component and can show lateralisation. These regions are also identified as part of a larger functional network, even at this high dimensionality.

Based on the findings in this chapter using TICA with data collected during movie watching is a viable method for identifying these regions of interest. Timeseries taken from participants at the primary visual cortex and MT+ regions (MT and MST) could be used to generate probabilistic maps of these regions, supporting the robustness of the technique for identifying the regions of interest.

The identification of functional networks at lower dimensionalities and functional regions at higher dimensionalities support the idea that components split into network sub-regions as dimensionality is increased (as explored in Chapter 5; see also Smith et.al., 2009). With the identification of robust components across individual subjects, Chapter 10 will explore a novel technique for examining the functional hierarchy of the visual system, by exploiting the splitting pattern of components across ICA dimensionalities.

In the next chapter I will apply ICA to MEG data collected during movie watching, with the overarching aim of comparing results across MRI and MEG modalities.

Chapter 7: Using movies and ICA to segment oscillatory activity in the brain

7.1. Introduction

In previous chapters a pipeline for finding the most reliable TICA components using fMRI bold signal collected during movie watching has been established. Further exploration of the results suggest that visual regions and networks of interest can be reliably identified at the group and individual level. One issue with the fMRI BOLD signal is that it is an indirect measure of neuronal activity as it measures changes in oxygenation in the blood, which is then used to infer activity. In fact, studies into the relationship between blood oxygenation and flow and the neuronal activity ('neurovascular coupling') reveals a more complex relationship (Attwell et.al., 2010).

As an alternative to fMRI, MEG data allows for a more direct insight into neuronal function by recording electro-magnetic signals of neurons as they process information and communicate. More recently, ICA has been used to segment resting state MEG data (e.g. Vigário et.al., 2000) and has allowed the mapping of functional networks within the brain (e.g. Brookes et.al., 2011). This research analysis has concentrated on activity in the alpha and beta frequency bands, where data are observed to produce reliable RSNs (e.g. Brookes et.al., 2011).

However, there is much evidence that functional networks in the brain are associated not only with beta and alpha, but with several frequency bands, depending on the brain region and cognitive demands applied by the environment (e.g. Morillon et.al., 2012; Mantini et.al., 2007; 2011). Gamma oscillations have been associated with the combining of sensory information, such as "feature binding" (e.g. Tallon-Baudry & Bertrand, 1999). Gamma frequencies are observed particularly in local synchronization of visual information (e.g. vonStein & Sarnthein, 2000). Given this finding, we would expect to see cross-frequency coupling between frequencies during visual tasks. Work by vonStein and Sarnthein (2000) also suggested synchronization by lower frequencies across larger scale neural connections. Synchronised beta (12-18Hz) was reported at temporal-parietal connections during sematic processing, while it was suggested that long-range fronto-parietal connections were sychronised by theta and alpha (4-8Hz and 8-12Hz, respectively). This

research suggests that integration of information across the brain involves multiple frequency bands. Using a rich broadband naturalistic stimulus such as a movie should be optimal for driving neural responses and producing measurable signals in regions involved in processing the visual input.

In this section of the thesis, I develop a novel broadband TICA technique that it can be used to investigate the relationship between oscillatory frequencies and between these frequencies and the BOLD signal. Cross-frequency synchronisation is relatively difficult to study in human subjects, and there is much more data in animal research on this topic, with use of sub-dural electrodes (e.g. Siapas, Lubenov & Wilson, 2005). One way to potentially further understand the activity in neural networks across the frequency bands would be to combine MEG data from different frequencies into a single TICA analysis.

Previous work by Nugent et.al. (2017) attempted this using MEG resting state data by concatenating all subject timeseries in each frequency band, at each voxel. Therefore, the data entering the ICA had subject and frequency band concatenated along the time axis. Nugent et.al. identified the sensorimotor network component in the ICA output, and used it for further analysis. They used linear regression to find the individual spatial maps at each frequency. Their results demonstrated a significant effect of frequency on the sensory-motor component spatial map.

One study by Aoki et.al. (2015) examined cross-frequency interactions using ICA and EEG resting state data by concatenating subject space-frequency maps along the x-axis and then stacking subject data along the time axis. This produced regions across the different frequency bands that were 'working together' across the subjects. Using 80 participants this study identified some cross-frequency interaction between alpha and beta at frontal and occipital regions (see Appendix 7.1). Oscillations in alpha at the right ventral visual pathway were correlated with beta oscillations in the ipsi-lateral prefrontal cortex (PFC; see Appendix 7.1). Alpha oscillations in the left dorsal visual pathway and MT+ were found to be anti-correlated with this activity (in the same component). This suggests that regions in the ventral and dorsal visual streams may have different patterns of cross-frequency correlations.

These are interesting findings, though are limited to understanding the intrinsic relationships between frequencies during rest. It would be really useful to understand cross-frequency interactions during tasks. The same procedure was also employed by a later group while subjects were engaged in different internal visualization tasks (Milz, Pascual-Marqui, Lehmann & Faber, 2016). Interactions were identified between

delta and alpha at the superior parietal lobule and dorsal visual pathway. Internalized object processing (visualization and verbalization) showed anti-correlated activity in alpha at the occipital-temporal-parietal regions and medial-central regions, such as the somatosensory cortex. This study and that of Aoki et.al. only identified a small number of components, and many of these were not cross-frequency interactions, but within the alpha band only. This may have been due to the tasks, as neither used an external sensory stimulus. When using resting-state data alpha and beta frequencies are the most prominent bands in spontaneous electromagnetic signals, with the largest amplitude when compared to faster gamma oscillations (Herrmann, Fründ & Lenz, 2010).

Although these studies used relatively large samples (80 and 70, respectively), one potential issue was their restriction of decomposition to a dimensionality of only 11 -13 components. This dimensionality restriction was based on a sphericity test (Bartlettt, 1954 *in* Aoiki et.al.). Extrapolating from our previous research with BOLD data, a larger dimensionality is identified when using an automated TICA analysis. Also, increasing the dimensionality will increase the number of signal components produced (explored in Chapters 1-6). Aoki et.al. also limited their frequency range to a maximum of 60Hz, however gamma ranges above this are known to be functionally significant in the human brain (e.g. Crone, Sinai & Korzeniewska, 2006).

It would be very useful to modify the techniques described above so the relationship between frequencies can be examined during different tasks. Another novel way to pull apart the different frequency bands and their interaction is to concatenate the data spatially, rather than along the time axis. If data is concatenated within a spatial dimension (x, y or z), then the assumption of spatial consistency is bypassed, and the ICA output will present spatial locations for each frequency band, where the timeseries show a correspondence. Using a movie stimulus, it is expected that a wider range of oscillatory activity is informative in the recorded data. This broadband frequency data can be spatially concatenated input into a TICA, potentially providing a neat and novel way to investigate cross-frequency interactions. This technique would not require an additional regression analysis to identify frequency-specific spatial maps. Use of the broadband stimulus also means the relationship between a range of frequency bands can be examined during natural viewing, and the technique can be applied to other task-based studies.

In this and the following chapters, I explore the usefulness of this novel technique for analysing cross-frequency and cross-modality activity. The technique inputs spatially concatenates data collected during

movie watching into a single TICA. By using a rich naturalistic stimulus multiple visually responsive regions and networks are activated and timelocked to the stimulus, across subjects (e.g. see Chapter 2 with BOLD data; Hasson et.al., 2010). It was expected that features of the movie stimulus will also drive activity in different frequency bands, and a cross-subject voxel-by-voxel correlation confirmed this was the case (discussed below). This means that the individual MEG timeseries do not need to be concatenated at each voxel and a single decomposition can be provided for all frequency band datasets.

Before applying this novel spatially concatenated TICA technique ("combined frequency"), three prerequisites need to be addressed. First, I need to establish that reliable visually driven components can be identified in each of the frequency bands. Second, I will check whether there are different cross-frequency relationships in different visual regions. If there is, this may allow for the segmentation of different visual regions or streams of processing. Finally, if the first two conditions are satisfied, I will assess the reliability of the combined frequency output by comparing it across different first-brain swapped permutations (see the same done for BOLD data in Chapter 2).

To anticipate the results, analyses support the investigation of cross-frequency relationships using a combined frequency TICA technique. In the next chapter I describe the reliable components identified in the combined-band output.

7.2 Can we identify visually driven components in a single MEG band?

Before performing a cross frequency TICA I needed to identify where reliable components were likely to be generated, using the different frequency bands. A cross-subject voxel-by-voxel correlation at each frequency band was performed to identify where oscillatory activity is being driven by the movie stimulus. This time-locking to the stimulus is indicative of regions being visually driven and is used in TICA to identify functional components. Following this analysis, I investigate whether reliable components can be identified in visually driven regions (defined as regions with significant cross- subject correlations) for each frequency band. First, I examine alpha and beta frequencies, which are commonly used for resting state analysis. Then I check the components in other frequency bands. Results show that reliable components covering sub-regions of visual functional networks are identified at each of the different frequency bands. Frequencies theta and

gamma in particular show multiple components representing visual regions that explain large amounts of variance in the data.

7.2.1 Methods

Defining components as visually driven

To identify where in the brain the oscillatory activity was being driven by the movie stimulus, a map of between subject cross-correlation was calculated for each frequency band. The mean of pair-wise correlations between each participant timeseries was plotted at each voxel. These maps show for each frequency band where temporal locking was observed between subjects, while watching the movie.

The significance threshold ($p<0.05$) was calculated for each cross-subject correlation using randomisation permutation testing across participants, to build a null distribution. These regions were then used as a spatial map to define MEG components as being 'visually driven'. Cross-subject correlation was seen at the occipital lobe across all frequency bands, moving anteriorly / parietally as frequencies increased though delta, theta, alpha and beta respectively.

At low gamma frequencies (40 – 60Hz) subject correlation become more focused at the occipital pole once more, before extending anteriorly/posteriorly again with the high and very high gamma frequencies. The overall cross-subject correlations were highest at theta and gamma ranges 60-140Hz, compared with the other frequency bands. The lowest overall cross-subject correlations were seen in alpha and the highest gamma band (140-200Hz).

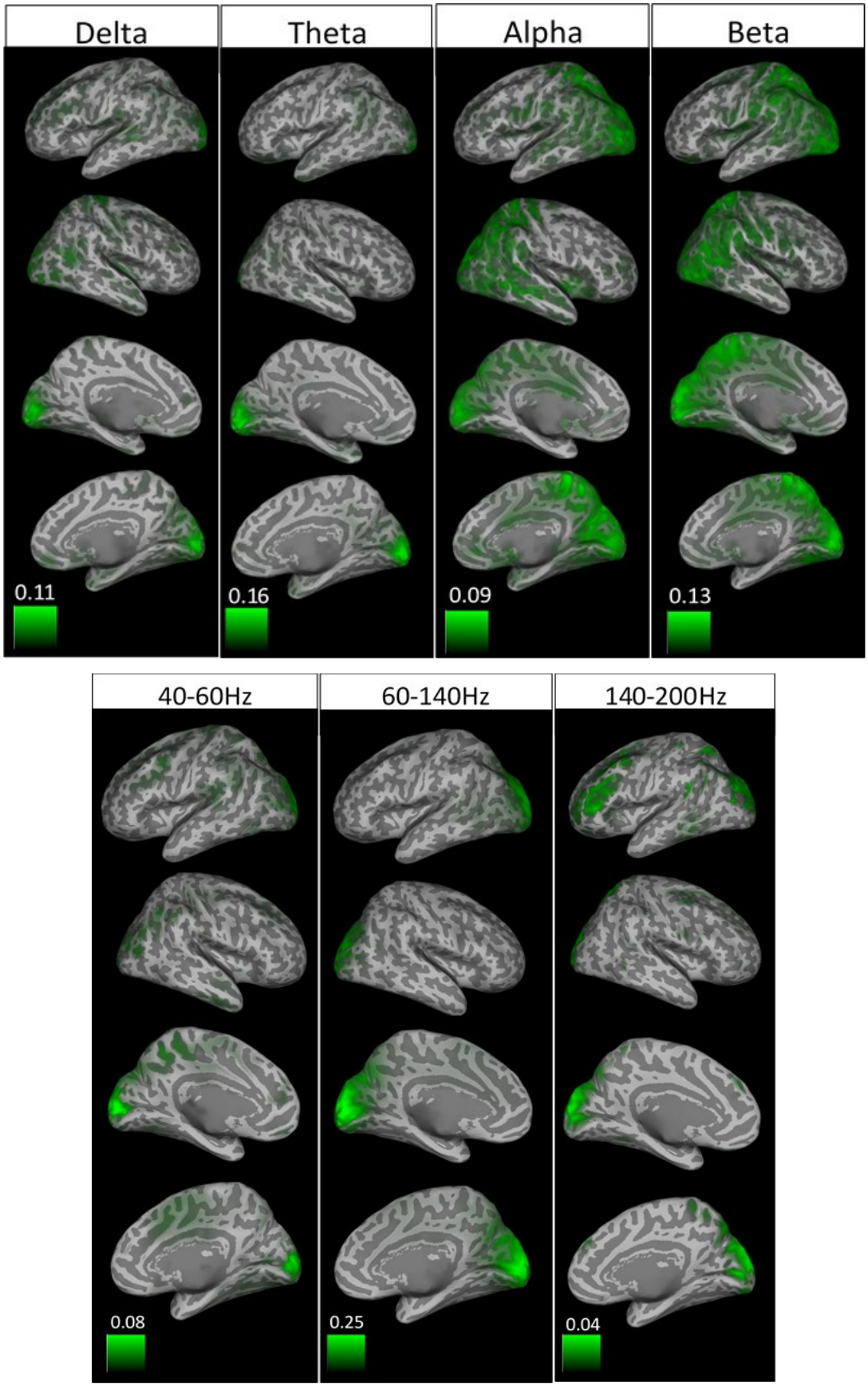

Figure 117. The results of a voxel-by-voxel cross-subject correlations at each frequency band. Primary visual regions show significant cross-subject correlations in all bands. Alpha and beta show the largest areas of significant correlation. Significant r-values ($p<0.05$) : Delta = > 0.017 ; Theta = > 0.024; Alpha = >0.014; Beta - >0.1; LG (40-60Hz) >0.012l; HG (60-140Hz) >0.045; VHG>0.006.

ICA Analysis

It has been demonstrated that decomposition of MEG data using ICA is more spatially accurate and robust to artefacts after source localization (Mantini et.al., 2011), therefore the beamformer virtual timeseries were used in our ICA analyses (Chapter 1, methods section 1.3). Once data had been processed for each subject, a group probabilistic tensor ICA (TICA) was performed for each frequency band. Previous work has shown that changing the first brain accounted for the variance between input permutations (Chapter 2). Therefore, 16 TICAs were run with each subject brain swapped into the first brain position. The representativeness of the ICA outputs was assessed as described in chapter one, using spatial and temporal comparisons of components across the different outputs.

Based on the number of components identified at each frequency band when left unrestricted (~60-125, depending on frequency), ICA outputs were restricted to 70 components. For each component in the representative output, the best matched component was found from each of the other permutation outputs based on the spatial – temporal correlation metric. Then these metrics were averaged across all matches for that component. This gave a measure of how reliable each component was across the permutations.

7.2.2. Results

Each of the frequency bands produced reliable TICA components in visually responsive areas. The three most reliable visually driven components in each theta, alpha, beta and high gamma frequencies (60-200Hz) are presented below. Delta and low gamma frequencies only returned two components within the selecting criterion and these are also presented. There were some reliable components that fell outside of this region for each frequency band (for example components in lateral occipital or frontal regions), that could be investigated in future research. First, I will report the visually driven components identified in alpha and beta, as these are the frequency bands usually used when working with resting state data. Alpha and beta are reported to play a role in attention and inhibition during visual tasks role in visually responsive regions (Jensen, Gips, Bergmann & Bonnefond, 2014; Wróbel, 2000), therefore it expected that reliable components should be identified using our technique.

Alpha and beta bands

Reliable alpha components were identified in dorsal and ventral regions of the visual pathway, and one lay at early visual regions in the medial occipital lobe (Figure 118).

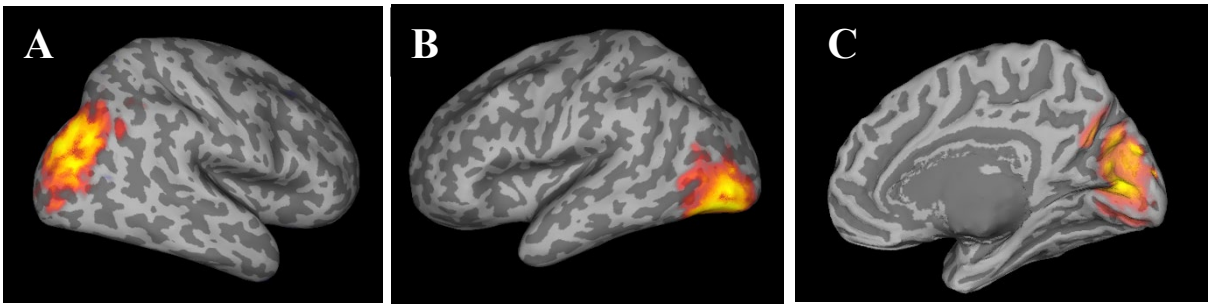

Figure 118. (A) right dorsal occipital regions, covering V3A and V6 *MNI coordinates [30, -73, 34]* (B) lateral occipital component *MNI coordinates [41, -81, 1]* (C) Alpha demonstrated a reliable component in early visual regions spanning early visual regions V1, V2 and V3 *MNI coordinates [14, -82, 18]*. This component is positioned at the posterior medial occipital lobe, where the central visual field is processed.

Reliable components were also identified in early visual regions and the dorsal and ventral regions of the visual pathway in the beta band (Figure 119).

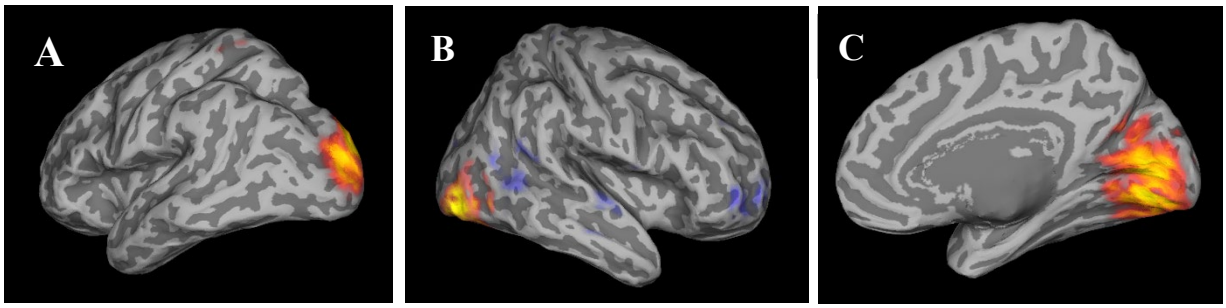

Figure 119. (A) A dorsal occipital component was identified in beta band, lying medially covering extrastriate regions *MNI coordinates [-10, -90, 26]*. (B) a reliable beta component lay lateralized at the ventro-lateral occipital lobe *MNI coordinates [-18, -96, -6]* (C) a medial occipital lobe covering early visual regions.

These results demonstrate that visually responsive components in the lateral and ventral visual streams can be identified in alpha and beta frequencies. These frequency bands are usually the focus of resting state analyses (e.g. Brookes et.al., 2011), however when combining the MEG data into a TICA analysis using my movie data I hope to investigate a wider range of frequencies. Other frequency bands which, though less informative when using RS data, are known to play important roles in processing visual information (e.g. Whittingstall & Logothetis, 2009).

Delta

The most reliable component in delta lay in the right hemisphere, with its peak activation at the cuneus, bounded by the parieto-occipital sulcus dorsally and the calcarine sulcus ventrally (MNI coordinates=18, -84, 24; see Figure 120A). A second component identified in a visually driven region lay at the occipital pole in the left hemisphere (see Figure 120B). The lower number of reliable components in the delta range suggests that delta plays less of a role during visual processing than other frequencies. This supports research showing theta and gamma bands driving oscillatory coupling in visual regions (Whittingstall & Logothetis, 2009), with alpha and beta important in visual attention and inhibition (e.g. Jensen, Gips, Bergmann & Bonnefond, 2014; Wróbel, 2000).

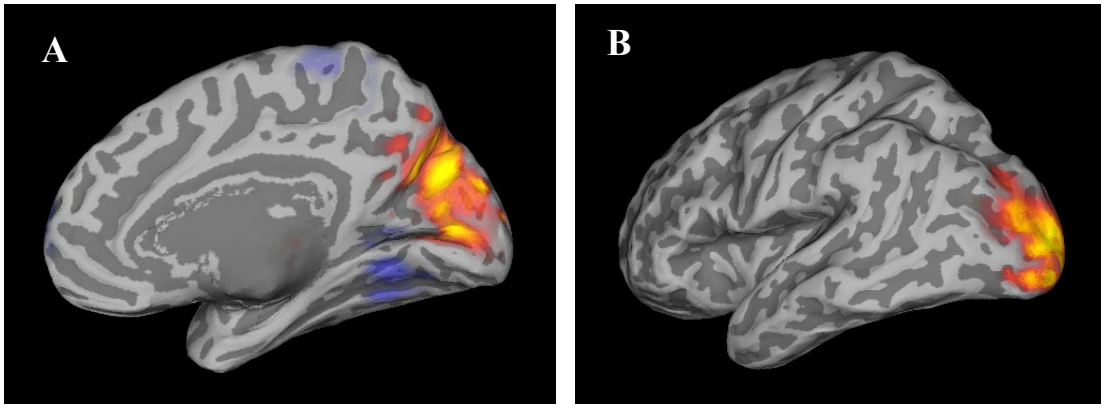

Figure 120. Activity on the inflated brain surface shows the most reliable Delta signal component, which lay in the right occipital cortex at the cuneus, extending into parietal regions, and anterior temporal regions.

Theta

One notable aspect of the components generated using data from the theta frequency was that the first six components that explained most of the variance were all in the occipital lobe. This was not as pronounced in other frequency bands which showed visually driven components later in the output.

The two most reliable components in the theta outputs were also the two that explained most variance in the data. The first component was bilateral, lying at the medial early visual region V1 (MNI coordinates 0, -96, 0; see Figure 121). This activity represented areas at the posterior of the calcarine sulcus which processes the peripheral visual field. Work in Chapter 6 showed how TICA separated BOLD activity in the primary

visual cortex into peripheral and central visual field regions (section 6.3.4). This finding shows similar patterns of component organisation, at the oscillatory level.

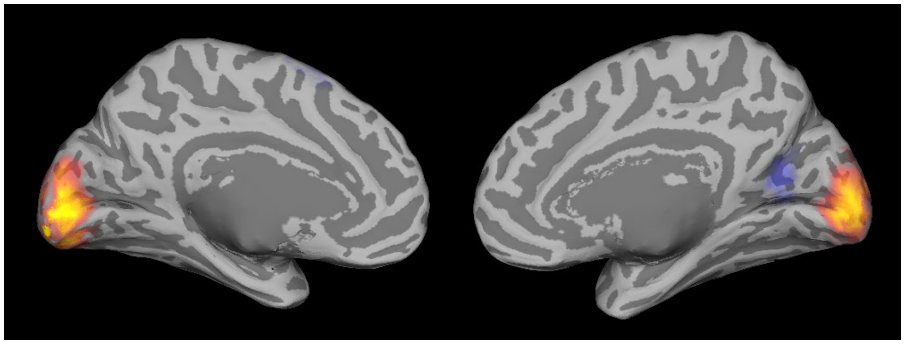

Figure 121. The most reliable theta component at the bilateral posterior medial occipital lobe (V1). This component also described the most variance of the theta components.

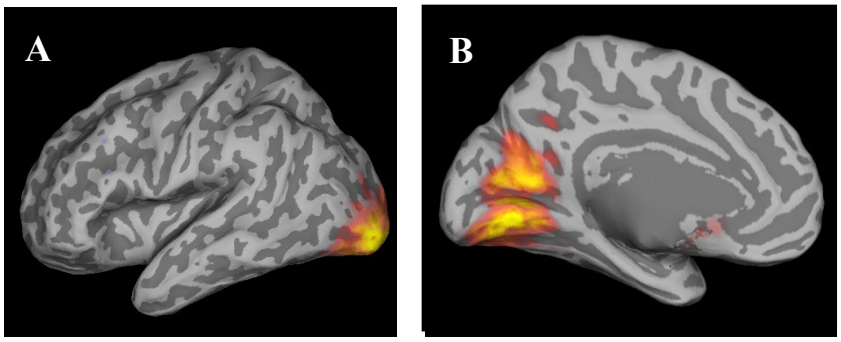

Figure 122. The second most reliable component in the theta output lay at the left occipital pole (A). Another component lay in early visual regions (B).

Gamma

Visually responsive regions can be identified using MEG data at frequencies between 1-30Hz, collected during movie watching. It is expected that regions responding to the movie stimulus will also be active in the gamma frequency ranges (40-200Hz; e.g. Whittingstall & Logothetis, 2009).

In low gamma the significant cross-subject correlation was restricted to only the early visual regions. Two reliable lateralized components were identified at these medial occipital lobe locations (see Figure 123A and B).

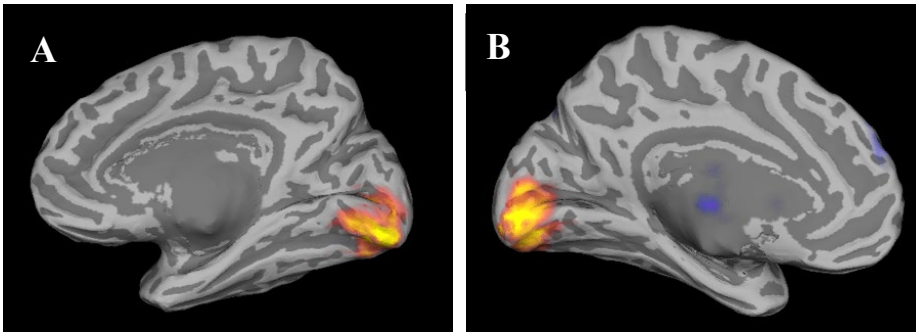

Figure 123. Lateralised (A) and bilateral (B) components in the primary and extrastriate visual regions processing central field information were highly reliable in the lower gamma ranges (40-60Hz)

At high gamma (60-140Hz) three reliable components were identified in the early visual and dorsal visually driven regions (Figure 124A- C).

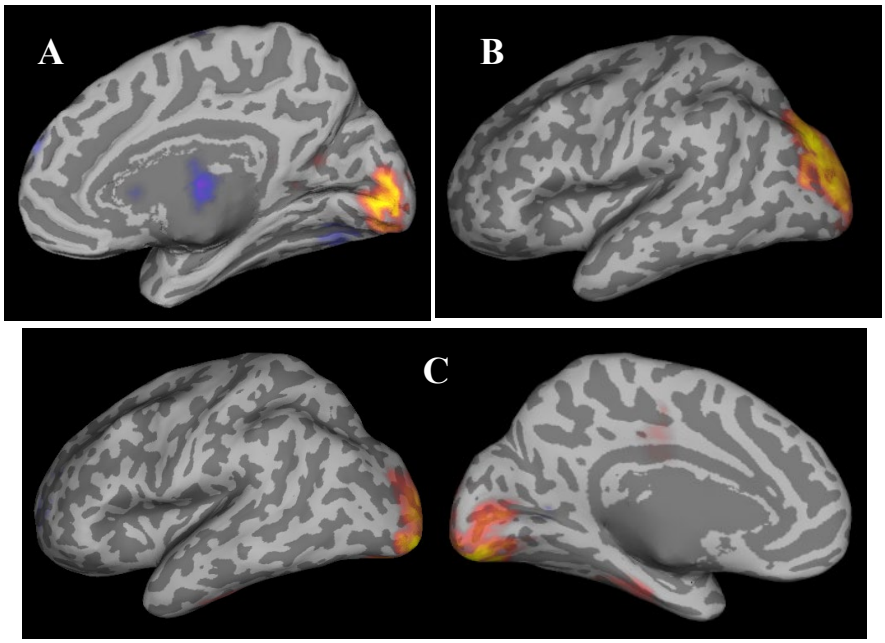

Figure 124. The reliable visually driven components in high gamma band (60-140Hz). Two lay in the primary visual cortex (A and C), another lay in the dorsal visual pathway (B).

Even at very high gamma (140-200Hz) reliable components were identified in the early visual regions (Figure 125A-C). The components represented regions in the dorsal stream (A) early visual cortex (B and C).

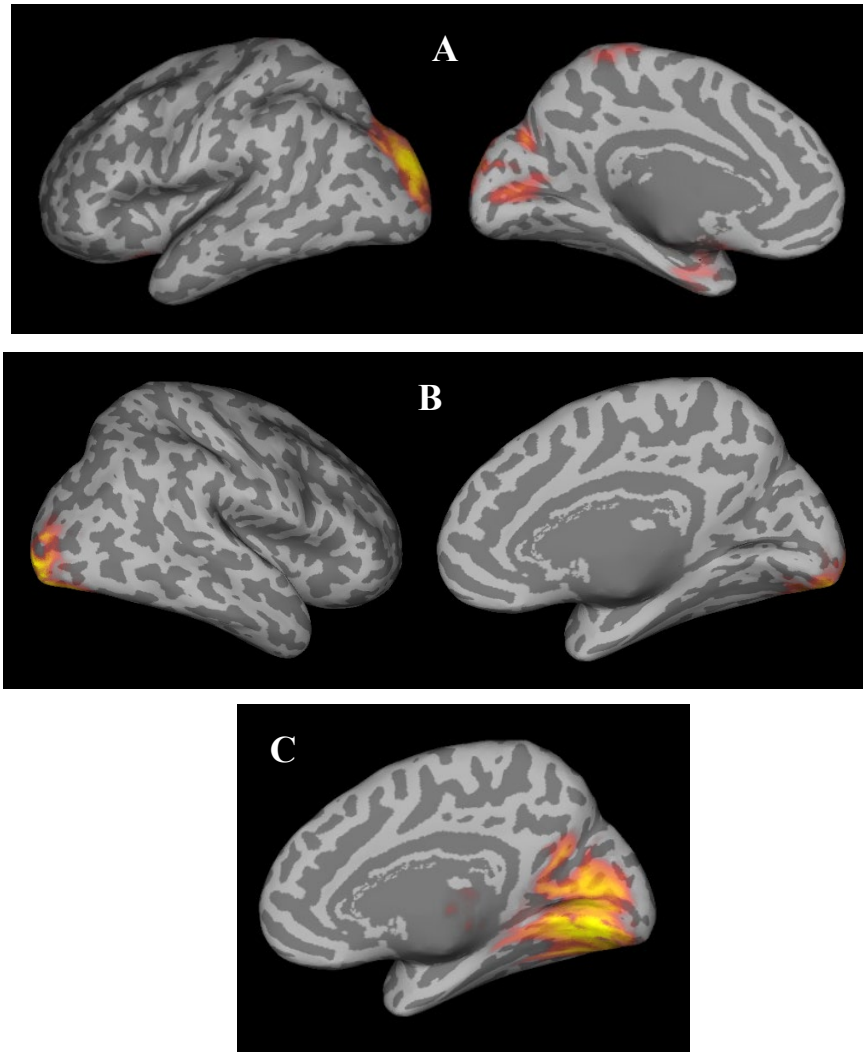

Figure 125. Three components lying in visually driven regions were reliably identified in the highest gamma range (140-200Hz). One lay in the dorsal visual stream (A), the second was centred at the occipital pole (B) and the third in the medial occipital lobe (C).

Summary

The results from single band TICAs demonstrate that reliable components in visually driven regions can be identified at each of the frequencies. This was important to establish before running a combined frequency TICA. In the next section of this chapter I investigate whether the correlations between frequency bands differs across different visual areas. Again, this is important to establish as if it is not the case a combined frequency TICA would not be able to differentiate between different visual areas.

7.3 Are there differences in the relationships between frequency bands in visually driven regions?

In the previous section I show that reliable and visually driven components can be identified in individual frequency bands at primary visual regions and in the dorsal and ventral visual pathways. Next, I cross-correlated the MEG beamformer data at each voxel to look at the relationship between the frequencies and see whether this altered across different visual regions. Based on the findings of Aoki et.al. (2015) and Milz et.al. (2016) that show differences in the cross-frequency coupling in dorsal and ventral visual streams, I am particularly interested in the relationship between oscillatory frequencies in these regions. Therefore, I selected motion region V3A in the dorsal pathway, MT+ in the ventral pathway and V1 (primary visual cortex) as regions for analysis of cross-frequency correlations. It is expected that the motion sensitive regions are activated while watching the movie, and research in Chapter 5 demonstrated that motion sensitive regions V3A and MT+ were reliably identified using BOLD data. If there are differences in the cross-band relationships between these regions, then they are potentially able to be differentiated in a combined frequency TICA.

7.3.1 Methods

MEG data were collected and pre-cleaned as described in the general introduction Chapter 1 (section 1.3). The average timeseries across subjects, was calculated at each voxel in the brain, for each frequency band. Voxel-by-voxel correlations were calculated (full linear correlation) between each pair of frequency bands. Regions of interest (ROI) were chosen at V1, lateral region MT+ and dorsal region V3A. The relationship between the frequency bands was analysed at these points, based on results using single band MEG data showing reliable components across different frequency bands at in early visual areas, lateral and dorsal areas.

7.3.2 Results

Primary visual

The first cross- frequency correlations were calculated at the anterior primary visual cortex (MNI [12, -78, 6]). Consecutive frequencies delta and theta, alpha and beta, and frequencies 40-60Hz and 60-140Hz

show the highest positive correlations (see panels in Figure 126). Delta and theta show a positive correlation with gamma, especially at 60-140Hz, supporting findings of theta-gamma functional coupling using ICA and in vivo recordings in this region (Logothetis & Whittingstall). Beta and gamma (60-140Hz) show negative correlations. These support the findings of a beta-gamma seesaw during visual attentions tasks (e.g. Michalareas et.al., 2016).

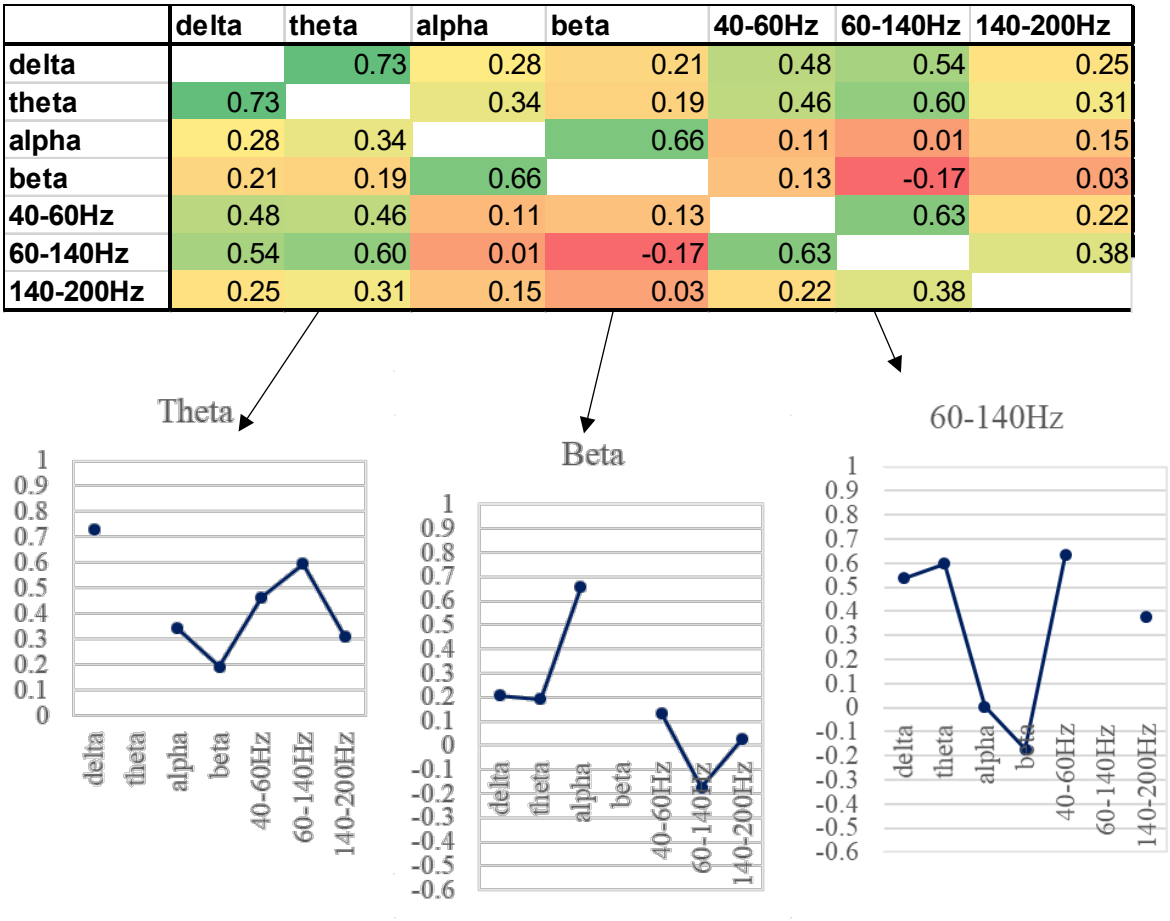

Figure 126. The cross-frequency correlations at a primary visual voxel (MNI coordinates [12, -102,6]). Consecutive frequencies delta and theta, alpha and beta, and frequencies 40-60Hz and 60-140Hz show the highest positive correlations. Delta and theta show a positive correlation with gamma, especially at 60-140Hz. Beta and gamma (60-140Hz) show negative correlations.

V3A

Another voxel chosen was at the expected region of V3A based on meta-analyses (Yeo et.al., 2011; MNI coordinates [20, -88, 22]). At this location the beta-gamma seesaw is present, with negative correlations between these frequency bands (see Figure 127). The positive correlation between theta and gamma frequencies is reduced, compared to earlier visual regions.

	delta	theta	alpha	beta	40-60Hz	60-140Hz	140-200Hz
delta		0.61	0.36	0.28	0.17	0.25	0.13
theta	0.61		0.47	0.33	0.19	0.18	0.15
alpha	0.36	0.47		0.76	-0.10	-0.31	-0.15
beta	0.28	0.33	0.76		-0.12	-0.46	-0.18
40-60Hz	0.17	0.19	-0.10	-0.12		0.48	0.26
60-140Hz	0.25	0.18	-0.31	-0.46	0.48		0.41
140-200Hz	0.13	0.15	-0.15	-0.18	0.26	0.41	

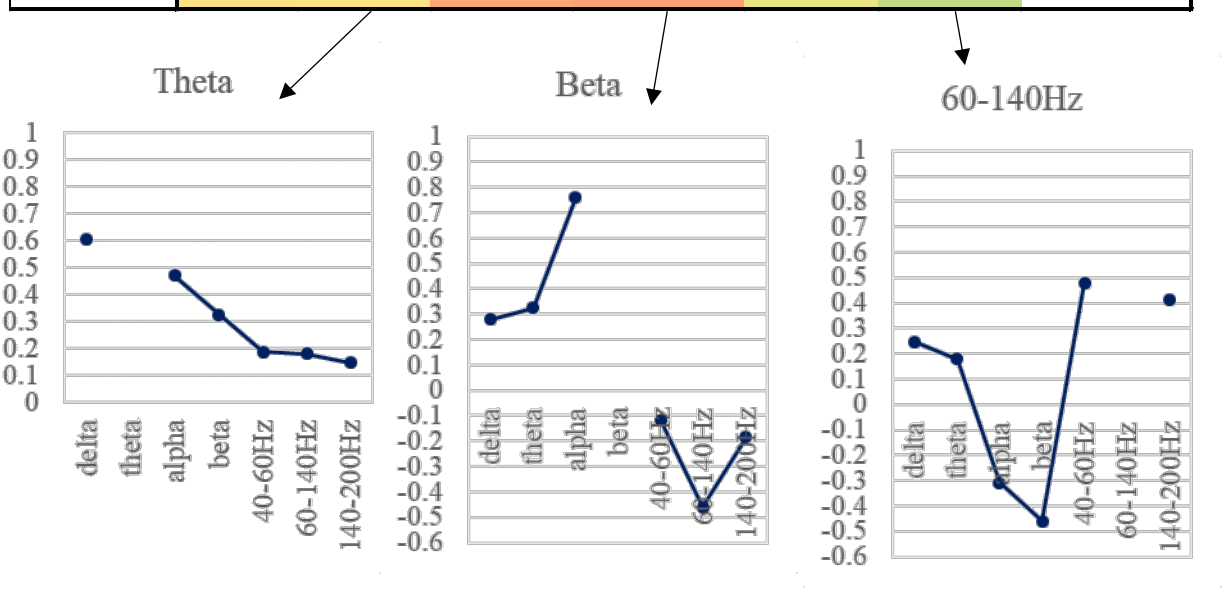

Figure 127. A coordinate at expted V3A was selected (MNI [20, -88, 22]). Cross-frequency correlations showed negative correlations between beta and gamma. The positive correlations between theta and gamma seen in the primary visual cortex was reduced in this extrastriate region.

MT+

At the MT+ region (MNI coordinates [42, -72, 0]) a similar pattern is observed (Figure 128). Alpha and beta frequencies show high correlation with each other, and both show anti-correlation with gamma frequencies. There is again high correlation between theta and delta, as well as between gamma frequencies. The beta/alpha – gamma see-saw has therefore been evidenced at both primary cortices and extrastriate regions, while the theta-gamma coupling has reduced outside of the visual cortex.

	delta	theta	alpha	beta	40-60Hz	60-140Hz	140-200Hz
delta		0.53	0.42	0.38	-0.05	0.01	0.05
theta	0.53		0.61	0.55	0.07	0.02	0.11
alpha	0.42	0.61		0.72	-0.06	-0.21	0.03
beta	0.38	0.55	0.72		-0.05	-0.18	0.04
40-60Hz	-0.05	0.07	-0.06	-0.05		0.56	0.43
60-140Hz	0.01	0.02	-0.21	-0.18	0.56		0.67
140-200Hz	0.05	0.11	0.03	0.04	0.43	0.67	

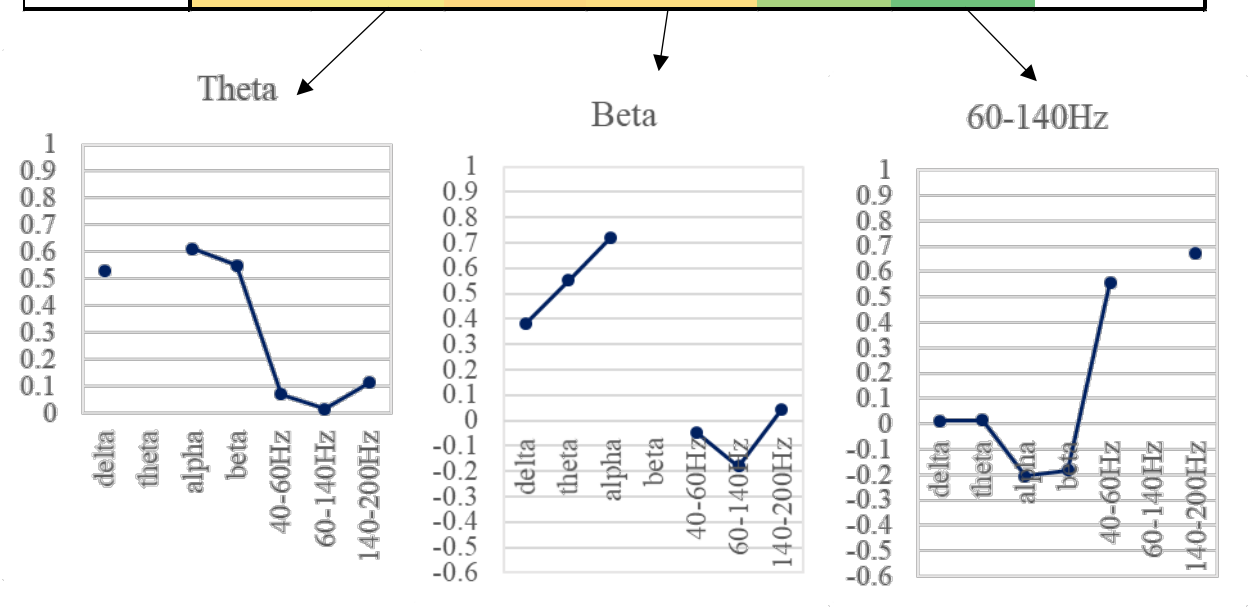

Figure 128. At MT+ (MNI [40, -88, 0]) there is strong positive correlation between lower frequency bands delta, theta, alpha and beta, and strong positive correlations across gamma frequencies ranging from 40 - 200Hz. Alpha and beta both show anti-correlated activity with gamma ranges, evidencing the see-saw between these frequencies during visual attention.

Summary

A cross-frequency correlation analysis at regions of interest in the visual pathway demonstrate that the relationship between the frequency bands differs across visual regions. This suggests that a multi-band TICA may provide useful results for identifying cross-band components in visually driven regions. Based on this I will run combined frequency analyses and assess the results.

7.4 Are multiband TICA outputs reliable across permutations?

The previous two sections have demonstrated that reliable visually driven components can be identified across the MEG frequency bands, and that the relationship between these frequencies changes across different visual regions. These findings support the exploration of a combined frequency TICA technique. Based on these findings I ran multiple TICA permutations using the combined band MEG data. I

first wanted to check whether outputs using this technique are reliable across outputs. Results show that reliable components are identified using this technique, across permutations.

7.4.1 Methods

For each frequency band the dataset consisted of a 4D dataset of dimensions (X, Y, Z, *t*) = [37 x 31 x 37 x 2360]. These 7 datasets were concatenated along the x-axis, creating a single dataset of size [259 x 31 x 37 x 2360. Probabilistic group tensor ICAs were run using FSL's MELODIC, via the command line to identify components in regions that were time-locked to the movie stimulus.

Movie clips of ten-minutes were used for analyses. This was due to MELODIC being unable to cope with the size of the dataset when clips were longer. The movie clips were taken from the middle of the movie clip (original length 19 minutes 40seconds). To assess the reliability of the components, the variability caused by changing the first brain was exploited (see Chapter 2). 16 permutations were generated, each with the first brain swapped so a different participant's data were the first input on each of the ICA runs. Unrestricted ICAs were conducted in the first instance to guide the restriction of dimensionality for direct comparisons across outputs. When a ten-minute clip was used between 85 and 87 components in each permutation were produced. These TICAs were then restricted to 85, based on the mean dimensionality. Analyses were also run at dimensionality 20, based on findings that components alter as dimensionality is changed (see Chapters 5 and 6). Outputs at different dimensionalities were used to check consistency.

The most reliable output was identified by finding the best matched components across the permutations and finding the average of the spatio-temporal correlations, a technique used previously with BOLD data (see Chapter 2). The most representative ICA output had components that showed higher spatio-temporal correlations with the other components generated, on average. The reliability of each of the components in the most reliable output was determined by finding the best matches in each of the other outputs and averaging the spatio-temporal similarity scores. The most reliable outputs were examined at a dimensionality of 20 and 85.

As a reality check and before the main analyses, the same frequency band was entered twice into the x-axis concatenation along with two other frequencies. The output was examined to check for duplication of

the components in the repeated frequency band. This was observed (see Figure 129), therefore we were reassured that the technique was doing what we expected.

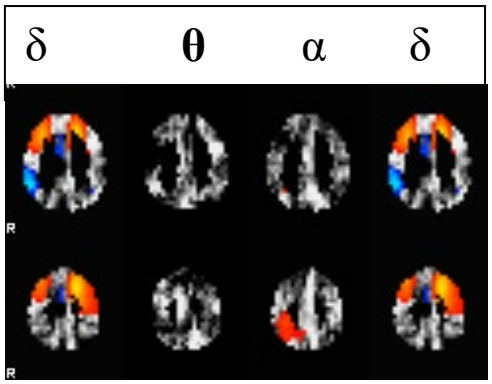

Figure 129. Repeated delta in an x-axis concatenation produced repeated spatial elements in cross-frequency components, providing validation to the technique.

7.4.2 Results

The reliability of the results was good across the sixteen permutations using ten-minute movie clips (see Figure 130 for reliability with 85 components).

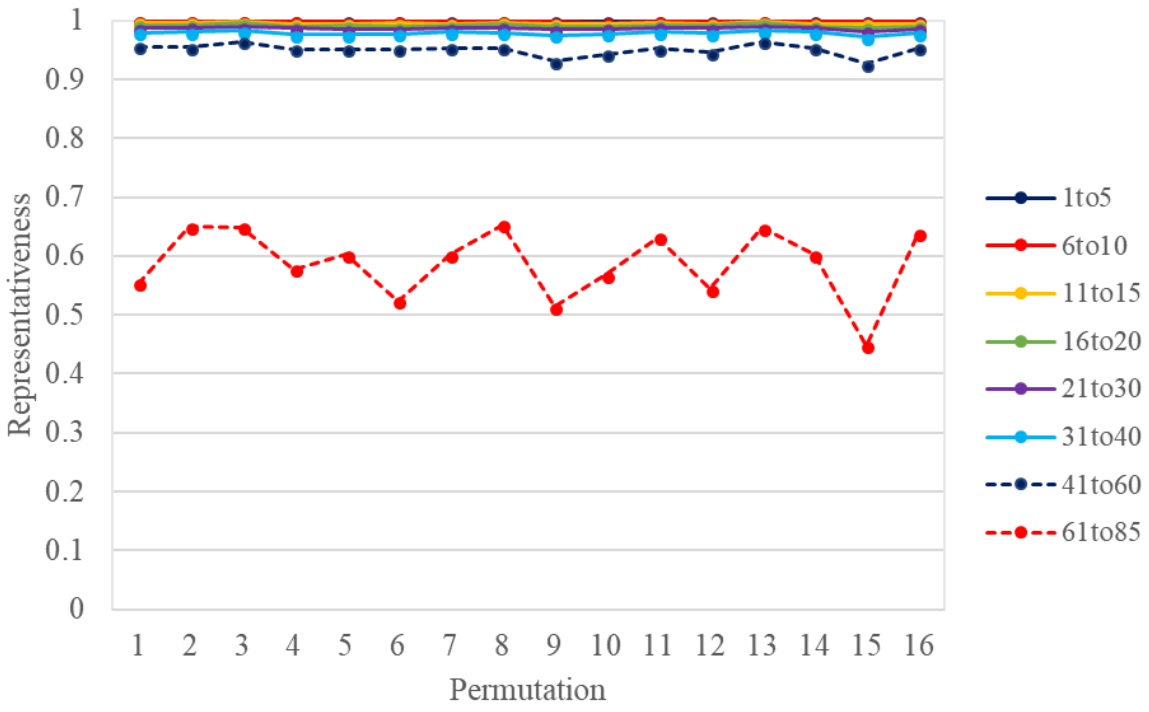

Figure 130. The similarity of TICA components across cross-frequency datasets using ten-minute movie clips. Shows very good reliability across permutations, supporting further investigation of the technique.

Signal and noise components

Components in the most representative output at dimensionality 85 were assessed as being either signal or noise, using the distribution of activation in the spatial maps and timeseries (Griffanti et.al., 2017). Components with evidence of motion artefacts were excluded as noise, as were components with scattered activation across a single frequency band or multiple bands. In the 85-component output I identified 12 noise components (15%; Griffanti, 2017). As this proportion was low (see Chapter Two), the variance explained was also used as a guidance for discarding components as noise. At 60 components 90% of the data were explained, meaning the rest of the 25 components represented only 10% of the variance (an average of less than 0.5% each). In Chapter 4 I found that components later in the output were more likely to be noise, therefore the first 60 components were taken forward in the analysis.

In the most reliable 20 component output, 4 components were identified as noise and only three components showed activity in visually driven regions. These components are presented in the following chapter, alongside additional components that were only identified in visual regions when using a higher dimensionality (85).

7.5 Summary: Chapter 7

The results in this chapter suggest that a combined frequency TICA technique using data collected during movie watching may be a valuable tool for investigating the relationship between different neural frequencies. Based on these findings, in the next chapter I present the reliable cross-frequency components identified using this technique.

Chapter 8: A novel combined-frequency technique to investigate MEG cross-frequency networks during natural viewing

8.1 Introduction

In the previous chapter, I lay the foundations for the use of a novel and potentially exciting technique for investigating cross-frequency relationships in the brain. First, I demonstrated that reliable visually driven components could be generated using each of the individual MEG frequency bands (1Hz – 200Hz) in a TICA. Next, I showed that the relationship between the frequency bands differed across different visually driven regions in the ventral and dorsal pathways. Finally, I showed that combined-band TICA outputs showed good reliability across different permutations. In this chapter I will present visually driven components in the combined-band output.

In my movie data, the visually responsive neural signal is driven by the broadband stimulus, therefore we expect multiple visual regions to be active, each with different timecourses responding to features in the stimulus. TICA works by grouping together voxels that are driven by the same underlying signal and should be able to identify correlated activity across frequency bands if the data is spatially concatenated.

8.2 Methods

As described in the previous chapter (section 7.4.1), I ran combined frequency TICAs at dimensionality 20 and 85. By cross-correlating the component outputs, I identified the most reliable outputs (for description of this method see Chapter 2, section 2.2.1.2, page 38). I used both outputs as a means of checking consistency, as it was difficult to identify noise components at a higher dimensionality (see previous Chapter 7, section 7.4.2). As this was an initial look at the results I looked only at components with peak activity in visually driven areas (occipital, parietal and posterior temporal). Two cross-frequency components were identified in the 20-dimensionality output based in these regions that were also present at the higher

dimensionality. Seven components were identified at the higher dimensionality with peaks in visually driven regions.

8.3 Results

Two components in the 20-dimensionality output had activation in visually driven areas. These represented two patterns of cross-frequency correlation, documented below. Very similar components were also identified at the higher dimensionality (85). I will first document these two cross-frequency patterns, and then present the additional components generated at a higher dimensionality.

8.3.1 Low dimensionality

1. Theta – Gamma positive correspondence

The most reliable component at 20-dimensionality showed correlated activity in theta, delta and gamma bands, in occipital and occipital-parietal regions (Figure 131). The component also explained a high proportion of variance in the data, lying 3rd in the TICA output. This supports previous research that shows cross-frequency correlations between these frequencies during visual tasks. For example, gamma-delta interactions have been identified in the monkey visual cortex during natural movies (Whittingstall & Logothetis, 2009). Evidence of gamma-theta driven coupling has been demonstrated in the inferior occipital gyrus during the viewing of human faces (Sato et.al., 2014). It is thought these frequency bands interact with higher gamma frequencies being 'nested' within the lower frequency bands (Buzsáki, & Wang, 2012) or that they exploit phase-amplitude coupling (e.g. Canolty & Knight, 2010). This cross-frequency coupling has been reported during visual working memory processes (e.g. Wolinski, Cooper, Sauseng & Romei, 2018; Demiralp et.al., 2007) and during visual discrimination tasks (Händel & Haarmeier, 2009).

Using this cross-frequency technique the gamma-theta and gamma-delta interaction could be explored further and across the brain by using different types of visual stimuli or task-based data using working memory tasks (Holz, Glennon, Prendergast & Sauseng, 2010) or declarative memory tasks (Osipova et.al., 2006).

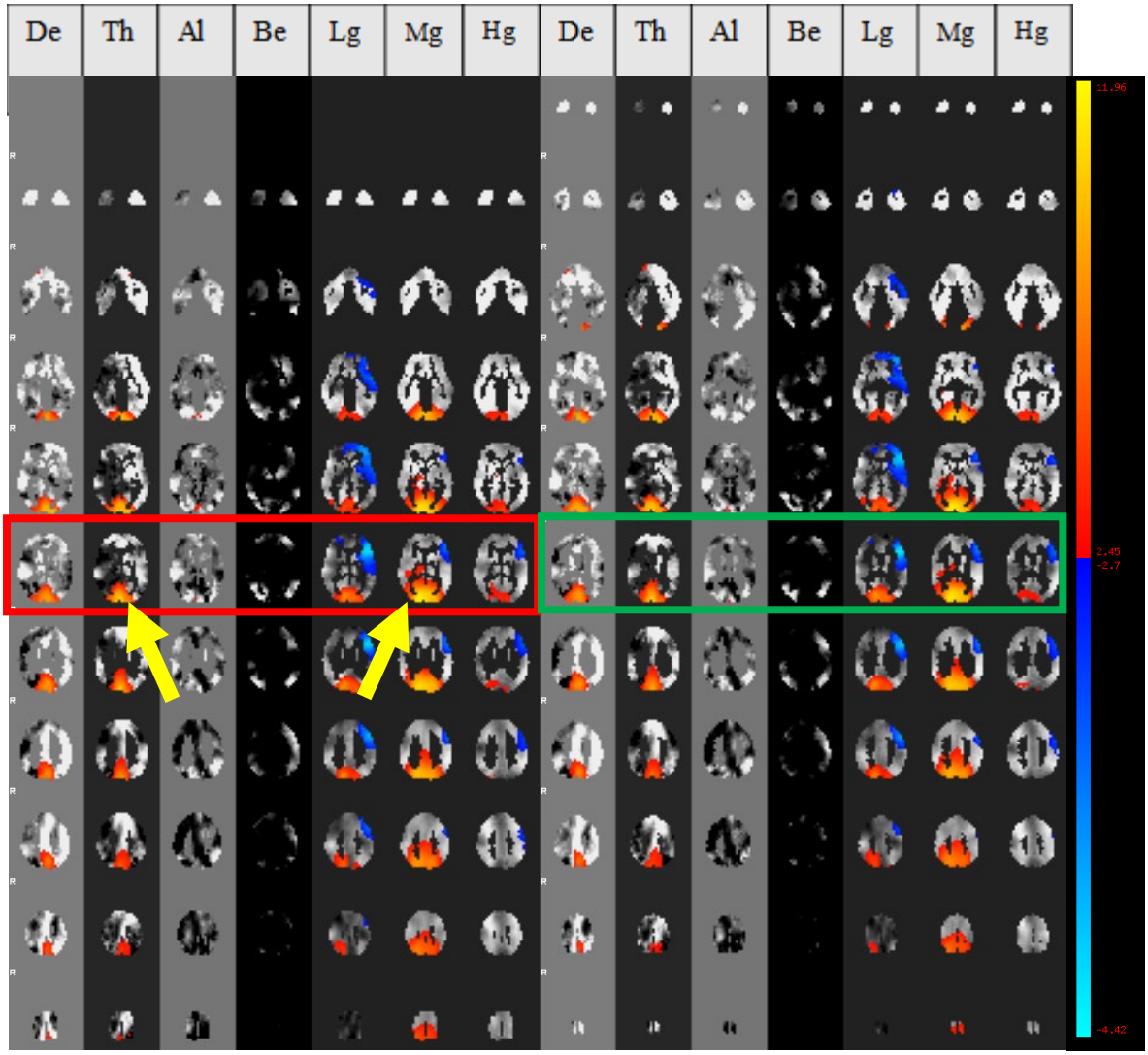

Figure 131. Alternating slices through the brain (L-R of figure) at each of the frequency bands. Two consecutive slices are highlighted with a red and green border, respectively, for demonstrative purposes. The most reliable component using a ten-minute movie clip showed correlated activity between gamma frequencies and theta/delta frequencies, in the occipital lobe (see yellow arrows).

Figure 132 shows the gamma and theta activation projected onto the 3D brain surface. The component activation in theta and 60-140Hz showed 76% and 52% overlap with the best matched single band components, respectively. Peak voxels lay in early visual regions at both the single band gamma range (MNI [-12, -78, 6]) and the merged band gamma output (MNI [6, -90, 0]). This was also the case for both single band theta (MNI [-24, -90, 6]) and theta when merged frequencies were input (MNI [-6, -84, 6]).

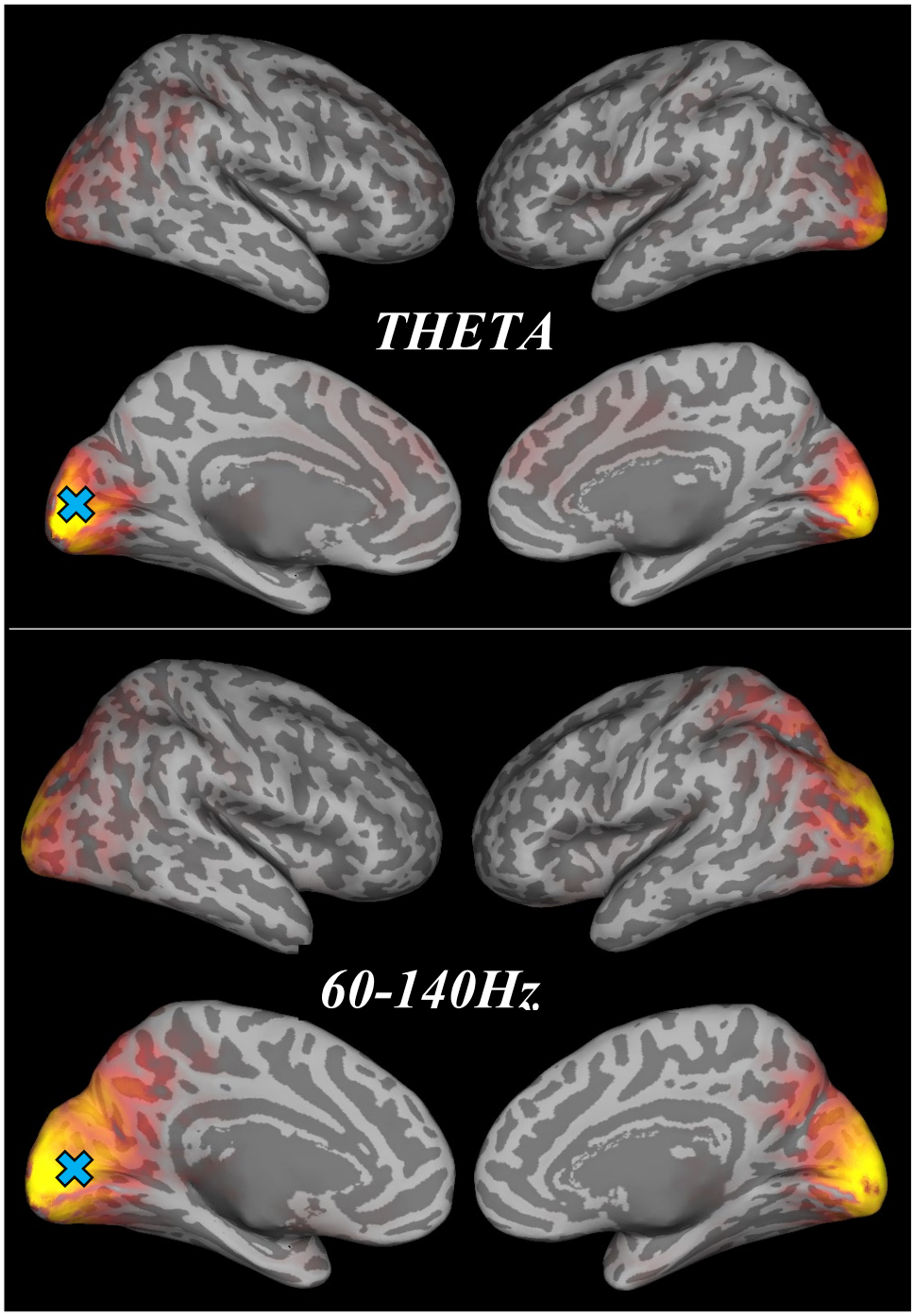

Figure 132. The (A) theta and (B) gamma (60-140Hz) elements of a cross-frequency correlation in the occipital lobe. Blue crosses show peak voxel

2. Beta - Gamma seesaw

One noticeable aspect to the results when examining the components, was the lack of components that show positive correspondence between beta and gamma bands. Instead a component showed antiphase activation between the two frequencies. The component shows negatively correlated beta and gamma

interaction, and a positive correlation between alpha and beta bands in the occipital and parietal lobes (see Figure 133). This interaction is supported in the literature where a reduction in alpha and beta bands are observed with the onset of visual stimulation and enhancement in the gamma band at occipital and parietal regions (Michalareas et.al., 2016). Presentation of moving and stationary stimuli in the central visual field also results in the same pattern in the early visual cortex (Swettenham, Muthukumaraswamy & Singh, 2009). Fluctuations in visual engagement, motion elements or low-level luminance could therefore cause the gamma – alpha/beta seesaw at these visually driven regions (e.g. Degwekar & Wyatt, 2013).

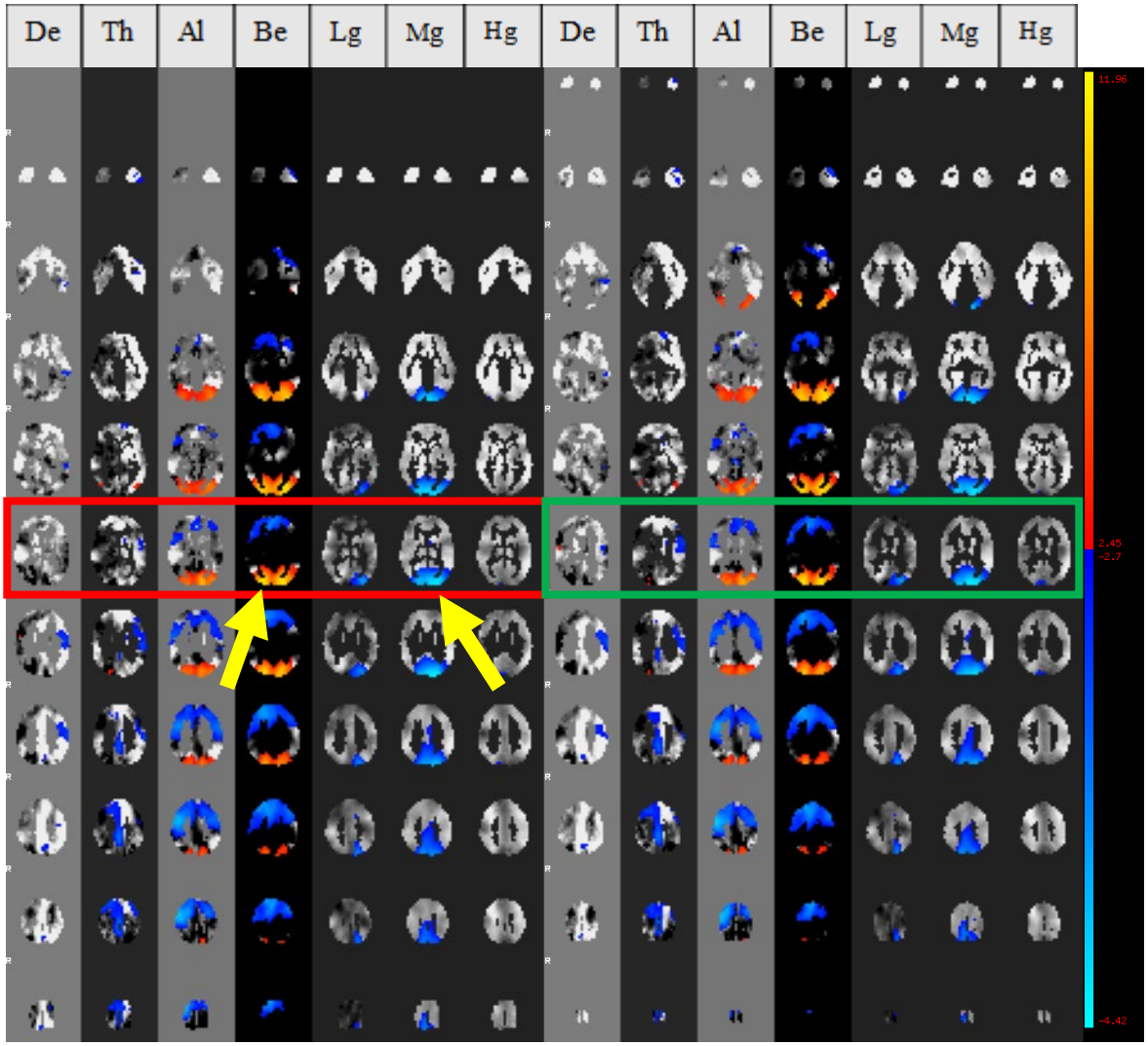

Figure 133. Alternating slices through the brain (L-R of figure) at each of the frequency bands. Two consecutive slices are highlighted with a red and green border, respectively, for demonstrative purposes Beta and alpha driven occipital activation shows anti-correlated activity in the gamma range during movie watching (see yellow arrows), and anti-correlated activity in frontal regions.

The anti-correlated activity in beta and MG (60-140Hz) covers early visual and lateral occipital regions (see Figure 134). Research into cross frequency-coupling during working memory has identified an interaction between gamma and alpha frequencies in early visual and dorsal regions (Popov, Jensen & Schoffelen, 2018). It is expected that visual working memory is active during the movie watching and investigation using targeted working memory tasks and the cross-frequency TICA technique would be useful in further understanding this interaction.

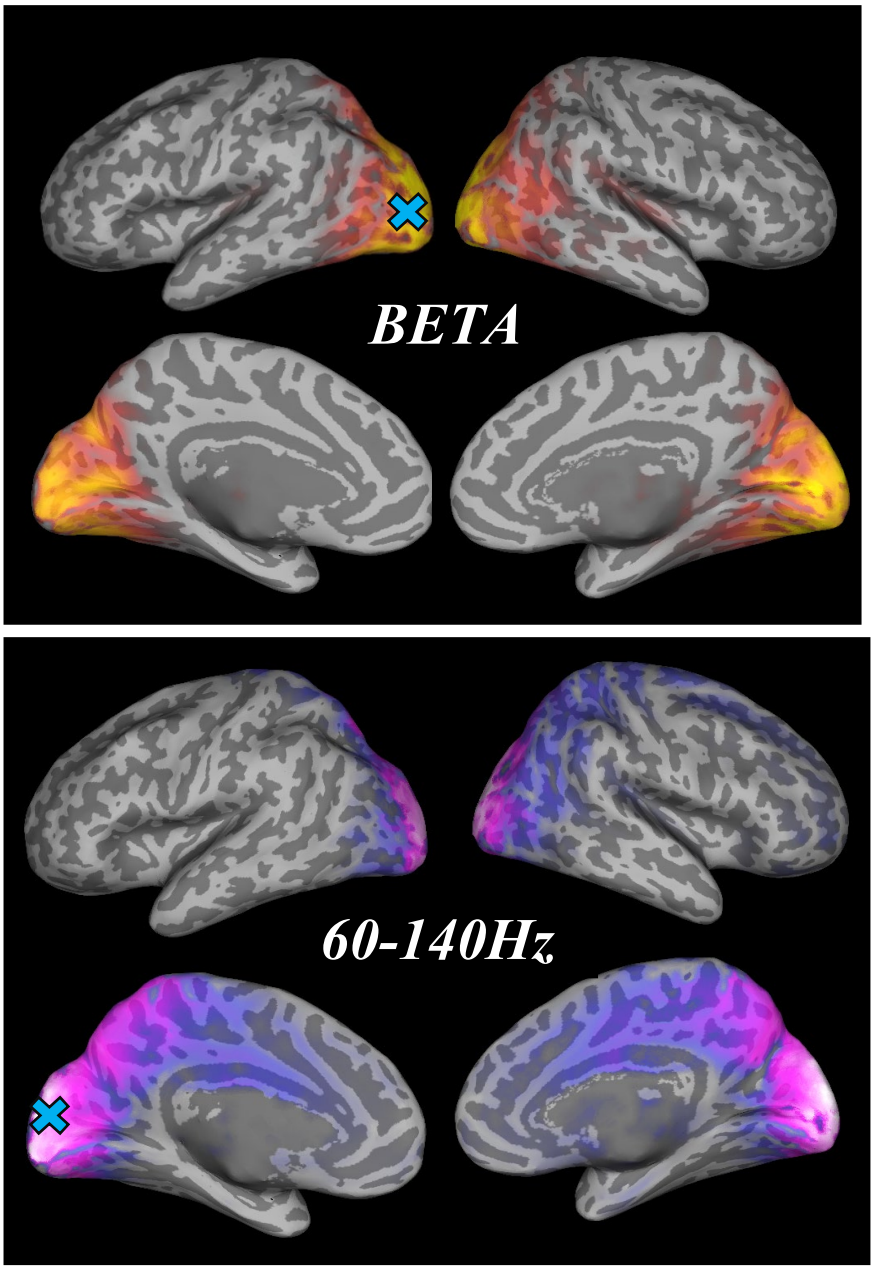

Figure 134. Antiphase beta and gamma activity was identified in early visual and lateral occipital regions. Locations of peak voxel activity are marked with a blue cross.

In a cross-frequency study using EEG data Aoki et.al. (2015) found a beta-gamma interaction with beta elements at post-central dorsal regions, and correlated gamma activity more anteriorly at the pre-SMA. Therefore, it may have been expected that these results would be replicated. One consideration is that Aoki et.al., (2015) used resting state data while we had the participants watch a movie clip. This may change the functional interaction profile of regions, across the frequency bands. Research has suggested that there may be distinct roles for beta and gamma in working memory (e.g. Lundqvist et.al., 2017) and monkey research has shown anti-correlated activity at the prefrontal cortex between beta and gamma frequencies during visual categorization tasks using working memory (Wutz et.al., 2018). The pre-SMA region has also been identified in previous research as being active during working memory tasks involving faces (Haxby, Petit, Ungerleider & Courtney, 2000).

Antiphase activity between gamma and alpha/beta frequencies is well documented during the presentation of visual stimuli (e.g. see Figure 135, adapted from Proudfoot, Woolrich, Nobre & Turner, 2014). Research has shown that lower frequency alpha/beta bands show suppression with afferent stimuli (Bauer, Oostenveld, Peeters & Fries, 2006), while higher gamma frequencies are enhanced (Donner & Siegel, 2011). The modulation in alpha/beta bands is understood to be modulated by the predictability of a visual stimulus rather than stimulus onset per se (Bauer, Stenner, Friston & Dolan, 2014). As our subjects were watching a movie clip, we would expect that the visual working memory was engaged to visually follow the plot (there was no audio during presentation of the movie). The engagement of visual working memory may mean that positive correlations between gamma and beta found in previous studies are disrupted.

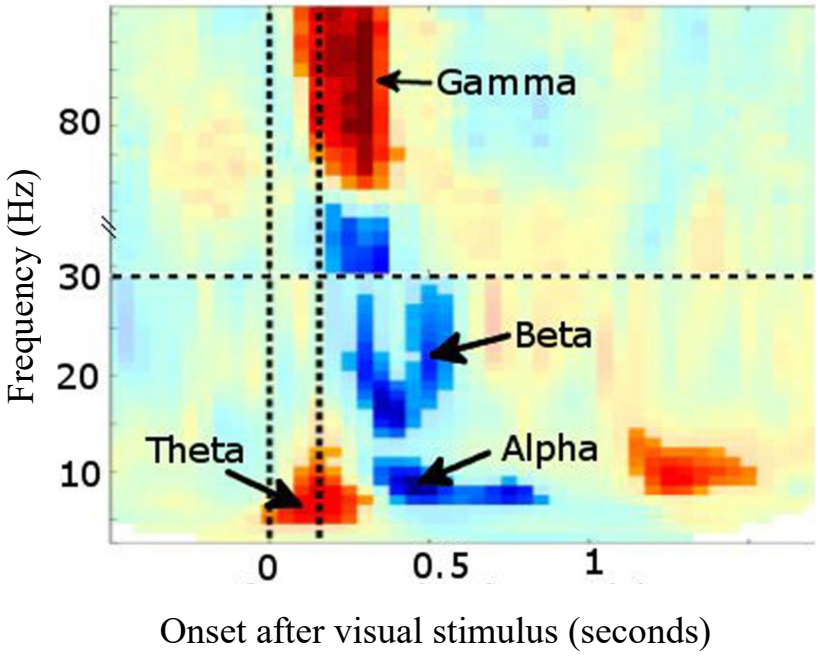

Figure 135. Adapted from Proudfoot et.al. (2014), antiphase activity in alpha/beta frequencies and gamma at presentation of visual stimulus.

Summary: low dimensionality

The two components identified at a low dimensionality demonstrate correlation and anti-correlation between low frequencies and higher gamma ranges. These are encouraging findings that suggest a usefulness for this merged frequency technique. The next sections will discuss components that were identified at the higher dimensionality of 85. A component was identified replicating the theta-gamma correlation in the occipital lobe. Two more components displayed beta-gamma anti-correlations in the occipital-parietal regions, supporting the robustness of the results above. Two components showed cross-gamma positive correspondence without associated theta activity that was not identified in the low dimensionality. Single band components (activity in only one band) were also not identified in the 20-dimensionality output. At a higher dimensionality one alpha only and one beta only component was generated.

8.3.2 Higher dimensionality

1. *Across gamma*

A component that was not identified at dimensionality 20 but was identified at a higher dimensionality (85) showed correlated activity across the gamma bands in the occipital lobe, predominantly at frequency bands 40-60Hz (LG) and 60-140Hz (MG) (see Figure 136). Gamma activation is thought to be important in the functional aspects of neuronal activation and systems levels functions (Merker, 2013). This means cortical oscillatory synchrony in the gamma range may help to enable infrastructural support functions, such as regional control of blood flow, or excitation-inhibition coupling. Gamma frequencies are also known to be modulated at the visual cortex by the presentation of visual stimuli (Bauer, Stenner, Friston & Dolan, 2014). Gamma shows feedforward patterns from early visual regions into the ventral stream, and modulations in power at higher order regions based on spatial attention (Magazzini & Singh, 2018).

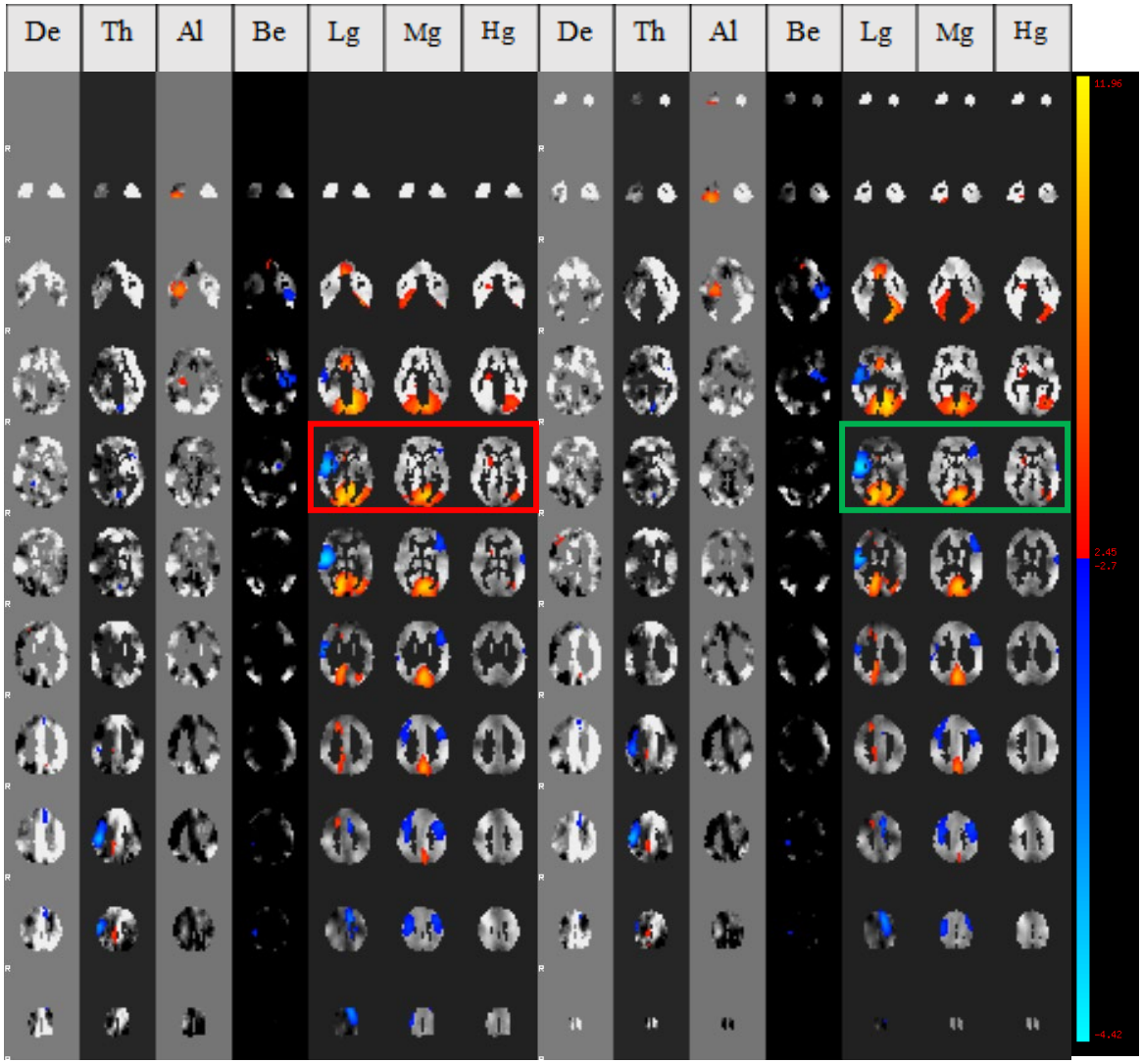

Figure 136. Alternating slices through the brain (L-R of figure) at each of the frequency bands Gamma driven components at the occipital lobe were reliably identified using the cross-frequency technique. Two consecutive slices are highlighted (red and green boxes) showing this gamma driven activation.

Within the lower gamma band there is an aspect of the component within the prefrontal cortex. It has been shown that long range gamma frequencies are elicited during face perception (e.g. Rodriguez et.al., 1999) and local synchronization takes place during visual processing (e.g. Von Stein & Sarnthein, 2000). The timecourse of this component could be further investigated alongside the movie clip to see which features of the movie this is responding to, and whether face processing is driving these long-range correlations.

Figure 137 shows the positive activation in the higher gamma frequency on the 3D surface. Both LG and MG gamma ranges have peak activation at the medial occipital lobe: MNI coordinates at 40-60Hz were [-

24,-60, 2] and at 60-140Hz [-12, -66, 18], near the calcarine sulcus. Some residual activity is also seen in the HG range (140-200Hz).

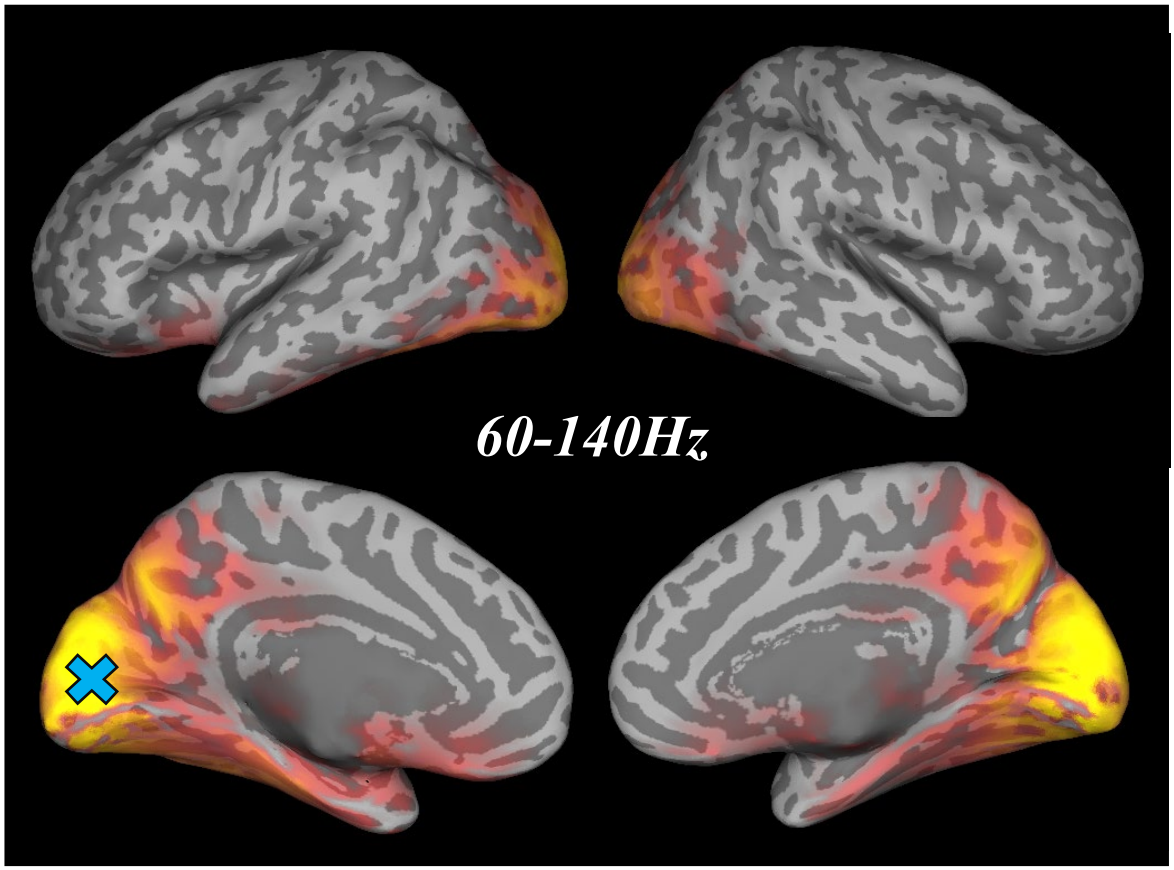

Figure 137. The activity in the 60-140Hz frequency range in a reliable gamma driven component shows medial occipital activation. Location of peak voxel of activity is marked with a blue cross.

Interestingly there is anti-correlated activity in this component, lying at dorsolateral pre-frontal regions in both theta and gamma ranges. There is also antiphase activity in anterior temporal regions/ventrolateral prefrontal regions in beta and gamma range 40-60Hz. These regions have been shown to be part of a functional network involved in cognitive and associative processed such as working memory, theory of mind and executive functions (DeLuca, Yates, Beale & Morrow, 2015;

Some research has demonstrated in the macaque brain that lower and higher gamma frequencies are anti-correlated in early visual regions (Ray & Maunsell, 2011). However, no components generated identified this interaction at this location. It may be that this effect (which was measured at the neural level), cannot be resolved at the whole brain scale, using this technique.

2. Centered in a single band

In the 20-dimensionality TICA output there were components with delta and theta activation only, but these were not in visually driven regions, but in more anterior regions; the lateral prefrontal cortex, the auditory cortex and the anterior temporal lobe. They also explained relatively little variance in the dataset. The only region associated directly with visual processing that was identified as a reliable delta driven component lay in the lingual gyrus, however it was 73rd/85 components therefore explaining only 0.38% of the variance in the data. Other cross-frequency components showed activity at early visual regions in delta and explained larger amounts of variance, suggesting that delta is synchronized with other frequencies during movie watching. It also means that components identified at the single-band level in early visual regions are in fact part of a cross-frequency component, recognized when the bands are combined (Chapter 7, section 7.2.2). However, theta activity, and to a lesser extent delta, appeared in very reliable cross-frequency components coupled with gamma frequencies. This suggests that components identified at the single band level are correlated with activity in gamma frequencies.

Although reliable components were identified in the occipital lobe using single band alpha and beta (see Chapter 7, section 7.2), there were no occipital components with alpha or beta only activation, using the combined band technique at 20 dimensionalities. Some residual activity alpha in this location can be seen in components centered in theta and gamma. This suggests some correlation between these frequencies that was not identified in the voxel-by-voxel correlation analysis (Chapter 7, section 7.2.1). It is possible that with using a broadband stimulus, multiple signals are underlying the data; these source signals can be identified using TICA but are lost due to mixing when you do a simple voxel-based correlation.

As well as correlated activity with theta/gamma, activity was correlated between alpha and beta in the occipital lobe, in anti-phase with gamma frequencies ("Beta-Gamma seesaw", section 8.3.1). Occipital-parietal regions are known to show synchronization in alpha and beta ranges based on cognitive engagement and disengagement with a visual task (e.g. Miller et.al., 2010). Research has shown that alpha power decreases with visual engagement (e.g. Klimesch, Sauseng & Hanslmayr, 2007), as subjects were attending to a visual stimulus, the power in alpha may have been lowered. A lack of alpha driven components in low dimensionality multiband analyses may reflect this, with activity in other bands explaining more of the variance, overall. Using only 20 components may have meant that alpha or beta centered components had not

split off from correlated activity in other bands. At the higher dimensionality of 85, new alpha centered components were generated in the medial parietal regions, though still not at the occipital lobe (see Appendix 8.1a). A beta occipital component (with a very small amount in the alpha band) was also very reliable at a higher dimensionality of 85 (see Appendix 8.1b). This suggests that the dimensionality chosen is critical for recovery of single band components in a multi-band output.

8.4 Summary: Chapter 8

Using ICA with MEG frequency bands merged across the x-axis provides a useful way to investigate cross-frequency interactions. A voxel-by-voxel correlation analysis across frequency bands provide support for the patterns of data seen in a merged frequency ICA. Results show a positive correlation between theta and gamma frequencies in visual regions, and a negative relationship between these frequencies with beta. A full correlation was calculated between frequencies; a further partial correlation could provide additional information about the relationship between frequency bands by regressing out other bands when comparing pairs of frequencies.

The use of movies increases the range of frequencies that can be examined and improves the signal to noise ratio. Using this method with data collected during different tasks will be useful for understanding how these interactions change depending on cognitive state. This technique may also be important for identifying changes in cross-frequency coupling with neurodevelopmental or clinical abnormalities.

Components displayed in the multi-band outputs were compared to the best matched single band components. Of interest was whether the same components can be identified using the multi-band technique, as well as the cross-frequency results. Components in the multiband ICA output show some overlap with matched components in the single band outputs. Further work could examine the dimensionality at which the best match could be found. Differences in spatial maps at a certain frequency band between the two techniques may indicate either changes in the output due to differences in the amount of data entered into the ICA, or a ‘pulling apart’ of components with multiband ICA creating different spatial maps.

This work demonstrates that you can get reliable and sensible components using a combined frequency technique, however dimensionality is critical. Although a dimensionality of 20 is fine for BOLD data, or single band MEG, it is not for multi-band MEG. Evidence of this is the is failing of the combined

multi-band technique to find some of the components that were clear in the single band analyses (Chapter 7). Therefore, more work is needed to document the results as dimensionality is changed. Based on the work in Chapters 4 and 6 it may be expected that single band elements of the coupled activity may split into separate components. This would be interesting to examine as splitting (or lack of) would give some indication of the strength of the coupling across different frequencies

In theory, the spatial concatenation ICA technique used in this chapter should work across modalities, if data is scaled to match. This will be examined in the following chapter, along with other analyses for investigating the relationship between the BOLD signal and neural oscillations.

Chapter 9: Combining MRI and MEG data collected during natural viewing

9.1 Introduction

In the previous chapter I discover that by combining MEG frequencies using spatial concatenation, reliable cross-frequency networks can be identified using TICA. This technique is an exciting and novel way to investigate cross-frequency coupling that could be applied to different tasks. In theory the same technique can be applied to combined BOLD and MEG frequency data, and if successful could be an important and useful tool. By combining MEG and fMRI data we can exploit the strengths of both of the techniques in one analysis for understanding functional activity in the brain. MEG data shows good temporal resolution, while BOLD data has a better spatial resolution. In previous Chapters of this thesis I have demonstrated that both BOLD fMRI recordings (Chapter 2; see also Hasson, Malach & Heeger, 2010) and MEG recordings (Chapter 7; see also Chang et.al., 2015) show reliable patterns of time locked activity during natural viewing. In this chapter I run some preliminary analyses comparing the MEG and BOLD data collected during movie watching, for combination into a spatially concatenated TICA analysis.

First, I will perform a voxel-by-voxel correlation between the MEG beamformer data and the BOLD timeseries to assess whether there are regions in each frequency band that show some coupling to the BOLD timeseries. Having established that there are different patterns of cross-modality correlation at the different frequency bands the voxel level, next I compare an fMRI component timeseries (generated using a BOLD only TICA) to the voxel-level MEG beamformer data. To anticipate the results, correlations are identified between the BOLD source signal (component timeseries) and the beamformer data in theta and gamma bands. The relationship between the couplings differs across different visual regions suggesting that a combined modality TICA may be able to segment different visual areas. Based on these results I run a combined modality TICA, which generates components with BOLD and oscillatory elements. The patterns of cross modality correlations identified in the TICA support previous work in the field and provide the foundation for use of BOLD and MEG frequency bands in a spatially combined TICA.

9.2 Methods

The data were collected in MEG and MRI scanners as described in Chapter 1 (section 1.3). Each of the sixteen participants took part in two scanning sessions, one in an MRI scanner and one in a MEG scanner. All subjects watched the same twenty-minute movie clip in each scanner, to allow comparison across the modalities. Half of the subjects had watched the movie clip in the MEG scanner before the MRI scan.

9.3 Voxel-wise correlation between MEG and MR data

First, a voxel-by-voxel correlation was run between the MEG beamformer data and BOLD timeseries to assess whether different patterns of correlations existed across the brain for the different frequency bands. Different correlation patterns between BOLD and the MEG frequencies support the potential use of a combined TICA analysis as it means we can examine different patterns of coupling during natural vision.

9.3.1 Methods

The mean timeseries was taken at each voxel in the brain for the fMRI data and each of the MEG frequency bands (HRF-convolved). In the cross-modality analysis, we correlated the mean fMRI voxel-timecourse the with MEG voxel-timecourse at each voxel, in each frequency band.

9.3.2 Results

Whole brain cross-correlations

The maps of these correlations in each frequency band are shown in Figure 138-Figure 144. In the primary visual cortex, with the notable exception of the alpha band (Figure 140), all MEG frequency ranges show significant positive temporal correlations with the BOLD signal (corrected to $p<0.05$, with FDR correction to account for multiple comparisons). In lateral extrastriate occipital regions, delta and theta bands showed a significant negative correlation ($p<0.05$; Figure 138 and Figure 139), as did alpha and beta frequencies ($p<0.05$; Figure 140 and Figure 141). In the gamma frequencies there were significant positive

correlations with BOLD, peaking at 60-140Hz (high gamma; Figure 143). Interestingly, positive correlations at the very high gamma range (140-200Hz) were also found (Figure 144).

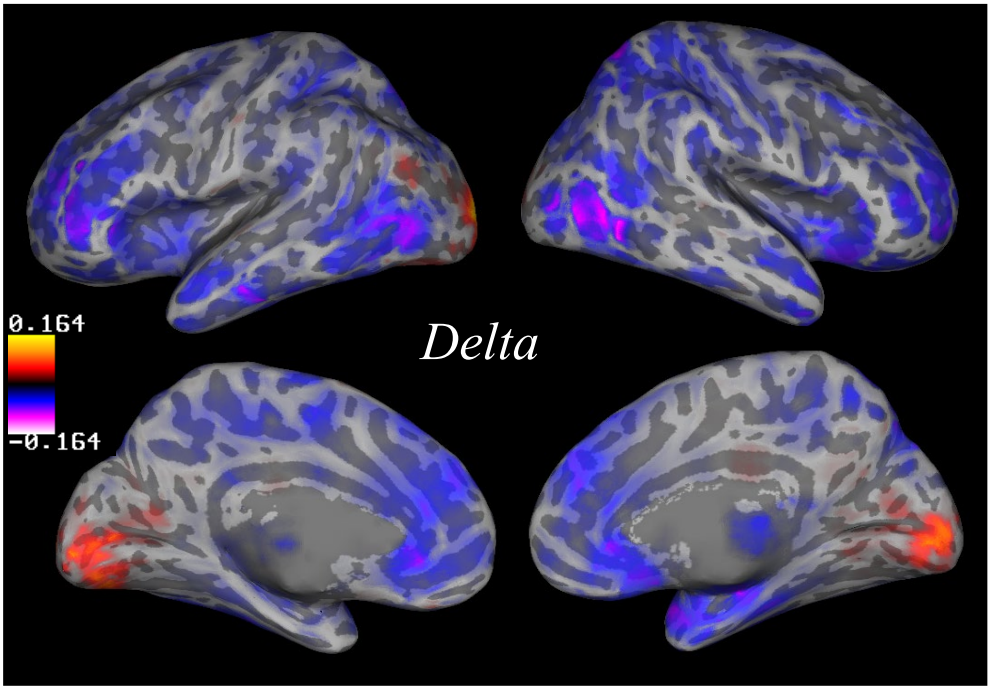

Figure 138. A voxel-by-voxel correlation between delta oscillatory activity and BOLD shows positive correlation only at early visual regions. Correlation values are displayed on a template brain in Montreal Neurological Institute (MNI) space. Significant correlations had a $p<0.0017$ (delta)

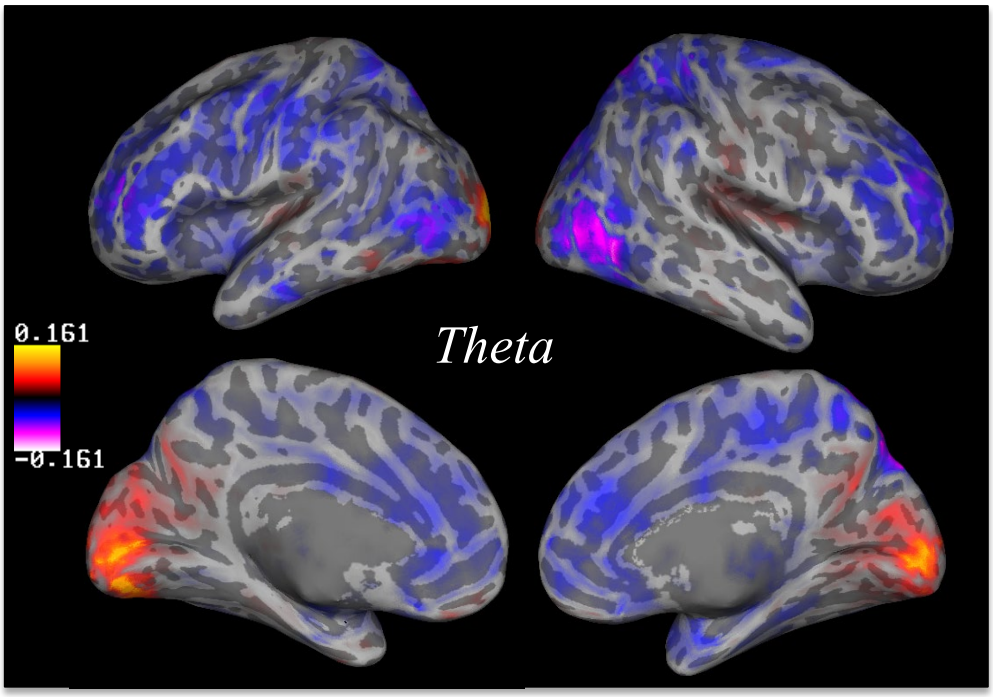

Figure 139. A voxel-by-voxel correlation between theta oscillatory activity and BOLD shows positive correlation only at early visual regions. Correlation values are displayed on a template brain in Montreal Neurological Institute (MNI) space. *p<0.0011 (theta).*

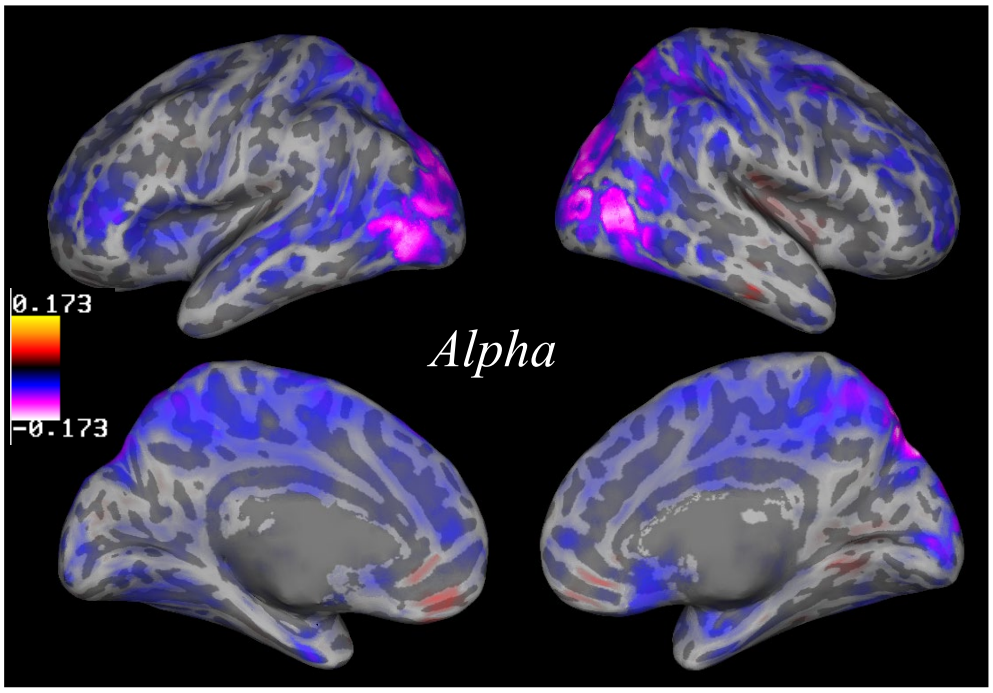

Figure 140. Alpha oscillatory activity shows negative correlation with the BOLD timeseries at lateral occipital and parietal regions. Alpha shows no correlation at early visual regions.

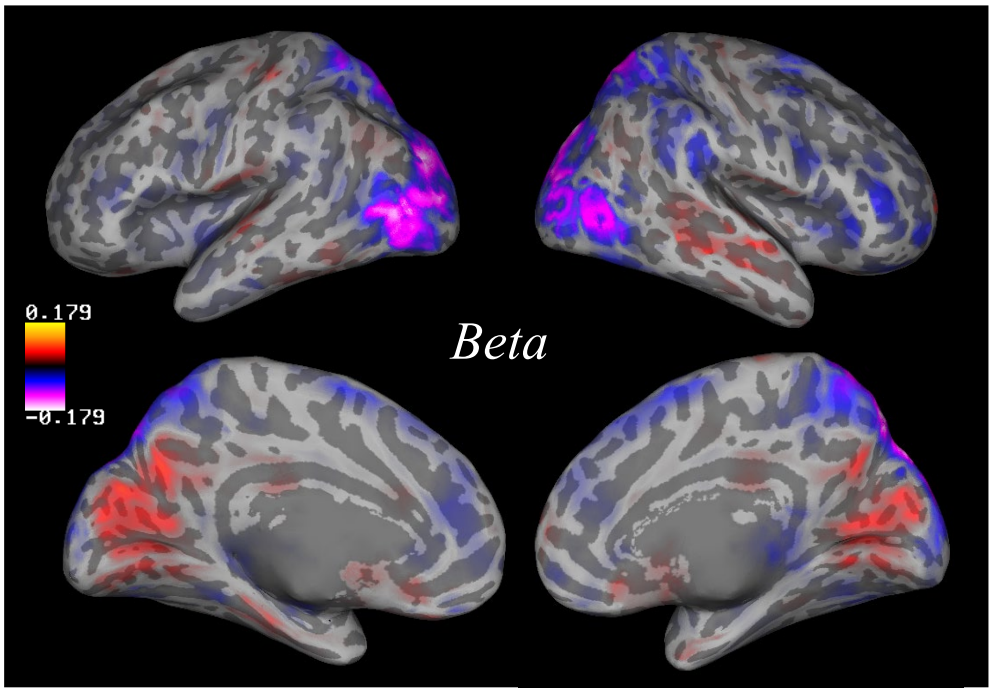

Figure 141. Beta oscillatory activity shows negative correlation with the BOLD timeseries at lateral occipital and parietal regions. Beta demonstrates some positive correlation at early visual regions, while alpha shows no correlation.

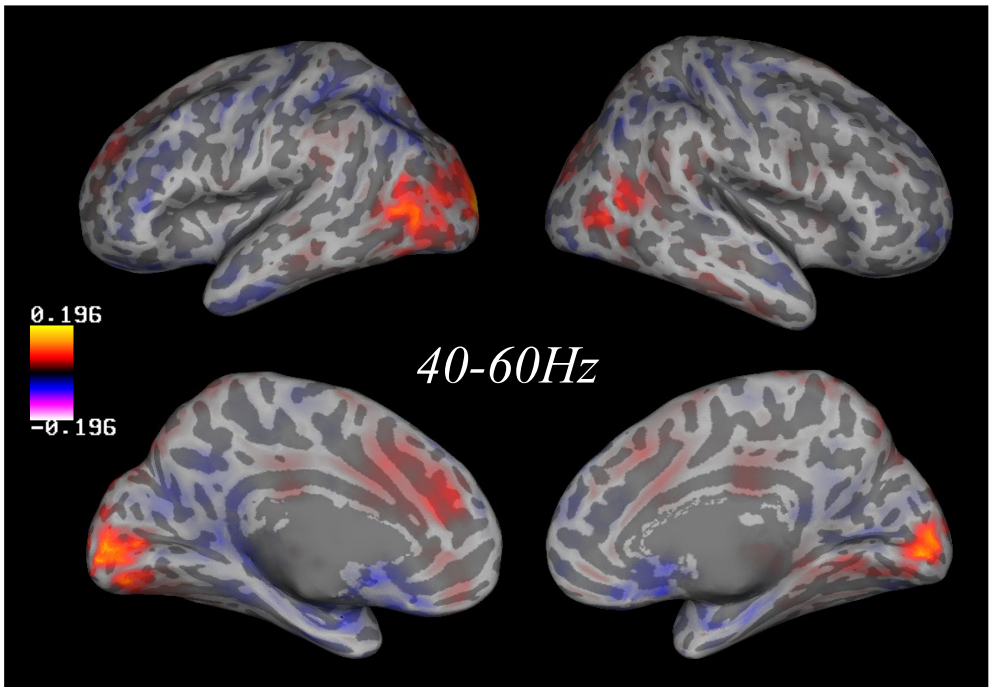

Figure 142. Low (40-60Hz) gamma frequencies show positive correlation with the BOLD timeseries in early and lateral occipital regions.

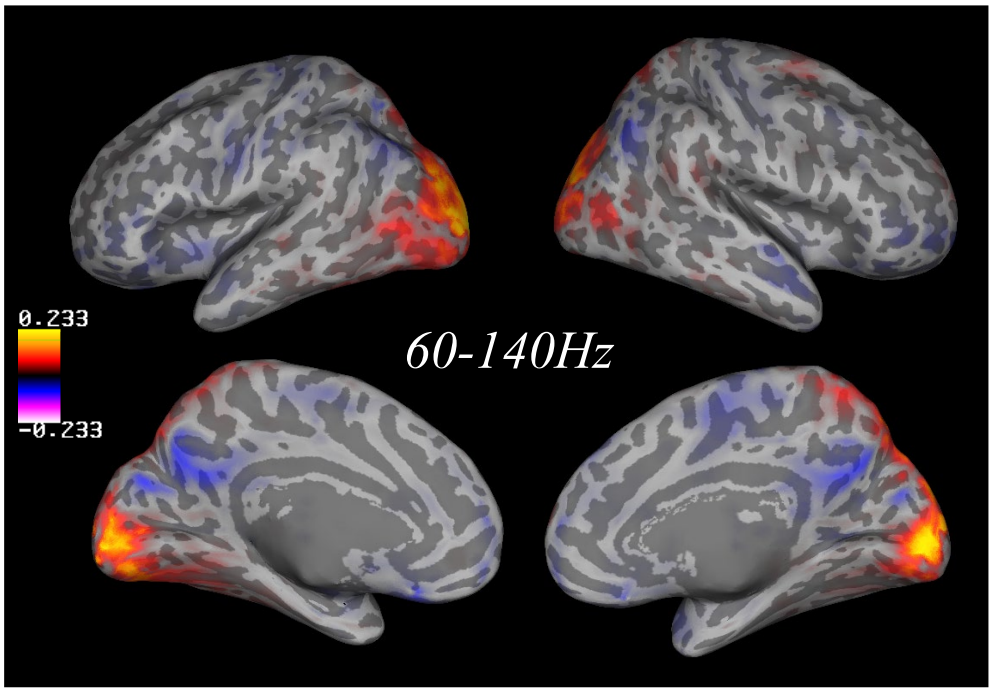

Figure 143. High (60-140Hz) gamma frequencies show positive correlation with the BOLD timeseries in early and lateral occipital regions.

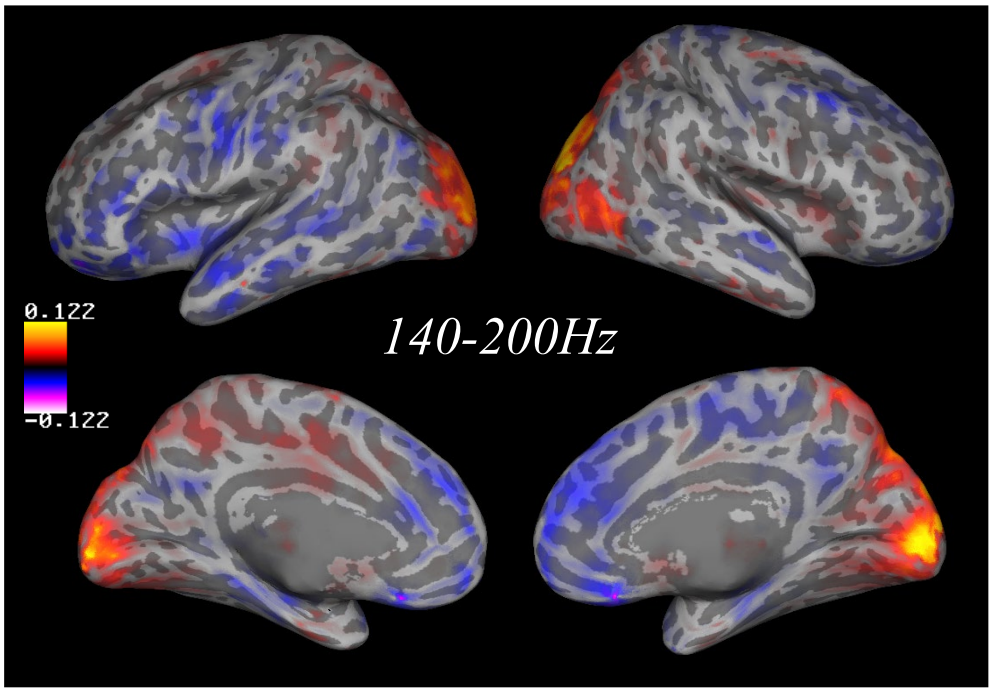

Figure 144. Even at high gamma frequencies a positive correlation with the BOLD timeseries can be seen at the occipital lobe.

It should be noted that using the mean timecourses will limit cross-frequency correlations to regions of cross-subject correlation found in the occipital lobe extending to parietal regions (see Chapter 7). Results demonstrate that cross-modality correlations differ dependent on which frequency band used. Points of interest were identified in the dorsal and ventral visual streams to closer inspect the relationship between the different frequency bands and the BOLD signal.

Cross modality correlation at point of interest

The correlation between the BOLD timeseries and each of the frequency bands was calculated at coordinates of interest in V1, V3A and MT+. The coordinates used matched those used in the previous chapter, where cross-frequency correlations were investigated. These coordinates were chosen as they represent motion sensitive regions expected to be active during the movie watching, and they also represent regions in the dorsal (V3A) and ventral (MT+) visual streams.

The pattern of cross-modality coupling was seen to differ across frequency bands and showed some differentiation across the visual regions. All three visually driven regions showed an anti-correlation between alpha and beta frequencies with the BOLD timeseries, though this was close to zero in V1 and lower in the motion sensitive regions (Figure 145). Low positive correlations are seen between the BOLD timeseries and delta and theta in V1. At both motion sensitive regions V3A and MT+, the correlation between BOLD with delta or theta was close to zero. All three regions showed positive correlation between the BOLD timeseries and gamma frequencies, peaking at 60-140Hz, supporting previous work (Logothetis et.al., 2001). This positive correlation was slightly lower at MT+ than in the other two regions.

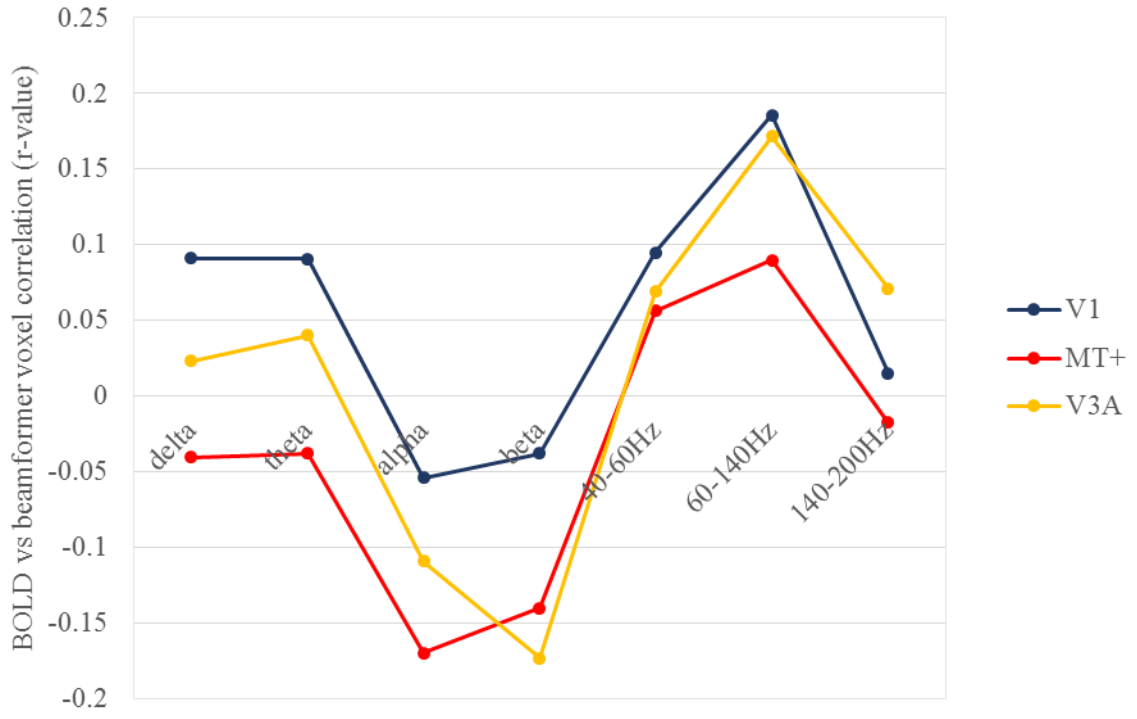

Figure 145. The correlation between the BOLD timeseries and each of the frequency bands at four points of interest in the brain. V1 MNI coordinates [12, -102, 6]; V3A MNI coordinates [20, -88, 22]; MT+ MNI coordinates [42, -72, 0]. All occipital regions show some positive correlation between gamma frequencies and the bold timeseries. V1 regions showed the highest correlation between BOLD and delta/theta frequencies. All visual regions showed negative correlation between alpha and beta with the BOLD timeseries (Mukamel et.al, 2005; see Figure 2, page 20).

These results support the exploration of a combined BOLD-beamformer TICA analysis as they show (a) different relationships between the BOLD signal with the different frequencies and (b) that these relationships alter across different visually driven regions. Next, I will examine whether the same source

signals identified using TICA with BOLD data can be used to describe the MEG beamformer voxel timeseries.

9.4 Correlation between fMRI component timeseries and MEG voxel timeseries

Having found different coupling relationships between the MEG frequencies and BOLD timeseries and within different visually driven regions, I next wanted to examine whether the source signals identified in BOLD only TICA could be correlated with the MEG timeseries. If correlations can be identified, it demonstrates that common source signals are driving the activity recorded across both of the techniques. Previous work by Mantini et.al., (2007) correlated fMRI component timeseries with MEG voxels using resting state networks (RSN). They took six RSN timeseries from a BOLD ICA output and correlated each with oscillatory brain activity in the delta, theta, alpha, beta and gamma bands. Each RSN showed a different pattern of correlation across the frequency bands (see Figure3, Mantini et.al.). By using a similar technique with visually driven component timeseries generated during movie watching, I also hope to find different patterns of coupling across the frequency bands. In the previous section of this chapter, BOLD in the primary visual cortex was found to be negatively correlated with low frequency oscillations and positively correlated with higher frequencies, supporting previous work in primary sensory areas (Mukamel, et.al., 2005). Based on these findings we expect to find this pattern using an fMRI component timeseries from the primary visual cortex. For the combined modality technique to be useful for differentiating coupling in different visual regions, this coupling pattern needs to show a change when we use component timeseries driven by other regions in the ventral or dorsal visual pathways.

9.4.1 Methods

Four components from visually driven regions were identified in the group fMRI TICA output (using data that had been grey matter masked and restricted at 70 components). The first component was located near the occipital pole with activity driven at the posterior primary visual cortex (Figure 146).

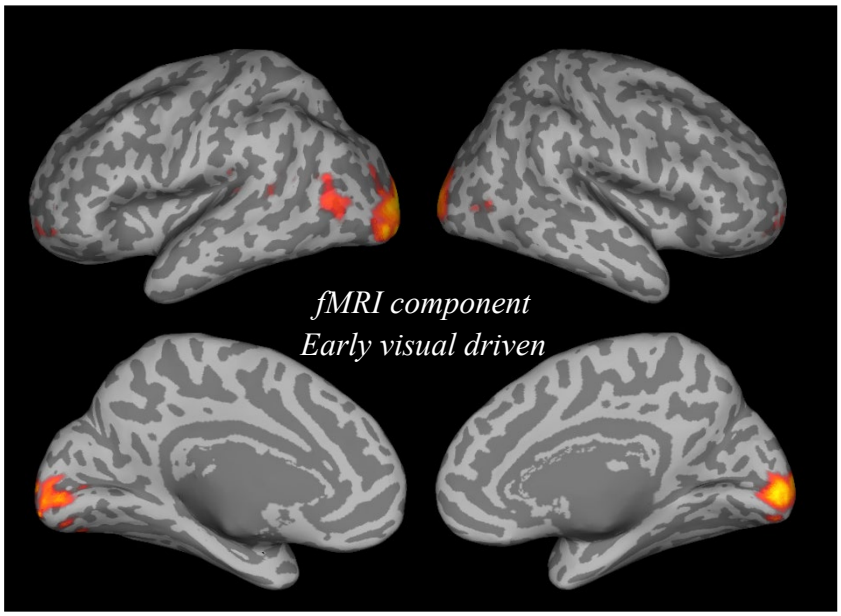

Figure 146. An fMRI component that covered the occipital pole and the posterior end of the calcarine sulcus was chosen for comparison between the unique component timeseries with the MEG beamformer at each voxel.

The second a bilateral component driven by MT+ regions and did not show activity elsewhere in the cortex (Figure 147).

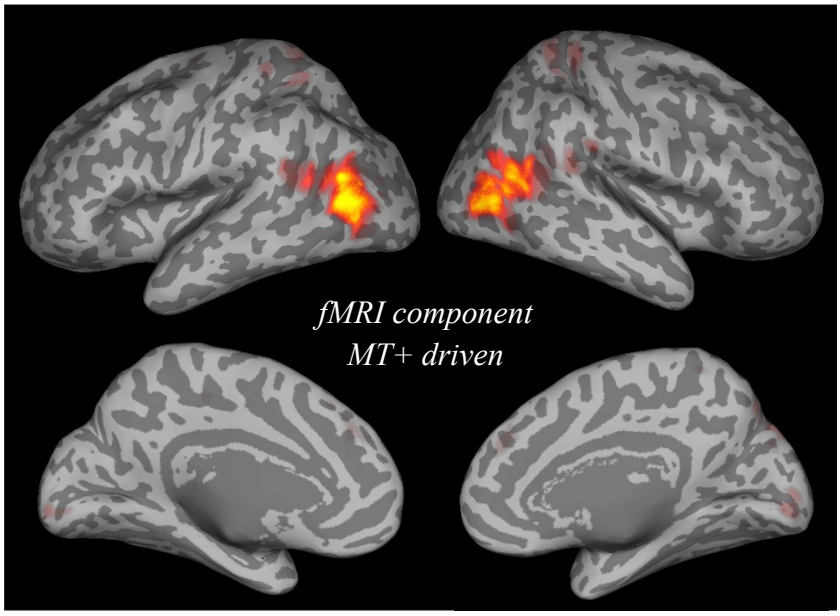

Figure 147. A second fMRI component chosen for a comparison between the timeseries and the beamformer at each voxel was located at MT+ regions, bilaterally.

The third component was driven by V3A and also showed activity at ventral occipital lobe at MT+ and V4.

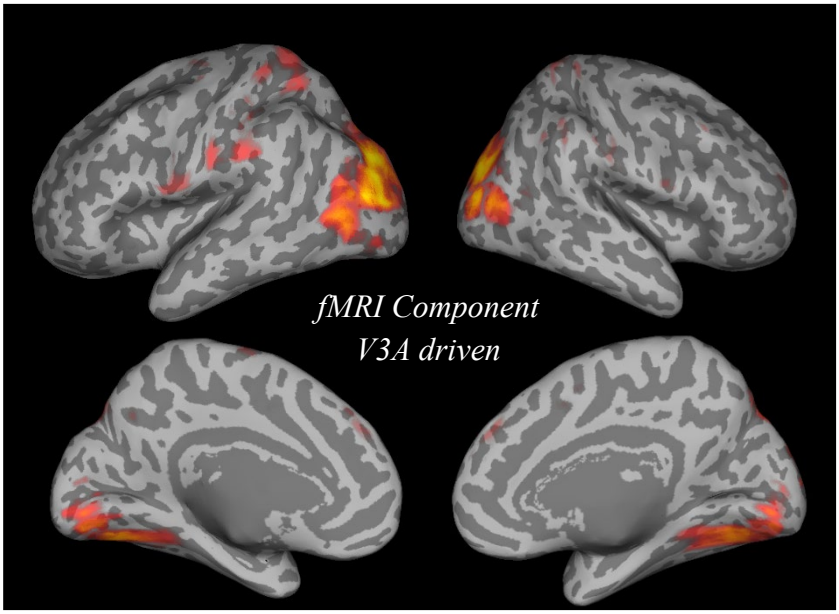

Figure 148. A component covering the dorsal region V3A, towards the IPS was chosen as the third component, for comparison with the beamformer timeseries at each voxel. Activitry peaked at V3A but also showed some coverage at lateral MT+ and ventrally at the fusiform gyrus.

Lastly, I used a component that represented activity driven by dorsal region V6, which has shown sensitivity to coherent motion (e.g. Cardin & Smith, 2009). This component had some associated activity at MT+, though this was lower than seen at the V6 region.

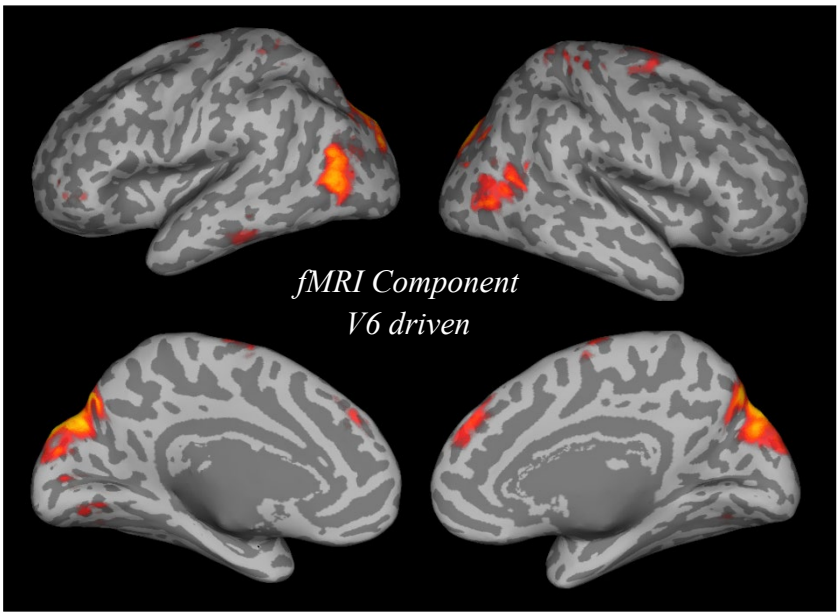

Figure 149. A fourth component was selected that had peak activity at dorsal region V6 (Cardin & Smith, 2009). As with the third component, some corresponding activity was also seen at MT+.

For each fMRI component, the timeseries was correlated with each voxel of oscillatory MEG data at seven frequency bands. This MEG voxel timeseries was a mean, averaged across all sixteen participants (the same sixteen participants whose BOLD data were used in the group ICA). The fMRI BOLD component was used as a weighted mask and the voxel correlations were averaged within this mask, for each frequency band. This provided me with a mean correlation value for each frequency band covering the same region as the fMRI component map.

9.4.2 Results

Component mask

The correlation results showed a similar pattern of coupling in the visually driven regions using the component timeseries as when using the BOLD voxel timeseries (Figure 150 and see previous section). This suggests that the same underlying signals identified using TICA with BOLD data also drive activity in MEG, where there are positive or negative correlations. V1 shows low positive correlations at delta and theta frequencies, while MT+ shows negative correlation. Both dorsally driven components show correlation values

close to zero. All visual regions demonstrate a negative relationship between the TICA timeseries and alpha/beta bands. This supports the assertion that the same underlying signal, driven by features in the movie stimulus, are also driving the activity in some of the BOLD frequency bands. This is closest to zero at the primary visual cortex, while other regions show a larger negative correlation. All visual regions show a positive correlation with the gamma ranges.

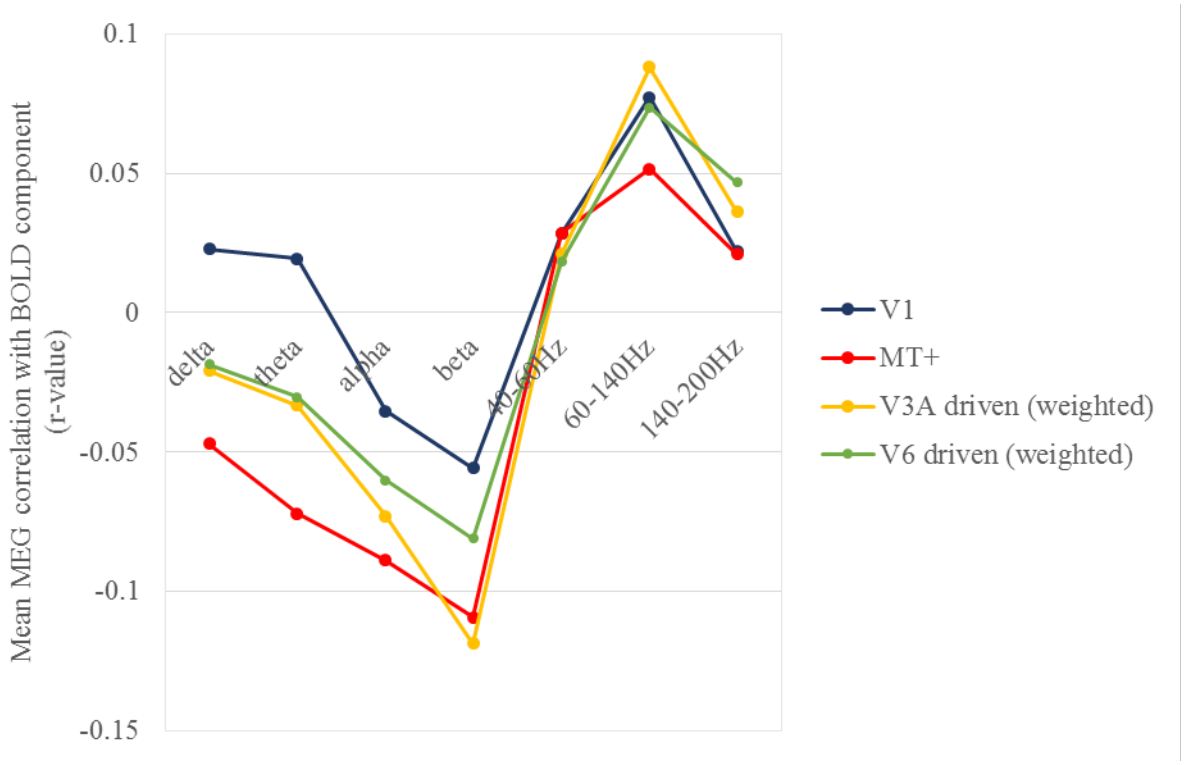

Figure 150. The mean correlation of Beamformer timeseries with four BOLD TICA component timeseries, averaged within the spatial mask of each component. Positive and negative correlations indicate that the same underlying signal is also influencing the frequency band activity.

These results support the use of a combined BOLD – Beamformer TICA, as they suggest that the same underlying signals driven by the movie stimulus are captured by both modalities.

9.5 Combined BOLD and single band TICA

The aim of the previous sections was to clarify whether MEG beamformer data and fMRI BOLD data may be appropriate for combination in a TICA analysis. The differentiation of the relationship between BOLD and the oscillatory frequencies and between different visual areas indicate that a combined modality TICA

may be successful. If a TICA can identify correlated activity across the modalities this would be an exciting new tool that could utilize the strengths of both techniques for understanding neural activity during natural viewing. To get a full picture of neural activity across BOLD and oscillatory activity, entering all of the frequencies with the BOLD data would be necessary. As an intermediate step I tried single band with BOLD merged modality TICA.

9.5.1 Methods

BOLD and beamformer timeseries data were normalized around zero and scaled across the modalities. Data were then combined spatially (along the x-axis). The combined data were entered into sixteen group TICA analyses, permutated so a different first brain was used for each. The most reliable output was identified for each of the frequency bands by cross correlating the spatio-temporal similarity of components in each of the outputs (as described in Chapter 2).

9.5.2 Results

Cross-modality outputs using single MEG bands produced reliable components with activity in both MRI and MEG brains, at each of the frequencies. Across all frequency band and MRI pairings there were up to five components with cross- modality activity in the first ten components. The components generated using delta or very high gamma (140-200Hz) did not produce cross-modality components based in visually responsive or attentional regions. The components using these bands showing cross-modality activation were noise elements (CSF and white matter). This reflects the reduced correlation between the MRI BOLD signal and these bands, compared to other frequencies (see Figure 145).

The pattern of activity in cross-modality components using the other frequencies (bands between 3-140Hz) showed cross-modality synchronization in visually driven regions. Positive correlations were generated as components in visual regions, for theta with BOLD and for gamma (40-60Hz and 60-140Hz) with BOLD. This supports the findings in sections 9.3 and 9.4. Alpha and beta showed anti-phase activity in early and lateral visually driven regions, also as predicted. These results support the use of a multi-band and BOLD combined TICA analysis. Based on these findings, in the next section I will present the initial results of a cross-modality multi-band TICA.

9.6 Combined BOLD and multi-band TICA

In the previous section I found that cross-modality components could be identified using a combined TICA with single frequency bands theta (3-8Hz), alpha (8-13Hz), beta (13-30Hz), or gamma (40-140Hz) and BOLD data. It would be useful to apply this technique across all the frequency bands and BOLD data to try to find interesting cross-modality and cross-frequency components. Therefore, I tested the technique using spatially concatenated BOLD with multiple MEG frequencies.

9.6.1 Methods

Based on the promising results in the single-band and BOLD TICA, normalized and scaled BOLD and beamformer timeseries data were used in the multi-band analysis. Ten-minute movie clips were used to reduce the computational demand (visually driven components can still be using a shorter length movie clip, see Chapter 2 and Chapter 8). All the frequency bands were combined spatially along the x-axis. For each frequency band the dataset consisted of a 4D dataset of dimensions (X, Y, Z, *t*) = [37 x 31 x 37 x 1200], the BOLD data were resampled to the same size (resolution $6mm^3$, TR=0.5). These 8 datasets were concatenated along the x-axis, creating a single dataset of size [296 x 31 x 37 x 1200].

The combined data were entered into sixteen group TICA analyses, permutated so a different first brain was used for each. TICA analyses were run at dimensionality 70 as the results in Chapter 8 demonstrated that using merged frequency technique increased the size of the components. As expected, output components represented large networks, covering multiple visual regions. As a first pass, the first ten components were examined, and three components showed cross-modality correlations. These components are discussed below.

9.6.2 Results

Four components in the top ten revealed cross-modality correlations. Other components were cross-frequency components (i.e. no BOLD correlation in thresholded spatial maps) displaying the same patterns described in Chapter 8 (namely: theta-gamma correlations, alpha-beta correlations and beta-gamma anti-correlations). In visually responsive regions two of the cross-modality outputs demonstrated a positive correlation with theta and gamma. A third component showed the gamma-beta seesaw pattern presented in the merged frequency output (Chapter 8, section 8.3.1, page 195), in early visual regions. BOLD showed

correlations with gamma at the same locations and into lateral occipital regions. A fourth component showed a more complex activation pattern. Regions of correlation and anti-correlation between gamma, beta and BOLD were seen in visually responsive areas. In this results section I present these four components.

1. Theta – Gamma and BOLD

The first cross-modality component showed BOLD activity correlated with theta and gamma in early visual regions (displayed on brain's surface in Figure 151). Activity in the early visual regions was present at delta and alpha bands (though was strongest in theta) and in gamma ranges 40-60Hz and 140-200Hz (but was strongest in the mid-range, 60-140Hz; see Appendix 9.1a for full output).

The activity in this component supports the findings in the previous sections and demonstrates that a merged modality TICA can pull out these relationships. It supports work by Whittingstall and Logothetis (2009) who showed a coupling between lower and higher frequencies during movie watching, which correlated with population spiking activity.

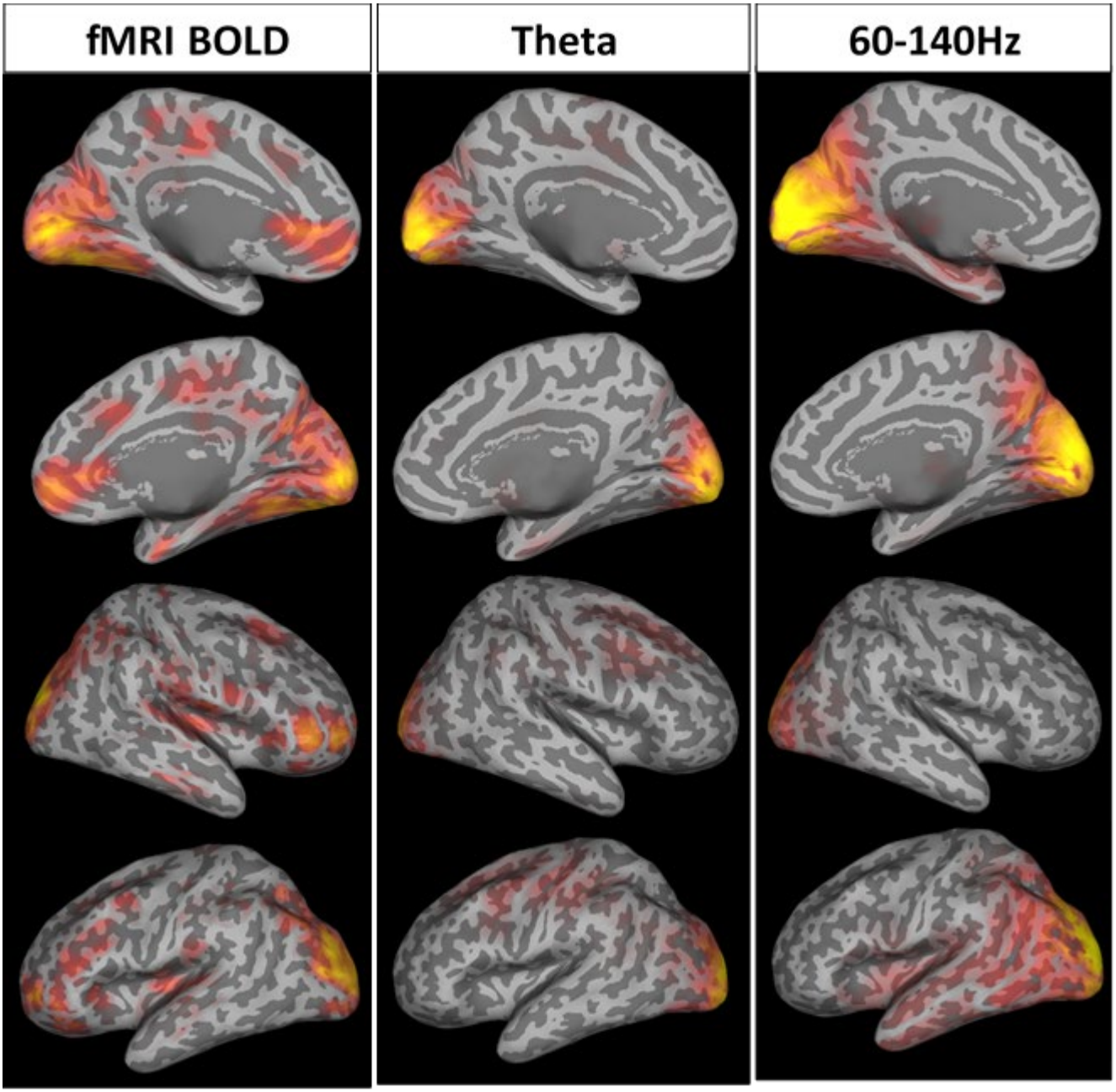

Figure 151. A component showing cross-modality activation showed correlated activity in the occipital lobe in BOLD signal, theta and gamma (60-140Hz). Some associated activity is also seen in frontal regions, in the BOLD signal.

The second component also showed correlations between gamma, theta and the BOLD signal in occipital and regions (see activity on brain surface in Figure 152). Bold signal in the lateral occipital lobe was correlated with theta and gamma in the primary cortex. Activity in the gamma range was also synchronized into medial parietal regions.

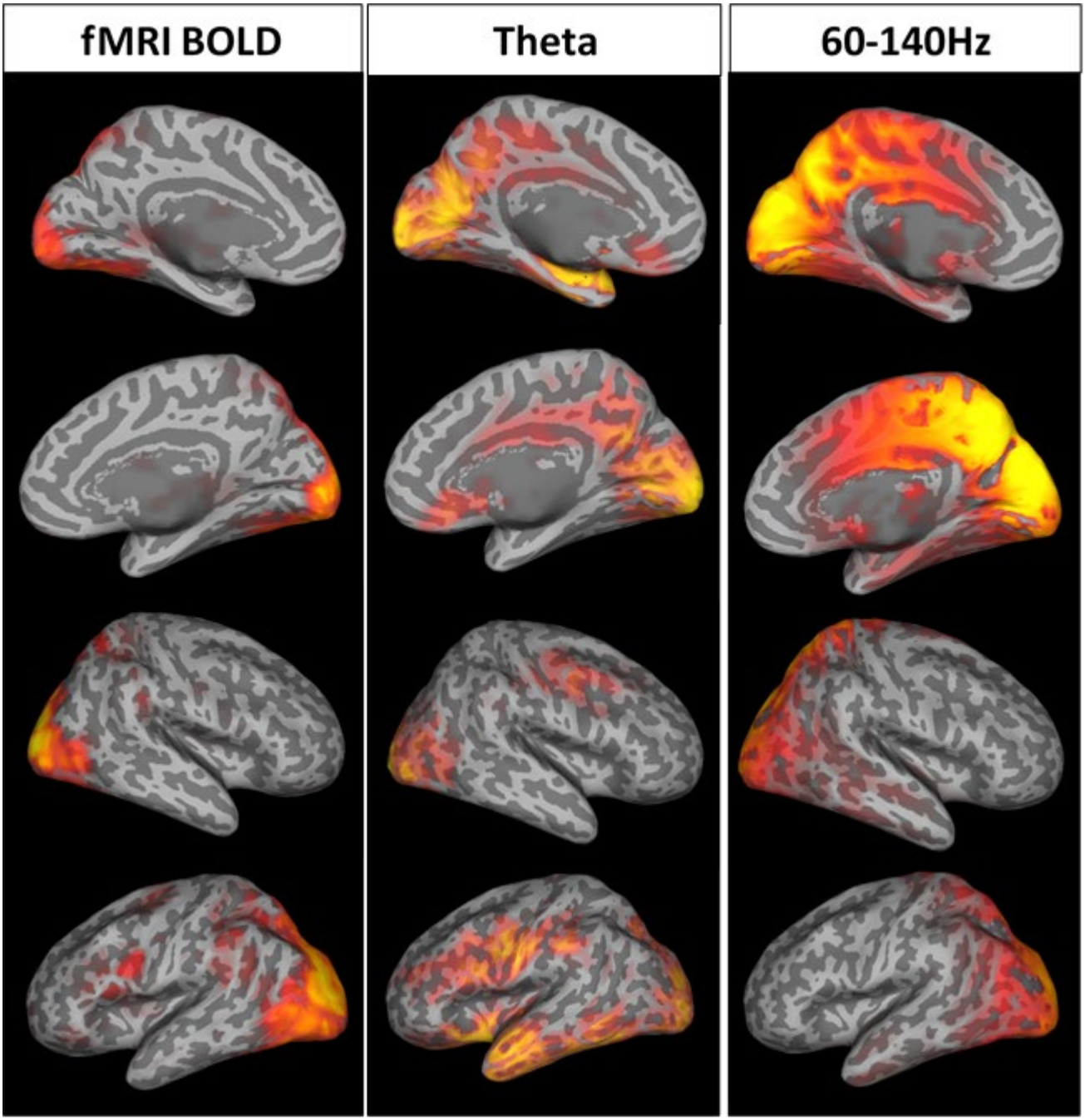

Figure 152. A second cross-modality component showed gamma and BOLD correlation in the occipital cortex. This component also showed small amounts of activity in other frequency bands (see Appendix 9.2b).

Unlike the first component, synchronized activity in other frequency bands was distributed outside of the occipital lobe. Delta showed correlation at the medial parietal lobe and right temporal lobe, while high gamma (140-200Hz) was synchronized in the right central sulcus (see Appendix 9.2b for full output).

My cross-frequency correlation analyses showed a positive correlation between theta and the BOLD at V1, but not in motion sensitive areas MT+ and V3A, supporting the findings of these two components (section 9.3.2).

2. Beta – Gamma and BOLD

In the merged bands (MEG only) TICA results, (Chapter 8, section 8.3.1, page 195) I found that a beta-gamma seesaw pattern was present in the component data; activity cross-frequency components showed anti-correlation between gamma and beta. There were not components with gamma-beta positive correlation. Two of the four cross-modality components also showed this pattern, with BOLD correlated with the gamma response, in visually driven regions.

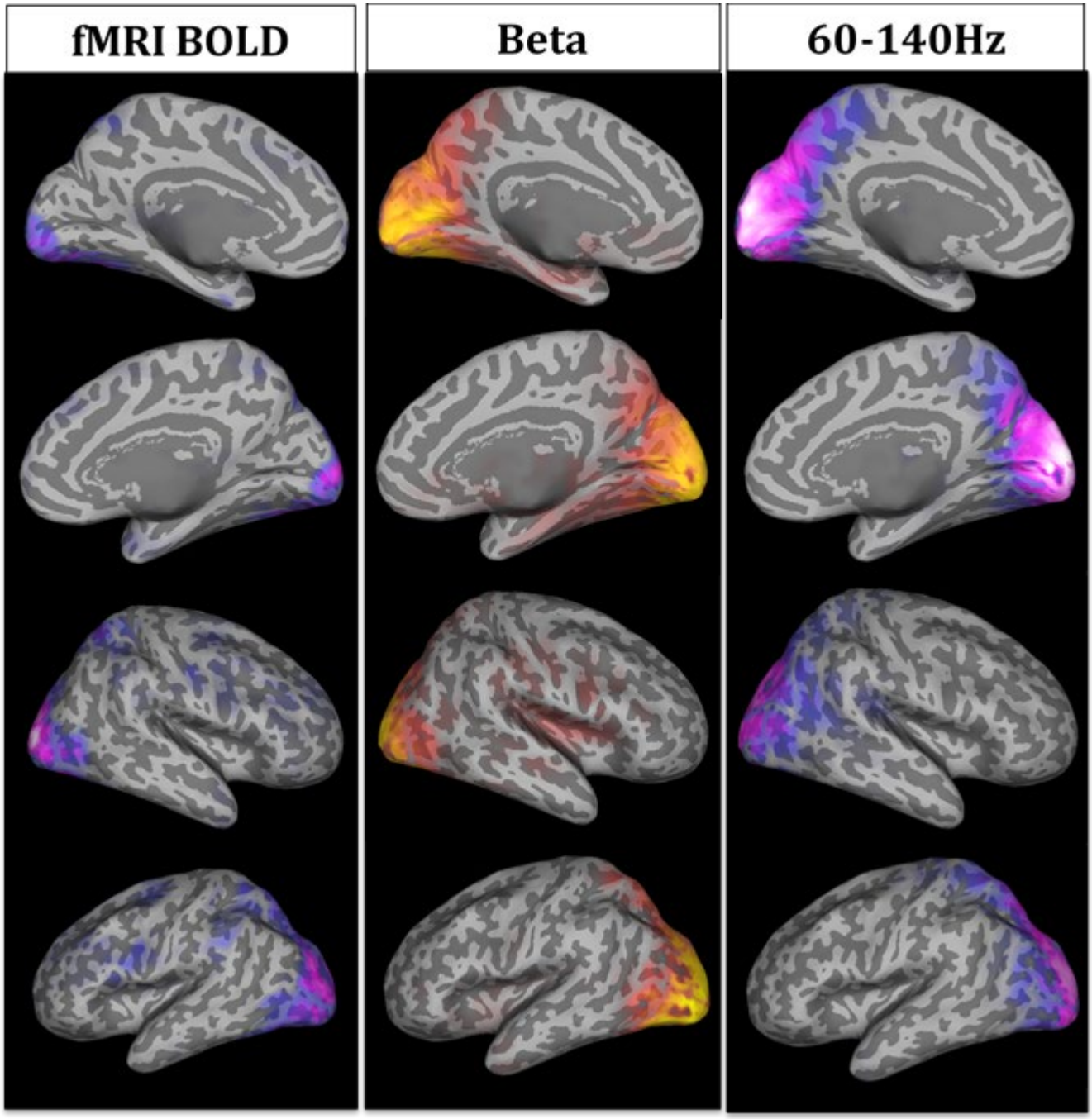

Figure 153. Beta and gamma were anticorrelated in early visual regions and lateral occipital areas. The BOLD signal showed positive synchronization with the gamma range at lateral occipital areas but not at the early visual regions.

The second beta-gamma seesaw component also showed anti-correlation between beta and gamma timeseries. In this component anticorrelated activity in was at parietal regions and did not cover the same areas across the bands; beta activity in medial-dorsal parietal lobe was anti-correlated with gamma at the lateral parietal lobe. The BOLD timeseries in the dorsal-medial parietal lobe was also anti-correlated with bold. Interestingly there was also some above threshold positive correspondence between beta in the medial

parietal regions and BOLD at the cuneus (see Appendix 9.1d for the full TICA component output). My voxelwise correlation between beta and BOLD demonstrated a positive correlation at this location (section 9.3.2), though in the component the positive activation does not overlap between BOLD and beta.

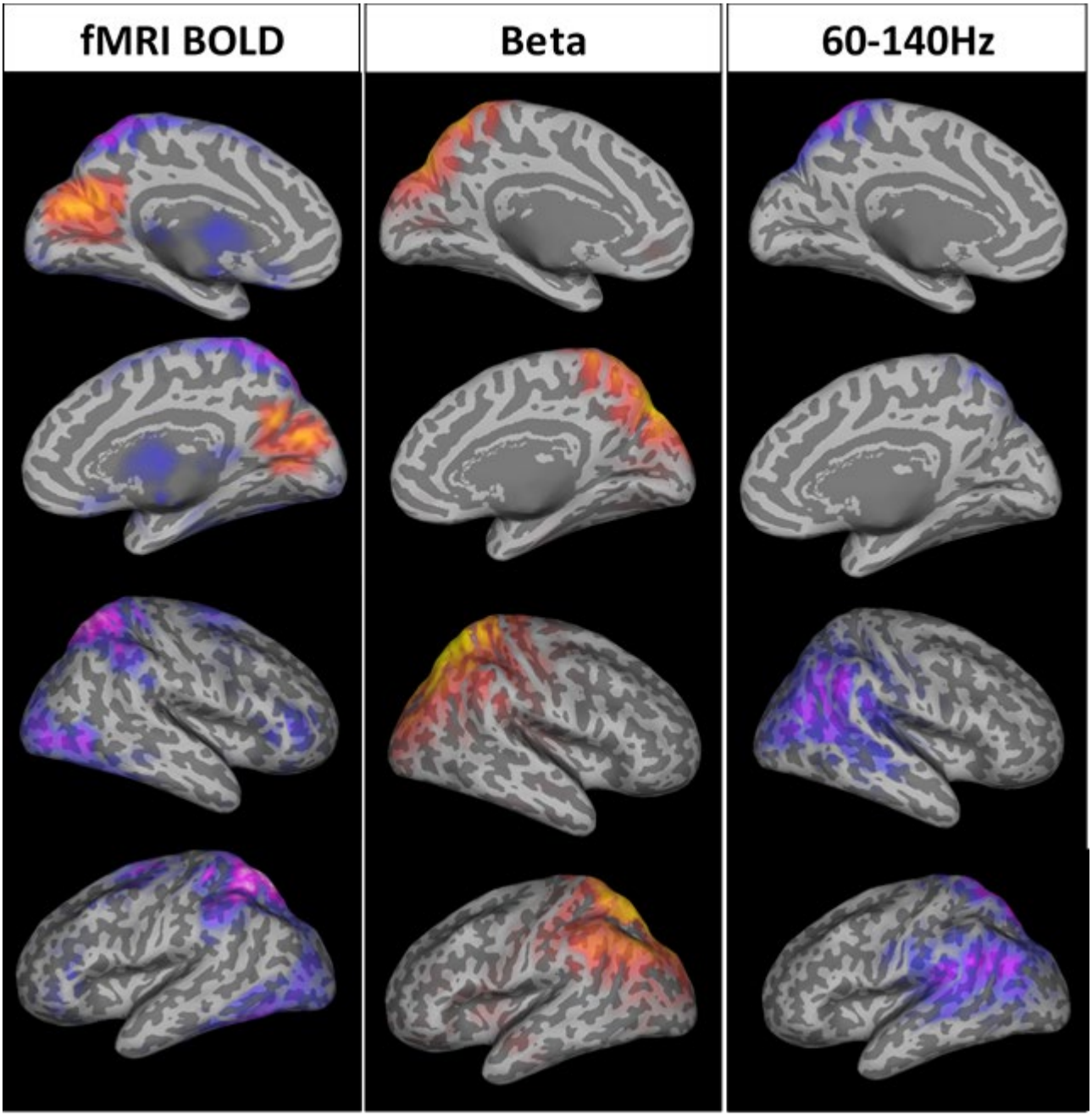

Figure 154. A fourth cross-modality component showed anti-correlated activity between gamma and beta in parietal regions. Medial-dorsal activity in beta was antic-correlated with gamma activity in more lateral parietal regions. BOLD also showed anti-correlation with beta at the dorsal parietal lobe, but also in inferior lateral occipital regions.

9.7 Summary: Chapter 9

In this chapter I aimed to establish whether BOLD and MEG data collected during movie watching would be potentially useful in a combined-modality TICA. The results of voxel-by-voxel correlations showed different relationships between BOLD and the frequency bands and suggested that regions of interest may be differentiated based on these relationships. Based on successful single-band and BOLD combined TICA outputs, I ran a multi-band combined modality TICA. The results show that multi-frequency cross-modality components can be identified using a TICA. This technique is an exciting and novel way to investigate the relationship between oscillatory activity and the BOLD signal. Combining the two modalities is useful for exploitation of MEG's higher temporal resolution, and fMRI's higher spatial resolution.

Chapter 10: Investigating neural hierarchies by changing ICA dimensionality

10.1 Introduction

In this thesis, I have demonstrated that visual regions and networks of interest can be reliably identified using data collected by MEG or fMRI during movie watching and segmented using ICA. In Chapter 5, I showed that at the group level components change as the dimensionality is altered, becoming smaller and representing sub-regions of the original component. In Chapter 6, I used single subject data and found that at lower dimensionalities functional networks are identified; at higher dimensionalities, although functional networks are still represented, components are also generated that identify sub-regions of interest in the visual processing pathways (e.g. central field and peripheral field processing, MT+, V3A, V4). In Chapters 7-9, I cofirmed the feasibility and usefulness of a novel technique for combining and comparing the BOLD and MEG signals recorded during the same task. Depending on the dimensionality of the combined ICA, different cross frequency and cross-modality components could be identified.

In this final chapter, I will explore the use of changing dimensionality for investigation of the hierarchy of the visual networks. This will focus on the merging and splitting of components across dimensionalities. As dimensionality is increased, functional activity is delineated into smaller parts, as more underlying source signals are incorporated into the output and components must 'split' to represent the different spatial basis of these source signals. Previous work has supported the view that as the dimensionality of ICA outputs increases, components can be identified as 'splitting' into sub-components. Smith et.al. (2009) measured 'splitting' by correlating the spatial maps of components at 20 and 70 dimensionalities and finding matches across the dimensionalities. Using this matching technique, they found multiple components at the higher dimensionality that showed significant spatial correlation with components at the lower dimensionality, in line with the findings presented in Chapters 5 and 6.

The pattern or order of splitting may provide insight into the hierarchy of the visual or attentional neural system. Regions that are the least functionally connected within a network are likely to 'split' and form separate components before other sub-regions. For example, a motion processing network

may include early visual regions, MT+, V3A and some parietal areas. The region with most independence from this network will be represented as a separate component before other regions, as dimensionality is increased. Neural regions that split/appear at a lower dimensionality show less similarity in function than regions that stay paired within a network until a higher dimensionality.

In this chapter I will explore the usefulness of examining the splitting pattern of components across dimensionalities for understanding functional hierarchy. Resting state studies usually restrict analyses to a dimensionality of ~20-30 to identify resting state networks in individuals (Bijsterbosch, Smith & Beckmann, 2017). Using a movie twenty-minute movie clip, I have found that ~200 components were identified using an unrestricted MELODIC single subject analysis (see Chapter 1 section for description of how dimensionality is estimated by MELODIC; see Beckmann & Smith, 2004). This is due to a) an engaging movie allowing for increase in length of a scan and hence the amount of data b) identification of functional sub-regions of networks due to an increase in the signal compared to noise and c) a movie is a rich stimulus, which should stimulate all the regions responsive during natural viewing, but each with a different timecourse (Bartels & Zeki, 2004). The range of dimensionalities available using a movie provides an opportunity for gaining insight into the hierarchy of visual functional networks (based on the image statistics of the movie).

Other standard techniques for investigating functional hierarchies include correlating component timeseries (e.g. Bartels & Zeki, 2004; FSLNets, Woolrich et.al., 2009) to find correlations (and/or partial correlations) between components. The strength of a correlation between the component timeseries is used to infer the functional connection between the regions identified by the ICA. There are a number of potential issues with this approach. One downside is that correlations are between components from the same ICA output which means the functional units are set based on the dimensionality chosen. Based on what I have shown in this thesis, we might expect that this set is somewhat arbitrary. The functional hierarchy *between* these component units can be inferred from the correlation values, however if multiple visual regions are represented in a single component any functional hierarchy *within* these networks remains unknown. This technique also means that intermediate components are inferred using the correlation statistics rather than observed directly.

Based on the findings in the previous chapter, I was interested in how the components split and changed across the intermediate dimensionalities. The aim of this chapter is to explore the use of splitting patterns to understand the hierarchy of functional visual networks during passive natural viewing. Before I can do that, I need to understand how stable components are across dimensionalities, by mapping components that are most similar as dimensionality is changed. In this chapter I use MATLAB's *'treeplot*' function to visualise how components merge and split across dimensionalities. These were exploratory steps and as a first stage, the results show some promise. I then compare the merging and splitting of regions of interest across ten subjects. Results show some variation across subjects. With development the technique could exploit the ICA process to offer a more in-depth picture of how networks and hierarchies change with task demands and/or stimuli.

10.2 Tracking components across dimensionalities: a case study

10.2.1 Methods

ICA was performed for four subjects at increasing dimensionalities from 20 to 200 (in steps of 4), producing a total of 46 ICA outputs. Signal components at visually driven regions were identified by eye for the subjects at dimensionality 200. Once these components of interest had been identified they were compared with each of the components in the dimensionality below (dimensionality 196). First the spatial correlation was calculated between the component of interest and the 196 components using FSL's '*fslcc'* command (provides a Pearson's r value). Then the peak voxel of the top five spatial matches was compared to the seed component. As components at lower dimensionalities were bilateral, and components at higher dimensionalities were splitting into lateralised parts, peak voxels were useful to help match these components to the correct hemisphere. The component that had the closest peak voxel was identified as the 'best match'. Matches were found iteratively through the dimensionalities using this technique, to track the component.

As an exploratory methodological step for the visualization of the merging and splitting, the matched components across dimensionalities were used to create trees representing the merging/splitting of visually driven components (using MATLAB's '*treeplot'* function). An example of the type of tree produced is presented in Figure 155. I wanted to see how stable components were across dimensionalities, and whether the

technique would be appropriate for visualizing the hierarchy of functional networks at the individual level. In this chapter I will report a single subject as a case study and see what I find as I vary the dimensionality.

10.2.2 Results

At higher dimensionalities matched components covered smaller regions of the networks identified at the lower dimensionality (see Chapter 5). The tree for the case study subject is seen in Figure 155. This subject had ten occipital components identified in the highest dimensionality. A pattern of functional splitting can be observed when components of interest are matched across the dimensionalities. The order of splitting for this component is displayed below (Figure 155).

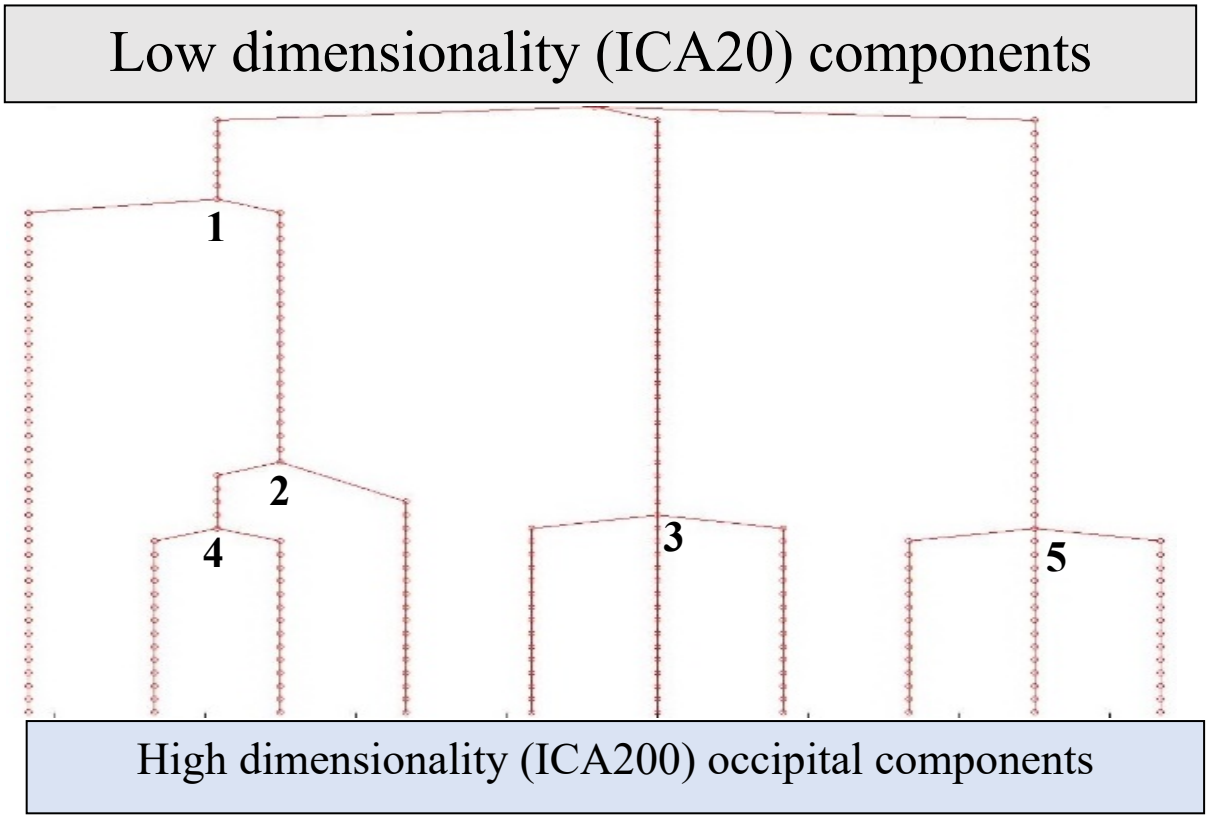

Figure 155. The splitting of components from ICA20 to a high dimensionality (ICA200). The best match for each component was identified based on spatio-temporal features. The splitting of components shows a hierarchy in the visual system with regions identified in previous research as having specialized functionality (1) and (2). Earlier visual regions show splitting later in the dimensionalities (e.g. 3).

The numbers below correspond to splitting branches in the tree presented in Figure 155:

1. Fusiform regions split from posterior and lateral occipital component (Figure 156).

2. V4 splits from early visual regions (Figure 157).

3. A dorsal visual network including V3A and early visual regions splits into three components showing different weightings across the network (ventral, V3A and LOC; Figure 158).
4. A component at the primary visual cortex splits into two. One lies dorsally and the other runs along the calcarine sulcus (Figure 157).
5. A component spanning the occipital lobe splits into three components; two in the primary visual cortex and another at MT+ (Figure 159).

In the following pages I will illustrate the components splitting off, based on this tree (Figure 155). In this observer, the earliest component to split from the seed networks is a ventral occipital component covering the fusiform face area and other lateral regions (see Figure 156). This suggests that in this subject's data these regions are more functionally distinct from early visual regions than other extra-striate regions such as MT+ or occipital-parietal visual areas. The finding in this participant supports research showing clear functional specialization of this region (Kanwisher, McDermott & Chun, 1997).

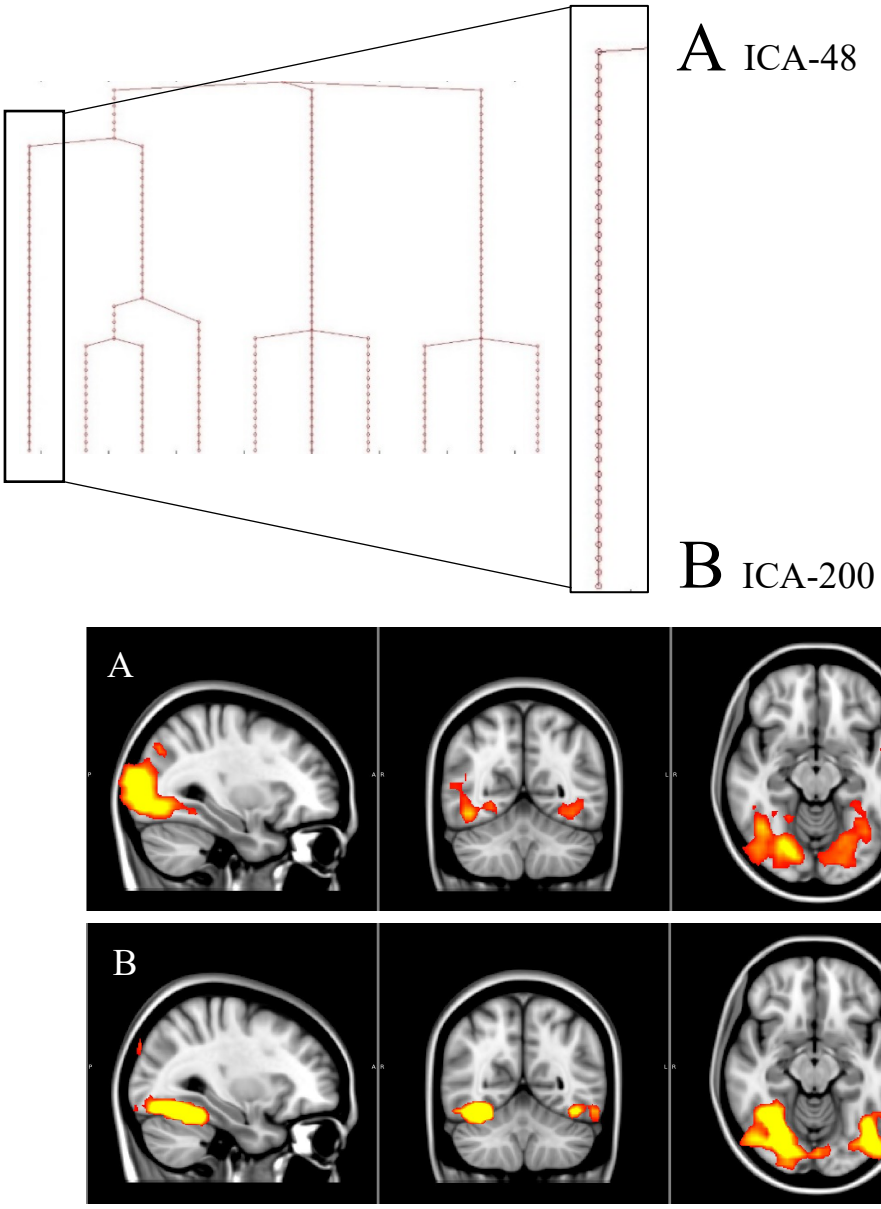

Figure 156. A large inferior occipital component splits early and remains stable across dimensionalities.

Next to split in this case study was a medial occipital component splitting into smaller regions representing two early visual regions (Figure 157A and B) and V4 (Figure 157C). The V4 component splits off first, suggesting it is more functionally distinct that the two early visual regions. This is expected as region V4 has been reported as higher in the visual hierarchy, processing features such as colour, texture and some types of motion (Norman, Heywood & Kentridge, 2017; Bannert & Bartels, 2018; Mikellidou et.al., 2018). The two early visual regions sit in the dorsal and central medial occipital lobe, respectively. In this subject there is not a clear separation between peripheral and central visual fields, as was reported in some individuals

in Chapter 6 and found averaging across subjects. This could be due to individual differences or noise in the signal.

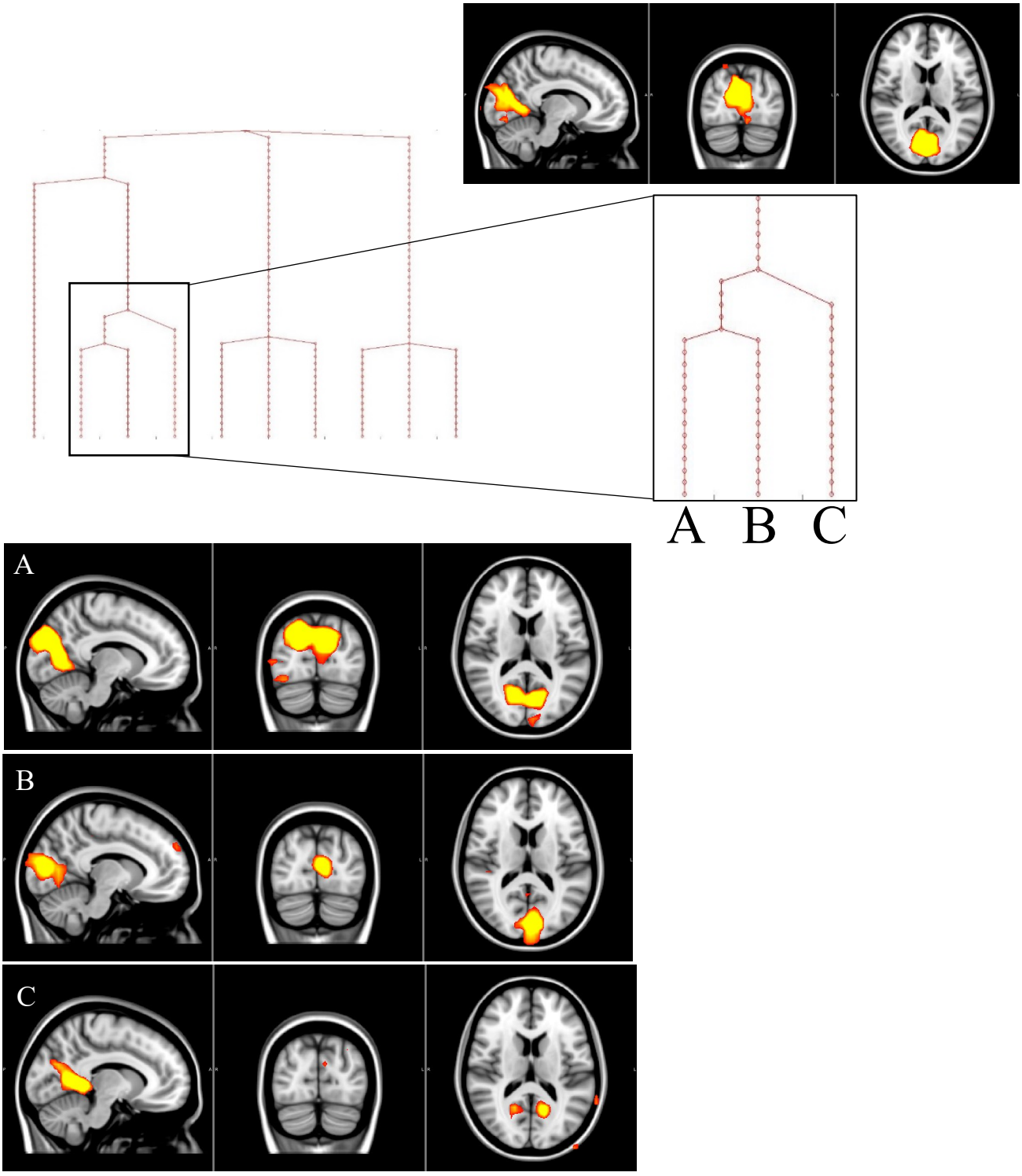

Figure 157. An early visual medial component was identified at ICA dimensionality 108. This was observed to split into three medial occipital components that represent distinct aspects of the early visual system. (A) lies at the superior occipital lobe. (B) lies at the calcarine sulcus and (C) shows activation at V4 and extends dorsally past the calcarine sulcus.

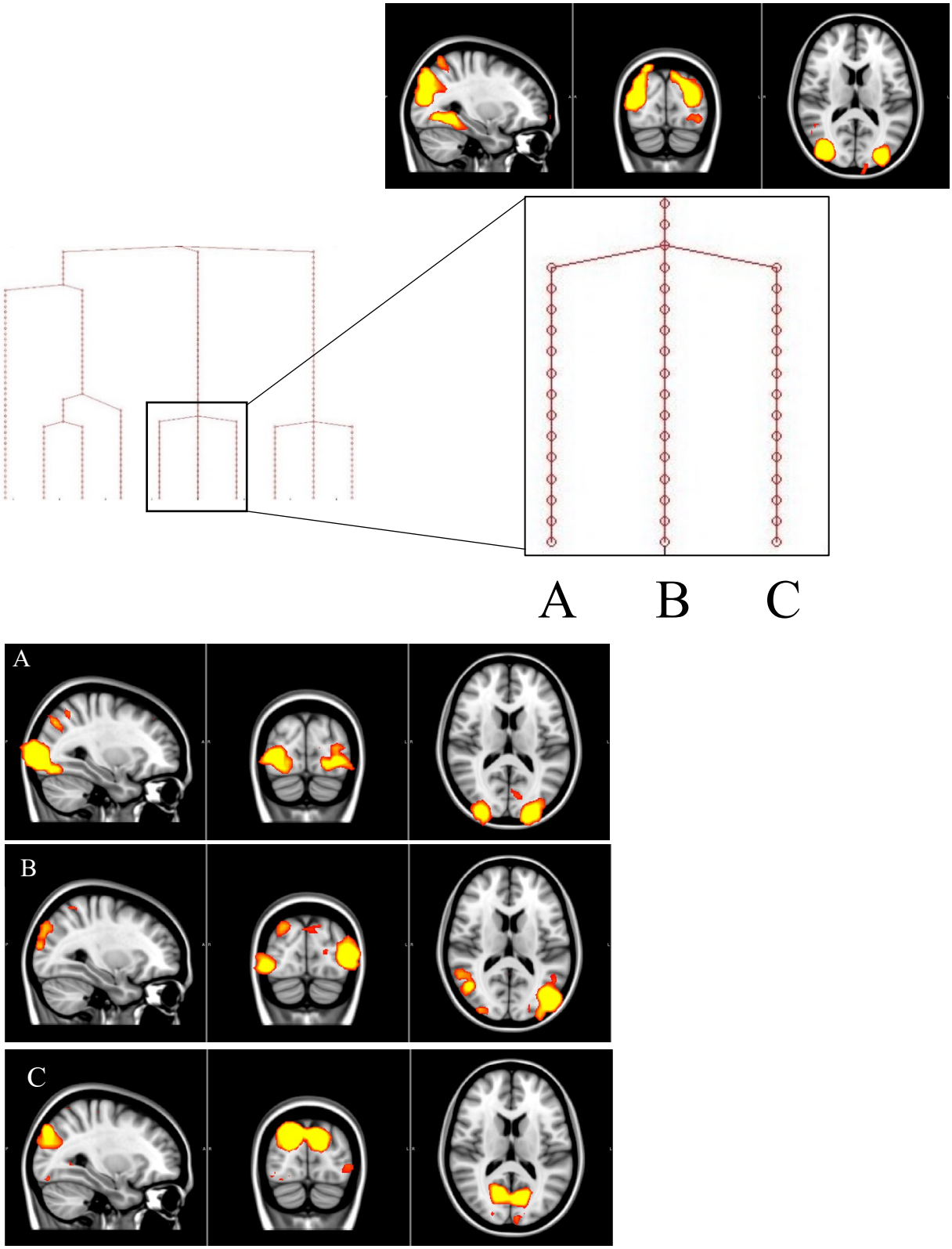

Figure 158. A network component at dimensionality 140 shows activation at V3A. lateral occipital and inferior occipital regions. This component splits into three components, representing smaller regions within the network as separate components (A-C).

In this example subject, the component splits demonstrate relatively high functional connection between early visual regions and V3A (Figure 158) and MT+ (Figure 159), shown to respond strongly to motion across the visual field. A network component covering V3A and some ventral occipital regions shows splitting into separate components representing different regions of the network (Figure 158). Interestingly, these components also showed remnants of activation at the rest of the functional network. The components represent areas in the inferior occipital cortex, V3A and LOC (potentially region MT+).

Another component lying at the lateral and posterior occipital lobe also splits into medial occipital regions in the primary visual cortex, and lateral regions representing the bilateral MT+ (Figure 7). The MT+ component (C) has very little overlap with the seed component, therefore these components must have been matched based on below threshold spatial information (as unthresholded maps were used for comparison).

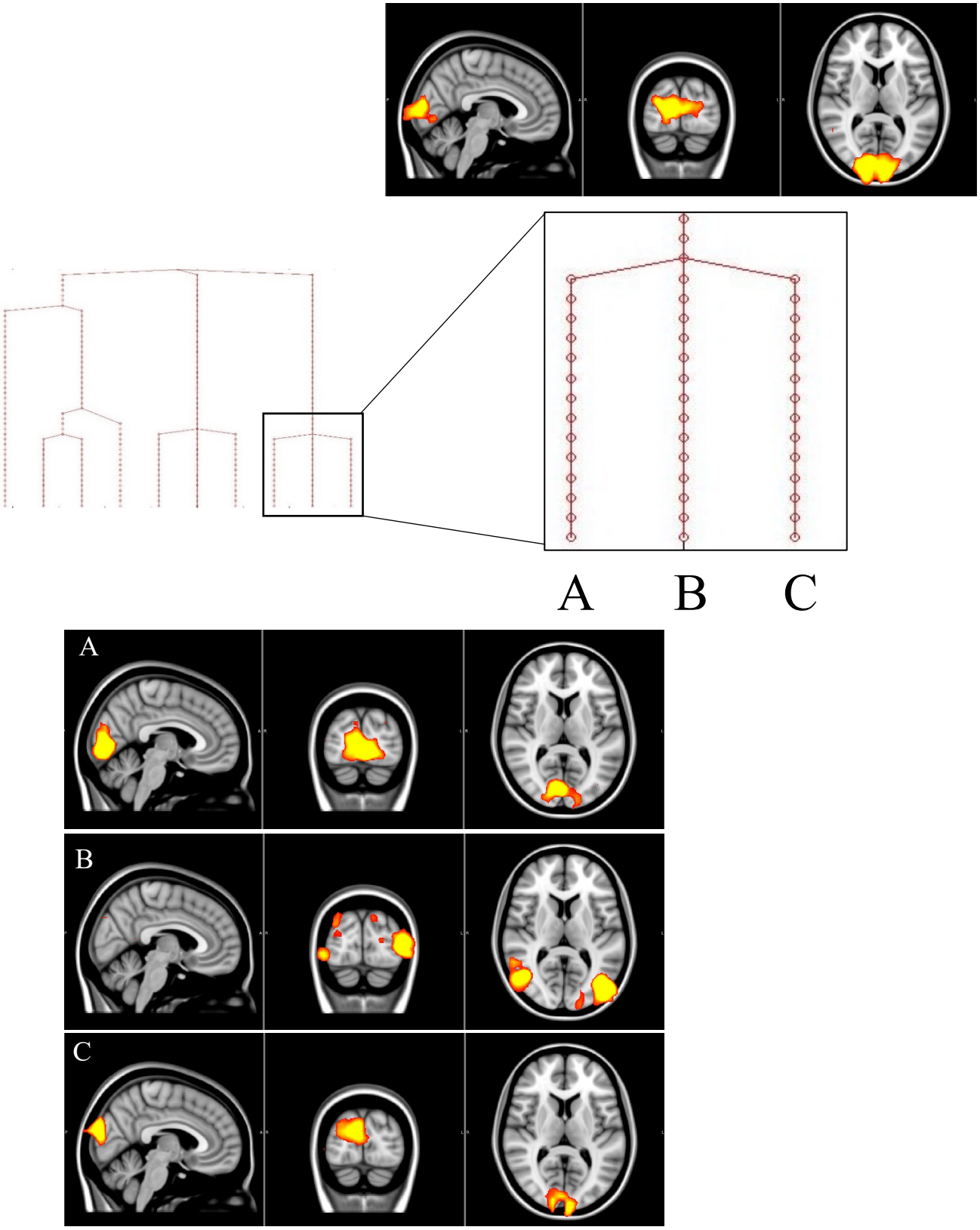

Figure 159. Early visual regions and MT+ components show splitting at higher dimensionalities (here A-C split at dimensionality 148), suggesting that these regions are relatively highly correlated in their functionality.

10.2.3 Discussion: Case study

One improvement that could be applied to this technique would be to identify stable seed components in a participant, rather than choosing components from the 200-dimensionality output. This is based on the finding that components jostle and oscillate across dimensionalities. For example, components chosen at dimensionality 200 may not be as stable or representative across dimensionalities as representing visual areas of interest, as those at a dimensionality of 188 or 202, for example. To develop this work stable components could be identified across the high dimensionalities (e.g. 180 – 220) and used as seed components.

Plotting the trees provides a nice way to examine how components change across TICA dimensionalities at the individual level. This technique could be extended to investigate the functional hierarchy using average components across subjects, as this may provide a more robust result. This technique could also be improved by using masked data to reduce noise caused by signal originating from CSF and white-matter (see Chapter 2).

10.3 How do the components merge and split across dimensionalities?

Having had an exploratory look at the merging/splitting trees generated using individual subjects. The question now is how consistent the pattern of components merging is across subjects. To address this question, I selected set of visually driven regions (V3A, V4 etc) and looked to see if or when they split or merge across a sample of observers. Results presented below demonstrate some consistency across subjects, but also some differences.

10.3.1 Methods

BOLD fMRI data were collected for each participant, as described in Chapter 1 (section 1.3). Each subject watched a clip from the James Bond Movie, Skyfall (19 minutes 40 seconds long). Subject data were pre-filtered as described in Chapter 6. As this was an exploratory analysis, data were unmasked; the next step in this research would be to repeat the analyses with masked data. Then ROI were identified for ten subjects at the dimensionality 200, and the pattern of merging and splitting of these components were compared.

TICA was performed for ten subjects at dimensionalities from 20 to 200 (in steps of 4), producing a total of 46 ICA outputs. Components at the highest dimensionality (200) were matched to the coordinates of

visual ROI at V1, V4, V3A and MT+ (Yeo et.al., 2011; see Chapter 6). Components were matched based on the distance of the peak voxel to the ROI coordinate and activation at the ROI coordinate. Components were ordered based on these matching criteria and checked by eye. A signal component was chosen that best represented the ROI. Using these components of interest, matches were identified iteratively through the dimensionalities using spatial correlation and peak voxel. As described above, the spatial correlation was calculated between the component of interest and the 196 components using FSL's '*fslcc'* command. Then the peak voxel of the top five spatial matches was compared to the seed component. The component that had the closest peak voxel was identified as the 'best match'.

All of the ROI are part of the visual network allowing observers to process the complex scene, and therefore all of these regions are functionally connected at some level. Here we are interested in the consistency across observers (how well the ICA technique picks up on these functional connections) and what it tells us about the strength of the functional connections (reflected in the ordering of the splits). To this end, two measures were taken:

(a) The percentage of participants showing the merging between two regions at lower dimensionality. This gives an indication of how reliably this functional connection can be identified using this technique (the consistency of structure across observers).

(b) The average point at which two regions merged (across those subjects showing merging).

10.3.2 Results

The results of this analysis demonstrate some differences in the splitting pattern of components, across subjects (see Figure 160 for merging statistics across observers). This may be reflecting real differences in the functional hierarchy during natural viewing but needs further investigation. However, there were also some similarities across subjects: all the observers showed some merging of components in early visual regions (covering V1/V2/V3; in Figure 160 this is notated at "any V1" merging). The statistics also lend support to the findings in Chapters 5 and 6 showing that different visual networks cover the anterior and posterior occipital lobe, at dimensionality 20. Only 3 of the 10 observers showed merging across the anterior (peripheral visual field) and posterior (foveal visual field) V1 components. Merging in V1 instead was across hemispheres, for example the V1 peripheral regions in the left and right hemisphere merged. 70% of the

observers showed a merging of V1 posterior components and 50% showed merging of the V1 anterior components. Interestingly, the 3 observers who showed merging across the central and peripheral components were all observers without merging of peripheral left and right hemispheres, suggesting a lateralization of activity in these observers.

Merging regions	Observers show merging
Any V1	100%
V4 and V3A	80%
Central V1	70%
MT and V3A	60%
Peripheral V1	50%
V4 and MT	40%
V3A across hemisphere	30%
MT across hemisphere	30%
MT and V1	30 %
V3A and V1	30%
V4 and V1	30%

Merging regions	Splitting level (average)
MT and V3A	140
V4 and V3A	124
Peripheral V1 (across hemis)	120
Central V1 (across hemis)	104

Functional similarity between regions **decreases**

Figure 160. Patterns of component merging as dimensionality was reduced were compared across subjects. Results show different across observers in their trees. This may be due to functional hierarchy differences or could be due to noise in the matching process.

Apart from early visual sub-regions, the most common merging across observers as dimensionality was lowered to 20 was between V4 and V3A, which showed 80% of subjects merging these two components. This suggests that these regions show functional connectivity during movie watching across the majority of the observers. Indeed, even at dimensionality 200 many of the subjects showed network components with both V3A and V4 activity. These statistics suggest that in some brains V4 and V3A remained separate even at dimensionality 20, but in others they were fused even at dimensionality 200. Motion sensitive regions MT and V3A also showed relatively high proportions of the subjects showing these regions merge into one component by dimensionality 20; 60% of subjects showed merging across these regions.

The regions that showed merging in 50% or more observers were taken forward to see when on average the merging occurred. It is interpreted that regions that split at higher dimensionalities show more similarity in function, compared to components that split at lower dimensionalities. The average dimensionality at which the regions of interest split suggest that MT and V3A are the regions that show most functional similarity, as they split at the highest dimensionality.

V3A and MT+ are both strongly responsive to motion (e.g. McKeefry et.al., 2008), which could be driving the correlation between processing while watching the movie. V4 and V3A are the next to split, suggesting a correlation in processing while watching the movie. Research has documented a diverse and complex functionality of V4, including processes related to colour, brightness and texture, shape, motion, motion contrast and depth (Roe et.al., 2012). Further research is needed to investigate this association. In the movie clip there are many camera movements creating motion parallax as well as moving objects, it could be that colour differences at the border of objects are being processed as an object moves across the background or as the camera moves.

Peripheral V1 components were matched across hemispheres at the next highest dimensionality, followed by central V1 components. These findings suggest that similarity in function may be higher across extrastriate regions than across hemispheres at early visual regions. The lack of merging in some participants between motion regions V3A/MT+ and early visual region V1 may be supported by the findings presented in Chapter 6. This showed that at dimensionality 20, individual participants showed separate components driven by the early visual regions and motion regions, respectively (see Chapter 6, section 6.3.2). Based on these findings it was expected that these regions would not merge by dimensionality 20 as they are still represented as part of different visual networks. The same can be said for the lack of merging between regions V4 and MT, with different networks representing lateral and medial aspects of the occipital lobe at dimensionality 20 (see also Smith et.al., 2009). This suggests that these regions are relatively functionally distinct, and a very low dimensionality (e.g. dimensionality 10 or 15) would be needed to see these components merging.

A lack of merging across hemispheres (V3A and MT+) is likely to be due to the methods used in the matching process. Component matches across dimensions were identified using peak voxel location and spatial map correlations. However, the peak voxels in both hemispheres were not used, only the absolute peak. This means that a bilateral component covering V3A in the right and left hemispheres, but with the peak voxel

in the right hemisphere may only get matched to the right V3A component, identified at a higher dimensionality. This problem has been recognized with hindsight and should be addressed for development of the technique. Components were more likely to be matched across hemispheres in the primary visual cortex as these peak coordinates sat more medially between the hemispheres.

10.4 Summary: Chapter 10

By increasing the dimensionality of ICA outputs using single subject BOLD data, an increased number of useful functional regions can be identified (up to a dimensionality of 200). This chapter has demonstrated a novel technique of investigating the visual functional hierarchy during natural viewing. By plotting the splitting of components as dimensionality is increased, the hierarchy of functional components can be examined.

The splitting and changing of components over different dimensionalities again highlight the importance of choosing the correct dimensionality to address your research question as the choice affects the parcellation of the brain. Choosing whether to limit the number of components to a fixed number or to allow an unrestricted ICA is a major analysis decision. The dimensionality chosen will be influenced by the stimulus used and the length of the scan; using a rich stimulus such as a movie allows for many different functional signals to be identified therefore increasing the number of informative components generated.

One area for future work is to look at how splitting at the same dimensionality may be different across observers, due to differences in noise factors. For example, at a dimensionality of 50 one subject may have 30 signal components, while another may have more motion artefacts meaning less components are available to represent signal. Differences in this "effective dimensionality" across subjects would cause different splitting patterns. Rather than start with components from an arbitrary dimensionality (here I used 200), a broader range could be used to search for stable and distinct components at ROIs for each of the observers.

The hierarchical structures identified in this chapter may be influenced by the task being performed by the observer (image statistics) or fixed by anatomy in the observer. This could be explored in future work by contrasting the hierarchy within subject while performing different tasks while watching the same movie clip. The technique could also be compared across different movie clips for the same observer to check for within

subject consistency of the hierarchy. The technique could also be used while performing tasks that do not involve watching a movie to see whether the hierarchies alter when a broadband stimulus is not being used.

If the technique proves to be robust then it can be applied to MEG data, using either single or multi-frequency band data. This would be interesting to see if cross-frequency band or area components split, and if they do, when they split. This technique should also be of use for examining how functional networks and hierarchies change during other tasks. Further research could input BOLD timeseries collected during tasks such as motion detection and assess the changes compared to natural viewing situations. This would have the aim of isolating and understanding the functional processes which occur during specific tasks.

Chapter 11: General discussion

11.1 Overview

The analyses reported in this thesis were designed to assess the use of a rich natural stimuli and ICA for:

(a) identifying multiple regions of interest in observers at the group and individual level using BOLD signal;

(b) investigating the relationship between MEG frequency bands, during natural viewing;

(c) investigating the relationship between oscillatory activity and the BOLD signal, during natural viewing;

(d) investigating the use of changing the dimensionality of TICA for mapping the functional hierarchy of visually driven regions, during natural viewing.

Based on previous work by Bartels and Zeki (2004; 2005) it was hypothesized that TICA could be used to segment visual functional regions using BOLD data collected during natural viewing. In the first section of this thesis I demonstrated that although TICA shows some sensitivity to analysis parameters, this is a promising technique that can produce reliable and robust visually driven components at the group and single subject level (Chapters 2, 3 and 6). Components represented established functional networks at low dimensionalities (Chapter 4 and 6), and visual regions of interest at higher dimensionalities (Chapters 5 and 6).

In the second section of this thesis I expanded on this technique and explored the use of TICA for examining the role of oscillatory activity in the brain, during natural vision. I found that using MEG beamformer data, reliable components could be identified in visually driven regions in individual frequency bands (Chapter 7) and across frequencies (Chapter 8). I proposed a novel technique using TICA that allows investigation of cross-frequency and cross modality relationships during natural viewing. Results supported established work in the field and offer an exciting new way to combine and investigate the MEG and BOLD signals, exploiting both of their strengths.

In the third section of this thesis I explore a novel way of investigating the functional hierarchy of the visual system, during natural viewing. The results are promising and with development could be a useful tool in future neuroscientific research.

In this final chapter I present the implications of these findings. I also discuss some future directions to build on what we have learnt and further improve our understanding of the functional and oscillatory activity in the visual system during natural viewing.

11.2 Implications and future directions

In Chapter 2, I build on the work started by Bartels and Zeki (2004) who showed that visual regions could be identified in subjects using ICA to delineate data collected during movie watching. This work presents an opportunity to be able to map visual areas in a group or an individual without the use of multiple localisers that are lengthy and uninteresting to observe. However, the reliability of the technique was unknown. With systematic analysis I demonstrated that although group TICA is sensitive to pre-processing parameters (including the order of subject input, smoothing, resampling, motion correction [FSL's AROMA] and grey matter masking), visually driven components remain relatively robust across outputs. With the use of a grey matter mask and by restricting dimensionality reliable components can be identified at the group level. These findings are important to contextualize findings using TICA, which is broadly used in neuroscientific research. They can also be used to inform future research in the field.

Another addition to this research could compare the timeseries BOLD data of each individual with the group TICA components. These results would be valuable as it may be that simple voxel-by-voxel correlations of timecourse obscure quite how high the correlation is between brains, due to noise at the individual level. It may also be that differences in the mixing of components across subjects' voxels masks functional similarities at the voxel-wise analysis level.

In Chapter 3 I found that these robust components can be identified across different subject group and movie clips. Although spatial maps showed some variability across sample, the peak voxel of reliable visually driven signal components was stable across different samples, suggesting that the same locations were being identified, but with slightly different spatial maps. These results are useful as they demonstrate how peak

voxels of components serve a useful tool for locating visual regions of interest at the group level. Future work should investigate whether the peak voxels of components remain stable across motion correction techniques and grey matter masking. It would also be useful to compare variability in peak voxel to variability in the location of the middle of a component. This could be identified by taking the mean voxel location for a component for the major cluster, or by taking a weighted mean where you weight the contribution of each voxel by its z value. It would be useful also to understand how the peak voxel relates to the "centre of mass" of the component.

A potential benefit of using movie clips and TICA rather than traditional localisers is the identification of functional networks. These networks would not be identified using simple functional localisers, which identify specific regions in a visual pathway rather than a whole network. Chapter 4 demonstrated that by using natural movies the same functional networks identified using resting state data can be identified using a low TICA dimensionality. An additional visual network was identified comprising of motion regions MT+, dorsal regions near the IPS and the ventral region V4. Being able to identify both functional networks and regions of interest using movies and TICA could prove very useful in neuroscientific research and work with clinical patients. Currently resting state data is widely used for comparison of neural function between clinical and non-clinical groups. However, the resting state sessions are usually only ~5 minutes long as participants find it difficult to stay awake and stay still in the scanner with the lack of stimulus. Using a movie could solve these restrictions increasing the attention of observers to the stimulus. Increasing the amount of data means more components can be generated (see Chapter 3), to identify networks and regions of interest. Temporally concatenated CICA could be used rather than TICA if there was an investigative focus on non-visually driven regions.

In Chapter 5, I compared the reliable functional regions identified using a high dimensionality group TICA to known regions of interest in the motion processing pathway. This pathway was chosen as it has been studied extensively and shows reliable activity when motion is observed (e.g. Tootell et.la., 1997; McKeefry et.al., 2008). It was expected that this pathway be activated as the movie clip included at least one type of motion in almost every scene. These findings provide support for the use of movies as a method of identifying regions of interest in the motion pathway at the group level. Used alongside an atlas, a movie and

TICA is a promising approach for identification of visual regions. It would also improve the experience of the observer and potentially cut scanning time.

The applications of this work are far reaching at the group level; if they could also be applied at the single subject level this would increase their potential in clinical and research settings. Work presented in Chapter 6 supported the use of this technique in single subjects. I demonstrate how at a low dimensionality, resting state networks and visual regions can be reliably identified at the individual subject level. In Chapter 6 I also demonstrated that at a high dimensionality TICA can identify separate components representing visually driven regions of interest in individuals. Regions in primary visual cortex processing the peripheral and central visual field were separate across most individuals. This may support conclusions developed by Trevarthen (1968) who suggested that vision is broken into central and ambient (peripheral) vision. This two-vision system model has largely been forgotten and replaced by ventral/dorsal, but it is still prominent in applied contexts like flying and clinical research. My research may support the functional splitting of early visual regions in this way. Alternatively, it may reflect the image statistics of the movie, which may show very distinct foregrounds (e.g. an object or actor) and backgrounds. Further investigations with stimuli with less defined foregrounds such as footage crowds or blizzards would be useful to see if this segregation is still robust.

Future work should also investigate the 'effective' dimensionalities at group and single subject level ICAs. In Chapter 6, single subject and group components were matched across the same dimensionalities. However, it may be that there are differences in the components that are due to features such as different levels of noise components or components driven by sub-groups in the group output. These would change the effective dimensionality of signal components, meaning they may differ in size or in the regions that they represent.

In Chapter 7, components generated using TICA with MEG data collected during natural viewing were documented. These were generated at a higher dimensionality than is usually used for the identification of RSN, therefore covered smaller sub-regions of networks. Components lying in regions with significant subject correlation were examined, therefore an obvious next step would be to assess whether resting state networks can also be identified using movies, at a lower dimensionality. It is expected that these functional

networks can be identified using either a TICA or CICA procedure, based on our work in Chapter 5 using the BOLD data.

When calculating cross-frequency correlations in the MEG data, voxel timecourses were averaged across subjects and then these mean brains were correlated in a voxel-by-voxel analysis. Using this method, the voxel timeseries will represent any signal timelocked to the movie stimulus across subjects. Another method that could be employed is to calculate the correlations between frequency bands at the subject level and then take a mean across participants. This will reveal cross-frequency correlations that are not stimulus driven.

In Chapters 8 and 9, I presented a novel technique for investigating cross-frequency and cross-modality coupling using a spatial concatenation technique. Currently, it is relatively difficult to investigate the relationship between BOLD signal and oscillatory activity. This approach will be of potential use in future neuroimaging projects and can be applied to different types of task data. Future research would be useful to understand the effect of increasing dimensionality in a combined frequency/modality analysis. Results in this thesis report large cross-modality components, covering multiple regions; increasing the ICA dimensionality may show a splitting of these components into smaller sub-regions, or across the frequencies/modalities. Using this spatially combined data technique, the relationship between activity in different layers of the cortex could also be examined with the development of MRI technologies achieving higher resolutions.

In Chapter 10, I begin to explore the potential use of ICA across dimensionalities for understanding the functional hierarchy within a brain. At an individual level it looks like a reliable hierarchy can be identified. Initial analysis suggests some similarities across observers, and some differences. Individual variation in tree hierarchy may be due to real individual differences in functionality, the matching methods across dimensions or a combination of both. Future work could investigate this further by examining the reliability of functional hierarchies in individuals across different movie clips. With development this would be a useful tool for the analysis of functional networks. Components in regions of interest are relatively robust at the individual level, but the merging and splitting of these components is less reliable. Future aims for the development of this work include plotting the trees with branches that represent the strength of correlation between the matched components. This would provide more useful information when examining a hierarchy. Another important step would be to create a tree using average components across subjects. To do this the

components would be matched across subjects at each dimensionality, and then averaged. The matching procedure would then work through these components to produce a probabilistic hierarchy. With this development in theory this technique could be applied to examine functional hierarchies across the brain and during different tasks, not just during natural viewing.

In summary, this thesis supports the use of TICA for the identification of visually driven regions and networks at the group and individual level, using BOLD data collected during movie watching (Bartels & Zeki, 2004). It expands on the technique and proposes a spatial concatenation approach for investigation of oscillatory activity during natural viewing and its relationship to the BOLD signal, which shows exciting promise. Additionally, the results show that changing the dimensionality of the ICA output may be a useful and novel way to examine functional hierarchies.

Appendices

Chapter 2

Appendix 2.1 *Spatial and temporal correlations across random permutations*

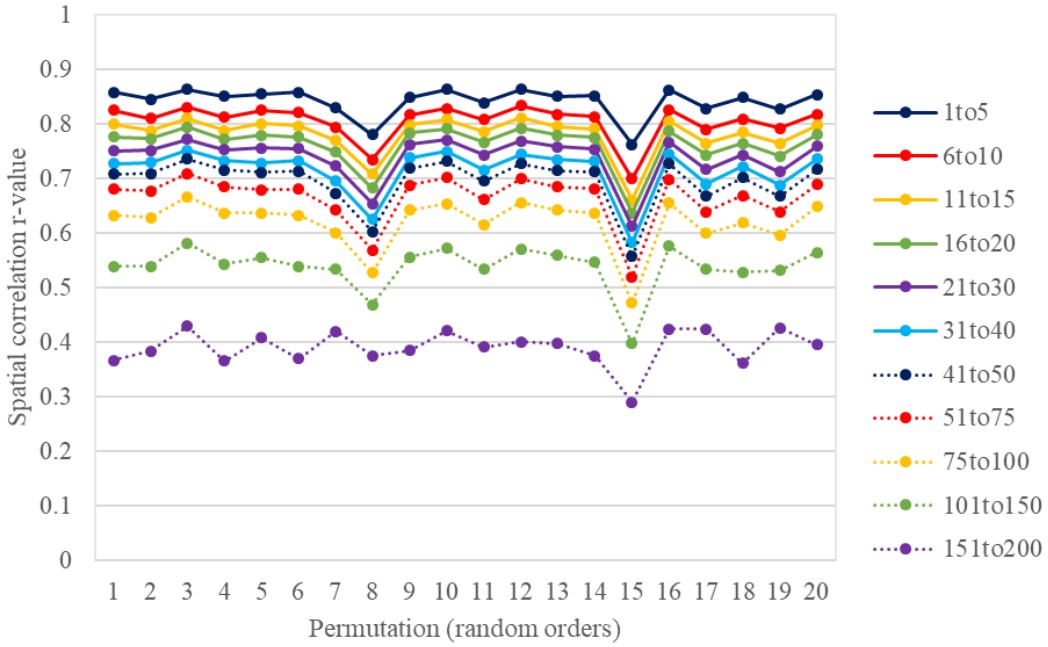

Appendix 2.1a Spatial correlations across random permutations. The average spatial correlations across random input permutations show spatial variation in the component maps.

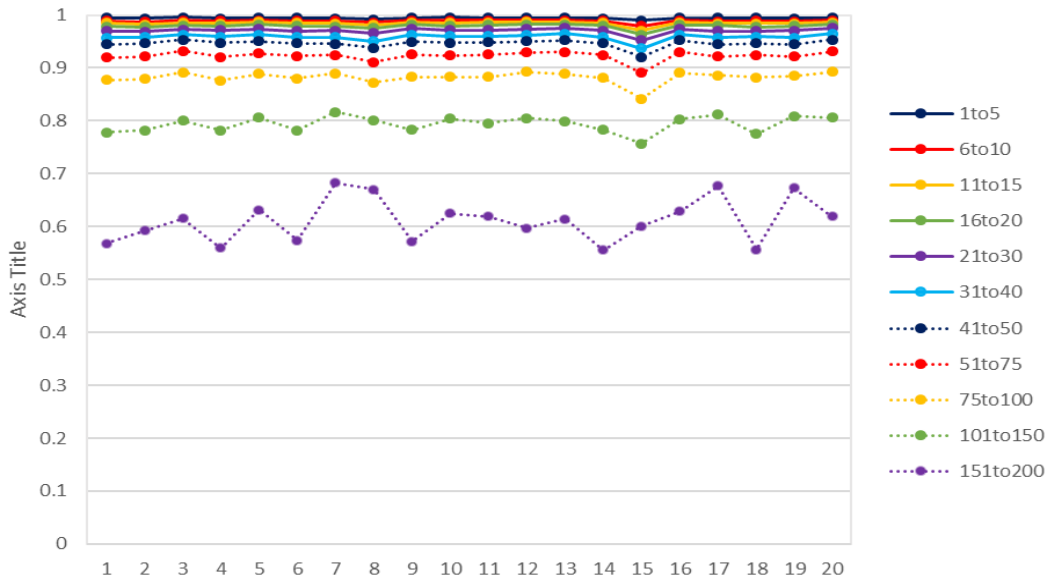

Appendix 2.1b Temporal correlations across random permutations. The average temporal correlations across random input permutations show low variation in the component timeseries.

Appendix 2.2 *Using an average brain as the first brain*

Given that the first brain seems to set the initial component conditions, using an average functional brain as the first input may lead to the most representative set of components being generated.
Each of the participant's functional data were averaged to create an 'average brain'. At each voxel the timeseries was averaged at each time-point, across all participants. This created a 4D file with an average timeseries at each point in the brain.

When the average brain was used on its own as input into MELODIC. The correspondence of the output to the ICAs generated using the full list of subjects is relatively low, shows similar levels of representativeness as a random one brain input (see Figure 13). The similarity is relatively stable across all the permutation comparisons.

Next, I added the mean functional data-set to the front of the most representative ICA output. Based on our previous findings that the first brain creates seeds for the components, the mean brain could be added to the front of a permutation to potentially create components that are more representative of components across the ICA outputs.

The mean movie brain being listed first generated components that represented the other components at an average standard across the runs (see Appendix 2.1 figure). Using the mean brain as the first brain may therefore be one way of directing the results to provide a more reliable result; i.e. know that it is not an outlying result. However, it does not necessarily allow you to generate the most representative output.

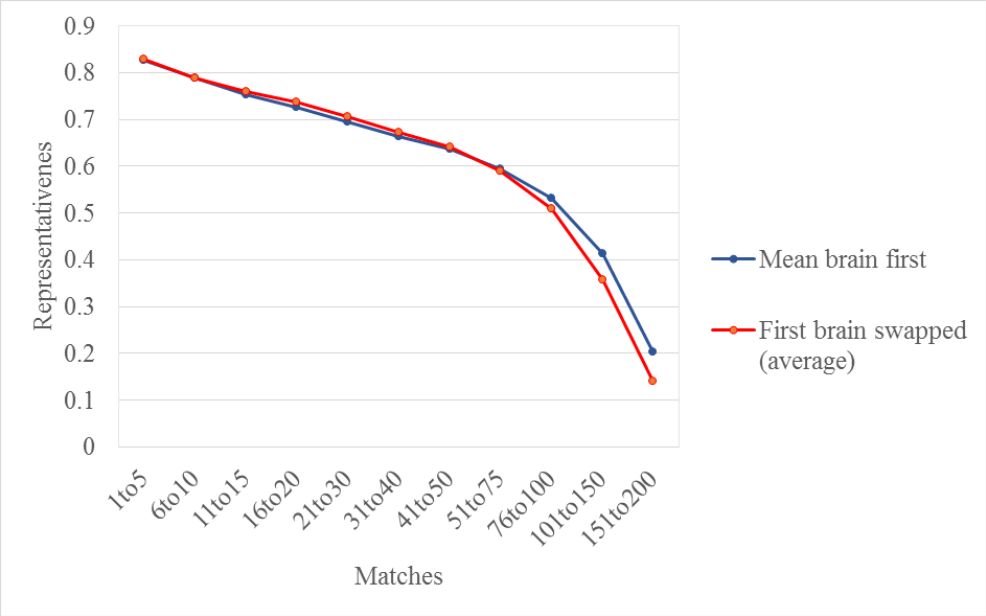

Appendix 2.2 Using a mean functional brain at the front of the full list of subjects created an ICA output that represented the other ICA outputs relatively well. The representativeness of the output was very similar to the average representativeness of the original permutations.

Appendix 2.3 *Representativeness of AROMA treated data permutations (first brain swapped)*

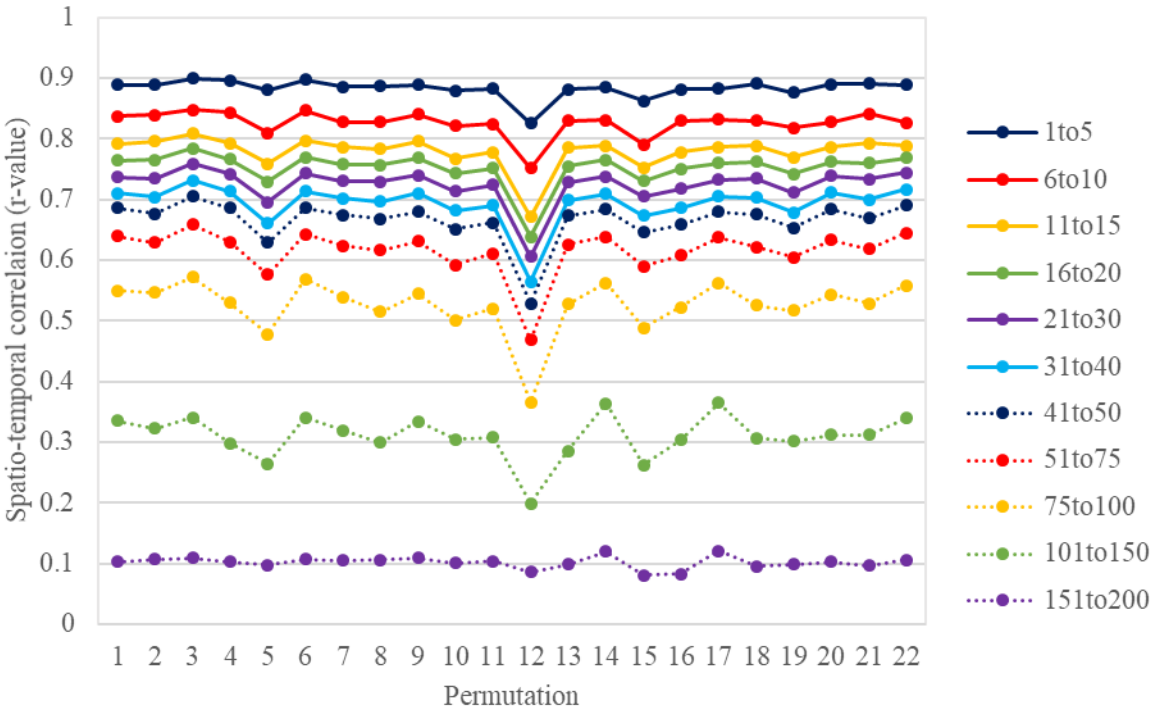

Appendix 2.3 When data is treated with AROMA the pattern of representativeness across permutations is similar to Vanilla (no-AROMA) outputs. For example, permutation 12 is the least representative permutation (see Figure 6)

Appendix 2.4a *The representativeness of grey matter masked data permutations (first brain swapped).*

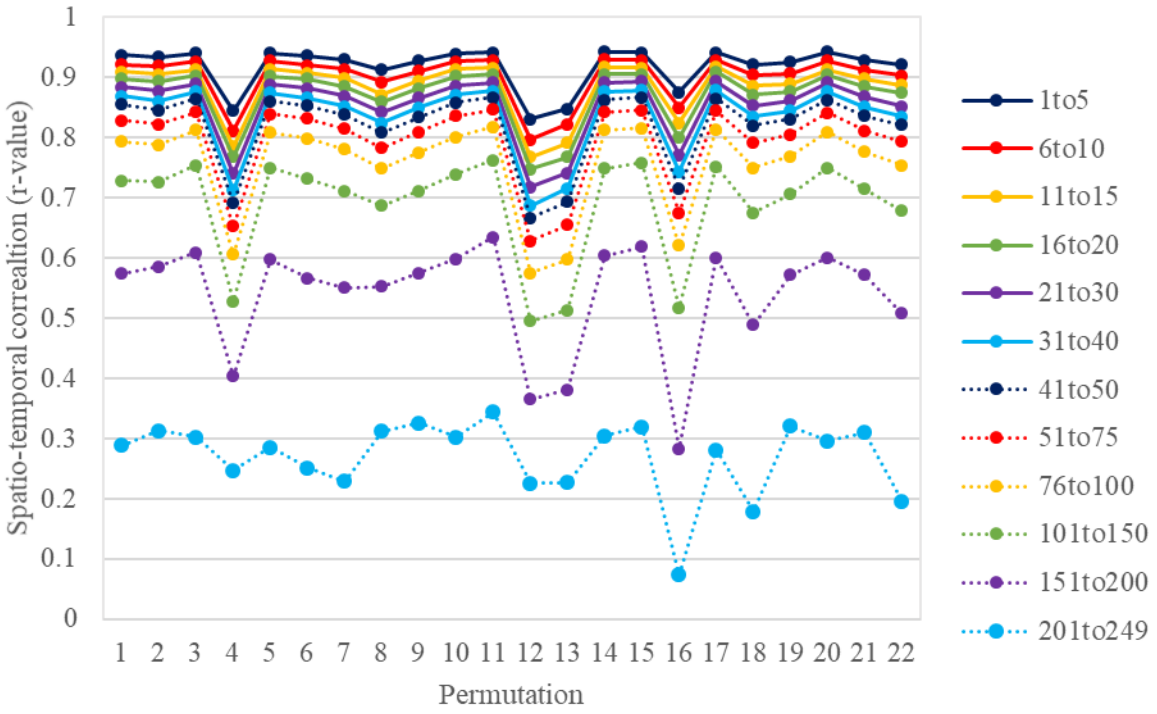

Appendix 2.4a When data grey matter masked the pattern of representativeness across permutations changes compared to Vanilla (no-mask) outputs. For example, permutation 12 no longer the least representative permutation (see Figure 6)

Appendix 2.5 *AROMA treated data versus no AROMA*

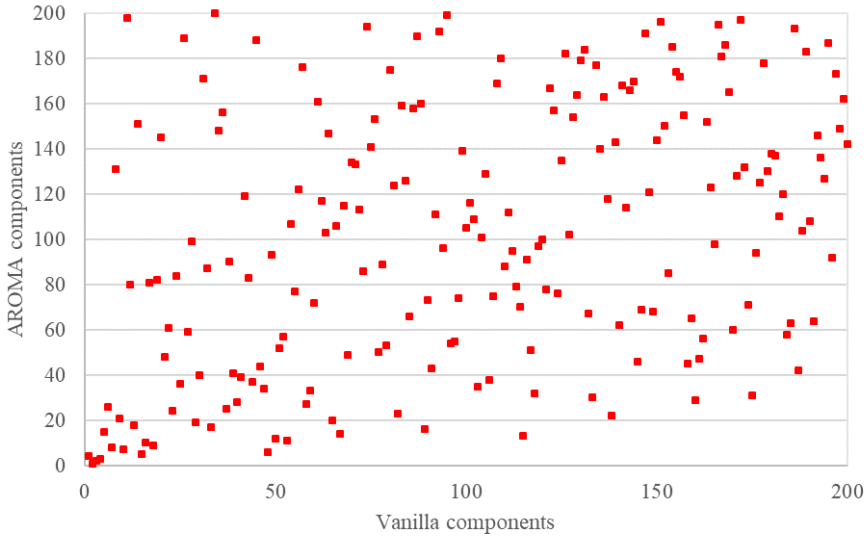

Appendix 2.5a The best component matches were recorded across the most representative AROMA and the most representative vanilla output. A map of the matched component numbers shows a no correspondence in position for most of the components.

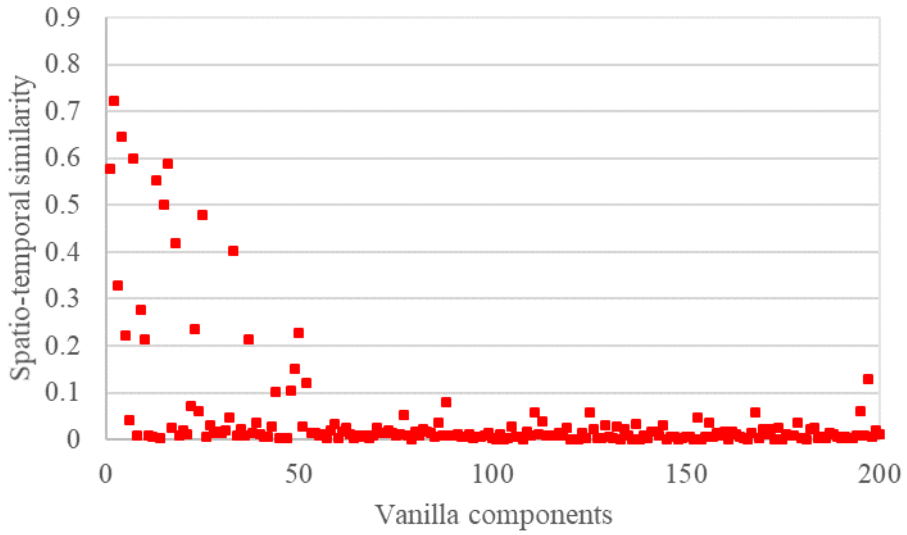

Appendix 2.5b Component number and reliability across AROMA and vanilla outputs. The components that showed good reliability all lay in the first fifty components of the Vanilla output.

Appendix 2.6 *Grey matter masked data versus no grey matter mask*

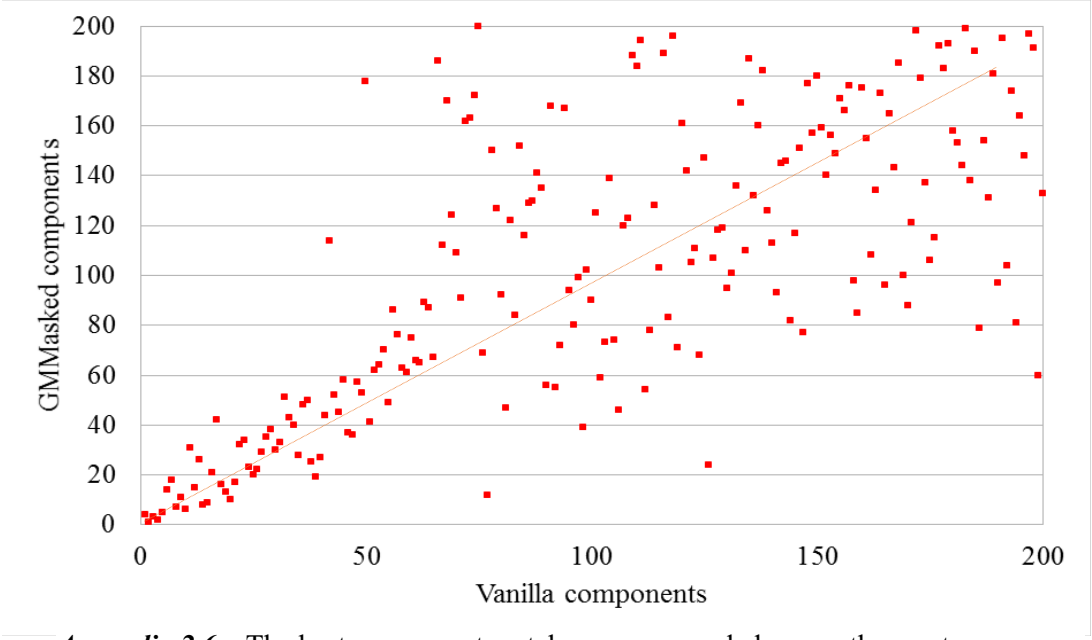

Appendix 2.6a The best component matches were recorded across the most representative grey matter masked and the most representative vanilla output. A map of the matched component numbers shows a correspondence in position for the first ~60 components.

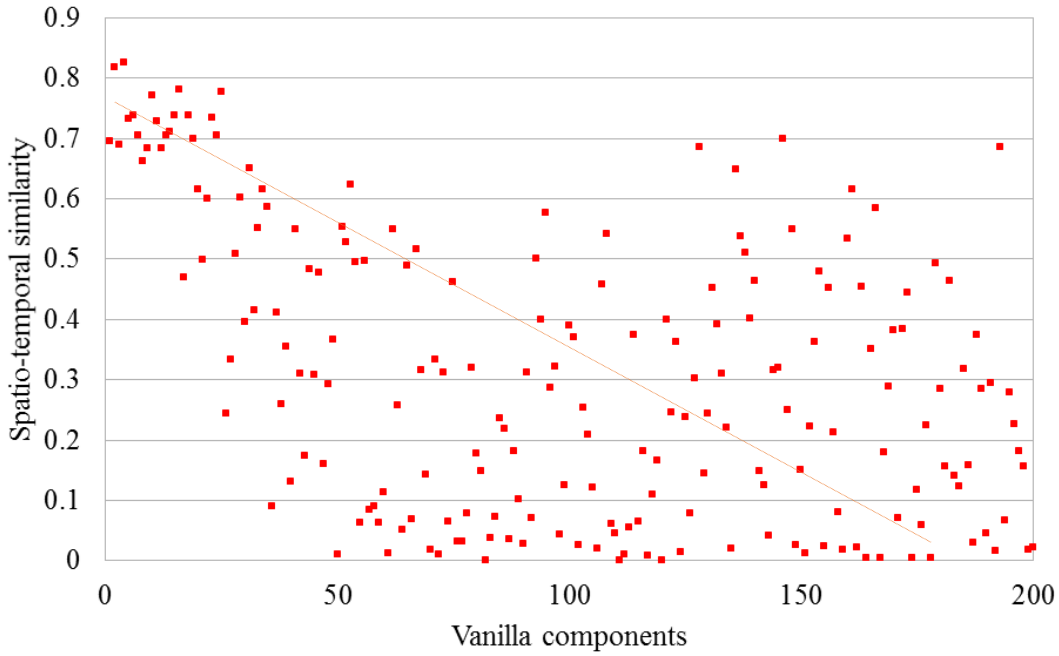

Appendix 2.6b Component number and reliability across grey matter masking: There was some positive correlation between component number and the best matched components across Vanilla and the grey matter masked data for the first 20 components and none, thereafter.

Chapter 3

Appendix 3.1 *Reliability of TICA outputs using the second half of the movie.*

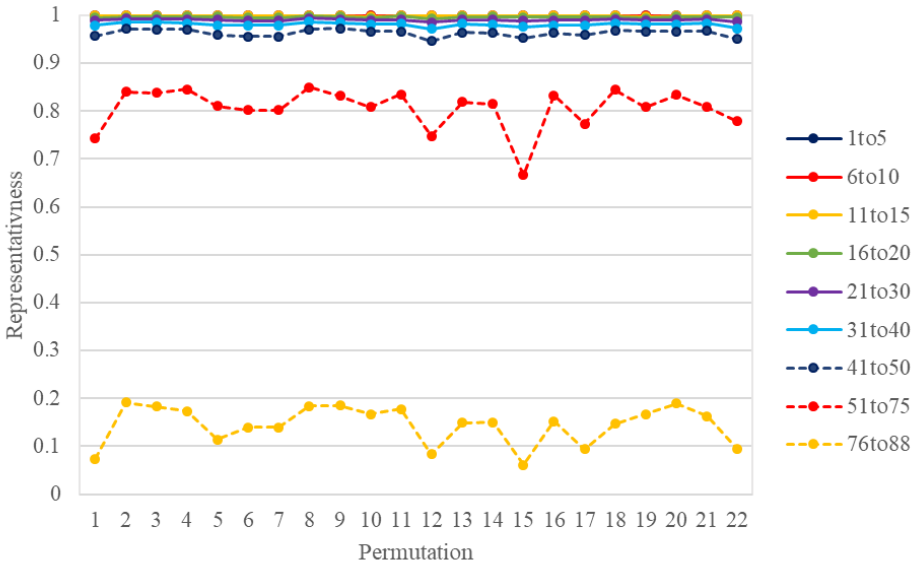

Appendix 3.1 **-** The reliability of the TICA components using the second 10-minute half of the James Bond clip, only. This is very similar to the pattern of reliability generated using the first half of the movie.

Appendix 3.2 *Reliability of spatial maps of the TICA outputs using eleven participants.*

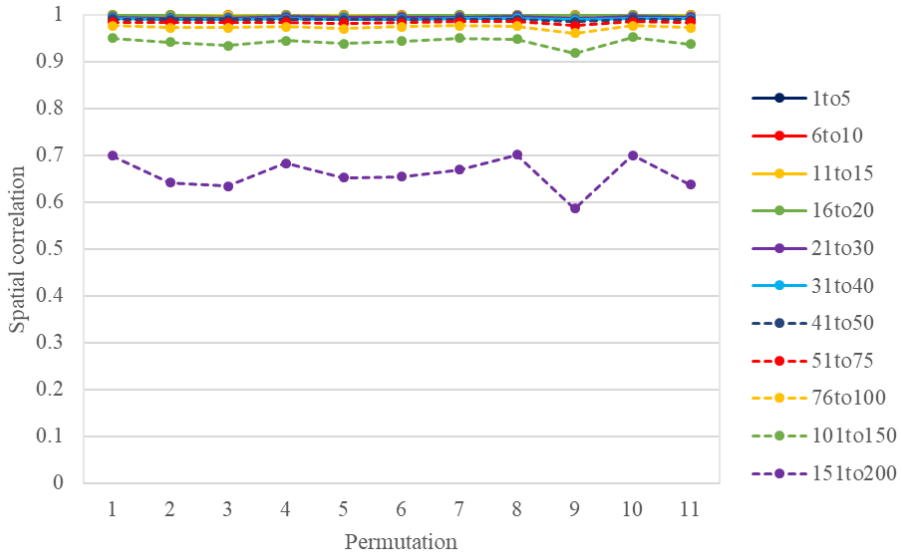

Appendix 3.2 - The spatial representativeness of different permutations of the same eleven participants. The first brain was swapped in each permutation and data were grey matter masked. Spatial correlations are very similar to the temporal correspondence.

Appendix 3.3: *Spatial correspondence between matched components generated using two different 5-minute clips*

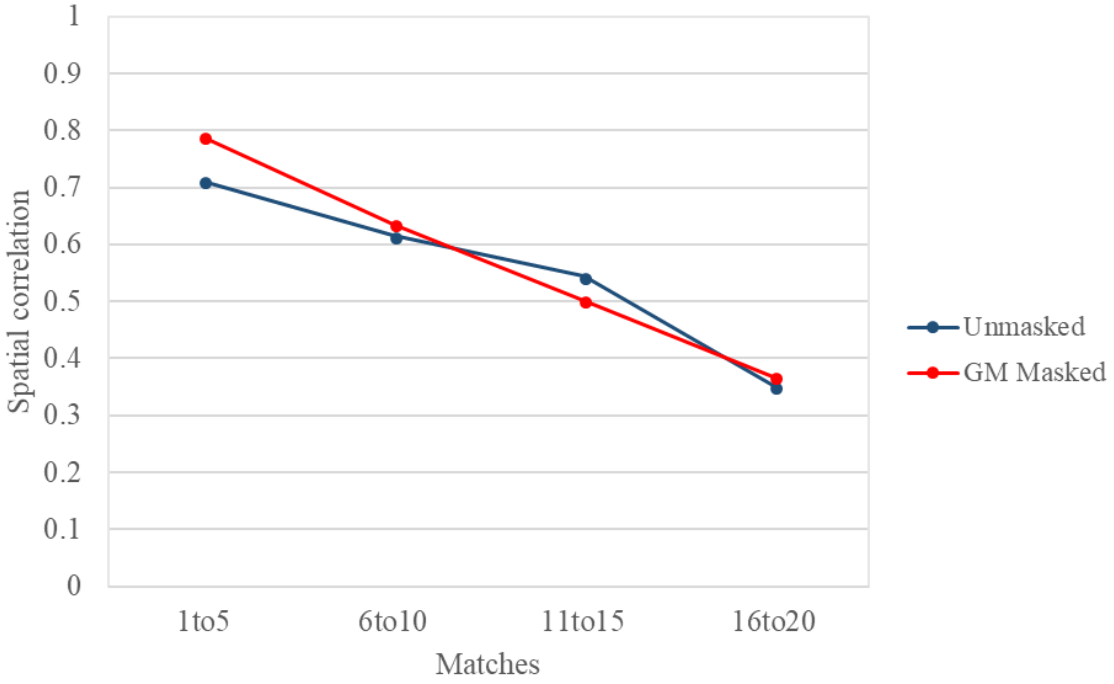

Appendix 3.3. The spatial correspondence between ICA components generated by different five-minute movie clips shows similar correspondence with or without grey matter masking. This spatial correaltion is similar to the matching seen across two different ten-minute clips (see section 3.2.3).

Chapter 4

Appendix 4.1: *The size of components best matched directly to the three seed visual network components at dimensionality 20.*

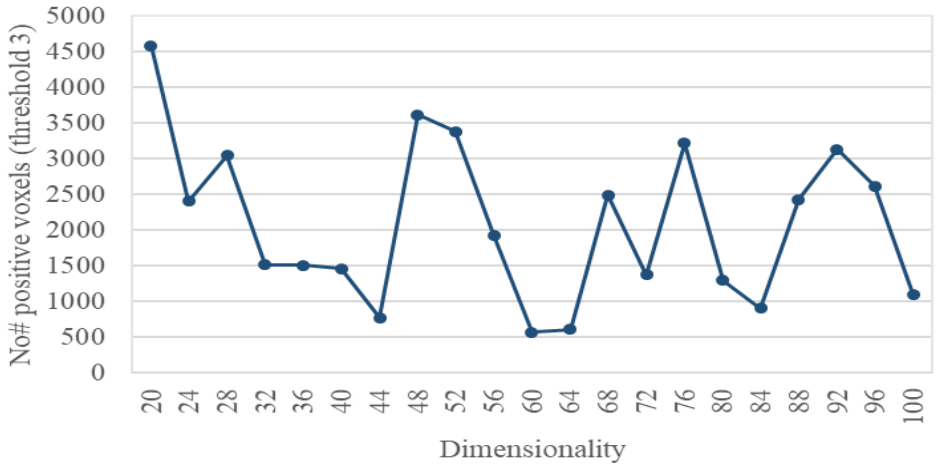

Appendix 4.1a Visual network 1: The size of the best matched components across dimensionalities from 20 to 100. The size fluctuates across dimensionalities signifying that neat splitting of the components is not taking place.

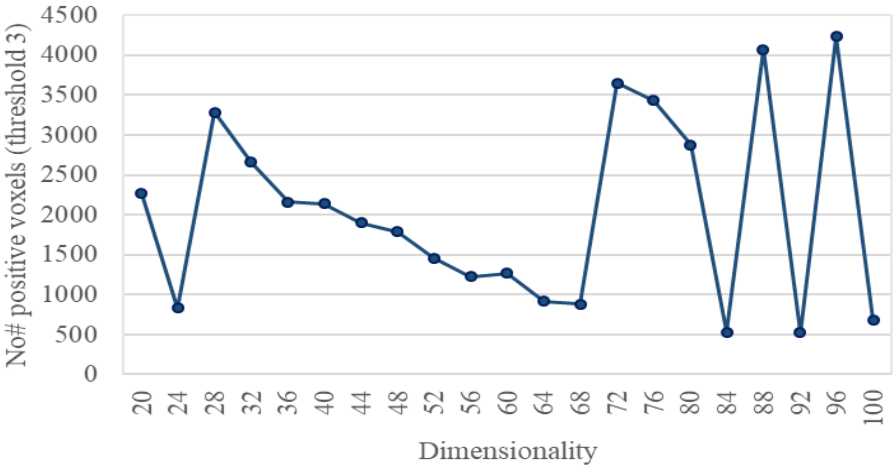

Appendix 4.1b Visual network 2: The size of the best matched components across dimensionalities from 20 to 100. The size fluctuates across dimensionalities particularly at the same point that changes in peak voxel are identified, signifying that neat splitting of the components is not taking place.

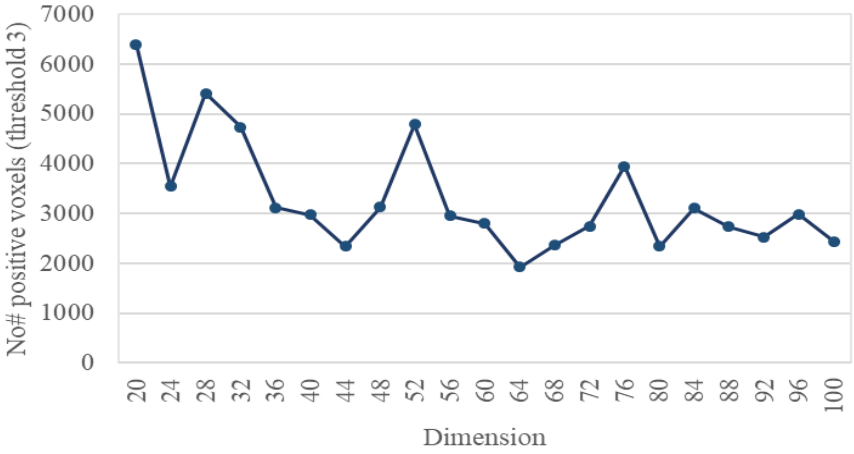

Appendix 4.1c Visual network 3: The size of the best matched components across dimensionalities from 20 to 100. The size shows some fluctuation across dimensionalities signifying that neat splitting of the components is not taking place.

Appendix 4.3 *Functional network identified using meta-analyses (Yeo et.al., 2009)*

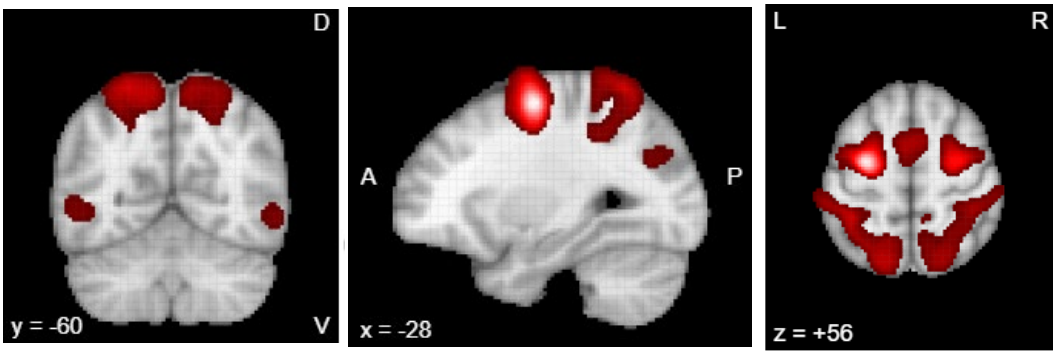

Appendix 4.3 **-** Meta-analyses of resting state data shows functional connectivity between post and pre-central regions and MT+ regions at the lateral occipital lobe (Yeo et.al., 2009). This is represented in the ICA output when using movies.

Chapter 5

Appendix 5.1 *The regions of signal components in the second half of the REPRUN TICA output (restricted at 200 components).*

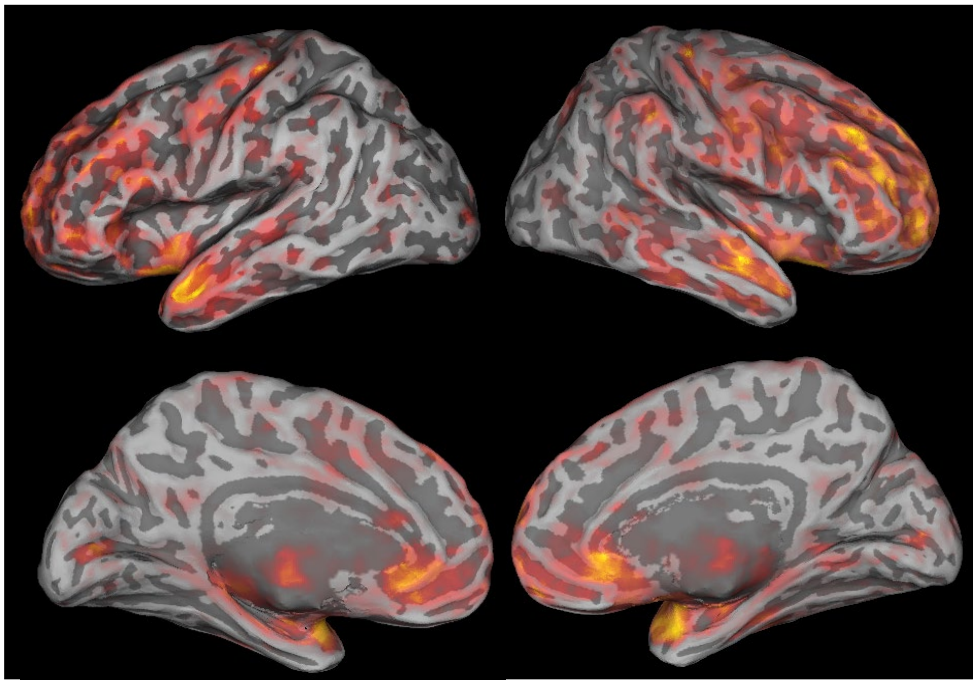

Appendix 5.1 **-** Signal components lying later in the ICA output (>position 73/200) tend to be in anterior regions of the brain, primarily in frontal and temporal regions. Signal components lying earlier in the TICA output were identified in the occipital and parietal regions, which showed significant cross-subject correlation of the BOLD timeseries.

Chapter 6

Appendix 6.1 *The average peak voxels across subjects for the components matched to the third group visual network.*

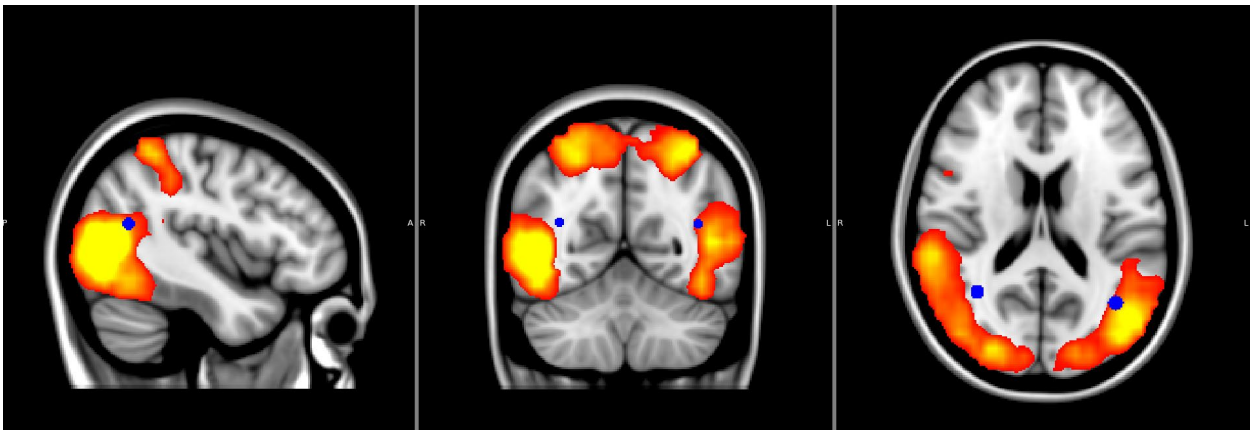

Appendix 6.1 The peaks are pulled anteriorly and dorsally between MT+ and V3A regions, as different participants showed peak voxels across both regions.

Appendix 6.2: *The MT+ localiser*

For each subject the MT+ region was identified for their individual brain. Localisers had been used for fourteen of the 22 participants to identify regions associated with motion processing, including MT. Analyses using FSL's FEAT identified regions matching the MT for these participants. For the remaining participants, the expected location of MT+ can be identified in each of the subjects using their own anatomical scan (Dumoulin et.al., 2000). Using these guidelines and the expected location based on the average coordinates, the expected MT+ could be identified for each subject.

Using the localisers the MT region could be identified by contrasting translational moving dots, with a static dot or contrasting full radial flow with static dots. Both resulting outputs were consulted to support the identification of MT+. An example image (Appendix 6.2 image, below) identifies the left (A) and right (B) MT+ for one participant. The average location identified across subjects was in line with previous findings with mean coordinates in the left hemisphere at MNI coordinates (-41,-78,1) and in the right hemisphere at (41,-75,1). There was a range of 10 MNI coordinates across the subject on the x-axis and a range of 12 coordinates difference, across the y and z axes.

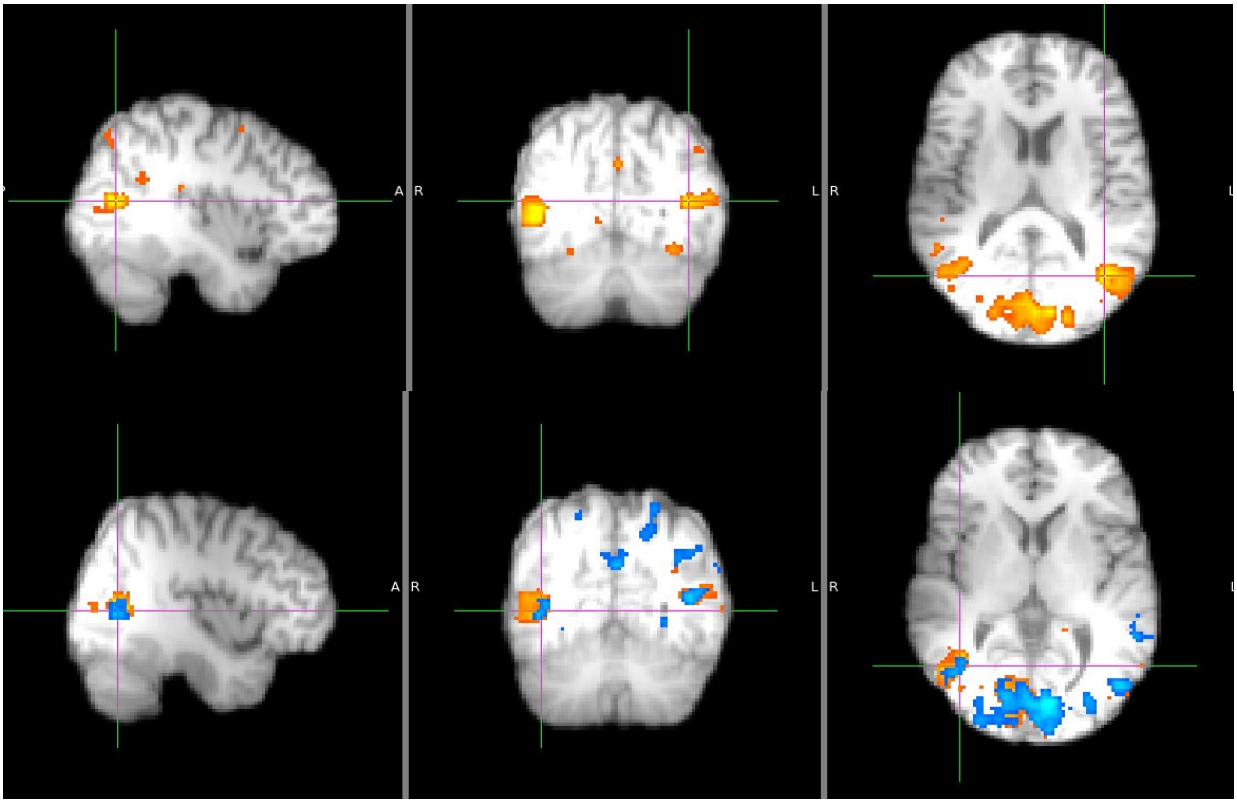

Appendix 6.2 A battery of localisers was used with some of the participants to localise MT+ and V3A regions. A representative example of the results is displayed. (A) An example subject shows activation at MT+ and early visual during fullscreen radial motion compared to static (B) Activation is seen at the same MT+ location during translational versus static stimuli.

These coordinates and anatomical markers could be used to identify components located at the subject specific MT+ and MST regions. Subject specific V1 components were also relatively trivial to identify, with peak around the calcarine sulcus. Activity at early visual regions was also often present in the localizer outputs (see figure Appendix 6.2).

Appendix 6.3: *Inputting an ICA component timeseries into FSL's FEAT*

Timeseries were entered as EVs in FEAT to see whether the MT region could be identified using the component timeseries. Each subject specific timeseries was entered in FEAT as the model, with no temporal derivative or filtering. The output was uncorrected to $p<0.001$. Using this method only the MT+ regions could be identified for each subject (examples in the figure below).

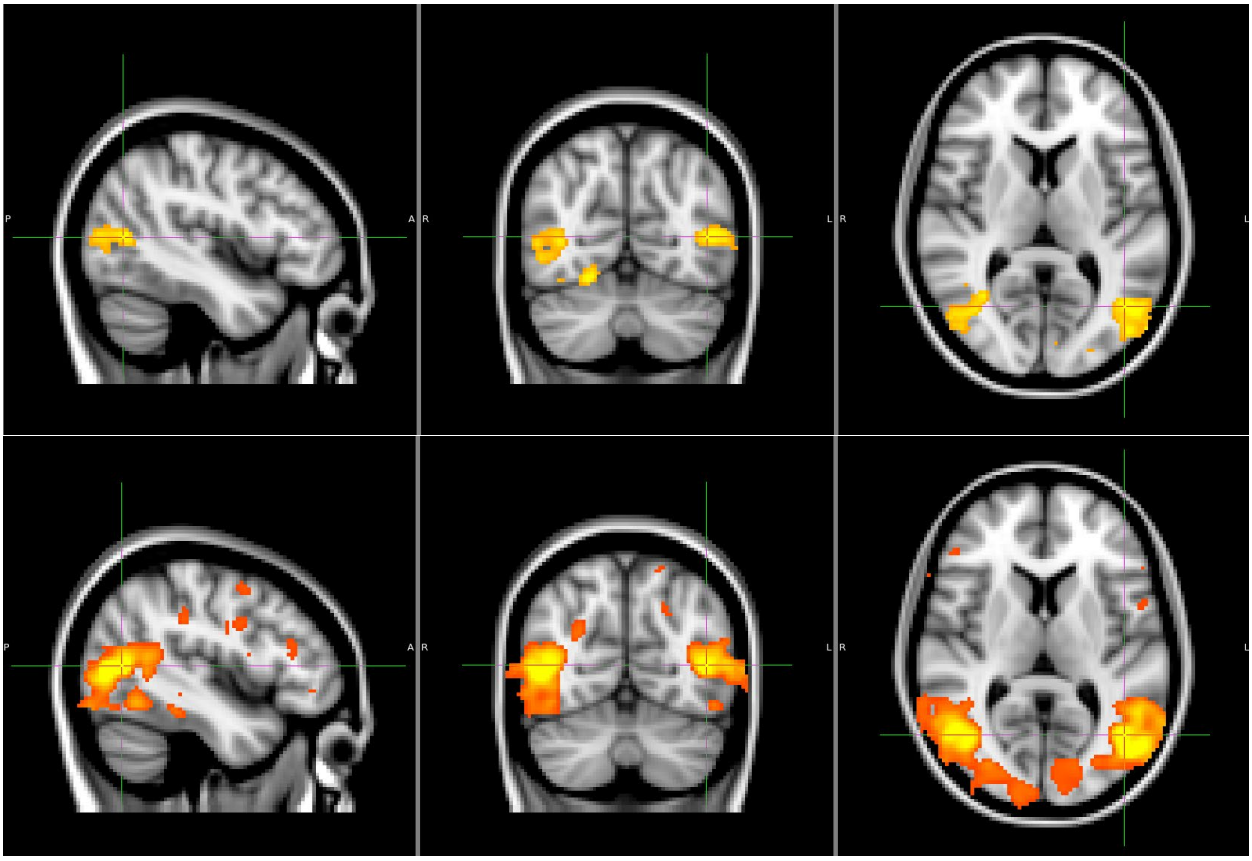

Appendix 6.3 Subject specific MT timeseries identified regions at the MT+ complex for all subjects.

Chapter 7

Appendix 7.1: *Aoki et.al., (2015)*

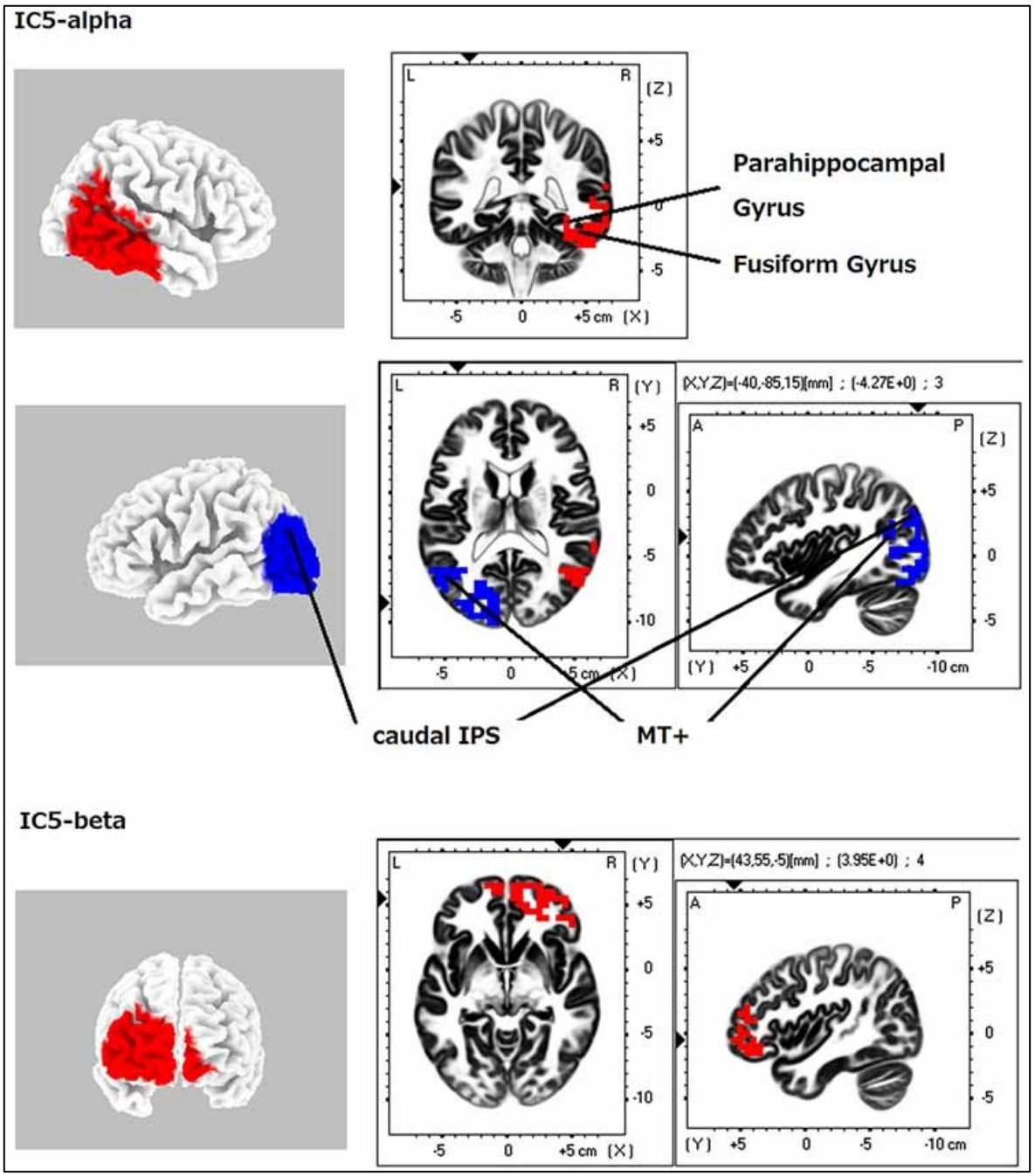

Appendix 7.1a. Cross frequency interactions during resting state at the prefrontal cortex (beta) and dorso-ventral visual pathways (alpha). Identified using EEG and cross-frequency ICA. Taken from Aoki et.al., 2015, p.5.

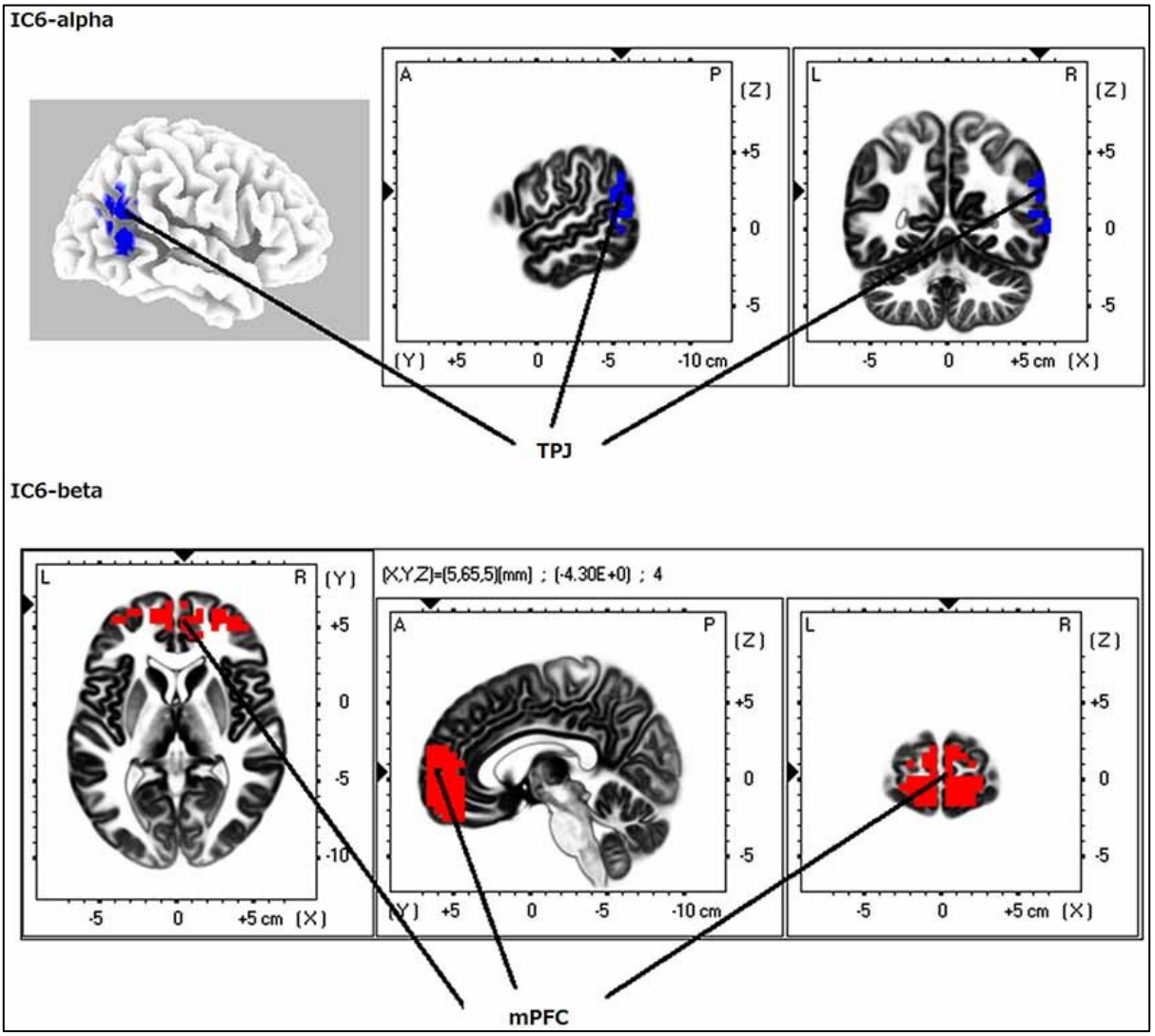

Appendix 7.1b Cross-frequency interactions at the medial pre-frontal cortex (beta) and the temporal-parietal junction (alpha). Identified using EEG and cross-frequency ICA. Taken from Aoki et.al., 2015, p.6.

Appendix 7.2 – *The reliability of components in the delta single band output.*

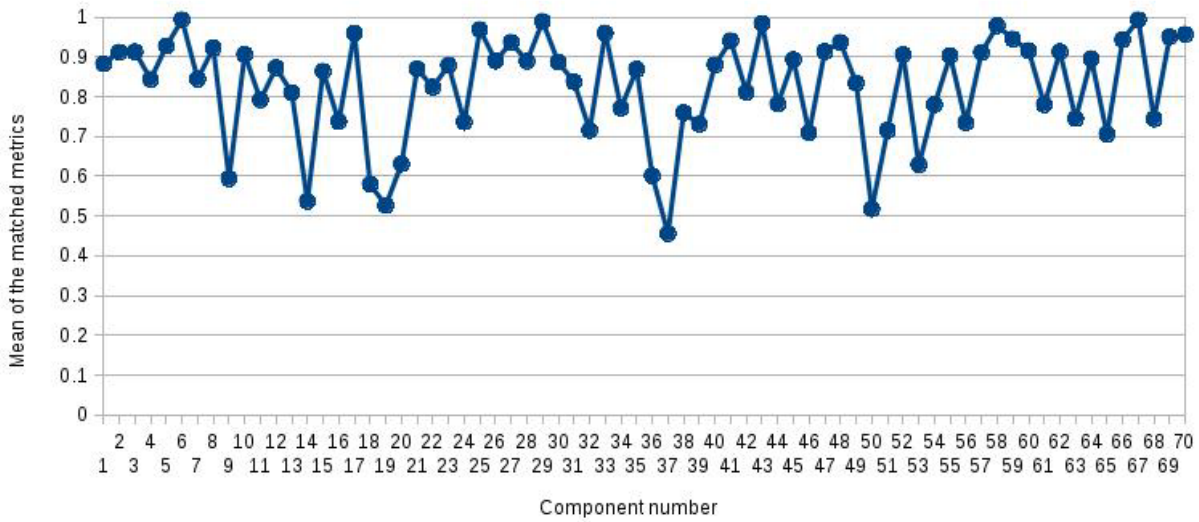

Appendix 7.2 . The reliability of each component in the most representative output across permutations for the delta frequency band.

Chapter 8

Appendix 8.1 – *Single band centered components identified using a higher dimensionality with a combined frequency TICA.*

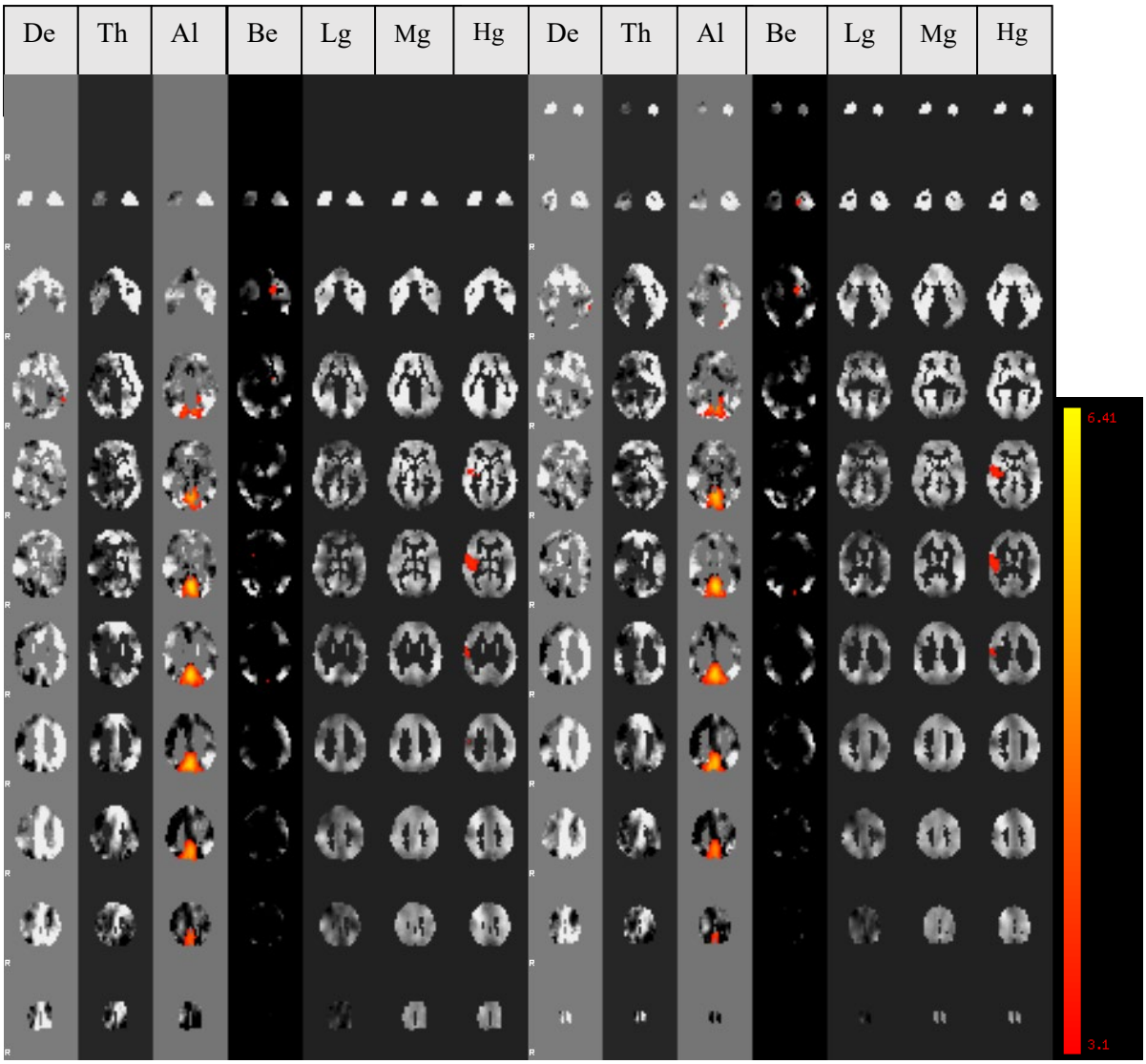

Appendix 8.1a *Alpha centered component*: A component with activation centred in Alpha was identified in a higher dimensionality (85) combined frequency output, that was not discoverable at a low dimensionality (20).

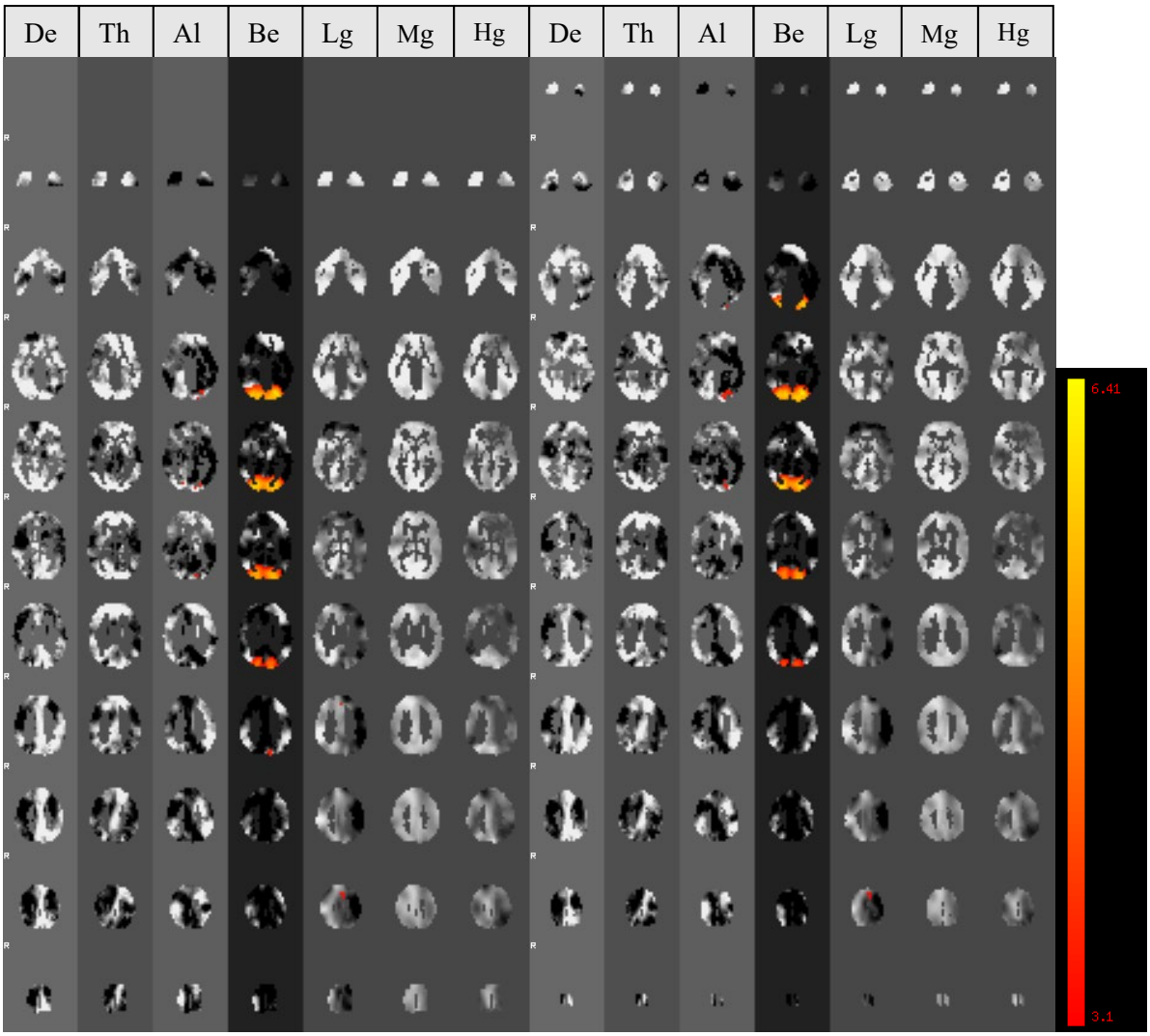

Appendix 8.1b *Beta centred component:* Components with activity centered in the beta frequency were not identified in a low dimensionality (20) TICA using combined frequency bands. However, they were generated when a higher dimensionality was used (85).

Chapter 9

Appendix 9.1 – *Example noise components from the cross-modality TICA output*

Noise components in cross-modality ICA were identified using the same guidance used for single frequency MEG and fMRI data (Griffanti, 2017). Example components that were excluded as noise due are displayed below in Appendix9.1a and b images.

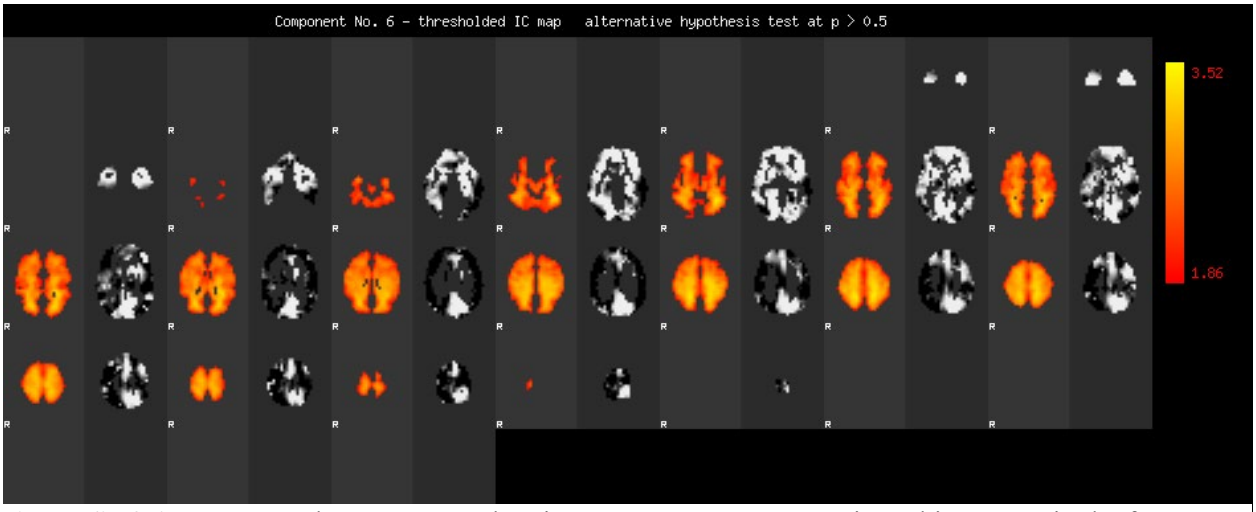

Appendix 9.1a. An example component showing a component representing white matter in the fMRI data. Here there is no cross-modality activity in the beta band.

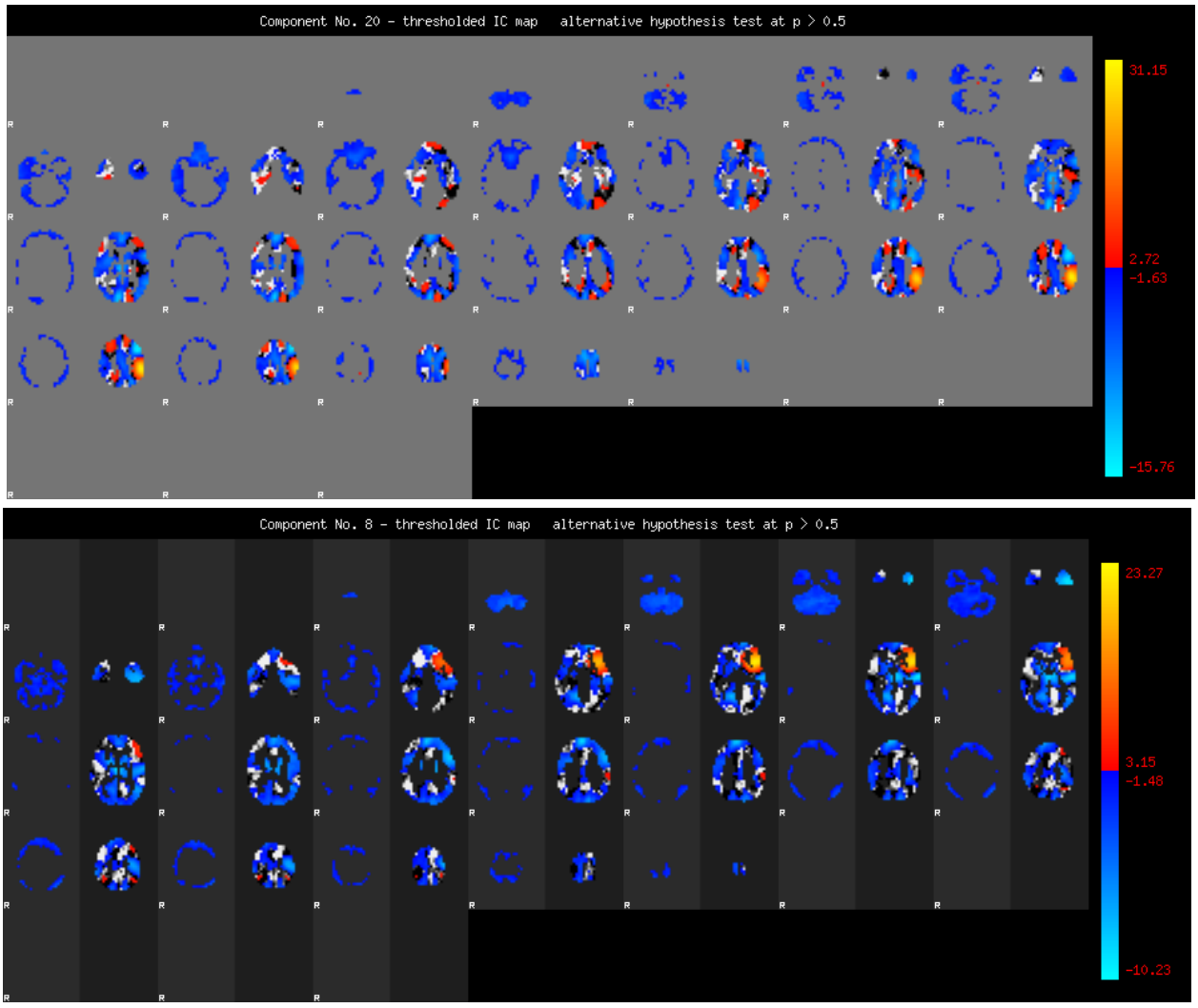

Appendix 9.1b Two example cross-frequency component showing some CSF artifact with 'ringing' pattern around the brain. (Top image shows slices of an MRI-Alpha component; bottom image is an MRI-Delta component). There is activity correlated with this in both the MEG bands.

Appendix 9.2 *– Full component outputs showing cross-modality activity in a merged modalities TICA.*

Appendix 9.2a: Component 1: Theta – Gamma and BOLD

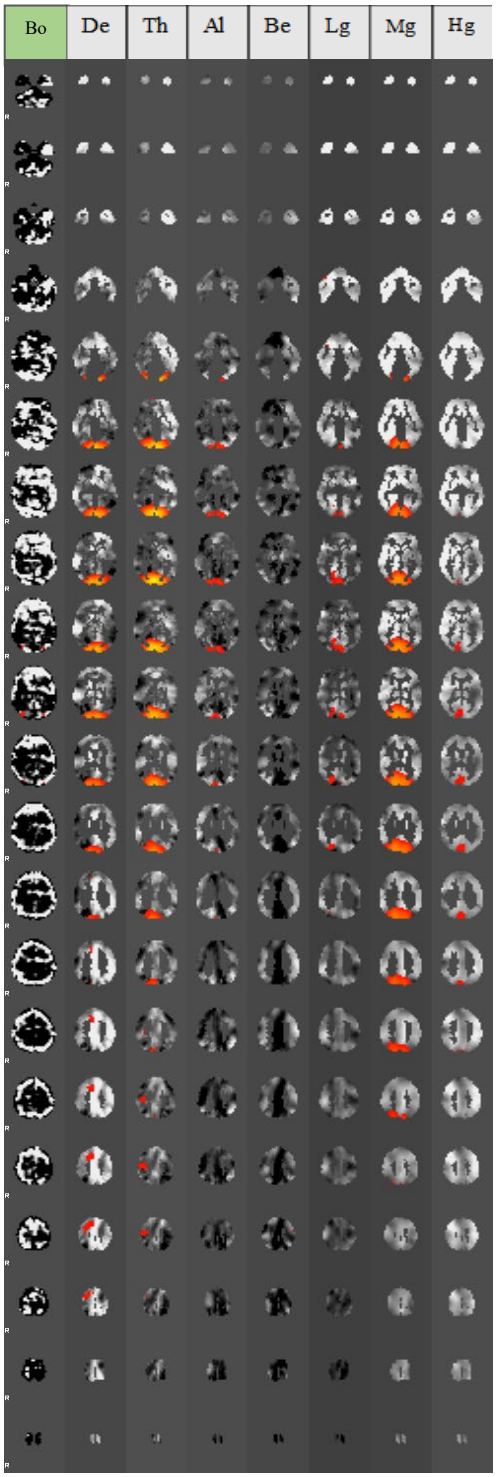

Appendix 9.2a. Theta- Gamma and BOLD correlation. The first cross modality component output shows correlation between BOLD, delta, theta and gamma.

Appendix 9.2b: *Component 2: Theta – Gamma and BOLD*

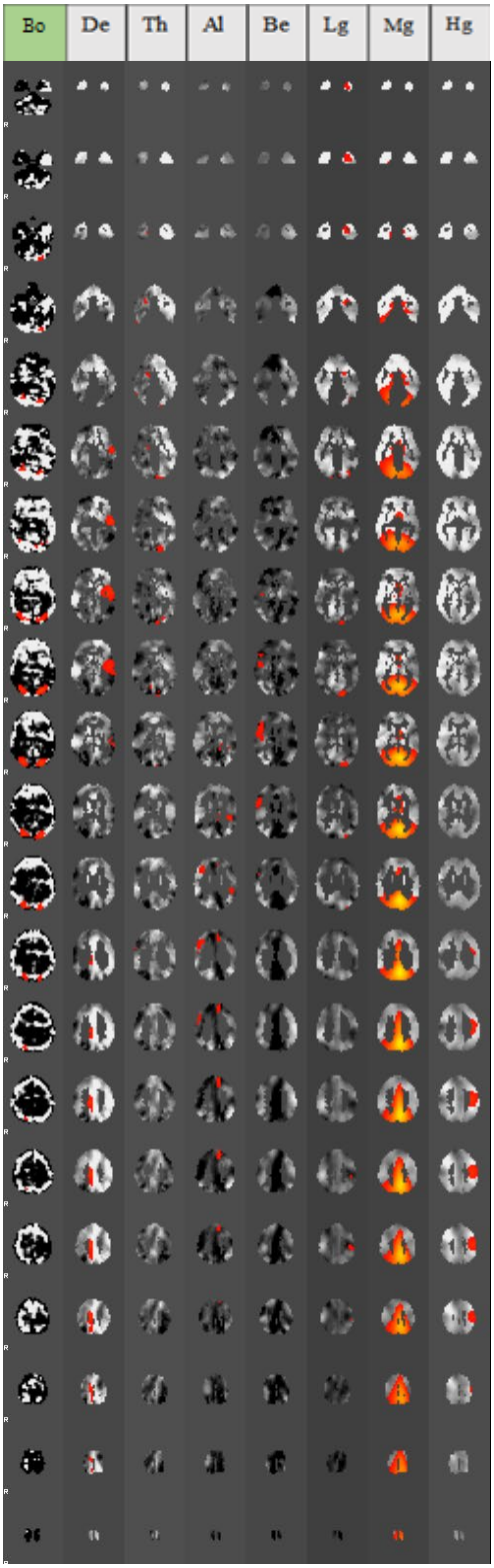

Appendix 9.2b. Theta- Gamma and BOLD correlation.
The second cross modality component output shows correlation between BOLD, delta, theta and gamma.

Appendix 9.2c: *Component 3: Beta – Gamma and BOLD*

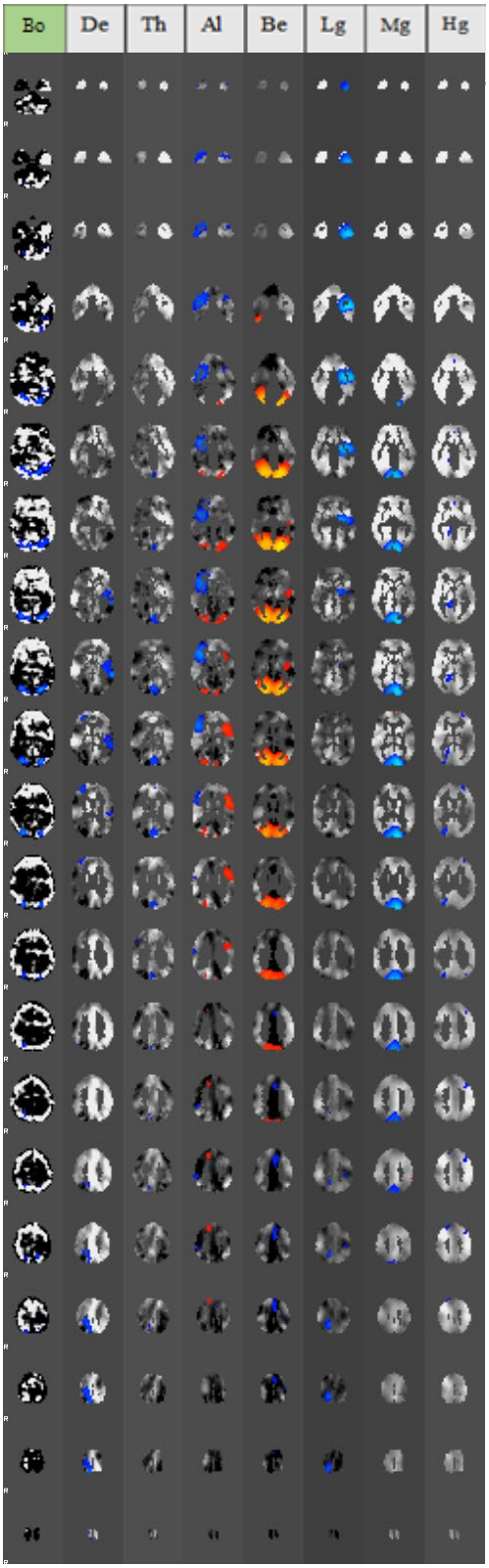

Appendix 9.2c. Beta- Gamma and BOLD correlation. The second cross modality component output shows anti-correlation between BOLD and beta in the occipital lobe. Activity in BOLD is paired with Gamma and theta.

Appendix 9.2d: *Component 2: Beta – Gamma and BOLD*

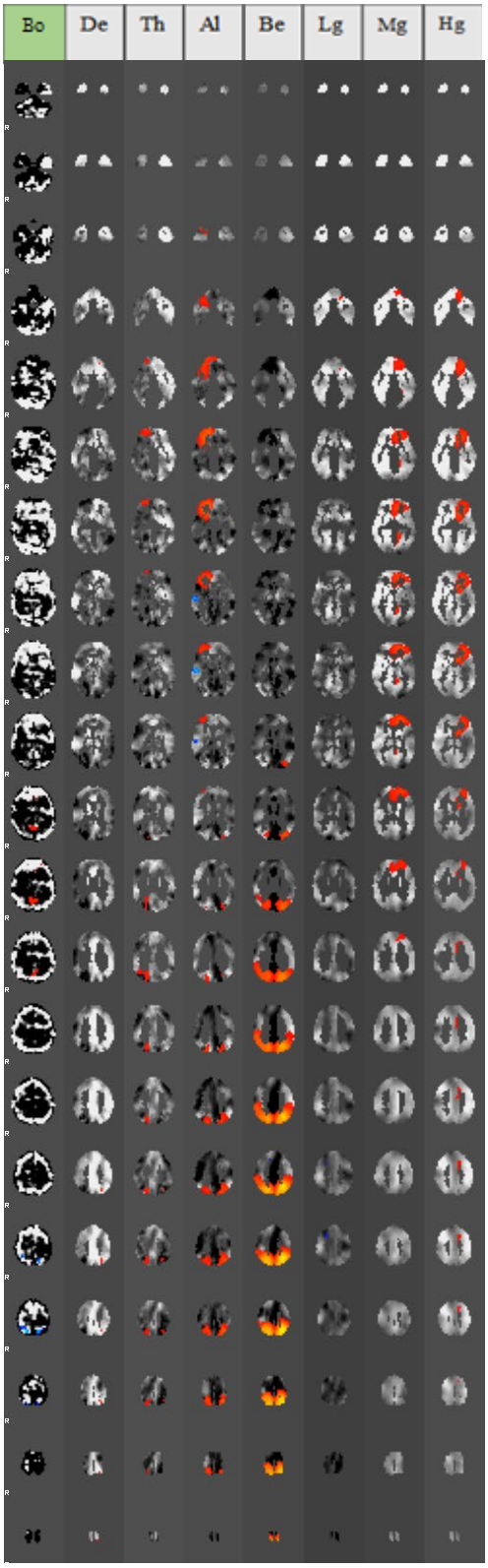

Appendix 9.2d. Beta - Gamma and BOLD correlation. The second cross modality component output shows anti-correlation between BOLD and beta frequency in the parietal lobe.

References

Allen, E. A., Erhardt, E. B., Wei, Y., Eichele, T., & Calhoun, V. D. (2012). Capturing inter-subject variability with group independent component analysis of fMRI data: a simulation study. *Neuroimage, 59(*4), 4141-4159.

Amano, K., Wandell, B. A., & Dumoulin, S. O. (2009). Visual field maps, population receptive field sizes, and visual field coverage in the human MT+ complex. *Journal of neurophysiology, 102*(5), 2704-2718.

Annese, J., Pitiot, A., Dinov, I. D., & Toga, A. W. (2004). A myelo-architectonic method for the structural classification of cortical areas. *Neuroimage, 21*(1), 15-26.

Arnoldussen, D. M., Goossens, J., & van den Berg, A. V. (2011). Adjacent visual representations of self-motion in different reference frames. *Proceedings of the National Academy of Sciences, 108*(28), 11668-11673.

Aoki, Y., Ishii, R., Pascual-Marqui, R. D., Canuet, L., Ikeda, S., Hata, M., ... & Iwase, M. (2015). Detection of EEG-resting state independent networks by eLORETA-ICA method. *Frontiers in human neuroscience, 9*, 31.

Artoni, F., Menicucci, D., Delorme, A., Makeig, S., & Micera, S. (2014). RELICA: a method for estimating the reliability of independent components. *NeuroImage, 103,* 391-400.

Attwell, D., Buchan, A. M., Charpak, S., Lauritzen, M., MacVicar, B. A., & Newman, E. A. (2010). Glial and neuronal control of brain blood flow. *Nature*, *468*(7321), 232.

Bannert, M. M., & Bartels, A. (2018). Human V4 Activity Patterns Predict Behavioral Performance in Imagery of Object Color. *Journal of Neuroscience*, 2307-17.

Bartels, A., & Zeki, S. (2004). The chronoarchitecture of the human brain—natural viewing conditions reveal a time-based anatomy of the brain. *Neuroimage, 22*(1), 419-433.

Bartels, A., & Zeki, S. (2005). The chronoarchitecture of the cerebral cortex. *Philosophical Transactions of the Royal Society of London B: Biological Sciences, 360*(1456), 733-750.

Bardi, L., Six, P., & Brass, M. (2017). Repetitive TMS of the temporo-parietal junction disrupts participant's expectations in a spontaneous Theory of Mind task. *Social cognitive and affective neuroscience, 12*(11), 1775-1782.

Battelli, L., Pascual-Leone, A., & Cavanagh, P. (2007). The 'when 'pathway of the right parietal lobe. *Trends in cognitive sciences, 11*(5), 204-210.

Bauer, M., Oostenveld, R., Peeters, M., & Fries, P. (2006). Tactile spatial attention enhances gamma-band activity in somatosensory cortex and reduces low-frequency activity in parieto-occipital areas. Journal of *Neuroscience, 26*(2), 490-501.

Bauer, M., Stenner, M. P., Friston, K. J., & Dolan, R. J. (2014). Attentional modulation of alpha/beta and gamma oscillations reflect functionally distinct processes. *Journal of Neuroscience, 34*(48), 16117-16125.

Beauchamp, M. S. (2015). The social mysteries of the superior temporal sulcus. *Trends in cognitive sciences, 19*(9), 489-490.

Beckers, G., & Zeki, S. (1995). The consequences of inactivating areas V1 and V5 on visual motion perception. *Brain*, *118*(1), 49-60.

Beckmann, C. F., DeLuca, M., Devlin, J. T., & Smith, S. M. (2005). Investigations into resting-state connectivity using independent component analysis. *Philosophical Transactions of the Royal Society of London B: Biological Sciences*, *360*(1457), 1001-1013.

Beckmann, C. F., & Smith, S. M. (2004). Probabilistic independent component analysis for functional magnetic resonance imaging. *IEEE transactions on medical imaging, 23*(2), 137-152.

Beckmann, C. F., & Smith, S. M. (2005). Tensorial extensions of independent component analysis for multisubject FMRI analysis. *Neuroimage, 25*(1), 294-311.

Beckmann, C. F., Mackay, C. E., Filippini, N., & Smith, S. M. (2009). Group comparison of resting-state FMRI data using multi-subject ICA and dual regression. *Neuroimage, 47*(Suppl 1), S148.

Benson, N. C., Butt, O. H., Brainard, D. H., & Aguirre, G. K. (2014). Correction of distortion in flattened representations of the cortical surface allows prediction of V1-V3 functional organization from anatomy. *PLoS computational biology, 10*(3), e1003538.

Benson, N. C., Butt, O. H., Datta, R., Radoeva, P. D., Brainard, D. H., & Aguirre, G. K. (2012). The retinotopic organization of striate cortex is well predicted by surface topology. *Current Biology*, *22*(21), 2081-2085.

Berger, H. (1929). Uber das Elektrenkephalogramm des Menschen. Arch. *Psychiat. Nerverkr. 87*, 527–570.

Betti, V., Della Penna, S., de Pasquale, F., Mantini, D., Marzetti, L., Romani, G. L., & Corbetta, M. (2013). Natural scenes viewing alters the dynamics of functional connectivity in the human brain. *Neuron*, *79*(4), 782-797.

Biswal, B. B., Kylen, J. V., & Hyde, J. S. (1997). Simultaneous assessment of flow and BOLD signals in resting-state functional connectivity maps. *NMR in Biomedicine*, *10*(4-5), 165-170.

Blanke, O., Spinelli, L., Thut, G., Michel, C. M., Perrig, S., Landis, T., & Seeck, M. (2000). Location of the human frontal eye field as defined by electrical cortical stimulation: anatomical, functional and electrophysiological characteristics. *Neuroreport, 11*(9), 1907-1913.

Bollimunta, A., Mo, J., Schroeder, C. E., & Ding, M. (2011). Neuronal mechanisms and attentional modulation of corticothalamic alpha oscillations. *Journal of Neuroscience, 31*(13), 4935-4943.

Bonnefond, M., Kastner, S., & Jensen, O. (2017). Communication between brain areas based on nested oscillations. *eneuro,* ENEURO-0153.

Boussaoud, D., Ungerleider, L. G., & Desimone, R. (1990). Pathways for motion analysis: cortical connections of the medial superior temporal and fundus of the superior temporal visual areas in the macaque. *Journal of Comparative Neurology*, *296*(3), 462-495.

Brennan, J., Nir, Y., Hasson, U., Malach, R., Heeger, D. J., & Pylkkänen, L. (2012). Syntactic structure building in the anterior temporal lobe during natural story listening. *Brain and language*, *120*(2), 163-173.

Bridge, H., Clare, S., Jenkinson, M., Jezzard, P., Parker, A. J., & Matthews, P. M. (2005). Independent anatomical and functional measures of the V1/V2 boundary in human visual cortex. *Journal of Vision, 5*(2), 1-1.

Brodmann, K. (1909). *Vergleichende Lokalisationslehre der Grosshirnrinde in ihren Prinzipien dargestellt auf Grund des Zellenbaues*. Barth.

Brookes, M. J., Woolrich, M., Luckhoo, H., Price, D., Hale, J. R., Stephenson, M. C., ... & Morris, P. G. (2011). Investigating the electrophysiological basis of resting state networks using magnetoencephalography. *Proceedings of the National Academy of Sciences,* 201112685.

Brovelli, A., Lachaux, J. P., Kahane, P., & Boussaoud, D. (2005). High gamma frequency oscillatory activity dissociates attention from intention in the human premotor cortex. *Neuroimage, 28(*1), 154-164.

Bullen, A. (2017). Movie-driven fMRI Reveals Network Asynchrony and Connectivity Alterations in Temporal Lobe Epilepsy. *University of Western Ontario, Electronic Thesis and Dissertation Repository.* https://ir.lib.uwo.ca/cgi/viewcontent.cgi?article=6720&context=etd

Bullier, J., Schall, J. D., & Morel, A. (1996). Functional streams in occipito-frontal connections in the monkey. *Behavioural brain research, 76*(1-2), 89-97.

Buzsáki, G., & Wang, X. J. (2012). Mechanisms of gamma oscillations. *Annual review of neuroscience, 35*, 203-225.

Cai, P., Chen, N., Zhou, T., Thompson, B., & Fang, F. (2014). Global versus local: double dissociation between MT+ and V3A in motion processing revealed using continuous theta burst transcranial magnetic stimulation. *Experimental brain research*, *232*(12), 4035-4041.

Calhoun, V. D., Adali, T., Hansen, L. K., Larsen, J., & Pekar, J. J. (2003). ICA of functional MRI data: an overview. In in *Proceedings of the International Workshop on Independent Component Analysis and Blind Signal Separation.*

Calhoun, V. D., Kiehl, K. A., & Pearlson, G. D. (2008). Modulation of temporally coherent brain networks estimated using ICA at rest and during cognitive tasks. *Human brain mapping*, *29*(7), 828-838.

Calhoun, V. D., Liu, J., & Adalı, T. (2009). A review of group ICA for fMRI data and ICA for joint inference of imaging, genetic, and ERP data. Neuroimage, 45(1), S163-S172.

Calhoun, V. D., Potluru, V. K., Phlypo, R., Silva, R. F., Pearlmutter, B. A., Caprihan, A., ... & Adalı, T. (2013). Independent component analysis for brain fMRI does indeed select for maximal independence. PloS one, 8(8), e73309.

Canolty, R. T., Edwards, E., Dalal, S. S., Soltani, M., Nagarajan, S. S., Kirsch, H. E., ... & Knight, R. T. (2006). High gamma power is phase-locked to theta oscillations in human neocortex. *Science, 313*(5793), 1626-1628.

Canolty, R. T., & Knight, R. T. (2010). The functional role of cross-frequency coupling. *Trends in cognitive sciences, 14*(11), 506-515.

Cardin, V., Hemsworth, L., & Smith, A. T. (2012). Adaptation to heading direction dissociates the roles of human MST and V6 in the processing of optic flow. Journal of neurophysiology, 108(3), 794-801.

Cardin, V., Sherrington, R., Hemsworth, L., & Smith, A. T. (2012). Human V6: functional characterisation and localisation. *PLoS One, 7*(10), e47685.

Cardin, V., & Smith, A. T. (2009). Sensitivity of human visual and vestibular cortical regions to egomotion-compatible visual stimulation. *Cerebral Cortex, 20*(8), 1964-1973.

Chang, W. T., Jääskeläinen, I. P., Belliveau, J. W., Huang, S., Hung, A. Y., Rossi, S., & Ahveninen, J. (2015). Combined MEG and EEG show reliable patterns of electromagnetic brain activity during natural viewing. *NeuroImage, 114*, 49-56.

Chelazzi, L., Miller, E. K., Duncan, J., & Desimone, R. (1993). A neural basis for visual search in inferior temporal cortex. *Nature, 363*(6427), 345.

Christoff, K., Gordon, A. M., Smallwood, J., Smith, R., & Schooler, J. W. (2009). Experience sampling during fMRI reveals default network and executive system contributions to mind wandering. *Proceedings of the National Academy of Sciences, 106*(21), 8719-8724.

Choi, E. Y., Yeo, B. T., & Buckner, R. L. (2012). The organization of the human striatum estimated by intrinsic functional connectivity. *Journal of neurophysiology*, *108*(8), 2242-2263.

Cichy, R. M., Pantazis, D., & Oliva, A. (2014). Resolving human object recognition in space and time. *Nature neuroscience, 17*(3), 455-462.

Clark, V. P., Courchesne, E., & Grafe, M. (1992). In vivo myeloarchitectonic analysis of human striate and extrastriate cortex using magnetic resonance imaging. *Cerebral Cortex, 2*(5), 417-424.

Clayton, M. S., Yeung, N., & Kadosh, R. C. (2015). The roles of cortical oscillations in sustained attention. *Trends in cognitive sciences*, *19*(4), 188-195.

Cohen D. (1972). Magnetoencephalography: detection of the brain's electrical activity with a superconducting magnetometer. *Science. 175* (4022), 664–66.

Collins, D. L., Neelin, P., Peters, T. M., & Evans, A. C. (1994). Automatic 3D intersubject registration of MR volumetric data in standardized Taliarach space. *Journal of computer assisted tomography, 18*(2), 192-205.

Condon, C. D., & Weinberger, N. M. (1991). Habituation produces frequency-specific plasticity of receptive fields in the auditory cortex. *Behavioral neuroscience, 105*(3), 416.

Crone, N. E., Sinai, A., & Korzeniewska, A. (2006). High-frequency gamma oscillations and human brain mapping with electrocorticography. *Progress in brain research, 159,* 275-295.

Culham, J., He, S., Dukelow, S., & Verstraten, F. A. (2001). Visual motion and the human brain: what has neuroimaging told us? *Acta psychologica*, *107*(1-3), 69-94.

Damoiseaux, J. S., Rombouts, S. A. R. B., Barkhof, F., Scheltens, P., Stam, C. J., Smith, S. M., & Beckmann, C. F. (2006). Consistent resting-state networks across healthy subjects. *Proceedings of the national academy of sciences, 103*(37), 13848-13853.

De Pasquale, F., Della Penna, S., Sporns, O., Romani, G. L., & Corbetta, M. (2016). A dynamic core network and global efficiency in the resting human brain. *Cerebral Cortex*, *26*(10), 4015-4033.

Degwekar, A. A., & Wyatt, D. (2013). U.S. Patent No. 8,358,262. Washington, DC: U.S. Patent and Trademark Office.

DeLuca, G. C., Yates, R. L., Beale, H., & Morrow, S. A. (2015). Cognitive impairment in multiple sclerosis: clinical, radiologic and pathologic insights. *Brain Pathology*, *25*(1), 79-98.

Demiralp, T., Bayraktaroglu, Z., Lenz, D., Junge, S., Busch, N. A., Maess, B., ... & Herrmann, C. S. (2007). Gamma amplitudes are coupled to theta phase in human EEG during visual perception. *International journal of psychophysiology, 64*(1), 24-30.

Desimone, R., & Duncan, J. (1995). Neural mechanisms of selective visual attention. *Annual review of neuroscience*, *18*(1), 193-222.

Devonshire, I. M., Papadakis, N. G., Port, M., Berwick, J., Kennerley, A. J., Mayhew, J. E. W., & Overton, P. G. (2012). Neurovascular coupling is brain region-dependent. *Neuroimage, 59*(3), 1997-2006. doi: https://doi.org/10.1016/j.neuroimage.2011.09.050.

De Pisapia, N., Bacci, F., Parrott, D., & Melcher, D. (2016). Brain networks for visual creativity: a functional connectivity study of planning a visual artwork. *Scientific reports, 6,* 39185.

Dmochowski, J. P., Bezdek, M. A., Abelson, B. P., Johnson, J. S., Schumacher, E. H., & Parra, L. C. (2014). Audience preferences are predicted by temporal reliability of neural processing. *Nature communications, 5*, 4567.

Donner, T. H., & Siegel, M. (2011). A framework for local cortical oscillation patterns. *Trends in cognitive sciences, 15*(5), 191-199.

Downing, P. E., Jiang, Y., Shuman, M., & Kanwisher, N. (2001). A cortical area selective for visual processing of the human body. *Science, 293*(5539), 2470-2473.

Du, W., Ma, S., Fu, G. S., Calhoun, V. D., & Adali, T. (2014, May). A novel approach for assessing reliability of ICA for FMRI analysis. In Acoustics, Speech and Signal Processing (ICASSP), 2014 *IEEE International Conference* (pp. 2084-2088). IEEE.

Duann, J. R., Jung, T. P., Makeig, S., & Sejnowski, T. J. (2003, April). Consistency of infomax ICA decomposition of functional brain imaging data. In *Proceedings of the 4th International Symposium on Independent Component Analysis and Blind Signal Separation* (ICA 2003). Nara, Japan (pp. 289-294).

Duffy, C. J., & Wurtz, R. H. (1991). Sensitivity of MST neurons to optic flow stimuli. I. A continuum of response selectivity to large-field stimuli. *Journal of neurophysiology*, *65*(6), 1329-1345.

Dukelow, S. P., DeSouza, J. F., Culham, J. C., van den Berg, A. V., Menon, R. S., & Vilis, T. (2001). Distinguishing subregions of the human MT+ complex using visual fields and pursuit eye movements. *Journal of neurophysiology, 86*(4), 1991-2000.

Dumoulin, S. O., Bittar, R. G., Kabani, N. J., Baker Jr, C. L., Le Goualher, G., Pike, G. B., & Evans, A. C. (2000). A new anatomical landmark for reliable identification of human area V5/MT: a quantitative analysis of sulcal patterning. *Cerebral cortex, 10*(5), 454-463.

Dumoulin, S. O., & Wandell, B. A. (2008). Population receptive field estimates in human visual cortex. *Neuroimage, 39*(2), 647-660.

Duncan, J., & Owen, A. M. (2000). Common regions of the human frontal lobe recruited by diverse cognitive demands. *Trends in neurosciences, 23*(10), 475-483.

Düzel, E., Habib, R., Schott, B., Schoenfeld, A., Lobaugh, N., McIntosh, A. R., ... & Heinze, H. J. (2003). A multivariate, spatiotemporal analysis of electromagnetic time-frequency data of recognition memory. *Neuroimage, 18*(2), 185-197.

Engel, A. K., Kreiter, A. K., König, P., & Singer, W. (1991). Synchronization of oscillatory neuronal responses between striate and extrastriate visual cortical areas of the cat. *Proceedings of the National Academy of Sciences*, *88*(14), 6048-6052.

Esposito, F., Scarabino, T., Hyvarinen, A., Himberg, J., Formisano, E., Comani, S., ... & Di Salle, F. (2005). Independent component analysis of fMRI group studies by self-organizing clustering. *Neuroimage, 25*(1), 193-205.

Euston, D. R., Gruber, A. J., & McNaughton, B. L. (2012). The role of medial prefrontal cortex in memory and decision making. *Neuron, 76(*6), 1057-1070.

Fabiani, M., Gordon, B. A., Maclin, E. L., Pearson, M. A., Brumback-Peltz, C. R., Low, K. A., ... & Gratton, G. (2014). Neurovascular coupling in normal aging: a combined optical, ERP and fMRI study. Neuroimage, 85, 592-607.

Fischer, E., Bülthoff, H. H., Logothetis, N. K., & Bartels, A. (2012). Human areas V3A and V6 compensate for self-induced planar visual motion. *Neuron, 73*(6), 1228-1240.

Fixot, R.S.: American Journal of Ophthalmology (1957) *in* Berger, A., Vokalova, A., Maly, F., & Poulova, P. (2017, August). Google glass used as assistive technology its utilization for blind and visually impaired people. *International Conference on Mobile Web and Information Systems* (pp. 70-82). Springer, Cham.

Formisano, E., Esposito, F., Di Salle, F., & Goebel, R. (2004). Cortex-based independent component analysis of fMRI time series. *Magnetic resonance imaging, 22*(10), 1493-1504.

Foxe, J. J., & Snyder, A. C. (2011). The role of alpha-band brain oscillations as a sensory suppression mechanism during selective attention. *Frontiers in psychology, 2*, 154.

Friston, K.J. et al. (1995) Characterizing evoked hemodynamics with fMRI. *Neuroimage 2*, 157–165

Friston, K.J. et al. (1995) Analysis of fMRI time-series revisited. *Neuroimage 2*, 45–53

Gallagher, H. L., Happé, F., Brunswick, N., Fletcher, P. C., Frith, U., & Frith, C. D. (2000). Reading the mind in cartoons and stories: an fMRI study of 'theory of mind' in verbal and nonverbal tasks. *Neuropsychologia, 38*(1), 11-21.

Galletti, C., Battaglini, P. P., & Fattori, P. (1990). 'Real-motion' cells in area V3A of macaque visual cortex. *Experimental Brain Research*, *82*(1), 67-76.

Gandhi, S. P., Heeger, D. J., & Boynton, G. M. (1999). Spatial attention affe*cts brain activity in human primary visual cortex.* Proceedings of the National Academy of Sciences, 96(6), 3314-3319.

Gaymard, B., Ploner, C. J., Rivaud, S., Vermersch, A. I., & Pierrot-Deseilligny, C. (1998). Cortical control of saccades. *Experimental Brain Research, 123*(1-2), 159-163.

Genç, E., Schölvinck, M. L., Bergmann, J., Singer, W., & Kohler, A. (2016). Functional connectivity patterns of visual cortex reflect its anatomical organization. *Cerebral cortex*, *26*(9), 3719-3731.

General Electric Company (2017). Milwaukee, Wisconsin.

Girouard, H., & Iadecola, C. (2006). Neurovascular coupling in the normal brain and in hypertension, stroke, and Alzheimer disease. *Journal of applied physiology*, *100*(1), 328-335.

Glasser, M. F., & Van Essen, D. C. (2011). Mapping human cortical areas in vivo based on myelin content as revealed by T1-and T2-weighted MRI. *Journal of Neuroscience, 31*(32), 11597-11616.

Goebel, R., Esposito, F., & Formisano, E. (2006). Analysis of functional image analysis contest (FIAC) data with brainvoyager QX: From single-subject to cortically aligned group general linear model analysis and self-organizing group independent component analysis. *Human brain mapping, 27*(5), 392-401

Goldstein, R. B., Woods, R. L., & Peli, E. (2007). Where people look when watching movies: Do all viewers look at the same place? *Computers in biology and medicine, 37*(7), 957-964.

Golland, Y., Bentin, S., Gelbard, H., Benjamini, Y., Heller, R., Nir, Y., ... & Malach, R. (2006). Extrinsic and intrinsic systems in the posterior cortex of the human brain revealed during natural sensory stimulation. *Cerebral cortex*, *17*(4), 766-777.

Goodale, M. A., & Milner, A. D. (1992). Separate visual pathways for perception and action. *Trends in neurosciences*, *15*(1), 20-25.

Grandchamp, R., Braboszcz, C., Makeig, S., & Delorme, A. (2012, August). Stability of ICA decomposition across within-subject EEG datasets. In Engineering in Medicine and Biology Society (EMBC), 2012 *Annual International Conference of the IEEE* (pp. 6735-6739). IEEE.

Greene, D. J., Koller, J. M., Hampton, J. M., Wesevich, V., Van, A. N., Nguyen, A. L., ... & Shimony, J. S. (2018). Behavioral interventions for reducing head motion during MRI scans in children. Neuroimage, 171, 234-245.

Greenlee, M. W. (2000). Human cortical areas underlying the perception of optic flow: brain imaging studies. *International review of neurobiology, 44*, 269-292.

Grefkes, C., & Fink, G. R. (2005). The functional organization of the intraparietal sulcus in humans and monkeys. *Journal of anatomy*, *207*(1), 3-17.

Griffanti, L., Douaud, G., Bijsterbosch, J., Evangelisti, S., Alfaro-Almagro, F., Glasser, M. F., ... & Beckmann, C. F. (2017). Hand classification of fMRI ICA noise components. *NeuroImage, 154*, 188-205.

Grill-Spector, K., & Malach, R. (2004). The human visual cortex. *Annu. Rev. Neurosci.*, *27*, 649-677.

Grossman, E. D., & Blake, R. (2002). Brain areas active during visual perception of biological motion. *Neuron*, *35*(6), 1167-1175.

Gu, H., Salmeron, B. J., Ross, T. J., Geng, X., Zhan, W., Stein, E. A., & Yang, Y. (2010). Mesocorticolimbic circuits are impaired in chronic cocaine users as demonstrated by resting-state functional connectivity. *Neuroimage*, *53*(2), 593-601.

Gusnard, D. A., Akbudak, E., Shulman, G. L., & Raichle, M. E. (2001). Medial prefrontal cortex and self-referential mental activity: relation to a default mode of brain function. *Proceedings of the National Academy of Sciences, 98*(7), 4259-4264.

Haak, K. V., Winawer, J., Harvey, B. M., Renken, R., Dumoulin, S. O., Wandell, B. A., & Cornelissen, F. W. (2013). Connective field modeling. *Neuroimage, 66*, 376-384.

Händel, B., & Haarmeier, T. (2009). Cross-frequency coupling of brain oscillations indicates the success in visual motion discrimination. *Neuroimage, 45*(3), 1040-1046.

Harrison, A., Jolicoeur, P., & Marois, R. (2010). "What" and "where" in the intraparietal sulcus: an fMRI study of object identity and location in visual short-term memory. *Cerebral Cortex*, *20*(10), 2478-2485.

Hasson, U., Nir, Y., Levy, I., Fuhrmann, G., & Malach, R. (2004). Intersubject synchronization of cortical activity during natural vision. *Science, 303*(5664), 1634-1640.

Hasson, U., Malach, R., & Heeger, D. J. (2010). Reliability of cortical activity during natural stimulation. *Trends in cognitive sciences, 14*(1), 40-48.

Hampson, M., Olson, I. R., Leung, H. C., Skudlarski, P., & Gore, J. C. (2004). Changes in functional connectivity of human MT/V5 with visual motion input. *Neuroreport, 15*(8), 1315-1319.

Herrmann, C. S., Fründ, I., & Lenz, D. (2010). Human gamma-band activity: a review on cognitive and behavioral correlates and network models. *Neuroscience & Biobehavioral Reviews*, *34*(7), 981-992.

Herrmann, C. S., Munk, M. H., & Engel, A. K. (2004). Cognitive functions of gamma-band activity: memory match and utilization. *Trends in cognitive sciences*, *8*(8), 347-355.

Hewson-Stoate, N., Jones, M., Martindale, J., Berwick, J., & Mayhew, J. (2005). Further nonlinearities in neurovascular coupling in rodent barrel cortex. *Neuroimage, 24*(2), 565-574. doi: https://doi.org/10.1016/j.neuroimage.2004.08.040

Hillebrand, A., Barnes, G. R., Bosboom, J. L., Berendse, H. W., & Stam, C. J. (2012). Frequency-dependent functional connectivity within resting-state networks: an atlas-based MEG beamformer solution. *Neuroimage, 59*(4), 3909-3921.

Hinds, O. P., Rajendran, N., Polimeni, J. R., Augustinack, J. C., Wiggins, G., Wald, L. L., ... & Fischl, B. (2008). Accurate prediction of V1 location from cortical folds in a surface coordinate system. *Neuroimage, 39*(4), 1585-1599.

Holmes, G. M. (1945). Ferrier Lecture-The organization of the visual cortex in man. *Proc. R. Soc. Lond. B*, *132*(869), 348-361.

Holz, E. M., Glennon, M., Prendergast, K., & Sauseng, P. (2010). Theta–gamma phase synchronization during memory matching in visual working memory. *Neuroimage, 52*(1), 326-335.

Huk, A. C., Dougherty, R. F., & Heeger, D. J. (2002). Retinotopy and functional subdivision of human areas MT and MST. *Journal of Neuroscience*, *22*(16), 7195-7205.

Igarashi, J., Isomura, Y., Arai, K., Harukuni, R., & Fukai, T. (2013). A θ–γ oscillation code for neuronal coordination during motor behavior. *Journal of Neuroscience, 33*(47), 18515-18530.

Ishai, A., Ungerleider, L. G., Martin, A., Schouten, J. L., & Haxby, J. V. (1999). Distributed representation of objects in the human ventral visual pathway. *Proceedings of the National Academy of Sciences*, *96*(16), 9379-9384.

Iwamura, Y. (1998). Hierarchical somatosensory processing. *Current opinion in neurobiology*, *8*(4), 522-528.

Jääskeläinen, I. P., Koskentalo, K., Balk, M. H., Autti, T., Kauramäki, J., Pomren, C., & Sams, M. (2008). Inter-subject synchronization of prefrontal cortex hemodynamic activity during natural viewing. *The open neuroimaging journal*, 2, 14.

Jenkinson, M., Beckmann, C.F., Behrens, T.E., Woolrich, M.W. & Smith, S.M. (2012). FSL. *NeuroImage, 62*, 782-90.

Jensen, O., Bonnefond, M., Marshall, T. R., & Tiesinga, P. (2015). Oscillatory mechanisms of feedforward and feedback visual processing. *Trends in neurosciences*, *38*(4), 192-194.

Jensen, O., & Colgin, L. L. (2007). Cross-frequency coupling between neuronal oscillations. *Trends in cognitive sciences, 11*(7), 267-269.

Jensen, O., Gips, B., Bergmann, T. O., & Bonnefond, M. (2014). Temporal coding organized by coupled alpha and gamma oscillations prioritize visual processing. *Trends in neurosciences*, *37*(7), 357-369.

Jo, H. J., Saad, Z. S., Simmons, W. K., Milbury, L. A., & Cox, R. W. (2010). Mapping sources of correlation in resting state FMRI, with artifact detection and removal. *Neuroimage, 52*(2), 571-582.

Jung, T. P., Makeig, S., Lee, T. W., McKeown, M. J., Brown, G., Bell, A. J., & Sejnowski, T. J. (2000, June). Independent component analysis of biomedical signals. In *Proc. Int. Workshop on Independent Component Analysis and Signal Separation* (pp. 633-644).

Kanwisher, N. (2010). Functional specificity in the human brain: a window into the functional architecture of the mind. *Proceedings of the National Academy of Sciences, 107*(25), 11163-11170.

Kanwisher, N., McDermott, J., & Chun, M. M. (1997). The fusiform face area: a module in human extrastriate cortex specialized for face perception. *Journal of neuroscience*, *17*(11), 4302-4311.

Kayser, C., Kim, M., Ugurbil, K., Kim, D. S., & König, P. (2004). A comparison of hemodynamic and neural responses in cat visual cortex using complex stimuli. *Cerebral Cortex*, *14*(8), 881-891.

Klaver, P., Lichtensteiger, J., Bucher, K., Dietrich, T., Loenneker, T., & Martin, E. (2008). Dorsal stream development in motion and structure-from-motion perception. *Neuroimage*, *39*(4), 1815-1823.

Kliemann, D., Richardson, H., Anzellotti, S., Ayyash, D., Haskins, A. J., Gabrieli, J. D., & Saxe, R. R. (2018). Cortical responses to dynamic emotional facial expressions generalize across stimuli, and are sensitive to task-relevance, in adults with and without Autism. *Cortex, 103*, 24-43.

Klimesch, W., Sauseng, P., & Hanslmayr, S. (2007). EEG alpha oscillations: the inhibition–timing hypothesis. *Brain research reviews, 53*(1), 63-88.

Komatsu, H., & Wurtz, R. H. (1988). Relation of cortical areas MT and MST to pursuit eye movements. I. Localization and visual properties of neurons. *Journal of Neurophysiology*, *60*(2), 580-603.

Kriegeskorte, N., Mur, M., & Bandettini, P. (2008). Representational similarity analysis–connecting the branches of systems neuroscience. *Frontiers in systems neuroscience, 2.*

Kragel, P. A., Kano, M., Van Oudenhove, L., Ly, H. G., Dupont, P., Rubio, A., ... & Ceko, M. (2018). Generalizable representations of pain, cognitive control, and negative emotion in medial frontal cortex. *Nature neuroscience, 1*.

Kubit, B., & Jack, A. I. (2013). Rethinking the role of the rTPJ in attention and social cognition in light of the opposing domains hypothesis: findings from an ALE-based meta-analysis and resting-state functional connectivity. *Frontiers in human neuroscience*, *7*, 323.

Lagae, L., Maes, H., Raiguel, S., Xiao, D. K., & Orban, G. A. (1994). Responses of macaque STS neurons to optic flow components: a comparison of areas MT and MST. *Journal of Neurophysiology*, *71*(5), 1597-1626.

Lankinen, K., Saari, J., Hlushchuk, Y., Tikka, P., Parkkonen, L., Hari, R., & Koskinen, M. (2018). Consistency and similarity of MEG- and fMRI-signal time courses during movie viewing. *Neuroimage.* doi: https://doi.org/10.1016/j.neuroimage.2018.02.045.

Li, Y. O., Adalı, T., & Calhoun, V. D. (2007). Estimating the number of independent components for functional magnetic resonance imaging data. *Human brain mapping, 28*(11), 1251-1266.

Lowe, M. J., Dzemidzic, M., Lurito, J. T., Mathews, V. P., & Phillips, M. D. (2000). Correlations in low-frequency BOLD fluctuations reflect cortico-cortical connections. *Neuroimage, 12*(5), 582-587.

Logothetis, N. K., Pauls, J., Augath, M., Trinath, T., & Oeltermann, A. (2001). Neurophysiological investigation of the basis of the fMRI signal. *Nature*, *412*(6843), 150.

Lundqvist, M., Herman, P., Warden, M. R., Brincat, S. L., & Miller, E. K. (2017). Gamma and beta bursts during working memory read-out suggest roles in its volitional control. *bioRxiv,* 122598.

Magazzini, L., & Singh, K. D. (2018). Spatial attention modulates visual gamma oscillations across the human ventral stream. *NeuroImage*, *166*, 219-229.

Manenti, R., Cappa, S. F., Rossini, P. M., & Miniussi, C. (2008). The role of the prefrontal cortex in sentence comprehension: an rTMS study. *cortex*, *44*(3), 337-344.

Mantini, D., Penna, S. D., Marzetti, L., De Pasquale, F., Pizzella, V., Corbetta, M., & Romani, G. L. (2011). A signal-processing pipeline for magnetoencephalography resting-state networks. *Brain connectivity, 1*(1), 49-59.

Mantini, D., Perrucci, M. G., Del Gratta, C., Romani, G. L., & Corbetta, M. (2007). Electrophysiological signatures of resting state networks in the human brain. *Proceedings of the National Academy of Sciences, 104*(32), 13170-13175.

Marsman, J. B. C., Renken, R., Haak, K. V., & Cornelissen, F. W. (2013). Linking cortical visual processing to viewing behaviour using fMRI. *Frontiers in systems neuroscience*, *7*, 109.

Mayhugh, R. E., Moussa, M. N., Simpson, S. L., Lyday, R. G., Burdette, J. H., Porrino, L. J., & Laurienti, P. J. (2016). Moderate-heavy alcohol consumption lifestyle in older adults is associated with altered central executive network community structure during cognitive task. *PloS one, 11*(8), e0160214.

Mazaheri, A., van Schouwenburg, M. R., Dimitrijevic, A., Denys, D., Cools, R., & Jensen, O. (2014). Region-specific modulations in oscillatory alpha activity serve to facilitate processing in the visual and auditory modalities. *Neuroimage*, *87*, 356-362.

McKeefry, D. J., Burton, M. P., & Morland, A. B. (2010). The contribution of human cortical area V3A to the perception of chromatic motion: a transcranial magnetic stimulation study. European Journal of Neuroscience, 31(3), 575-584.

McKeefry, D. J., Burton, M. P., Vakrou, C., Barrett, B. T., & Morland, A. B. (2008). Induced deficits in speed perception by transcranial magnetic stimulation of human cortical areas V5/MT+ and V3A. *Journal of Neuroscience*, *28*(27), 6848-6857.

McKeown, M.J. Deterministic and stochastic features of fMRI data: Implications for data averaging. in Exploratory Analysis and Data Modeling in Functional Neuroimaging (Eds Sommer, F.T. & Wichert, A.) 63 (*The MIT Press, Cambridge,* Massachusetts, 2002). Accessed on 08.11.2017 using https://books.google.co.uk/

McKeown, M. J., Makeig, S., Brown, G. G., Jung, T. P., Kindermann, S. S., Bell, A. J., & Sejnowski, T. J. (1998). Analysis of fMRI data by blind separation into independent spatial components. *Human brain mapping*, *6*(3), 160-188.

McKeown, M. J., Varadarajan, V., Huettel, S., & McCarthy, G. (2002). Deterministic and stochastic features of fMRI data: implications for analysis of event-related experiments. Journal of neuroscience methods, 118(2), 103-113.

Meinecke, F. C., Ziehe, A., Kawanabe, M., & Müller, K. R. (2002). Estimating the reliability of ICA projections. InAdvances in Neural Information Processing Systems (pp. 1181-1188).

Merker, B. (2013). Cortical gamma oscillations: the functional key is activation, not cognition. Neuroscience & Biobehavioral Reviews, 37(3), 401-417.

Michalareas, G., Vezoli, J., Van Pelt, S., Schoffelen, J. M., Kennedy, H., & Fries, P. (2016). Alpha-beta and gamma rhythms subserve feedback and feedforward influences among human visual cortical areas. Neuron, 89(2), 384-397.

Mikellidou, K., Frijia, F., Montanaro, D., Greco, V., Burr, D. C., & Morrone, M. C. (2018). Cortical BOLD responses to moderate-and high-speed motion in the human visual cortex. *Scientific reports*, *8*(1), 8357.

Miller, K. J., Hermes, D., Honey, C. J., Sharma, M., Rao, R. P., Den Nijs, M., ... & Makeig, S. (2010). Dynamic modulation of local population activity by rhythm phase in human occipital cortex during a visual search task. Frontiers in human neuroscience, 4, 197.

Milner, A. D., & Goodale, M. A. (2008). Two visual systems re-viewed. *Neuropsychologia*, *46*(3), 774-785.

Milz, P., Pascual-Marqui, R. D., Lehmann, D., & Faber, P. L. (2016). Modalities of thinking: State and trait effects on cross-frequency functional independent brain networks. *Brain topography*, *29*(3), 477-490.

Minka, T. P. (2001). Automatic choice of dimensionality for PCA. In Advances in neural information processing systems (pp. 598-604).

Mishkin, M., Ungerleider, L. G., & Macko, K. A. (1983). Object vision and spatial vision: two cortical pathways. *Trends in neurosciences*, *6*, 414-417.

Mitchell, J. P., Banaji, M. R., & MacRae, C. N. (2005). The link between social cognition and self-referential thought in the medial prefrontal cortex. Journal of cognitive neuroscience, 17(8), 1306-1315.

Miyashita, Y. (1993). Inferior temporal cortex: where visual perception meets memory. *Annual review of neuroscience*, *16*(1), 245-263.

Moran, J., & Desimone, R. (1985). Selective attention gates visual processing in the extrastriate cortex. Science, 229(4715), 782-784.

Motter, B. C. (1994). Neural correlates of attentive selection for color or luminance in extrastriate area V4. Journal of Neuroscience, 14(4), 2178-2189.

Muller, L., Chavane, F., Reynolds, J., & Sejnowski, T. J. (2018). Cortical travelling waves: mechanisms and computational principles. *Nature Reviews Neuroscience*.

Mukamel, R., Gelbard, H., Arieli, A., Hasson, U., Fried, I., & Malach, R. (2005). Coupling between neuronal firing, field potentials, and FMRI in human auditory cortex. Science, 309(5736), 951-954.

Naci, L., Cusack, R., Anello, M., & Owen, A. M. (2014). A common neural code for similar conscious experiences in different individuals. Proceedings of the National Academy of Sciences, 111(39), 14277-14282.

Nishimoto, S., & Gallant, J. L. (2011). A three-dimensional spatiotemporal receptive field model explains responses of area MT neurons to naturalistic movies. *Journal of Neuroscience*, *31*(41), 14551-14564.

Norman, L. J., Heywood, C. A., & Kentridge, R. W. (2017). Texture segmentation without human V4. *Visual cognition*, *25*(1-3), 184-195.

Nugent, A. C., Luber, B., Carver, F. W., Robinson, S. E., Coppola, R., & Zarate, C. A. (2017). Deriving frequency-dependent spatial patterns in MEG-derived resting state sensorimotor network: A novel multiband ICA technique. Human brain mapping, 38(2), 779-791.

Nybakken, G., Quigley, M., Moritz, C., Cordes, D., Haughton, V., & Meyerand, M. (2002). Test-retest precision of functional magnetic resonance imaging processed with independent component analysis. Neuroradiology, 44(5), 403-406.

Ohlendorf, S., Kimmig, H., Glauche, V., & Haller, S. (2007). Gaze pursuit,'attention pursuit'and their effects on cortical activations. *European Journal of Neuroscience*, *26*(7), 2096-2108.

Osipova, D., Takashima, A., Oostenveld, R., Fernández, G., Maris, E., & Jensen, O. (2006). Theta and gamma oscillations predict encoding and retrieval of declarative memory. Journal of neuroscience, 26(28), 7523-7531.

Palva, J. M., & Palva, S. (2017). Functional integration across oscillation frequencies by cross-frequency phase synchronization. *European Journal of Neuroscience*.

Pérez-González, D., Malmierca, M. S., & Covey, E. (2005). Novelty detector neurons in the mammalian auditory midbrain. European Journal of Neuroscience, 22(11), 2879-2885.

Petit, L., & Haxby, J. V. (1999). Functional anatomy of pursuit eye movements in humans as revealed by fMRI. *Journal of Neurophysiology*, *82*(1), 463-471.

Pitzalis, S., Fattori, P., & Galletti, C. (2013). The functional role of the medial motion area V6. *Frontiers in behavioral neuroscience, 6,* 91.

Pitzalis, S., Bozzacchi, C., Bultrini, A., Fattori, P., Galletti, C., & Di Russo, F. (2013a). Parallel motion signals to the medial and lateral motion areas V6 and MT+. *Neuroimage, 67*, 89-100.

Pitzalis, S., Sdoia, S., Bultrini, A., Committeri, G., Di Russo, F., Fattori, P., ... & Galati, G. (2013b). Selectivity to translational egomotion in human brain motion areas. *PLoS One*, *8*(4), e60241.

Poldrack, R. A., Mumford, J. A., & Nichols, T. E. (2011). Handbook of functional MRI data analysis. *Cambridge University Press.*

Popov, T., Jensen, O., & Schoffelen, J. M. (2018). Dorsal and ventral cortices are coupled by cross-frequency interactions during working memory. *NeuroImage.*

Poppe, A. B., Wisner, K., Atluri, G., Lim, K. O., Kumar, V., & MacDonald, A. W. (2013). Toward a neurometric foundation for probabilistic independent component analysis of fMRI data. *Cognitive, Affective, & Behavioral Neuroscience, 13*(3), 641-659.

Prados, N. W. C. L. E., & Deriche-Olivier, R. (2007). Anatomical connections in the human visual cortex: validation and new insights using a DTI Geodesic Connectivity Mapping method.

Proudfoot, M., Woolrich, M. W., Nobre, A. C., & Turner, M. R. (2014). Magnetoencephalography. *Practical neurology, practneurol*-2013.

Pruim, R. H., Mennes, M., van Rooij, D., Llera, A., Buitelaar, J. K., & Beckmann, C. F. (2015). ICA-AROMA: A robust ICA-based strategy for removing motion artifacts from fMRI data. *Neuroimage, 112*, 267-277

Raichle, M. E. (2015). The brain's default mode network. *Annual review of neuroscience*, *38*, 433-447.

Raichle, M. E., MacLeod, A. M., Snyder, A. Z., Powers, W. J., Gusnard, D. A., & Shulman, G. L. (2001). A default mode of brain function. *Proceedings of the National Academy of Sciences, 98*(2), 676-682.

Ray, S., & Maunsell, J. H. (2011). Different origins of gamma rhythm and high-gamma activity in macaque visual cortex. *PLoS biology, 9*(4), e1000610.

Recanzone, G. H., Wurtz, R. H., & Schwarz, U. (1997). Responses of MT and MST neurons to one and two moving objects in the receptive field. *Journal of Neurophysiology*, *78*(6), 2904-2915.

Ribary, U. (2005). Dynamics of thalamo-cortical network oscillations and human perception. *Progress in brain research*, *150*, 127-142.

Ridderinkhof, K. R., Ullsperger, M., Crone, E. A., & Nieuwenhuis, S. (2004). The role of the medial frontal cortex in cognitive control. *Science, 306*(5695), 443-447.

Riecke, L., Sack, A. T., & Schroeder, C. E. (2015). Endogenous delta/theta sound-brain phase entrainment accelerates the buildup of auditory streaming. Current Biology, 25(24), 3196-3201.

Rilling, J. K., Barks, S. K., Parr, L. A., Preuss, T. M., Faber, T. L., Pagnoni, G., ... & Votaw, J. R. (2007). A comparison of resting-state brain activity in humans and chimpanzees. *Proceedings of the National Academy of Sciences*, *104*(43), 17146-17151.

Rodriguez, E., George, N., Lachaux, J. P., Martinerie, J., Renault, B., & Varela, F. J. (1999). Perception's shadow: long-distance synchronization of human brain activity. Nature, 397(6718), 430.

Roe, A. W., Chelazzi, L., Connor, C. E., Conway, B. R., Fujita, I., Gallant, J. L., ... & Vanduffel, W. (2012). Toward a unified theory of visual area V4. *Neuron*, *74*(1), 12-29.

Romei, V., Cooper, N., Sauseng, P., & Wolinski, N. (2017). P187 Individual differences in parietal theta frequency drive spatial working memory capacity. *Clinical Neurophysiology, 128*(3), e107.

Roux, F., & Uhlhaas, P. J. (2014). Working memory and neural oscillations: alpha–gamma versus theta–gamma codes for distinct WM information? *Trends in cognitive sciences*, *18*(1), 16-25

Rzucidlo, J. K., Roseman, P. L., Laurienti, P. J., & Dagenbach, D. (2013). Stability of whole brain and regional network topology within and between resting and cognitive states. *PloS one, 8*(8), e70275.

Salmi, J., Glerean, E., Jääskeläinen, I. P., Lahnakoski, J. M., Kettunen, J., Lampinen, J., ... & Sams, M. (2014). Posterior parietal cortex activity reflects the significance of others' actions during natural viewing. *Human brain mapping*, *35*(9), 4767-4776.

Sanes, J. N., & Donoghue, J. P. (1993). Oscillations in local field potentials of the primate motor cortex during voluntary movement. *Proceedings of the National Academy of Sciences*, *90*(10), 4470-4474.

Sasaki, Y., & Watanabe, T. (2016). V3A takes over a job of MT+ after training on a visual task. *Proceedings of the National Academy of Sciences, 113*(22), 6092-6093.

Sato, W., Kochiyama, T., Uono, S., Matsuda, K., Usui, K., Inoue, Y., & Toichi, M. (2014). Rapid, high-frequency, and theta-coupled gamma oscillations in the inferior occipital gyrus during face processing. *Cortex, 60*, 52-68.

Saxe, R., & Wexler, A. (2005). Making sense of another mind: the role of the right temporo-parietal junction. *Neuropsychologia, 43*(10), 1391-1399.

Schölvinck, M. L., Maier, A., Frank, Q. Y., Duyn, J. H., & Leopold, D. A. (2010). Neural basis of global resting-state fMRI activity. *Proceedings of the National Academy of Sciences*, 200913110.

Schweinberger, S. R., Pickering, E. C., Jentzsch, I., Burton, A. M., & Kaufmann, J. M. (2002). Event-related brain potential evidence for a response of inferior temporal cortex to familiar face repetitions. *Cognitive Brain Research*, *14*(3), 398-409.

Seymour, K., Clifford, C. W., Logothetis, N. K., & Bartels, A. (2009). The coding of color, motion, and their conjunction in the human visual cortex. *Current Biology*, *19*(3), 177-183.

Sheth, S. A., Nemoto, M., Guiou, M., Walker, M., Pouratian, N., & Toga, A. W. (2004). Linear and Nonlinear Relationships between Neuronal Activity, Oxygen Metabolism, and Hemodynamic Responses. *Neuron, 42*(2), 347-355. doi: https://doi.org/10.1016/S0896-6273(04)00221-1

Siapas, A. G., Lubenov, E. V., & Wilson, M. A. (2005). Prefrontal phase locking to hippocampal theta oscillations. *Neuron, 46*(1), 141-151.

Skipper, J. I., Goldin-Meadow, S., Nusbaum, H. C., & Small, S. L. (2009). Gestures orchestrate brain networks for language understanding. *Current Biology*, *19*(8), 661-667.

"Skyfall" (2012) Sam Mendes, MGM & Columbia Pictures.

Sliwa, J., & Freiwald, W. A. (2017). A dedicated network for social interaction processing in the primate brain. *Science, 356*(6339), 745-749.

Smith, S. M. (2012). The future of FMRI connectivity. *Neuroimage, 62(*2), 1257-1266.

Smith, S. M., Fox, P. T., Miller, K. L., Glahn, D. C., Fox, P. M., Mackay, C. E., ... & Beckmann, C. F. (2009). Correspondence of the brain's functional architecture during activation and rest. *Proceedings of the National Academy of Sciences, 106*(31), 13040-13045.

Smith, A. T., Wall, M. B., Williams, A. L., & Singh, K. D. (2006). Sensitivity to optic flow in human cortical areas MT and MST. *European Journal of Neuroscience, 23*(2), 561-569.

Strong, S. L., Silson, E. H., Gouws, A. D., Morland, A. B., & McKeefry, D. J. (2016). A direct demonstration of functional differences between subdivisions of human V5/MT+. *Cerebral Cortex, 27*(1), 1-10.

Strong, S. L., Silson, E. H., Gouws, A. D., Morland, A. B., & McKeefry, D. J. (2017). Higher Neural Functions and Behavior: Differential processing of the direction and focus of expansion of optic flow stimuli in areas MST and V3A of the human visual cortex. *Journal of Neurophysiology, 117*(6), 2209.

Smith, S. M., Vidaurre, D., Beckmann, C. F., Glasser, M. F., Jenkinson, M., Miller, K. L., ... & Barch, D. M. (2013). Functional connectomics from resting-state fMRI. *Trends in cognitive sciences*, *17*(12), 666-682.

Sunaert, S., Van Hecke, P., Marchal, G., & Orban, G. A. (1999). Motion-responsive regions of the human brain. *Experimental brain research*, *127*(4), 355-370.

Swettenham, J. B., Muthukumaraswamy, S. D., & Singh, K. D. (2009). Spectral properties of induced and evoked gamma oscillations in human early visual cortex to moving and stationary stimuli. *Journal of neurophysiology*, *102*(2), 1241-1253.

Tagliazucchi, E., & Laufs, H. (2014). Decoding wakefulness levels from typical fMRI resting-state data reveals reliable drifts between wakefulness and sleep. *Neuron*, *82*(3), 695-708.

Tallon-Baudry, C., & Bertrand, O. (1999). Oscillatory gamma activity in humans and its role in object representation. *Trends in cognitive sciences*, *3*(4), 151-162.

Taylor, P. C., Nobre, A. C., & Rushworth, M. F. (2006). FEF TMS affects visual cortical activity. *Cerebral Cortex, 17*(2), 391-399.

Thompson, R. F., & Spencer, W. A. (1966). Habituation: a model phenomenon for the study of neuronal substrates of behavior. *Psychological review*, *73*(1), 16.

Tikka, P., Kauttonen, J., & Hlushchuk, Y. (2018). Narrative comprehension beyond language: Common brain networks activated by a movie and its script. PloS one, 13(7), e0200134.

Tootell, R. B., Dale, A. M., Sereno, M. I., & Malach, R. (1996). New images from human visual cortex. *Trends in neurosciences*, *19*(11), 481-489.

Tootell, R. B., Hadjikhani, N. K., Mendola, J. D., Marrett, S., & Dale, A. M. (1998). From retinotopy to recognition: fMRI in human visual cortex. *Trends in cognitive sciences*, *2*(5), 174-183.

Tootell, R. B., Mendola, J. D., Hadjikhani, N. K., Ledden, P. J., Liu, A. K., Reppas, J. B., ... & Dale, A. M. (1997). Functional analysis of V3A and related areas in human visual cortex. *Journal of Neuroscience, 17*(18), 7060-7078.

Tootell, R. B., Reppas, J. B., Kwong, K. K., Malach, R., Born, R. T., Brady, T. J., ... & Belliveau, J. W. (1995). Functional analysis of human MT and related visual cortical areas using magnetic resonance imaging. *Journal of Neuroscience, 15*(4), 3215-3230.

Tootell, R. B., Silverman, M. S., Switkes, E., & De Valois, R. L. (1982). Deoxyglucose analysis of retinotopic organization in primate striate cortex. *Science*, *218*(4575), 902-904.

Tremblay, P., & Small, S. L. (2011). On the context-dependent nature of the contribution of the ventral premotor cortex to speech perception. *NeuroImage*, *57*(4), 1561-1571.

Treue, S., & Maunsell, J. H. (1996). Attentional modulation of visual motion processing in cortical areas MT and MST. *Nature*, *382*(6591), 539.

Trevarthen, C. B. (1968). Two mechanisms of vision in primates. *Psychologische Forschung*, *31*(4), 299-337.

Valyear, K. F., Culham, J. C., Sharif, N., Westwood, D., & Goodale, M. A. (2006). A double dissociation between sensitivity to changes in object identity and object orientation in the ventral and dorsal visual streams: a human fMRI study. *Neuropsychologia*, *44*(2), 218-228.

Vanderwal, T., Kelly, C., Eilbott, J., Mayes, L. C., & Castellanos, F. X. (2015). Inscapes: A movie paradigm to improve compliance in functional magnetic resonance imaging. *NeuroImage, 122,* 222-232.

Van Essen, D. C., Glasser, M. F., Dierker, D. L., Harwell, J., & Coalson, T. (2011). Parcellations and hemispheric asymmetries of human cerebral cortex analyzed on surface-based atlases. *Cerebral cortex*, *22*(10), 2241-2262.

Van Dijk, K. R., Hedden, T., Venkataraman, A., Evans, K. C., Lazar, S. W., & Buckner, R. L. (2009). Intrinsic functional connectivity as a tool for human connectomics: theory, properties, and optimization. *Journal of neurophysiology, 103*(1), 297-321.

Van Dijk, K. R., Sabuncu, M. R., & Buckner, R. L. (2012). The influence of head motion on intrinsic functional connectivity MRI. *Neuroimage, 59*(1), 431-438.

van Schie, H. T., Koelewijn, T., Jensen, O., Oostenveld, R., Maris, E., & Bekkering, H. (2008). Evidence for fast, low-level motor resonance to action observation: a MEG study. *Social Neuroscience*, *3*(3-4), 213-228.

Vigário, R., Sarela, J., Jousmiki, V., Hamalainen, M., & Oja, E. (2000). Independent component approach to the analysis of EEG and MEG recordings. *IEEE transactions on biomedical engineering*, *47*(5), 589-593.

Vinberg, J., & Grill-Spector, K. (2008). Representation of shapes, edges, and surfaces across multiple cues in the human visual cortex. Journal of neurophysiology.

Visser, M., & Lambon Ralph, M. A. (2011). Differential contributions of bilateral ventral anterior temporal lobe and left anterior superior temporal gyrus to semantic processes. *Journal of Cognitive Neuroscience*, *23*(10), 3121-3131.

Von Stein, A., & Sarnthein, J. (2000). Different frequencies for different scales of cortical integration: from local gamma to long range alpha/theta synchronization. *International journal of psychophysiology*, *38*(3), 301-313.

Wandell, B. A., Dumoulin, S. O., & Brewer, A. A. (2007). Visual field maps in human cortex. *Neuron*, *56*(2), 366-383.

Wang, X. J. (2010). Neurophysiological and computational principles of cortical rhythms in cognition. *Physiological reviews, 90*(3), 1195-1268.

Wang, K., Liang, M., Wang, L., Tian, L., Zhang, X., Li, K., & Jiang, T. (2007). Altered functional connectivity in early Alzheimer's disease: A resting-state fMRI study. *Human brain mapping*, *28*(10), 967-978.

Wang, L., Mruczek, R. E., Arcaro, M. J., & Kastner, S. (2014). Probabilistic maps of visual topography in human cortex. *Cerebral Cortex, 25*(10), 3911-3931.

Whitney, C., Huber, W., Klann, J., Weis, S., Krach, S., & Kircher, T. (2009). Neural correlates of narrative shifts during auditory story comprehension. *Neuroimage*, *47*(1), 360-366.

Whitney, C., Kirk, M., O'Sullivan, J., Lambon Ralph, M. A., & Jefferies, E. (2010). The neural organization of semantic control: TMS evidence for a distributed network in left inferior frontal and posterior middle temporal gyrus. *Cerebral Cortex*, *21*(5), 1066-1075.

Whittingstall, K., & Logothetis, N. K. (2009). Frequency-band coupling in surface EEG reflects spiking activity in monkey visual cortex. *Neuron, 64*(2), 281-289.

Wieczorek, K. (2015). *Investigating the relationship between microsaccades and oscillations in the human visual cortex.* (Doctoral dissertation, Cardiff University).

Wilson, S. M., Molnar-Szakacs, I., & Iacoboni, M. (2007). Beyond superior temporal cortex: intersubject correlations in narrative speech comprehension. *Cerebral cortex, 18*(1), 230-242.

Winder, A.T., Echagarruga, C., Zhang, Q., & Drew, P.J. (2017). Weak correlations between hemodynamic signals and ongoing neural activity during the resting state. *Nature Neuroscience*. doi:10.1038/s41593-017-0007-y

Winawer, J., Horiguchi, H., Sayres, R. A., Amano, K., & Wandell, B. A. (2010). Mapping hV4 and ventral occipital cortex: the venous eclipse. Journal of vision, 10(5), 1-1.

Wisner, K. M., Atluri, G., Lim, K. O., & MacDonald, A. W. (2013). Neurometrics of intrinsic connectivity networks at rest using fMRI: retest reliability and cross-validation using a meta-level method. *NeuroImage, 76*, 236-251.

Wolinski, N., Cooper, N. R., Sauseng, P., & Romei, V. (2018). The speed of parietal theta frequency drives visuospatial working memory capacity. *PLoS biology, 16*(3), e2005348.

Womelsdorf, T., Fries, P., Mitra, P. P., & Desimone, R. (2006). Gamma-band synchronization in visual cortex predicts speed of change detection. *Nature*, *439*(7077), 733.

Worsley, K.J., Marrett, S., Neelin, P., and Evans, A.C. (1992). A three-dimensional statistical analysis for CBF activation studies in human brain. *Journal of Cerebral Blood Flow and Metabolism*, **12**:900-918.

Wright, N. D., Mechelli, A., Noppeney, U., Veltman, D. J., Rombouts, S. A., Glensman, J., ... & Price, C. J. (2008). Selective activation around the left occipito-temporal sulcus for words relative to pictures: Individual variability or false positives? *Human brain mapping, 29*(8), 986-1000.

Wróbel, A. (2000). Beta activity: a carrier for visual attention. *Acta neurobiologiae experimentalis, 60*(2), 247-260.

Wutz, A., Loonis, R., Roy, J. E., Donoghue, J. A., & Miller, E. K. (2018). Different Levels of Category Abstraction by Different Dynamics in Different Prefrontal Areas. *Neuron, 97*(3), 716-726.

Yarkoni, T., Poldrack, R. A., Nichols, T. E., Van Essen, D. C., & Wager, T. D. (2011). Large-scale automated synthesis of human functional neuroimaging data. *Nature methods, 8*(8), 665.

Yeo, B. T., Krienen, F. M., Sepulcre, J., Sabuncu, M. R., Lashkari, D., Hollinshead, M., ... & Fischl, B. (2011). The organization of the human cerebral cortex estimated by intrinsic functional connectivity. *Journal of neurophysiology, 106*(3), 1125-1165.

Ylipaavalniemi, J., & Vigário, R. (2008). Analyzing consistency of independent components: An fMRI illustration. *NeuroImage, 39*(1), 169-180.

Yuan, H., Perdoni, C., Yang, L., & He, B. (2011). Differential Electrophysiological Coupling for Positive and Negative BOLD Responses during Unilateral Hand Movements. *The Journal of Neuroscience, 31*(26), 9585-9593. doi: 10.1523/jneurosci.5312-10.2011

Zacks, J. M., Braver, T. S., Sheridan, M. A., Donaldson, D. I., Snyder, A. Z., Ollinger, J. M., ... & Raichle, M. E. (2001). Human brain activity time-locked to perceptual event boundaries. *Nature neuroscience, 4*(6), 651.

Zhang, H., Zuo, X. N., Ma, S. Y., Zang, Y. F., Milham, M. P., & Zhu, C. Z. (2010). Subject order-independent group ICA (SOI-GICA) for functional MRI data analysis. *Neuroimage, 51*(4), 1414-1424.

Zeki, S. M. (1974). Functional organization of a visual area in the posterior bank of the superior temporal sulcus of the rhesus monkey. *The Journal of Physiology, 236*(3), 549-573.

Zeki, S. M. (1978). Functional specialisation in the visual cortex of the rhesus monkey. *Nature*, *274*(5670), 423.

Zeki, S., Watson, J. D., Lueck, C. J., Friston, K. J., Kennard, C., & Frackowiak, R. S. (1991). A direct demonstration of functional specialization in human visual cortex. *Journal of neuroscience, 11*(3), 641-649.

Zuo, X. N., & Xing, X. X. (2014). Test-retest reliabilities of resting-state FMRI measurements in human brain functional connectomics: a systems neuroscience perspective. *Neuroscience & Biobehavioral Reviews, 45*, 100-118.